Dissertation
submitted to the
Combined Faculties of the Natural Sciences and Mathematics
of the Ruperto-Carola-University of Heidelberg, Germany
for the degree of
Doctor of Natural Sciences

Put forward by

Simon Alexander Weißenborn-Bresch

born in: Heidelberg, Germany

Oral examination: 13^{th} of July 2016

On the Impact of Pion Fluctuations on the Dynamics of the Order Parameter at the Chiral Phase Transition

Referees:

PD Dr. Jürgen Schaffner-Bielich

Prof. Dr. Joerg Jaeckel

Über den Einfluss pionischer Fluktuationen auf die Dynamik des Ordnungsparameters am chiralen Phasenübergang

Auf der Suche nach möglichen Signaturen des chiralen Phasenübergangs in Schwerionenkollisionen kommt den Pionen vermutlich eine entscheidende Rolle zu. Wir untersuchen den Einfluss pionischer Fluktuationen auf die Relaxationsdynamik des chiralen Ordnungsparameters im Rahmen eines Langevinansatzes für das Quark-Meson Modell.
Von der effektiven Wirkung ausgehend leiten wir, motiviert durch den Formalismus des "Influence"-Funktionals, eine Bewegungsgleichung für die chiralen Felder her, welche eine Ankopplung an ein Wärmebad bestehend aus Quarks und harten mesonischem Moden beinhaltet.
In diesem Zuge erweitern wir bestehende Studien, in welchen die Pionen vernachlässigt wurden. Als Ergebnis erhalten wir, dass pionische Fluktuationen am chiralen Phasenübergang spürbare Auswirkungen auf die Dynamik des sigma-Feldes haben. Bei einem Phasenübergang erster Ordnung können sich die pionischen Fluktuationen entweder beschleunigend oder bremsend auf die Relaxation des Systems auswirken, je nach gewählten Anfangsbedingungen. Am kritischen Punkt eines Phasenübergangs zweiter Ordnung erwirken die pionischen Fluktuationen eine Verschiebung des Gleichgewichtserwartungswertes des sigma-Feldes.
Desweiteren testen wir unser Modell im Kontext einer Schwerionenkollision, indem wir das Temperaturprofil eines expandierenden Plasmas für das Wärmebad annehmen. In dieser Näherung zeigen die pionischen Fluktuationen jedoch keinen merklichen Effekt.

On the Impact of Pion Fluctuations on the Dynamics of the Order Parameter at the Chiral Phase Transition

In the search for possible signatures of the chiral phase transition in heavy ion collisions, pions are expected to play an important role. We investigate the impact of pion fluctuations on the relaxation of the chiral order parameter in the framework of nonequilibrium Langevin dynamics in the quark-meson model.
Starting from the effective action and motivated by the influence functional formalism, we derive an equation of motion for the chiral fields coupled to a heat bath of quarks and hard meson modes.
Thereby, we extend existing studies in which the pions have been neglected.
We find that at the chiral phase transition the pion fluctuations have a noticeable effect on the dynamics of the sigma field. For a first order phase transition, the pion fluctuations can speed up or delay relaxation of the system, depending on the initial conditions. For a critical point scenario, the pion fluctuations shift the equilibrium expectation value of the order parameter at the phase transition.
Further, we test our model in the context of a heavy ion collision by imposing the temperature profile for an expanding plasma on the heat bath. We find that within this approximation the model shows no effect from pion fluctuations.

Contents

Chapter 1.

Introduction

One of the four fundemental interactions known today is the so-called strong interaction. It acts between quarks and gluons as well as between all kinds of hadrons, which are particles composed of quarks. Since nearly all of the visible matter in the universe belongs to this category, understanding the strong interaction is of great interest.

The most easily accessible pieces of strongly interacting matter are atomic nuclei. However, the information we gain from these nuclei at "normal" conditions are hard to extrapolate to high temperatures and densities. Unfortunately, natural environments for very hot or dense strongly interacting matter as e.g. the early universe, supernova explosions and neutron stars are far less accessible for observations and often require indirect measurements.

With the advent of accellerator experiments in the second half of the last century, strongly interacting matter at high temperatures and densities could be created and closely observed. Apart from the discovery of the quarks as constituent particles of the baryons, it was found, that the strength of the interaction between the quarks decreases with higher energy. This effect is known as asymptotic freedom. In combination with the lack of observing lumps of quarks that consist of less than either three quarks, respectively antiquarks, or a quark-antiquark pair, which is known as confinement, the question arises whether there will be a phase transition to a plasma of quarks (and gluons), and if so, where precicely does it occur and of what type is it? To answer these questions, we need a theory on the quark level.

To this day, the best and most widely accepted candidate for a theory of strongly interacting matter is quantum chromodynamcis (QCD). Besides incorporating confinement

and asymptotic freedom, QCD is approximately symmetric under chiral transformations at low energies. However, this symmetry is broken in the vacuum, but can it be restored at finite temperature?

The great interest in this particular symmetry of QCD is that we have probably already found the possible quasi-Goldstone bosons in the chirally broken vacuum, the pions. Moreover, the breaking, respectively restoration of the symmetry may explain the difference between the current and constituent quark masses of the two lightest quark flavors. What we still lack is the (experimental) finding of some characteristic signature of the phase transition for a proof of its existence.

The strength and so the experimental recognizability of such a signature depends on the order of the phase transition. If it is of second order, the correlation length of the thermal fluctuations diverges at the critical point and the microscopic properties of the system become unimportant which leads to universal scaling. If the phase transition is of first order, the formation of disoriented chiral condensates (DCC) is considered a possible footprint of the phase transition[1]. DCCs arise when the chiral quark condensate is driven out of its equilibrium direction and acquires a finite component in pion direction. During the decay of the DCCs, soft pion modes are enhanced. DCCs can form by spinodal decomposition or from tachyonic instabilities of the order parameter. However, no traces of DCC formation and decay have yet been found in experiment. Nevertheless, we can expect pion fluctuations to become important at the chiral phase transition.

The main goal of this work is to study the impact of pionic fluctuations on the dynamics of the chiral fields near and at the chiral phase transition. The dynamics of the fields are governed by a Langevin equation which is obtained from the quark-meson model in the framework of the closed time path effective action and motivated by the influence functional formalism.

In the present work, we build upon existing studies in which the role of dissipation and noise on the dynamics of the chiral order parameter has been investigated [Nah11,

[1] There exist many studies of DCC formation and their signatures, see e.g. [Bjo92, RW93, SD99, XG00] to name just a few amongst many. An extensive review is provided in [MS05] and a short overview is found in [Nah11]

NLHB11, NLB12, NHL$^+$13]. Therein, the dynamics of the sigma mean field is described by a Langevin equation which is obtained from the quark-meson model in the framework of the influence functional formalism and the closed time path effective action. From the effective interaction of the sigma field and the quarks which serve as a heat bath, dissipative terms and noise enter the equation of motion. In the cited works, pions have not been taken into account. However, at the chiral phase transition they are expected to become important.

In this work, we extend the model of [Nah11] by including the pions. This is done in two steps: In a first approach, we allow for a finite pion field, and then we also account for the contributions of hard meson modes to the heat bath in terms of disspation and noise[2]. We then investigate the impact of pionic fluctuations on the dynamics of the sigma field close and at the chiral phase transition.

This thesis is organized as follows: in chapter 2, we will go into more detail about chiral symmetry as an approximate symmetry of QCD. Then, we will motivate and discuss the quark-meson model. In chapter 3 we will collect the various concepts that we need to derive a Langevin equation of motion which is at the heart of our numerical studies. These concepts include the imaginary as well as the closed time path formalism (section 3.1), but also basic Langevin theory and the influence functional formalism (section 3.2). At the end of the chapter, the 1PI and 2PI effective action on the closed time path are presented. The whole of chapter 4 is devoted to the derivation of the equations of motion. The first part of the chapter contains our first extenstion to the model of [Nah11] by including explicitly propagated pion mean fields. In the second part, we extend the model further by accounting for the dissipative effects from interactions of the mean fields with the hard meson modes. Then we finally present our numerical results in chapters 5-7. While in chapter 5 we restrict calculations to the case where we propagate the pion mean fields alongside the sigma field, chapter 6 contains the corresponding results for the case of additional hard meson modes in the heat bath. Both chapters 5 and 6 are of identical structure: first, thermal equilibrium is discussed and the model parameters chosen for the different types of phase transition. Second, for the case of a static heat bath the nonequilibrium dynamics of the sigma field is examined in the presence of the pion fluctuations. And finally, the energy dissipation of the

[2]This can be considered as combining our first upgrade to the model of [Nah11] with parts of the model of [Ris98] in a (slightly) different framework.

chiral fields to the heat bath is taken into account. In chapter 7, we apply our model in the context of a heavy ion collision and investigate relaxation and particle production in the soft meson modes. In chapter 8, we summarize our results and present an outlook.

Throughout this work, we use natural units $\hbar = c = k_B = 1$.

Chapter 2.

QCD, Chiral Symmetry and the Quark-Meson Model

In this chapter, we will very briefly review the history of QCD. Thereafter, we shortly discuss chiral symmetry and introduce the quark-meson model as the basis upon which we build our studies.

2.1. Quantum Chromodynamics

Today's state of the art description for the physics of strong interactions is the theory of quantum chromodyamics (QCD). It is very successful in describing many of the observed features of strong interactions. Historically, the evolution of QCD followed the enormous progress in collider experiments which began in the late 1940s and revealed the existence of many formerly unknown particles.[1]

Amongst these particles, the large variety of observed hadrons could successfully be explained by assuming hadrons to be composed of other particles, the quarks and anti-quarks [Ne'61, GM62, GM64, Zwe64a, Zwe64b]. Furthermore, the observed existence of certain hadrons made it necessary for the quarks to be given a new degree of freedom: otherwise, e.g. the nucleonic resonance Δ^{++} which consists of three up-quarks with zero orbital angular momentum and all three spins aligned in the same direction could not be explained to exist as a consequence of the Pauli principle. The new degree of freedom was introduced via an additional $SU(3)$ symmetry and the quarks were given

[1] Introductions to QCD, its historical development and key concepts can be found in many textbooks, as e.g. [Gri08, Col11], but also in countless works. The presentation in this section is strongly influenced by [Sti14] where also many of the references cited here are found.

a corresponding charge, the color [Gre64, HN65, FGM72].

Apart from explaining the patterns in the quantum numbers and masses of the different hadrons found in experiments, the assumption of quarks as constituents of baryons and mesons was successfully applied to describe the outcome of deep inelastic scattering experiments [Tay, BEF$^+$68, B$^+$69, Fey69b, Fey69a, BP69]. However, with these findings new questions arose: at low energies quarks only appear in their hadronic bound states and no isolated free quark has ever been detected. Instead, only composite particles have been found and all of them can be described as singlets of color SU(3). This is known as confinement. Moreover, the quarks tend to behave more and more like free particles at higher energies. This effect is called asymptotic freedom. Both these properties of quarks were successfully incorporated into a theory by coupling the quarks to a massless, non-abelian gauge field [YM54, GW73b, GW73a, GW74, Pol73, Pol74]. The corresponding gauge group is elegantly identified with the color SU(3) symmetry group. The outcome is the theory governed by the Lagrangian:

$$\mathcal{L}_{QCD} = \sum_{flavor} \overline{\psi} \left(i \not{D} - m \right) \psi - \frac{1}{4} F^a_{\mu\nu} F^{\mu\nu}_a \tag{2.1}$$

with the gauge covariant derivative

$$D_\mu = \partial_\mu - i g t^a A^a_\mu \tag{2.2}$$

and field strength tensor

$$F^a_{\mu\nu} = \partial_\mu A^a_\nu - \partial_\nu A^a_\mu - g f^{abc} A^b_\mu A^c_\nu \tag{2.3}$$

The particles associated with the eight gauge vector fields A^a_μ are named gluons and t^a denote the corresponding generators of the SU(3) gauge group. They satisfy the relations:

$$\left[t^a, t^b \right] = i f^{abc} t^c \tag{2.4}$$

with SU(3) structure constants f^{abc}. The sum in (2.1) runs over the six known quark flavors (u,d,s,c,b,t).

With properties such as confinement and asymptotic freedom one might ask if at sufficiently high temperatures or densities there is a phase transition to a quark-gluon

plasma, i.e. a state of strongly interacting matter, where the quarks behave like free particles (see e.g. [Hag65, CP75a, Ito70, CP75b] amongst many others). Firm and clear evidence for such a phase transition has not yet been found experimentally despite good hints for successful creation of a quark-gluon plasma (see for instance [A$^+$05]). While collider experiments keep on probing the QCD phase diagram for signs of a phase transiton, it is also difficult to make theoretical predictions, because of the non-abelian nature of the gluon fields: an exact analytic solution to QCD at finite temperature is not at hand and standard perturbative techniques which rely on a sufficiently small coupling constant are only valid at high enough energy scales where the quarks are asymptotically free. At the QCD phase transition however, these methods are no longer applicable.

In order to treat QCD at the phase transition non-perturbative approaches are needed. Probably the most prominent example is lattice QCD where the partition function is solved on a discrete space-time lattice[2]. The corresponding calculations are computationally very expensive. This is why they are usually performed on big computer clusters. At zero quark-chemical potential, lattice QCD predicts a crossover at the QCD phas transition [BFH$^+$10, BP10, B$^+$12]. For finite quark chemical potential, lattice QCD faces the famous sign problem.

If one does not wish to employ a non-perturbative method for practical reasons, but nevertheless wishes to explore the QCD phase diagram at low temperatures and energies, it is customary to choose an effective model of QCD [FS13]. Such a model cannot of course fully reproduce QCD in its full glory. Instead, such models are designed so that they are of simpler structure and feature only certain desired properties. The property we are interested in is chiral symmetry, which we discuss in the following section.

[2] The field of lattice QCD is very wide (and deep). An introduction to the subject is e.g. given in [Cre83, DH09, Phi10].

2.2. Chiral Symmetry

[3] Apart from its color $SU(3)$ symmetry, the QCD Lagrangian (2.1) features several other symmetries, probably the most obvious one being invariance under global $U(1)_V$ transformations, given by:

$$\psi(x) \to e^{-i\theta}\psi(x) \tag{2.5}$$

with real valued parameter θ. The conserved Noether charge associated with this symmetry is the baryon number. Further, the Lagrangian (2.1) is also invariant under global $U(1)_A$ transformations,

$$\psi(x) \to e^{-i\gamma_5\theta}\psi(x) \ . \tag{2.6}$$

However, during the quantization of the theory this symmetry is explicitly broken which gives rise to the mass splitting in the meson multiplets [DGH14]. If we restrict to two flavor QCD, i.e. if we only consider up and down quark flavors which share the same mass, $m_u = m_d$, we find another symmetry of (2.1), namely $SU(2)_V$ with corresponding transformations

$$\psi(x) \to e^{-i\frac{\vec{\tau}}{2}\vec{\theta}}\psi(x) \tag{2.7}$$

where $\psi = (\psi_u, \psi_d)^t$ and τ_j, $(j = 1, 2, 3)$ are the Pauli matrices acting on flavor space. The associated conserved quantity is the isospin current. Finally, in the limit of vanishing quark masses (2.1) is invariant under so called chiral transformations, which in the case of two quark flavors read

$$\psi(x) \to e^{-i\gamma_5\frac{\vec{\tau}}{2}\vec{\theta}}\psi(x) \tag{2.8}$$

and belong to the group $SU(2)_A$. The axial vector current

$$\vec{A}^\mu(x) = \overline{\psi}(x)\gamma^\mu\gamma_5\frac{\vec{\tau}}{2}\psi(x) \tag{2.9}$$

is conserved if the symmetry is exact. The combined group $SU(2)_V \times SU(2)_A$ is isomorphic to $SU(2)_L \times SU(2)_R$, the chiral symmetry group, which seperately transforms spinors of left (L) and right (R) handed chirality, $\psi_{R/L} = \frac{1}{2}(1 \pm \gamma_5)\psi$. In real two flavor QCD, whith up and down quark masses nonzero but very small compared to e.g. the hadron masses, we can expect that the violation of axial vector current conservation is only small. However, this approximate symmetry would require a corresponding degen-

[3] The symmetries of QCD and in particular chiral symmetry are discussed in various books and articles (see e.g. [Mos89, Koc97]). Our presentation of the subject has been greatly inspired by [Mal12, Nah11].

eracy of hadronic states with nearly the same mass which is not observed. Therefore, if chiral symmetry is an approximate symmetry of QCD, it must be broken in the vacuum. But if a symmetry is spontaneously broken, the Goldstone theorem predicts the existence of massless particles. For an approximate, but not exact, symmetry which is broken, these Goldstone bosons acquire a small but finite mass. In nature, suitable candidates are found in shape of the pions: with a vacuum mass of $m_\pi = 138$ MeV, they are much lighter than any other observed hadrons. As for the order parameter of the broken chiral symmetry, the scalar quark condensate $\langle\overline{\psi}\psi\rangle$ is identified with the sigma meson.

2.3. The Quark-Meson Model

In order to explore the QCD phase diagram near the chiral phase transition we choose an effective model[4] of QCD which contains the necessary ingredients for chiral symmetry breaking. A simple model which meets this requirement is the (chiral) quark-meson model or linear sigma model with constituent quarks which is obtained from the original linear sigma model with nucleons [GML60] by using light quarks instead of nucleons. Collecting the up and down quarks into $\psi = (\psi_u, \psi_d)^t$ the Lagrangian of the quark meson model is given by

$$\mathcal{L}_{QM} = \overline{\psi}\left[i\partial\!\!\!/ - g\left(\sigma + i\gamma_5\vec{\tau}\vec{\pi}\right)\psi\right] + \frac{1}{2}\partial_\mu\sigma\partial^\mu\sigma + \frac{1}{2}\partial_\mu\vec{\pi}\partial^\mu\vec{\pi} - V_{cl}(\sigma,\vec{\pi}) \tag{2.10}$$

with the scalar isoscalar field σ and the pseudoscalar isovector field $\vec{\pi}$. The bosonic potential reads

$$V_{cl}(\sigma,\vec{\pi}) = \frac{\lambda}{4N}\left(\sigma^2 + \vec{\pi}^2 - v^2\right)^2 - h\sigma \ . \tag{2.11}$$

The potential reflects the kind of symmetry breaking in the model: for the choice $h = 0$ the potential is invariant under chiral transformations, but in the ground state, the vacuum expectation value of the vector $\vec{\varphi} = (\sigma, \vec{\pi})$ has finite length $\vec{\varphi}^2 = v^2$ and therefore, the quarks acquire a mass term which breaks chiral symmetry. The breakdown of symmetry occurs spontaneously, since the vector $\vec{\varphi}$ may point in any direction, i.e. the ground state is degenerate. By defining the σ direction to coincide with the direction of

[4] A review on chiral effective models of QCD is found in [FS13]. Our presentation of the subject is guided by [Sti14, Nah11].

the ground state vector, i.e. $\vec{\varphi} = (v, \vec{0})$ we see that the pions are indeed massless

$$m_\pi^2 = \left.\frac{\partial^2 V_{cl}}{\partial \pi_j^2}\right|_{\substack{\sigma=v \\ \vec{\pi}=0}} = 0 \tag{2.12}$$

in agreement with the Goldstone theorem. However, the choice $h > 0$ tilts the potenial in the σ direction and explicitly breaks chiral symmetry, thus leading to a finite pion mass

$$m_\pi^2 = \frac{h}{\langle\sigma\rangle} \tag{2.13}$$

with vacuum expectation value $\langle\sigma\rangle > 0$ while $\langle\vec{\pi}\rangle$ is forced to zero. The vacuum expectation value $\langle\sigma\rangle$ then serves as order parameter for chiral symmetry breaking and generates a finite quark mass in the broken phase, $m_q = g\langle\sigma\rangle$. The parameters of the model are fixed to reproduce the phenomenological values [O+14]

$$\langle\sigma\rangle = f_\pi = 93\ MeV \tag{2.14}$$

$$m_\pi = 138\ MeV \tag{2.15}$$

$$m_\sigma^2 = \left.\frac{\partial^2 V_{cl}}{\partial \sigma^2}\right|_{\substack{\sigma=f_\pi \\ \vec{\pi}=0}} = \frac{2\lambda}{N} f_\pi^2 + m_\pi^2 \approx (600\, MeV)^2 \tag{2.16}$$

which suggests

$$\frac{\lambda}{N} = 20 \tag{2.17}$$

$$h = f_\pi m_\pi^2 \tag{2.18}$$

$$v^2 = f_\pi^2 - \frac{N}{\lambda} m_\pi^2 \tag{2.19}$$

For later convenience, it should be noted that in the absence of the explicit symmetry breaking term the purely mesonic part of the Lagrangian (2.10) coincides with more general $O(N)$ invariant

$$\mathcal{L}_\varphi = \frac{1}{2}\partial_\mu \varphi_a \partial^\mu \varphi_a - \frac{\lambda}{4N}\left(\varphi_a \varphi_a - v^2\right)^2 \tag{2.20}$$

for a N-component scalar field $\vec{\varphi}$ in the special case of $N = 4$ meson flavors.

The quark-meson model is widely used for studies of chiral symmetry breaking (see

for instance [JW96, SP99, LRSB00, BJW03, BK09]), but it is of course not the only suitable model. Another important chiral effective model is the Nambu-Jona-Lasinio model [NJL61a, NJL61b] which in contrast to the quark-meson model is however not renormalizable.

Chapter 3.

The Tool Box

In the previous chapter we have discussed the quark-meson model as the basis upon which we want to build our studies of mesonic fluctuations in the context of the chiral phase transition. What we need now is a way to get from the Lagrangian (2.10) to an equation of motion which explicitly reflects the impact of these fluctuations on the dynamics of the meson fields in a way that we can handle numerically. Furthermore, the desired equation of motion should allow for nonequilibrium meson field configurations to first relax to and then remain in thermal equilibrium. This means, that we require an irreversible (partial) conversion of the potential and kinetic energy of the meson fields into thermal energy. In other words, we want dissipation in our equation of motion.

In this chapter, we present the concepts neccessary for the derivation of such an equation of motion. These are the real-time contour formalism, the influence functional and its relation to Langevin dynamics and the (2PI) effective action formalism.

3.1. Time Paths in Finite Temperature Field Theory

A discussion of the following can be found in many textbooks on finite temeperature field theory, as e.g. [Das97] which has influenced our presentation of the subject most, but also [KG06, Bel11].

3.1.1. Imaginary time formalism

Probably the most widely used concept in finite temperature field theory is the Matsubara formalism [Mat55]. It is based on the idea that the density matrix,

$$\rho = e^{-\beta H} \tag{3.1}$$

of a statistical ensemble with Hamiltonian H and inverse temperature $\beta = 1/T$ may be regarded as a quantum mechanical time evolution operator in imaginary time, $t \to -i\tau$, with τ ranging from 0 to β. For the ensemble averages of quantum mechanical operator products this ansatz leads to periodicity conditions in imaginary time direction[1], known as Kubo-Martin-Schwinger relations [Kub57, MS59]:

$$\langle A(t)B(t')\rangle = \langle B(t')A(t+i\beta)\rangle \tag{3.2}$$

where the ensemble average is defined in the standard way

$$\langle A\rangle = (Tr\ \rho)^{-1}\, Tr\ \rho A \tag{3.3}$$

For the two point functions $G(\tau, \tau')$ of boson respectively fermion fields, relation (3.2) implies

$$G(0,\tau) = \pm G(\beta,\tau) \tag{3.4}$$

where the minus sign corresponds to the fermionic case. This (anti)periodicity leads to a discrete Fourier spectrum, the so-called Matsubara frequencies:

$$\begin{aligned} \omega_{n,b} &= \frac{2\pi n}{\beta} \\ \omega_{n,f} &= \frac{(2n+1)\pi}{\beta} \end{aligned} \tag{3.5}$$

for bosons (b) and fermions (f) with $n \in \mathbb{Z}$. The Matsubara formalism allows to rather intuitively apply zero temperature field theory techniques as e.g. diagrammatic expansions to the finite temperature case and has been very successfully used to study systems in thermal equilibrium on countless occasions.

[1] This requires time dependence of the operators and so a treatment e.g. in the Heisenber picture [Das97].

3.1.2. Closed real time path formalism

However, if one is interested in dynamic aspects as e.g. the behaviour of a system evolving through a phase transition, the imaginary time formalism is not well suited, since it gives up the time variable in favour of introducing temperature. In order to obtain thermal n-point functions defined for real time arguments, one can search for analytic continuation of the imaginary time Green's functions in the complex time plane (see e.g. [BM61, DJ74]). However, a more convenient apporoach (in our case) follows from the basic observation that the time evolution of an ensemble average of an operator $\langle A(t)\rangle_\beta$ can be rewritten as tracing over time evolution operators from initial time t_0 to $t > t_0$ where $A(t)$ is inserted, then on to some $t' > t$ and somehow back to $t_0 - i\beta$. A special case of this is the so-called closed time path, where time is evolved back along the real axis from t' to t_0 and then in negative imaginary direction from t_0 to $t_0 - i\beta$. The three parts of the time contour $\mathcal{C}$ are usually denoted as $\mathcal{C}_+$, $\mathcal{C}_-$ for the paths along the real axis in positive (+) respectively negative (-) direction, and $\mathcal{C}_3$ for the remaining part in imaginary direction. The closed time path formalism goes back to Schwinger [Sch61] and Keldysh [Kel64] and is designed to treat nonequilbrium dynamics from the start.

The partition function, given by the trace over the time evolution operators along the contour, can be generalized by adding sources on the contour which allows for the definition of a generating functional for correlation functions in the standard fashion. In the limit of $t_0 \to -\infty$, $t' \to +\infty$, the partition function factorizes into one partition function for the real time paths and another for the path in imaginary direction. Thus, we need not worry about the path $\mathcal{C}_3$ when considering correlation functions with real time arguments and may neglect $\mathcal{C}_3$ in the derivations in the next chapter. However, it should be noted, that $\mathcal{C}_3$ still has an impact on the real time correlation functions in the sense that they have to fulfill the according (anti)periodicity conditions in imaginary time[2]. Furthermore, if one is interested in equilibrium properties as e.g. pressure, the partition function of $\mathcal{C}_3$ must be taken into account.

The time integration along the contour $\mathcal{C}$ in the limits $t_0 \to -\infty$, $t' \to +\infty$ and ne-

[2]This means, the notion of temperature is still implemented in the formalism. This is in contrast to a "full" nonequilibrium treatment which does not know about temperature [Ber04].

glecting $\mathcal{C}_3$ is given by:

$$\int_{\mathcal{C}} \varphi(t)dt = \int_{-\infty}^{+\infty} \varphi(t_+)dt_+ - \int_{-\infty}^{+\infty} \varphi(t_-)dt_- \tag{3.6}$$

for some field φ, where the first integral on the right hand side is along the path $\mathcal{C}_+$ and the other integral along $\mathcal{C}_-$. Accordingly, the delta function on the contour is defined via

$$\int_{\mathcal{C}} \varphi(t')\delta_{\mathcal{C}}(t-t')dt' = \varphi(t') \tag{3.7}$$

and thus $\delta_{\mathcal{C}}(t-t') = \pm\delta(t-t')$ for t, t' both on $\mathcal{C}_\pm$. If t, t' lie on different branches of the contour, the delta function equates to zero of course. It is customary, to view $\varphi(t_+)$ and $\varphi(t_-)$ as two separate variables $\varphi^+(t)$, $\varphi^-(t)$ with t on the standard real time axis:

$$\int_{\mathcal{C}} \varphi(t) = \int_{-\infty}^{+\infty} \left(\varphi^+(t) - \varphi^-(t)\right)\, dt \tag{3.8}$$

Accordingly, the sources in the generating functional are also split into independent sources for fields on the different time branches. The propagators which require time ordering along the contour $\mathcal{C}$ take on a matrix form:

$$G^{ab} = \begin{pmatrix} G^{++} & G^{+-} \\ G^{-+} & G^{--} \end{pmatrix} \tag{3.9}$$

with

$$\begin{aligned} G^{++}(t,t') &= \langle T\varphi^+(t)\varphi^+(t')\rangle \\ G^{+-}(t,t') &= \langle \varphi^-(t')\varphi^+(t)\rangle \\ G^{-+}(t,t') &= \langle \varphi^-(t)\varphi^+(t')\rangle \\ G^{--}(t,t') &= \langle T^*\varphi^-(t)\varphi^-(t')\rangle \end{aligned} \tag{3.10}$$

with T denoting the standard time ordering and T^* anti time ordering. In the case of fermion fields, G^{+-} gets a minus sign on the right hand side. Of the four propagator components, only three are independent, since G^{++} and G^{--} can be expressed as

$$\begin{aligned} G^{++}(t,t') &= \Theta(t-t')G^{-+}(t,t') + \Theta(t'-t)G^{+-}(t,t') \\ G^{--}(t,t') &= \Theta(t-t')G^{+-}(t,t') + \Theta(t'-t)G^{-+}(t,t') \end{aligned} \tag{3.11}$$

which allows to eliminate one of the components. For a real scalar field of mass m, the propagator in momentum space reads:

$$G^{++}(p) = \frac{i}{p^2 - m^2 + i\epsilon} + 2\pi\, n_B\left(|p^0|\right)\, \delta\left(p^2 - m^2\right) \tag{3.12}$$

$$G^{--}(p) = \frac{-i}{p^2 - m^2 - i\epsilon} + 2\pi\, n_B\left(|p^0|\right)\, \delta\left(p^2 - m^2\right) \tag{3.13}$$

$$G^{+-}(p) = 2\pi\left(n_B\left(|p^0|\right) + \Theta\left(-p^0\right)\right)\, \delta\left(p^2 - m^2\right) \tag{3.14}$$

$$G^{-+}(p) = 2\pi\left(n_B\left(|p^0|\right) + \Theta\left(p^0\right)\right)\, \delta\left(p^2 - m^2\right) \tag{3.15}$$

and for a fermion field of mass m:

$$S^{++}(p) = (\not{p} + m)\left(\frac{i}{p^2 - m^2 + i\epsilon} - 2\pi n_F(|p^0|)\delta(p^2 - m^2)\right) \tag{3.16}$$

$$S^{--}(p) = (\not{p} + m)\left(\frac{-i}{p^2 - m^2 - i\epsilon} - 2\pi n_F(|p^0|)\delta(p^2 - m^2)\right) \tag{3.17}$$

$$S^{+-}(p) = -2\pi(\not{p} + m)\left[n_F(|p^0|) - \Theta(-p^0)\right]\delta(p^2 - m^2) \tag{3.18}$$

$$S^{-+}(p) = -2\pi(\not{p} + m)\left[n_F(|p^0|) - \Theta(p^0)\right]\delta(p^2 - m^2) \tag{3.19}$$

where n_B and n_F denote the boson (B) and fermion (F) distribution functions. Often, the off-diagonal propagator components are also denoted as $G^{+-} = G^{<}$ and $G^{-+} = G^{>}$.

3.2. Influence functional and Langevin Dynamics

3.2.1. Classical Langevin equation

What we are still missing in our tool box for crafting a suitable equation of motion is a way to incorporate dissipation. A good candidate for this is the Langevin [Lan08, LG97] equation which historically was introduced in the context of Brownian motion: a test particle of mass m moving with velocity v in a liquid of light particles gets random kicks in any direction by colliding with the particles of the liquid which is modelled by a stochastic force ξ. On average, these collisions slow down the test particle, i.e. they effectively exert a frictional force, $\sim -v$. The equation of motion for the test particle

may thus be written as (see e.g. [Sch06]):

$$m\dot{v}(t) = -\eta v(t) + \xi(t) \tag{3.20}$$

The light particles are usually assumed to equilibrize on a time scale much shorter than the time scale for the evolution of the test particle, meaning that the random kicks by the stochastic force are uncorrelated for different times, i.e. it is of Markovian type. The first two moments of ξ are then

$$\langle \xi(t) \rangle = 0 \tag{3.21}$$

$$\langle \xi(t)\xi(t') \rangle = \lambda\delta(t - t') \tag{3.22}$$

where the average over an ensemble of configurations of the stochastic force is considered. For the sake of simplification, it is customary to assume that the distribution of ξ is Gaussian and thus no higher moments are needed for a full characterization of the stochastic force. Demanding that the test particle is in thermal equilibrium with the liquid for large times $t \gg m/\eta$ leads for the average kinetic energy for each spatial degree of freedom to the condition

$$\frac{1}{2}m\langle v^2(t) \rangle = \frac{1}{2}k_B T \tag{3.23}$$

due to the equipartition theorem. This allows to connect the variance of the stochastic field to the damping coefficient:

$$\lambda = 2\eta k_B T \tag{3.24}$$

which is known as the fluctuation-dissipation theorem.

In principle, on the classical level, the motion of the test particle as well as of every light particle is fully deterministic, given full knowledge of the position and momentum of all particles involved and keeping track of every single one of them during the time evolution. Apart from being highly impractical for even the simplest applications, such a description is also invariant under time reversal[3], i.e. the system is not dissipative. However, the Langevin ansatz focuses only on the evolution of those degrees of freedom which are of interest, namely the movement of the test particle. The light particles of the liquid act as a heat bath and we only consider their average effect (plus stochastic fluctuations) on the relevant part of the system. And it is at this point where dissipation

[3]This statement assumes of course interactions modelled as elastic two-body scattering.

enters. In our case, the relevant degrees of freedom are the meson soft modes and the irrelevant part of the system is a heat bath of quarks (and hard meson modes). Thus, we might look for a (quantum)field theoretical technique which helps in averageing over the irrelevant degrees of freedom in order to obtain a Langevin-like equation of motion for the relevant part of the system. This leads us directly to the influence functional formalism. Its presentation in the following section is based on [GL98, Nah11, Ris98].

3.2.2. Influence functional formalism

The idea of the influence functional goes back to Feyman and Vernon [FV63] and starts with a system governed by the action $S[x, q]$ where all relevant field variables, i.e. the ones whose dynamics we are interested in, are collected in x, while all other variables of the system are considered irrelevant and collectively denoted by q. The latter constitute a background for the dynamics of the relevant variables and serve as a heat bath if one assumes the fields q to be thermalized. At initial time t_i the entire system is described by the density matrix ρ_i with matrix elements $\rho_i(x_i, q_i, x_i', q_i')$. At time t_f, the density matrix $\rho_f = \rho(t_f)$ is obtained from ρ_i via

$$\begin{aligned}\rho_f(x_f, q_f, x_f', q_f', t_f) = \int dx_i \int dx_i' \int dq_i \int dq_i'\, U(x_f, q_f, t_f, x_i, q_i, t_i)\times \\ \times\, \rho_i(x_i, q_i, x_i', q_i')\, U^\dagger(x_f', q_f', t_f, x_i', q_i', t_i)\end{aligned} \tag{3.25}$$

where the time evolution operator, expressed as a path integral, reads

$$U(x_f, q_f, t_f, x_i, q_i, t_i) = \int \mathcal{D}x \int \mathcal{D}q\; exp(iS[x, q]) \tag{3.26}$$

with boundary conditions $x(t_i) = x_i$, $x(t_f) = x_f$ and likewise for q. With this, there appears a term

$$\sim exp(iS[x, q] - iS[x', q']) \tag{3.27}$$

under the functional integral in expression (3.25). This term is rewritten by splitting the action $S[x, q]$ into three parts,

$$S[x, q] = S_0[x] + S_0[q] + S_{int}[x, q] \tag{3.28}$$

with $S_0[x]$, $S_0[q]$ containing only terms involving x, respectively q, and $S_{int}[x, q]$ consisting of the remaining interaction terms between the two sectors. To simplify matters,

it is convenient to assume Bogoliubov initial conditions, i.e. that the relevant and the irrelevant sectors are initially uncorrelated which leads to a factorization of the initial density matrix:

$$\rho_i(x_i, q_i, x_i', q_i') = \rho_i^S(x_i, x_i') \otimes \rho_i^E(q_i, q_i') \tag{3.29}$$

where we adopted the notation of [Nah11] for the density matrix of the system (S) of relevant degrees of freedom, and the environment (E) constituted by the irrelevant fields. Integrating out the environment then leads to a reduced density matrix ρ_r of the relevant fields:

$$\rho_r(x_f, x_f', t_f) = \int dx_i \int dx_i' \, \rho_i^S(x_i, x_i') \int \mathcal{D}x \int \mathcal{D}x' \, exp(iS_0[x] - iS_0[x'] + iS_{IF}[x, x']) \tag{3.30}$$

with the influence functional S_{IF} defined by

$$\begin{aligned} exp(iS_{IF}[x, x']) = \int dq_i \int dq_i' \, \rho_i^E(q_i, q_i') \int \mathcal{D}q \int \mathcal{D}q' \\ \times exp(iS_0[q] + iS_{int}[x, q] - iS_0[q'] - iS_{int}[x', q']) \end{aligned} \tag{3.31}$$

The influence functional contains all information about the (ensemble averaged) interactions of the relevant variables x with the environment. From its definition, the influence functional fulfills the relations:

$$S_{IF}[x, x'] = 0 \tag{3.32}$$

$$S_{IF}[x, x'] = -S_{IF}^*[x, x'] \tag{3.33}$$

For practical use, it is convenient to approximate the term $exp(iS_{IF})$ so that ρ_r can be computed. Often, one expands the interaction part:

$$exp(iS_0[q]+iS_{int}[x, q]-iS_0[q']-iS_{int}[x', q']) = exp(iS_0[q]-iS_0[q']) \sum_{n=0}^{\infty} \frac{i^n}{n!} (S_{int}[x, q]-S_{int}[x', q'])^n \tag{3.34}$$

and truncates the series at the desired order which corresponds to a perturbative expansion in the coupling between the system and the heat bath. By virtue of the expansion it becomes clear that equation (3.31) can be viewed as a sum of correlation functions in x and q which are ensemble averages with respect to the environment. Expanding also $log(1 + a) = a - a^2/2 + ...$ we can express the influence functional itself in terms of n-

point functions which can be reduced to products of two point functions in the standard way (e.g. by explicitly constructing the partition function and generating functional and successive functional differentiation with respect to the source).

In the limit $t_i \to -\infty$, $t_f \to \infty$ and with an equilibrium density matrix ρ_i^E it is natural to identify $x \to x^+$ and $x' \to x^-$ as fields on different branches of the closed real time contour. The aforementioned two-point functions are then given by the real-time contour propagators. Trading the varibles $x^\pm$ for center and relative variables on the contour,

$$\overline{x} = \frac{1}{2}(x^+ + x^-) \tag{3.35}$$

$$\Delta x = x^+ - x^- \tag{3.36}$$

allows to identify effects from fluctuations off equilibrium, since in thermal equilibrium $\Delta x = 0$. An equation of motion for $\overline{x}$ is then obtained from equation (3.30) by the stationary phase condition:

$$\left.\frac{\delta(S_0[x^+] - S_0[x^-] + S_{IF}[\overline{x}, \Delta x])}{\delta(\Delta x)}\right|_{\Delta x = 0} \tag{3.37}$$

As we will later see in our model, the influence functional S_{IF} can have a term linear in Δx (in the next chapter, x will be the replaced by the chiral fields),

$$\int d^4z \, D(z)\Delta x(z) \tag{3.38}$$

with standard space-time integration. This will lead to a damping term in the equation of motion. Real valued terms at $\mathcal{O}(\Delta x^2)$ vanish of course as do terms of any higher order. However, the influence functional might come with an imaginary part of the form:

$$Im(S_{IF}[\overline{x}, \Delta x]) = \frac{i}{2}\int d^4z \int d^4z' \, \Delta x(z)\mathcal{N}(z, z')\Delta x(z') \tag{3.39}$$

which is not neccessarily suppressed for large Δx. To get the influence functional (and thus the action) real, a stochastic field ξ is introduced and the term in question is

expressed as an average over the stochastic field [Sch82]

$$exp(i\, Im(S_{IF}[\overline{x}, \Delta x])) = \int \mathcal{D}\xi\; P[\xi]\; exp\left(i \int d^4z \xi(z) \Delta x(z)\right) \tag{3.40}$$

where the factor

$$P[\xi] = \tilde{N}\; exp\left(-\frac{1}{2}\int d^4z\; d^4z' \xi(z) \mathcal{N}^{-1}(z,z') \xi(z')\right) \tag{3.41}$$

is a Gaussian weight and $\tilde{N}$ an appropriate normalization constant. Due to the Gaussian distribution of the field ξ, it is characterized by its first and second moment:

$$\langle \xi(z) \rangle_\xi \;=\; 0 \tag{3.42}$$

$$\langle \xi(z)\xi(z') \rangle_\xi \;=\; \mathcal{N}(z,z') \tag{3.43}$$

Finally, the semi classical equation of motion for $\overline{x}$ is

$$\frac{\delta S_0[\overline{x}]}{\delta \overline{x}(z)} + D(z) + \xi(z) = 0 \tag{3.44}$$

We have obtained a Langevin equation with the stochastic field ξ acting as a random force. Assuming that D acts as a damping term (which we will se in the next chapter) we have now a tool for obtaining an equation of motion for the relevant fields which incorporates dissipation and noise as an averaged effect from the interaction with a thermal heat bath. However, equation (3.44) does not account for thermal mass shifts: apart from damping and noise terms the equation of motion only features the field derivative of the classical action, but there is no thermal contribution to the potential. For such an upgrade in our equation of motion, we will consider the effective action formalism in the following section.

3.3. The nPI effective action

3.3.1. 1PI effective action

A great tool for studying symmetry breaking in quantum field theory is the one-particle-irreducible (1PI) effective action.[4] In quantum field theory, the generating functional of connected n-point functions, $W[J]$, in the presence of a linear source J is defined as:

$$Z[J] = exp(iW[J]) = \int \mathcal{D}\varphi \, exp\left(iS_{cl}[\varphi] + \int J\varphi\right) \tag{3.45}$$

where we consider for simplicity the case of a neutral scalar field φ governed by the classical action S_{cl}. The mean field π in the presence of the source J is then obtained via functional differentiation as

$$\phi = \frac{\delta W[J]}{\delta J} = \langle\varphi\rangle_J \tag{3.46}$$

and the effective action, $\Gamma[\phi]$, is defined as the Legendre transform of $W[J]$:

$$\Gamma[\phi] = W[J] - \int J\phi \tag{3.47}$$

and the equation of motion for the mean field is given by:

$$\frac{\delta\Gamma[\phi]}{\delta\phi} = J \tag{3.48}$$

Considering the full field shifted to the mean field plus fluctuations, $\varphi \to \phi + \varphi$ allows to write Γ as the sum of the classical action of the mean field plus quantum corrections. The latter allow for a diagrammatic expansion,

$$\Gamma[\phi] = S_{cl}[\phi] + \frac{i}{2} Tr \, log \, G_0^{-1} + \Gamma_1 \tag{3.49}$$

with the trace-log term resumming the one-loop contributions of the "classical" propagator,

$$iG_0^{-1}(x,y) = \frac{\delta^2 S_{cl}[\phi]}{\delta\phi(x)\delta\phi(y)} \tag{3.50}$$

[4] Introductions to the 1PI effective action at zero temperature can be found in almost every book on quantum field theory, e.g. [PS95, Wei95, Sre07]. For our discussion at finite temperatures and also for the 2PI effective action, we rely on [Ber04, Nah11].

and the term Γ_1 containing only connected 1PI-diagrams (i.e. diagrams which are still connected if a single line is removed) beginning at two-loop order. Finite temperature physics enter the formalism when specifying the time integration contour accordingly, as e.g. the closed real time path.

3.3.2. 2PI effective action

To go beyond mean field dynamics, one might add a bilocal source term

$$\int \varphi(x) R(x,y) \varphi(y) \tag{3.51}$$

in the exponential on the right hand side of equation (3.45) and perform a second Legendre transform, trading the source R for the connected two-point function G. The expansion of the effective action (3.49) then takes the form:

$$\Gamma[\phi, G] = S_{cl}[\phi] + \frac{i}{2} Tr\, log\, G^{-1} + \frac{i}{2} Tr\, G_0^{-1} G + \Gamma_2[\phi, G] \tag{3.52}$$

where at one loop order, i.e. in the trace-log term, the self-consistent propagator G enters. The latter satisfies the stationarity condition:

$$\frac{\delta \Gamma}{\delta G} = -\frac{1}{2} R \tag{3.53}$$

and Γ_2 is given by the sum of all two-particle irreducible diagrams (i.e. diagrams which cannot be separated by the removal of two lines). The equations of motion in the absence of sources are:

$$\frac{\delta \Gamma}{\delta \phi} = 0 \qquad \frac{\delta \Gamma}{\delta G} = 0 \tag{3.54}$$

For the propagator, this is a Schwinger-Dyson equation:

$$G_0^{-1} G - \Sigma G = \mathbb{1} \tag{3.55}$$

with the proper self energy Σ defined as

$$\Sigma(x, y, \phi, G) = 2i \frac{\delta \Gamma_2[\phi, G]}{\delta G(x, y)} \tag{3.56}$$

where we have restored the various dependencies for now. The Schwinger-Dyson equation ensures that 1PI self-energy contributions are automatically and self-consistently resummed in the propagator.

This is a welcome feature and it may be extended to the description of n-point functions by successively introducing 3-point sources, 4-point sources and so on with subsequenct Legendre transformations. At the n-th step, this leads to the n-particle-irreducible effective action with a self-consistent (up to n-th loop order) set of equations of motion for all n'-point functions with $n' \leq n$.

For fermion fields, the 2PI effective action also depends on the fermion propagator S which appears in the expansion in equation (3.52) as:

$$- i\, Tr\, log\, S^{-1} - i\, Tr\, S_0^{-1} S \tag{3.57}$$

as well as in the 2PI diagrams entering Γ_2 which determine the fermion self-energy $\Sigma_f = -i\delta\Gamma_2/\delta S$.

In order to solve the equations of motion, one needs to truncate Γ_2, e.g. at a given order in loops or in the coupling constant. Despite such approximations, the self-consistency of the 2PI ansatz is still given within the limits of the truncation. While the aforementioned examples provide a finite number of diagrams contributing to Γ_2, there are also ways to resum an infinite number of diagrams. A prominent example is provided by a an expansion in powers of $1/N$ in O(N) symmetric models (see e.g. [Ber02, Ber04]).

Choosing the closed real time contour for the time integration (as introduced above), the 2PI effective action is capable of describing dynamics in a thermodynamic context, where temperature has a meaning. However, for "true" nonequilbrium dynamics the time path from initial time to present time t and back to initial time is chosen. The system is then evolved in time by increasing t and at each point in time the current evolution is determined by the full past of the fields and correlators. The boundary problem from the (anti)periodicity conditions in imaginary time are not present in this apporach (nor is temperature), instead it is an initial value problem. If in the nonequilbrium 2PI effective action ansatz the system relaxes to a stable state which can be identified as thermal equilibrium, then it is an outcome of the theory which has not been put in by

hand [Ber04]. In our studies, however, we would like to have more control over the final state of the system which is why we stick to the Schwinger-Keldysh contour.

Chapter 4.

Mesonic Fluctuations and Langevin Dynamics

In this section we will derive a Langevin equation for the σ mean field taking into account dissipative and noise terms originating from mesonic fluctuations. Starting from the effective action for the quark meson model, we will extend the approach of Nahrgang ([NLHB11, Nah11]) by including pionic degrees of freedom. Before we continue, it should be stressed that in [NLHB11, Nah11] the notion of the 2PI effective action differs from the one delineated e.g. in [Ber04]. We shall adopt the latter notion and emphasize differences to [NLHB11, Nah11] whenever neccessary.

Probably the most appealing property of the 2PI effective action formalism is that it automatically leads to a self-consistent quantum theory which also featueres thermodynamic consistency. However, in the notion of [Ber04] and as opposed to the claim in [NLHB11, Nah11], we will sacrifice the self-consistency in favor of obtaining a semi-classical equation of motion. Nevertheless the 2PI formalism will help us in deriving self consistent thermal meson propagators in section 4.2. But first, we will restrict to the case of a pure quark heat bath during the derivations in section 4.1. We will work at vanishing quark chemical potential.

4.1. Dissipation and noise for pure quark heat bath

In order to find a semi-classical equation of motion for the meson fields we follow [Nah11, NLHB11] and (at least formally) start with the 2PI effective action for the quark-meson model. As outlined in the previous chapter, the first step in the derivation of the 2PI effective action is to split the quantum fields into their ensemble averages (i.e.

the "classical" or "mean" fields) plus fluctuations.
Likewise, the Lagrangian splits into a part consisting only of classical fields and a fluctuation part. The classical part constitutes the so-called classical action S_{cl} which enters into the loop expansion of the 2PI effective action, equation (3.52), while the fluctuation part provides the vertices needed for the construction of the 2PI diagrams entering Γ_2. The classical Lagrangian is given by equation (2.10) with classical instead of full fields. From S_{cl} the inverse classical propagators for the quarks (S_0) and mesons (G_0) can be read off immediately as ($\vec{\varphi} = (\sigma, \vec{\pi})$):

$$iS_0^{-1}(x,y) = (i\partial\!\!\!/_x - g[\sigma(x) + i\gamma_5 \vec{\tau}\vec{\pi}(x)])\delta(x-y) \tag{4.1}$$

$$iG_{ab,0}^{-1}(x,y) = -\left([\Box_x + \frac{\lambda}{N}\varphi_c(x)\varphi^c(x) - v^2]\delta_{ab} - 2\frac{\lambda}{N}\varphi_a(x)\varphi_b(x)\right)\delta(x-y) \tag{4.2}$$

From the above one sees that in general both propagators could have non-zero off-diagonal elements in quark respectively meson flavor space. However, for vanishing pion mean field and thus especially in thermal equilibrium the structure of the propagators reduces to flavor-diagonal form.

Next, we need to specify how to truncate Γ_2. In the spirit of Nahrgang [NLHB11], we will for now fully neglect the meson propagators, i.e. we choose

$$G = 0 \tag{4.3}$$

$$\Longrightarrow \Gamma = \Gamma[\sigma, \vec{\pi}, S] \quad . \tag{4.4}$$

This choice however makes it impossible to draw any 2PI diagrams containing quark propagators, since the quark-meson model lacks a quark-quark self-interaction term. Thus, the current approximation results in

$$\Gamma_2 = 0 \tag{4.5}$$

and therefore causes a vanishing quark self-energy:

$$\Sigma_q = -i\frac{\delta\Gamma_2[\sigma, \vec{\pi}, S]}{\delta S} = 0 \tag{4.6}$$

As a consequence, the equation of motion for the quark propagator also becomes trivial:

$$\frac{\delta\Gamma}{\delta S} = 0 \Longrightarrow S_0^{-1}S = \mathbb{1} \Longleftrightarrow S = S_0 \tag{4.7}$$

i.e., the full propagator is just given by the classical one. Further, the $Tr(S_0^{-1}S)$ term in the loop expansion of the 2PI effective action is reduced to an (infinite) constant which may be dropped. The ansatz for the effective action melts down to the simple form:

$$\Gamma[\sigma, \vec{\pi}, S_0] = S_{cl}[\sigma_0, \vec{\pi}] + i\, Tr\, ln\, S_0(\sigma, \vec{\pi}) \tag{4.8}$$

This is just the standard (1PI) effective action with the quark one-loop potential in meson mean-field approximation. In other words, within the chosen approximation we would not have needed the full 2PI effective action ansatz. However, as soon as we include the meson propagator, we will need the 2PI formalism (see section 4.2).

At this point it is important to note that the previous statements follow from using the 2PI framework in the sense of e.g. [Ber04]. In [NLHB11, Nah11] on the other hand a different definition of the classical propagator is used which leads to Γ_2 consisting of a quark loop with a mean field insertion. However, following [Ber04], the contributions from any one-loop diagrams are already accounted for by the one-loop part of the 2PI effecitve action, i.e. the trace terms. Of course, within the current approximations both points of view will finally result in the same equations of motion.

It is clear that by assuming a vanishing meson propagator we loose all information about mesonic quantum fluctuations, which are hidden in the n point correlation functions of the meson fields [Ber04]. The only degrees of freedom left are the macroscopic meson fields and the fermion propagator as a function of these fields. In order to reintroduce mesonic fluctuations into the model we follow Nahrgang et al. and allow for a (microscopic) spatial variation of the (macroscopic) meson mean fields [NLHB11]. These meson fields are then split into a slowly varying part and a fluctuating rest:

$$\sigma(x) \longrightarrow \sigma_0(x) + \delta\sigma(x) \tag{4.9}$$

$$\vec{\pi}(x) \longrightarrow \vec{\pi}(x) + \delta\vec{\pi}(x) \tag{4.10}$$

where we adopt the notation of [NLHB11] by assigning a "δ" to the fluctuations and using the index "0" for the slowly varying fields. Similarly to the meson fields, the quark propagator is replaced by a sum of a thermal propagator S_{th} plus fluctuations [NLHB11]:

$$S_0(x,y) \longrightarrow S(x,y) = S_{th}(x,y) + \delta S(x,y) + \delta^2 S(x,y) \tag{4.11}$$

The splitting of the meson fields is chosen such that the "slowly" varying part depends only weakly on space-time coordinate compared to the quark propagator. Further, it is assumed that the fluctuations in the propagator and the fields are small. Therefore, the above replacements allow to solve the equation of motion for the quark propagator, equation (4.7), order by order in the fluctuations, i.e. the following three equations:

$$\mathcal{O}(\delta^0) \quad : \quad (i\partial\!\!\!/_x - g[\sigma_0^a(x) + i\gamma_5\vec{\tau}\vec{\pi}_0^a(x)])S_{th}^{ab}(x,y) = i\delta_{\mathcal{C}}^{ab}(x-y) \tag{4.12}$$

$$\begin{aligned}\mathcal{O}(\delta^1) \quad : \quad & (i\partial\!\!\!/_x - g[\sigma_0^a(x) + i\gamma_5\vec{\tau}\vec{\pi}_0^a(x)])\delta S^{ab}(x,y) - g[\delta\sigma^a(x) + i\gamma_5\vec{\tau}\delta\vec{\pi}^a(x)]S_{th}^{ab}(x,y) \\ & = 0\end{aligned} \tag{4.13}$$

$$\begin{aligned}\mathcal{O}(\delta^2) \quad : \quad & (i\partial\!\!\!/_x - g[\sigma_0^a(x) + i\gamma_5\vec{\tau}\vec{\pi}_0^a(x)])\delta^2 S^{ab}(x,y) - g[\delta\sigma^a(x) + i\gamma_5\vec{\tau}\delta\vec{\pi}^a(x)]\delta S^{ab}(x,y) \\ & = 0\end{aligned} \tag{4.14}$$

Here we have restored the real-time contour indices. Since we require a much weaker space-time dependence of σ_0, $\vec{\pi}_0$ than S_{th},the solution to the lowest order equation is given by the thermal fermion propagator on the real time contour. The propagators mass matrix features off-diagonal elements due to the pseudo-scalar coupling of the pions and quarks. In momentum space, the four components of S_{th} on the real-time contour read:

$$S_{th}^{++}(p) = (p\!\!\!/ + g(\sigma_0 - i\gamma_5\vec{\tau}\vec{\pi}_0))\left(\frac{i}{p^2 - m_q^2 + i\epsilon} - 2\pi n_F(|p^0|)\delta(p^2 - m_q^2)\right) \tag{4.15}$$

$$S_{th}^{--}(p) = (p\!\!\!/ + g(\sigma_0 - i\gamma_5\vec{\tau}\vec{\pi}_0))\left(\frac{-i}{p^2 - m_q^2 - i\epsilon} - 2\pi n_F(|p^0|)\delta(p^2 - m_q^2)\right) \tag{4.16}$$

$$S_{th}^{+-}(p) = -2\pi(p\!\!\!/ + g(\sigma_0 - i\gamma_5\vec{\tau}\vec{\pi}_0))\left[n_F(|p^0|) - \Theta(-p^0)\right]\delta(p^2 - m_q^2) \tag{4.17}$$

$$S_{th}^{-+}(p) = -2\pi(p\!\!\!/ + g(\sigma_0 - i\gamma_5\vec{\tau}\vec{\pi}_0))\left[n_F(|p^0|) - \Theta(p^0)\right]\delta(p^2 - m_q^2) \tag{4.18}$$

with the dynamic quark mass $m_q = g\sqrt{\sigma_0^2 + \vec{\pi}_0^2}$. Now that we have the solution of equation (4.12), we note that we can solve equation (4.13) by a Green's function ansatz:

$$\delta S^{ab}(x,y) = -ig \int_{\mathcal{C}} d^4z S_{th}^{ac}(x,z) \left[\delta\sigma^c(z) + i\gamma_5 \vec{\tau}\delta\vec{\pi}^c(z)\right] S_{th}^{cb}(z,y) \tag{4.19}$$

Similarly, one finds for the solution of equation (4.14):

$$\begin{aligned}\delta^2 S^{ab}(x,y) \;\; &= -g^2 \int_{\mathcal{C}} d^4z d^4z' \;\; S_{th}^{ac}(x,z) \left[\delta\sigma^c(z) + i\gamma_5 \vec{\tau}\delta\vec{\pi}^c(z)\right] S_{th}^{cd}(z,z') \\ &\qquad \left[\delta\sigma^d(z') + i\gamma_5 \vec{\tau}\delta\vec{\pi}^d(z')\right] S_{th}^{db}(z',y)\end{aligned} \tag{4.20}$$

Plugging the quark propagator into the effective action, we find up to an infinite constant

$$\Gamma = S_{cl}[\sigma_0 + \delta\sigma, \vec{\pi}_0 + \delta\vec{\pi}] + i\, Tr\, ln\, (S_{th} + \delta S + \delta^2 S) \tag{4.21}$$

and expand in orders of fluctuations. For this purpose, we write the trace-log term as:

$$i\, Tr\, ln\, S \;\; = \;\; i\, Tr\, ln\, S_{th} + i\, Tr\, ln\, (\mathbb{1} + S_{th}^{-1}(\delta S + \delta^2 S)) \tag{4.22}$$

with all indices suppressed. Using

$$ln(1+x) = x - \frac{x^2}{2} + ... \tag{4.23}$$

we obtain:

$$\begin{aligned} i\, Tr\, ln\, S \;\; &= \;\; i\, Tr\, ln\, S_{th} + g\, Tr\, (\delta\phi\, S_{th}) \\ &\qquad -\frac{ig^2}{2}\, Tr\, (\delta\phi\, S_{th}\, \delta\phi\, S_{th}) + \mathcal{O}(\delta^3) \end{aligned} \tag{4.24}$$

where we inserted the solutions for δS, $\delta^2 S$, i.e. equations (4.19), (4.20), and introduced the shorthand notation:

$$\delta\phi = \delta\sigma + i\gamma_5 \vec{\tau}\delta\vec{\pi} \quad . \tag{4.25}$$

Following [NLHB11, Nah11], we combine the fields on the two time branches of the Keldysh contour into center and relative variables:

$$\delta\overline{\sigma} = \frac{1}{2}(\delta\sigma^+ + \delta\sigma^-) \tag{4.26}$$

$$\Delta\delta\sigma = \delta\sigma^+ - \delta\sigma^- \tag{4.27}$$

$$\delta\overline{\pi}_j = \frac{1}{2}(\delta\pi_j^+ + \delta\pi_j^-), \quad (j = 1, 2, 3) \tag{4.28}$$

$$\Delta\delta\vec{\pi} = \delta\vec{\pi}^+ - \delta\vec{\pi}^- \tag{4.29}$$

As in equation (4.28), we will always write the pion center field with an isospin index such that it cannot be confused with the vector notation. To ensure better readability, we further define

$$\delta\overline{\phi} = \frac{1}{2}(\delta\phi^+ + \delta\phi^-) = \delta\overline{\sigma} + i\gamma_5\tau_j\delta\overline{\pi}_j \tag{4.30}$$

$$\Delta\delta\phi = \delta\phi^+ - \delta\phi^- = \Delta\delta\sigma + i\gamma_5\vec{\tau}\Delta\delta\vec{\pi} \quad . \tag{4.31}$$

which has a non-trivial structure in Dirac and quark flavor spaces due to the pion contribution. With the replacements of equations (4.24) and (4.26)-(4.31) we rewrite the effective action, equation (4.21). Further, we switch to the common notation $S^< = S^{+-}$, $S^> = S^{-+}$. Finally, the effective action takes the following form (see appendix A.2 for computational details):

$$\begin{aligned}
&\Gamma[\sigma_0, \vec{\pi}_0, \delta\sigma, \delta\vec{\pi}, S] = \\
&\qquad S_{cl}[\sigma_0 + \delta\sigma, \vec{\pi}_0 + \delta\vec{\pi}] \;+\; i\,Tr\;ln\;S_{th} + \;g\int d^4x\;\; tr\left(\Delta\delta\phi(x)S_{th}^{++}(x,x)\right) \\
&+ig^2\int d^4x d^4y\Theta(x^0-y^0)tr\left(\Delta\delta\phi(x)S_{th}^<(x,y)\delta\overline{\phi}(y)S_{th}^>(y,x) - \Delta\delta\phi(x)S_{th}^>(x,y)\delta\overline{\phi}(y)S_{th}^<(y,x)\right) \\
&- \frac{ig^2}{4}\int d^4x\, d^4y\; tr\left(\Delta\delta\phi(x)S_{th}^<(x,y)\Delta\delta\phi(y)S_{th}^>(y,x) + \Delta\delta\phi(x)S_{th}^>(x,y)\Delta\delta\phi(y)S_{th}^<(y,x)\right) \\
&\qquad\qquad + \mathcal{O}(\delta^3)
\end{aligned} \tag{4.32}$$

This is the one loop effective action plus corrections linear and quadratic in the meson fluctuations. Also, for all pion contributions set to zero, we almost recover the result presented in [NLHB11, Nah11]. The only difference lies in the presence of the one loop mean field quark potential, i.e. the trace-log term, which will drop out in the equation of motion. Moreover, comparing our equation (4.32) to the corresponding equation (48) in [NLHB11], respectively equation (5.42) in [Nah11], we note that in the cited work the term with the theta-function carries an additional factor 1/2. However, since we cannot reproduce this factor even by precisely following the derivations in [NLHB11, Nah11], we assume that it must be a typo.

From equation (4.32) the equation of motion for the meson center fields is obtained by:

$$\left.\frac{\delta\Gamma}{\delta(\Delta\delta\sigma)}\right|_{\substack{\Delta\delta\sigma=\Delta\sigma_0=0\\ \Delta\delta\vec{\pi}=\Delta\vec{\pi}_0=0}} = 0 \tag{4.33}$$

$$\left.\frac{\delta\Gamma}{\delta(\Delta\delta\pi_j)}\right|_{\substack{\Delta\delta\sigma=\Delta\sigma_0=0\\ \Delta\delta\vec{\pi}=\Delta\vec{\pi}_0=0}} = 0 \quad (j=1,2,3) \tag{4.34}$$

In equation (4.32) we recognize the structure of the damping and noise kernels as motivated by the influence functional in the previous chapter[1]. Denoting the damping kernel as D_a and introducing the stochastic force as in the influence functional approach, equations (4.33), (4.34) turn into (j=1,2,3):

$$0 = \left.\frac{\delta S_{cl}[\sigma,\vec{\pi}]}{\delta(\Delta\delta\sigma(x))}\right|_{\substack{\Delta\delta\sigma=\Delta\sigma_0=0\\ \Delta\delta\vec{\pi}=\Delta\vec{\pi}_0=0}} + g\,tr\,S_{th}^{++}(x,x) + D_\sigma(x) + \xi_\sigma(x) \tag{4.35}$$

$$0 = \left.\frac{\delta S_{cl}[\sigma,\vec{\pi}]}{\delta(\Delta\delta\pi_j(x))}\right|_{\substack{\Delta\delta\sigma=\Delta\sigma_0=0\\ \Delta\delta\vec{\pi}=\Delta\vec{\pi}_0=0}} + ig\,tr\left(\gamma_5\,\tau_j\,S_{th}^{++}(x,x)\right) + D_{\pi_j}(x) + \xi_{\pi_j}(x) \tag{4.36}$$

[1]Explicitly evaluating the influence functional for the quark-meson model at the meson mean field level, indeed leads to the very same expressions at $\mathcal{O}(g^2)$ (see [Nah11, NLHB11] for the case of $\vec{\pi}=0$)

4.1.1. Classical action and (pseudo)scalar density

For the classical action on the real time contour we have:

$$\left.\frac{\delta S_{cl}[\sigma,\vec{\pi}]}{\delta(\Delta\delta\sigma)}\right|_{\substack{\Delta\delta\sigma=\Delta\sigma_0=0\\ \Delta\delta\vec{\pi}=\Delta\vec{\pi}_0=0}} = \left(\frac{\delta S_{QM}[\sigma^+,\vec{\pi}^+]}{\delta(\Delta\delta\sigma)} - \frac{\delta S_{QM}[\sigma^-,\vec{\pi}^-]}{\delta(\Delta\delta\sigma)}\right)\Bigg|_{\substack{\Delta\delta\sigma=\Delta\sigma_0=0\\ \Delta\delta\vec{\pi}=\Delta\vec{\pi}_0=0}} \tag{4.37}$$

$$\tag{4.38}$$

and similarly for $\delta S_{cl}/\delta(\Delta\delta\pi_j)$, (j=1,2,3). Since $\sigma^{\pm} = \overline{\sigma}_0 \pm \frac{1}{2}\Delta\sigma_0 + \delta\overline{\sigma} \pm \frac{1}{2}\Delta\delta\sigma$ (and likewise for the pions), we obtain:

$$\left.\frac{\delta S_{cl}[\sigma,\vec{\pi}]}{\delta(\Delta\delta\sigma)}\right|_{\substack{\Delta\delta\sigma=\Delta\sigma_0=0\\ \Delta\delta\vec{\pi}=\Delta\vec{\pi}_0=0}} = \frac{\delta S_{QM}[\overline{\sigma}_0,\overline{\pi}_{0,j}\ (j=1,2,3)]}{\delta(\overline{\sigma}_0)} \tag{4.39}$$

$$\left.\frac{\delta S_{cl}[\sigma,\vec{\pi}]}{\delta(\Delta\delta\pi_k)}\right|_{\substack{\Delta\delta\sigma=\Delta\sigma_0=0\\ \Delta\delta\vec{\pi}=\Delta\vec{\pi}_0=0}} = \frac{\delta S_{QM}[\overline{\sigma}_0,\overline{\pi}_{0,j}\ (j=1,2,3)]}{\delta(\overline{\pi}_{0,k})} \qquad (k=1,2,3) \tag{4.40}$$

where we have already applied a further approximation which causes the fluctuating fields $\delta\overline{\sigma}$, $\delta\overline{\pi}_j$ (j=1,2,3) to vanish from the above expressions. This approximation will be introduced during the computation of the damping kernel later on (see equation (4.74)).

From now on we are always dealing with expressions in which only the meson center variables appear. Therefore, we can savely drop the bar in the notation and write e.g. σ_0, $\delta\sigma$ instead of $\overline{\sigma}_0$, $\delta\overline{\sigma}$ and so on.

Let us turn towards the computation of the $tr\ S^{++}$ terms in the equations of motion. These terms are of zeroth order in meson fluctuations, since we found the solution to S_{th} by treating σ_0, $\vec{\pi}_0$ as quasi mean fields. Thus, the thermal propagator is approximately translation invariant, $S_{th}(x,y) \approx S_{th}(x-y)$. However, this is indeed not an exact relation which is especially noticeable in the case of $S_{th}(x,x) \approx S_{th}(0)$ which still carries an implicit x-dependence through $\sigma_0(x)$, $\vec{\pi}_0(x)$. Bearing this in mind and neglecting the propagator's vacuum contribution, we find using

$$\delta(p^2 - m_q^2) = \delta((p^0)^2 - (\vec{p}^2 + m_q^2)) = \frac{1}{2E_p}\left[\delta(p^0 - E_p) + \delta(p^0 + E_p)\right] \tag{4.41}$$

and the eplicit form of S_{th}^{++}, i.e. equation (4.15):

$$\begin{aligned} g\,tr\,S_{th}^{++}(x,x) &\approx g\,tr\int\frac{d^4p}{(2\pi)^4}S_{th}^{++}(p) \\ &= -2\pi g\int\frac{d^4p}{(2\pi)^4}tr\left(\not{p}+g(\sigma_0-i\gamma_5\vec{\tau}\vec{\pi}_0)\right)n_F(|p^0|)\delta(p^2-m_q^2) \\ &= -2n_q g^2\sigma_0\int\frac{d^3p}{(2\pi)^3}\frac{n_F(E_p)}{E_p} \\ &= -g\rho_s(x) \end{aligned} \tag{4.42}$$

Here, $n_q = 12$ is the quark degeneracy factor and $E_p = \sqrt{\vec{p}^2 + m_q^2}$ the quark energy with dynamic mass $m_q = g\sqrt{\sigma_0^2 + \vec{\pi}_0^2}$. In the last line of equation (4.42) we have restored the x-dependency omitted in the intermediate steps. Further, we identify the one-loop scalar density ρ_s. Equation (4.42) is in agreement with [NLHB11, Nah11].

Similarly to equation (4.42), for the j-th pion component, using $\gamma_5\gamma_5 = \mathbb{1}$ and $tr(\tau_i\tau_j) = d_{flavor}\delta_{ij}$, we arrive at:

$$\begin{aligned} ig\,tr\,\left(\gamma_5\tau_j S_{th}^{++}(x,x)\right) &\approx -2n_q g^2\pi_{0,j}\int\frac{d^3p}{(2\pi)^3}\frac{n_F(E_p)}{E_p} \\ &= -g\rho_{ps,j}(x) \end{aligned} \tag{4.43}$$

i.e. the according component of the one-loop pseudo-scalar density, $\vec{\rho}_{ps}$.

In the following, it will be convenient to group the mesons into the four vector $\vec{\varphi} = (\sigma, \vec{\pi})$. In this sense, we collect the scalar and pseudo-scalar densities, into the four vector $\vec{\rho}$ with components:

$$\rho_a(x) = 2n_q g\varphi_a(x)\int\frac{d^3p}{(2\pi)^3}\frac{n_F\left(E_p\right)}{E_p} \tag{4.44}$$

4.1.2. The damping kernel

In order to evaluate the damping kernels $D_\sigma(x)$, $D_{\pi_j}(x)$ in equations (4.35), (4.36) we will first clean up our notation: we group the mesons into the four vector $\vec{\varphi} = (\sigma, \vec{\pi})$ with component index running from $a = 0$ (σ) to 3. Further, we will drop any index 0 in the mean fields and also omit the index th in the thermal quark propagator. Just like

the mesons, we can collect the damping kernels into a vector and write

$$D_a(x) = ig^2 \int d^4y\, \Theta(x^0 - y^0)\, \delta\varphi_b(y)\, \mathcal{M}_{ab}(x-y) \tag{4.45}$$

with summation over repeated indices. Hereby, we have defined $\mathcal{M}_{ab}(x-y)$, which is a matrix in meson flavor space. Its components read $(j,k = 1,2,3)$:

$$\begin{aligned}
\mathcal{M}_{00}(x-y) &= tr\left(S^<(x-y)S^>(y-x) - S^>(x-y)S^<(y-x)\right) && (4.46)\\
\mathcal{M}_{0j}(x-y) &= tr\left(S^<(x-y)i\gamma_5\tau_j S^>(y-x) - S^>(x-y)i\gamma_5\tau_j S^<(y-x)\right) && (4.47)\\
\mathcal{M}_{j0}(x-y) &= tr\left(i\gamma_5\tau_j S^<(x-y)S^>(y-x) - i\gamma_5\tau_j S^>(x-y)S^<(y-x)\right) && (4.48)\\
\mathcal{M}_{jk}(x-y) &= tr\left(i\gamma_5\tau_j S^<(x-y)i\gamma_5\tau_k S^>(y-x)\right) \\
&\quad -tr\left(i\gamma_5\tau_j S^>(x-y)i\gamma_5\tau_k S^<(y-x)\right) && (4.49)
\end{aligned}$$

By neglecting the pion contributions, the only surviving component of $\mathcal{M}$ would be the 00 (i.e. $\sigma\sigma$) component, which is in agreement with [NLHB11, Nah11]. The Fourier transform of $\mathcal{M}$ is given by:

$$\mathcal{M}_{00}(k) = \int \frac{d^4p}{(2\pi)^4}\, tr\left(S^<(p+k)S^>(p) - S^>(p+k)S<(p)\right) \tag{4.50}$$

and likewise for the other components. Inserting the parts of the propagator relevant for the evaluation of the trace we have for the 00 component:

$$tr\left[\left(\not{p} + \not{k} + g\sigma - ig\gamma_5\vec{\tau}\vec{\pi}\right)\left(\not{p} + g\sigma - ig\gamma_5\vec{\tau}\vec{\pi}\right)\right] = 2\, n_q\left((p+k)p + g^2\sigma^2 - g^2\vec{\pi}^2\right) \tag{4.51}$$

The $0j$ and $j0$ components $(j = 1,2,3)$ evaluate to:

$$\begin{aligned}
& tr\left[\left(\not{p} + \not{k} + g\sigma - ig\gamma_5\vec{\tau}\vec{\pi}\right) i\gamma_5\tau_j \left(\not{p} + g\sigma - ig\gamma_5\vec{\tau}\vec{\pi}\right)\right] \\
= \;& tr\left[i\gamma_5\tau_j\left(\not{p} + \not{k} + g\sigma - ig\gamma_5\vec{\tau}\vec{\pi}\right)\left(\not{p} + g\sigma - ig\gamma_5\vec{\tau}\vec{\pi}\right)\right] = 4\, n_q\, g^2\sigma\pi_j \qquad (4.52)
\end{aligned}$$

and the jl $(j,l = 1,2,3)$ component is given by:

$$\begin{aligned}
& tr\left[i\gamma_5\tau_j\left(\not{p} + \not{k} + g\sigma - ig\gamma_5\vec{\tau}\vec{\pi}\right) i\gamma_5\tau_k \left(\not{p} + g\sigma - ig\gamma_5\vec{\tau}\vec{\pi}\right)\right] \\
= \;& 2\, n_q\left((p+k)p\,\delta_{jl} + 2g^2\pi_j\pi_l - g^2\,\vec{\varphi}^2\,\delta_{jl}\right) \qquad (4.53)
\end{aligned}$$

Obviously, the terms (4.51)-(4.53) can be collected into the single expression

$$A_{ab}(p,k) = 2\,n_q\left((p+k)p\,\delta_{ab} + 2g^2\varphi_a\varphi_b - m_q^2\,\delta_{ab}\right) \tag{4.54}$$

where we identified the dynamic quark mass $m_q = g\sqrt{\vec{\varphi}^2} = g\sqrt{\sigma^2+\vec{\pi}^2}$. We note, that in comparison to [NLHB11, Nah11], our $\sigma\sigma$ component A_{00} is altered by contributions from the pions. Only in the case of a vanishing pion mean field and thus especially in thermal equilibrium the quark mass reduces to $m_q = g\sigma$ and we recover for A_{00} the corresponding results of [NLHB11, Nah11]. However, since we allow for a nonzero pion mean field off equilibrium this corresponds to a rotation of the meson mean field vector $\vec{\varphi}$ away from the pure σ-direction. Thus, the σ field is no longer the longitudinal component of $\vec{\varphi}$. Only in the defining (thermal) ground state we have $\vec{\varphi} = (\sigma, \vec{0})$ due to the explicit symmetry breaking. Therefore, it is convenient to split all quantities in meson flavor space into longitudinal (L) and transversal (T) components with respect to the mean field vector. For this purpose, we introduce the projection operators

$$P^L_{ab} = \frac{\varphi_a\varphi_b}{\varphi^2} \tag{4.55}$$

$$P^T_{ab} = \delta_{ab} - \frac{\varphi_a\varphi_b}{\varphi^2} \tag{4.56}$$

and rewrite

$$A_{ab}(p,k) = A_L(p,k)P^L_{ab} + A_T(p,k)P^T_{ab} \tag{4.57}$$

with components:

$$A_L(p,k) = 2n_q(p+k)p + m_q^2 \tag{4.58}$$

$$A_T(p,k) = 2n_q(p+k)p - m_q^2 \tag{4.59}$$

and we can identify the longitudinal component $A_L(p,k)$ with the σ-component A_{00} in thermal equilibrium. It should be noted, that such splitting into longitudinal and transversal parts with respect to the mean field vector is most commonly used in $O(N)$ symmetric models with spontaneous symmetry breaking (see e.g. [Ber04, vHK02a]).

Including all parts of the thermal propagator, we find:

$$\begin{aligned}\mathcal{M}_{ab}(k) = \frac{1}{4\pi^2}\int d^4p\, A_{ab}(p,k)\,\delta\left((p+k)^2 - m_q^2\right)\,\delta\left(p^2 - m_q^2\right)\times \\ \times\Big\{\left(n_f(|p^0+k^0|) - \Theta(-p^0-k^0)\right)\left(n_f(|p^0|) - \Theta(p^0)\right) \\ -\left(n_f(|p^0+k^0|) - \Theta(p^0+k^0)\right)\left(n_f(|p^0|) - \Theta(-p^0)\right)\Big\}\end{aligned} \tag{4.60}$$

which can be split into longitudinal $\mathcal{M}_L$ and transversal $\mathcal{M}_T$ parts as well:

$$\mathcal{M}_{ab}(k) = \mathcal{M}_L(k)P^L_{ab} + \mathcal{M}_T(k)P^T_{ab} \tag{4.61}$$

Recalling the definition of the quark energy $E_p = \sqrt{\vec{p}^2 + m_q^2}$ (and likewise E_{p+k}) we can perform the p^0 integration and evaluate the theta functions. The result is:

$$\begin{aligned}\mathcal{M}_L(\omega,\vec{k}) = \frac{n_q}{8\pi^2}\int d^3p\,\frac{1}{E_pE_{p+k}}\Big\{\left[-E_p(E_p+E_{p+k}) - \vec{k}\vec{p} + 2m_q^2\right]\times \\ \times\Big(\delta(\omega - E_p - E_{p+k})\left[n_f(E_p)n_f(E_{p+k}) - (1-n_f(E_p))\,(1-n_f(E_{p+k}))\right] \\ +\delta(\omega + E_p + E_{p+k})\left[(1-n_f(E_p))\,(1-n_f(E_{p+k}) - n_f(E_p)n_f(E_{p+k}))\right]\Big) \\ +\left[-E_p(E_p-E_{p+k}) - \vec{k}\vec{p} + 2m_q^2\right]\times \\ \times\Big(\delta(\omega + E_p - E_{p+k})\left[n_f(E_p)\,(1-n_f(E_{p+k})) - (1-n_f(E_p))\,n_f(E_{p+k})\right] \\ +\delta(\omega - E_p + E_{p+k})\left[\,(1-n_f(E_p))\,n_f(E_{p+k}) - n_f(E_p)\,(1-n_f(E_{p+k}))\,\right]\Big)\Big\}\end{aligned} \tag{4.62}$$

For $\mathcal{M}_T$, replace:

$$\left[-E_p(E_p \pm E_{p+k}) - \vec{k}\vec{p} + 2m_q^2\right] \longrightarrow \left[-E_p(E_p \pm E_{p+k}) - \vec{k}\vec{p}\right] \tag{4.63}$$

Here, we have followed [NLHB11, Nah11] and chosen the notation $k^0 = \omega$ as well as sorted the the various terms according to their energy balance. The reason for this is that we more easily recognize the phyical meaning of the different terms. Since the structure for longitudinal and transversal components of $\mathcal{M}$ is exactly the same as in

[NLHB11, Nah11], we may closely follow the discussion in the cited references which is in turn based on [Wel83]: While $n_f(E_p)n_f(E_{p+k})$ equals the probability of a quark-antiquark pair to decay into a certain meson mode, the decay of a meson mode into a quark-antiquark pair comes with the probability $(1 - n_f(E_p))(1 - n_f(E_{p+k}))$. The decay of a quark into a meson and a quark (and likewise for antiquark decay) as well as the respective inverse processes come with terms like $n_f(E_p)(1 - n_f(E_{p+k}))$. Each delta function in $\mathcal{M}$ is accompanied by the difference of the probabilities of two mutually inverse processes, i.e. it can be viewed as a gain minus a loss term for each type of process. For each delta function, the loss and gain terms fulfill the universal relation

$$\frac{\Gamma_{loss}}{\Gamma_{gain}} = exp\left(\frac{\omega}{T}\right) \tag{4.64}$$

which is typical for the interaction of test particles with a heat bath in equilibrium [Wel83, NLHB11].
For our further calculations it is important to note that from the structure of $\mathcal{M}_{ab}(\omega, \vec{k})$ in its explicit form (4.61)-(4.63) we can infer that substituting $\omega \longrightarrow -\omega$ simply leads to a pairwise swapping of the delta functions and thus to an overall change of sign:

$$\mathcal{M}_{ab}(-\omega, \vec{k}) = -\mathcal{M}_{ab}(\omega, \vec{k}) \tag{4.65}$$

This antisymmetry in ω will be useful in evaluating the damping kernel. We write:

$$\begin{aligned} D_a(x) &= ig^2 \int d^4y\, \Theta(x^0 - y^0)\delta\varphi_b(y)\mathcal{M}_{ab}(x - y) \\ &= ig^2 \int d^4y\, \Theta(x^0 - y^0)\delta\varphi_b(y) \int \frac{d^4k}{(2\pi)^4} exp(-ik(x - y))\mathcal{M}_{ab}(\omega, \vec{k}) \end{aligned} \tag{4.66}$$

Performing the spatial y integration leads to the spatial Fourier transform of the meson fluctuations:

$$\delta\varphi_b(y^0, \vec{k}) = \int d^3y\, exp(-i\vec{k}\vec{y})\, \delta\varphi_b(y) \tag{4.67}$$

Additionaly, we introduce the time variable $t' = y^0 - x^0$ and denote $x^0 = t$. Then, we change the time integration variable from $y^0 = t - t'$ to t' which allows for a simple evaluation of the Theta function and yields for the damping kernel (see also [NLHB11,

Nah11] for $a = b = 0$):

$$D_a(x) = ig^2 \int \frac{d^3k}{(2\pi)^3}\, exp(i\vec{k}\vec{x}) \int_0^\infty dt' \int \frac{d\omega}{2\pi}\, exp(-i\omega t')\, \mathcal{M}_{ab}(\omega, \vec{k})\, \delta\varphi_b(t - t', \vec{k}) \quad (4.68)$$

It is $t - t' < t = x^0$ within the above integration region and thus at each point in time fluctuations from the past contribute to the damping kernel and therefore to the evolution of the meson fields themselves. The trouble is, that for every infinitesimal step in time $t \to t + dt$ not just some "local" past but the full past of the field evolution is contributing to the present evolution. This means that in principle we have to keep track of all field configurations $\varphi_a(t, \vec{k})$ from the very start of the evolution at $t = t_0$. For this reason, numerical studies including the full history of the fields become very memory and time consuming with increasing number of time steps. This is a known problem, especially for self-consistent frameworks as e.g. the nonequilibrium 2PI effective action formalism. To simplify our computations we approximate the memory effects so as to get an analytic expression for the damping kernel. For this purpose, we choose a linear harmonic approximation to the meson fields. But first, let us reinstate the index 0 for the mean fields. The full field is then given by:

$$\varphi_a = (P^L_{ab} + P^T_{ab})(\varphi_{0,b} + \delta\varphi_b) = \varphi_{0,a} + P^L_{ab}\delta\varphi_b + P^T_{ab}\delta\varphi_b \quad (4.69)$$

(Note, that since the the mean field $\varphi_{0,a}$ defines the longitudinal direction, it does not have a transversal part.) Assume now a linear harmonic approximation with different frequencies for the longitudinal and transversal parts:

$$P^L_{ab}\varphi_b(t - t', \vec{k}) = a^L_a(t)cos(E^L_k t') + b^L_a(t)sin(E^L_k t') \quad (4.70)$$

$$P^T_{ab}\varphi_b(t - t', \vec{k}) = a^T_a(t)cos(E^T_k t') + b^T_a(t)sin(E^T_k t') \quad (4.71)$$

Since $(P^L)^2 = P^L$ and $(P^T)^2 = P^T$ as well as $P^L P^T = P^T P^L = 0$ it follows that the coefficients obey:

$$P^L_{ab}a^L_b(t) = a^L_a(t) \qquad P^T_{ab}a^L_b(t) = 0 \quad (4.72)$$

$$P^T_{ab}b^T_b(t) = b^T_a(t) \qquad P^L_{ab}b^T_b(t) = 0 \quad (4.73)$$

In the above ansatz, the coefficients $a_a^L(t)$, $a_a^T(t)$, $b_a^L(t)$, $b_a^T(t)$ are fixed by the constraints:

$$\varphi_a(t-t',\vec{k})\Big|_{t'=0} = \varphi_{0,a}(t,\vec{k}) \tag{4.74}$$

$$\frac{\partial\varphi_a(t-t',\vec{k})}{\partial t'}\Big|_{t'=0} = -\frac{\partial\varphi_a(t,\vec{k})}{\partial t} \tag{4.75}$$

The first requirement leads to

$$a_a^L(t) + a_a^T(t) = \varphi_{0,a}(t,\vec{k}) \tag{4.76}$$

which is purely longitudinal and thus:

$$a_a^L(t) = \varphi_{0,a} \qquad a_a^T(t) = 0 \tag{4.77}$$

The second constraint corresponds to

$$b_a^L(t)E_k^L + b_a^T(t)E_k^T = -\partial_t\varphi_a(t,\vec{k}) \tag{4.78}$$

After multiplying this line with P^L respectively P^T one finds:

$$b_a^L(t) = -\frac{1}{E_k^L}P_{ab}^L\partial_t\varphi_b(t,\vec{k}) \tag{4.79}$$

$$b_a^T(t) = -\frac{1}{E_k^T}P_{ab}^T\partial_t\varphi_b(t,\vec{k}) \tag{4.80}$$

Applying again (4.74), we arrive at the expression

$$\begin{aligned}\varphi_a(t-t',\vec{k}) = \varphi_{0,a}(t,\vec{k})cos(E_k^Lt') - \frac{1}{E_k^L}sin(E_k^Lt')P_{ab}^L\partial_t\varphi_{0,b}(t,\vec{k}) \\ -\frac{1}{E_k^T}sin(E_k^Tt')P_{ab}^T\partial_t\varphi_{0,b}(t,\vec{k})\end{aligned} \tag{4.81}$$

for the full field. Comparing this result to equation (4.69), we see that the fluctuations

are

$$P^L_{ab}\delta\varphi_b(t-t',\vec{k}) = \Big(\varphi_{0,a}(t,\vec{k})cos(E^L_k t') - \varphi_{0,a}(t-t',\vec{k})\Big) - \frac{1}{E^L_k}sin(E^L_k t')P^L_{ab}\partial_t\varphi_{0,b}(t,\vec{k}) \tag{4.82}$$

$$P^T_{ab}\delta\varphi_b(t-t',\vec{k}) = -\frac{1}{E^T_k}sin(E^T_k t')P^T_{ab}\partial_t\varphi_{0,b}(t,\vec{k}) \tag{4.83}$$

If we expand the dynamical quark mass $m_q = g\sqrt{\sigma^2+\vec{\pi}^2}$ in fluctuations, we see that the first term in equation (4.82) causes a correction at lowest order ($\sim\varphi_0$). This correction is assumed to be small [NLHB11, Nah11], i.e.:

$$\varphi_{0,a}(t,\vec{k})cos(E^L_k t') - \varphi_{0,a}(t-t',\vec{k}) \approx 0 \tag{4.84}$$

and so the remaining part of the fluctuations is the term proportional to the time-derivative of the mean field itself. From now on, we will again omit the index 0 for the mean fields. With the approximated fluctuations, the damping kernel becomes:

$$\begin{aligned} D_a(x) = & -ig^2\int\frac{d^3k}{(2\pi)^3}\frac{1}{E^L_k}exp(i\vec{k}\vec{x})P^L_{ab}\partial_t\varphi_b(t,\vec{k})\times \\ & \times\int_0^\infty dt'\int\frac{d\omega}{2\pi}\,exp(-i\omega t')\mathcal{M}_L(\omega,\vec{k})\,sin(E^L_k t') \\ & -ig^2\int\frac{d^3k}{(2\pi)^3}\frac{1}{E^T_k}exp(i\vec{k}\vec{x})P^T_{ab}\partial_t\varphi_b(t,\vec{k})\times \\ & \times\int_0^\infty dt'\int\frac{d\omega}{2\pi}\,exp(-i\omega t')\mathcal{M}_T(\omega,\vec{k})\,sin(E^T_k t') \end{aligned} \tag{4.85}$$

Using

$$sin(E_k t') = -\frac{i}{2}\left(exp(iE_k t') - exp(-iE_k t')\right) \tag{4.86}$$

we perform the integrations in the second line (and analogously in the fourth line) of

equation (4.85):

$$
\begin{aligned}
-\frac{i}{2}\int\frac{d\omega}{2\pi}\int_0^\infty dt'\ \left\{exp\left(i(E_k^L-\omega)t'\right)-exp\left(-i(E_k^L+\omega)t'\right)\right\}\mathcal{M}_L(\omega,\vec{k})\\
=-\frac{i}{2}\int\frac{d\omega}{2\pi}\left\{\int_{-\infty}^\infty dt'\,exp\left(i(E_k^L-\omega)t'\right)-\int_{-\infty}^0 dt'\,exp\left(i(E_k^L-\omega)t'\right)\right.\\
\left.+\int_0^{-\infty}dt' exp\left(i(E_k^L+\omega)t'\right)\right\}\mathcal{M}_L(\omega,\vec{k})\qquad(4.87)\\
=-\frac{i}{2}\int\frac{d\omega}{2\pi}\mathcal{M}_L(\omega,\vec{k})\left\{2\pi\,\delta(\omega-E_k^L)+\int_0^{-\infty}dt'\,exp\left(i(E_k^L-\omega)t'\right)\right.\\
\left.-\int_0^{-\infty}dt' exp\left(i(E_k^L-\omega)t'\right)\right\}
\end{aligned}
$$

where in the first step we "added a zero" to the first term and in the second term we changed the integration variable from t' to $-t'$. Then, in the second step we evaluated the first t' integral and swapped integration limits in the second term. For the last term we substituted $\omega\to-\omega$ and used the antisymmetry property $\mathcal{M}_{ab}(-\omega,\vec{k})=-\mathcal{M}_{ab}(\omega,\vec{k})$. The last two terms in the last line of equation (4.87) cancel and the omega integration can easily be carried out. Thus, we arrie at:

$$
D_a(x)=-\frac{1}{2}g^2\int\frac{d^3k}{(2\pi)^3}\,exp(i\vec{k}\vec{x})\left(\frac{1}{E_k^L}\,\mathcal{M}_L(E_k^L,\vec{k})\,P_{ab}^L+\frac{1}{E_k^T}\,\mathcal{M}_T(E_k^T,\vec{k})\,P_{ab}^T\right)\partial_t\varphi_b(t,\vec{k})\qquad(4.88)
$$

which is in agreement with [NLHB11, Nah11] for the longitudinal component. Our interest lies in the behaviour of the long range oscillations of the meson fields. Therefore, we evaluate $\mathcal{M}_{ab}$ within a zero mode approximation, i.e. we assume $\mathcal{M}_{ab}(\omega,\vec{k})\approx\mathcal{M}_{ab}(\omega,\vec{0})$ [NLHB11, Nah11]. With $\omega=E_k^{L/T}=\sqrt{m_{L/T}^2+\vec{k}^2}$ this corresponds to the replacement $\mathcal{M}_{L/T}(E_k^{L/T},\vec{k})\to\mathcal{M}_{L/T}(m_{L/T},\vec{0})$ in equation (4.88). Further, due to the zero mode approximation, in equation (4.62) only the term including

$$
\delta(\omega-E_p-E_{p+k})\longrightarrow\delta(\omega-2E_p)\qquad(4.89)
$$

survives, while the other delta functions all equate to zero. We obtain:

$$\begin{aligned}\mathcal{M}_L(m_L,\vec{0}) &= \frac{n_q}{\pi}\int_0^\infty dp\,\frac{p^2}{E_p^2}\left(-E_p^2+m_q^2\right)\left(2n_f(E_p)-1\right)\delta(m_L-2E_p)\\ &= -\frac{n_q}{\pi\,m_L}\left(\frac{m_L^2}{4}-m_q^2\right)^{3/2}\left(2n_f(\frac{m_L}{2})-1\right) \qquad (4.90)\end{aligned}$$

$$\begin{aligned}\mathcal{M}_T(m_T,\vec{0}) &= -\frac{n_q}{\pi}\int_0^\infty dp\,p^2\left(2n_f(E_p)-1\right)\delta(m_T-2E_p)\\ &= -\frac{n_q}{4\pi}\,m_T\,\left(\frac{m_T^2}{4}-m_q^2\right)^{1/2}\left(2n_f(\frac{m_T}{2})-1\right) \qquad (4.91)\end{aligned}$$

for $m_{L/T} > 2m_q$ and $\mathcal{M}_{L/T} = 0$ otherwise. We apply the same approximation, $E_k^{L/T} \approx m_{L/T}$, also to the damping kernel, which allows us to perform the integration over spatial momenta:

$$\begin{aligned}D_a(x) &\approx -\frac{1}{2}g^2\left(\frac{1}{m_L}\mathcal{M}_L(m_L,\vec{0})P_{ab}^L+\frac{1}{m_L}\mathcal{M}_T(m_T,\vec{0})P_{ab}^T\right)\left(\int\frac{d^3k}{(2\pi)^3}\,exp(i\vec{k}\vec{x})\,\partial_t\varphi_b(t,\vec{k})\right)\\ &= -\eta_{ab}\,\partial_t\varphi_b(x) = -\left(\eta_L P_{ab}^L+\eta_T P_{ab}^T\right)\partial_t\varphi_b(x) \qquad (4.92)\end{aligned}$$

with the components of the damping coefficient η_{ab} given by:

$$\eta_L = g^2\frac{n_q}{2\pi\,m_L^2}\left(\frac{m_L^2}{4}-m_q^2\right)^{3/2}\left(1-2n_f\left(\frac{m_L}{2}\right)\right) \qquad (4.93)$$

$$\eta_T = g^2\frac{n_q}{8\pi}\left(\frac{m_T^2}{4}-m_q^2\right)^{1/2}\left(1-2n_f\left(\frac{m_T}{2}\right)\right) \qquad (4.94)$$

In comparison to [NLHB11, Nah11] we find an additional factor 1/2 in the longitudinal component of the damping coefficien, η_T. This difference is independent of the one discussed after equation (4.32). Instead, we assume that in equation (54) of [NLHB11] (respectively equation (5.50) of [Nah11]) a factor of 1/2 is missing in the derivation of $\mathcal{M}(\omega,\vec{k})$ which then remains absent in η.

4.1.3. The noise kernel

The noise kernel is defined as:

$$\mathcal{N}_{ab}(x-y) = -\frac{1}{2}g^2\, tr\left(\chi_a S^{<}_{th}(x-y)\chi_b S^{>}_{th}(y-x) + \chi_a S^{>}_{th}(x-y)\chi_b S^{<}_{th}(y-x)\right) \quad (4.95)$$

with $\vec{\chi} = (\mathbb{1}, i\gamma_5\vec{\tau})$. Just as for the damping kernel, we take the Fourier transform of $\mathcal{N}_{ab}(x-y)$. Since the traces are the same as calculated before in equation (4.54), we find:

$$\begin{aligned}
\mathcal{N}_{ab}(\omega,\vec{k}) = -\frac{n_q}{16\pi^2}g^2\int d^3p\,\frac{1}{E_pE_{p+k}}\times \\
\times\Bigg\{\left(\left[-E_p(E_p+E_{p+k}) - \vec{k}\vec{p}\right]\delta_{ab} + 2g^2\varphi_a\varphi_b\right)\times \\
\times\Big(\delta(\omega - E_p - E_{p+k})\left[n_f(E_p)n_f(E_{p+k}) + (1-n_f(E_p))\,(1-n_f(E_{p+k}))\right] \\
+\delta(\omega + E_p + E_{p+k})\left[(1-n_f(E_p))\,(1-n_f(E_{p+k}) + n_f(E_p)n_f(E_{p+k}))\right]\Big) \\
+\left(\left[E_p(-E_p+E_{p+k}) - \vec{k}\vec{p}\right]\delta_{ab} + 2g^2\varphi_a\varphi_b\right)\times \\
\times\Big(\delta(\omega + E_p - E_{p+k})\left[n_f(E_p)\,(1-n_f(E_{p+k})) + (1-n_f(E_p))\,n_f(E_{p+k})\right] \\
+\delta(\omega - E_p + E_{p+k})\left[\,(1-n_f(E_p))\,n_f(E_{p+k}) + n_f(E_p)\,(1-n_f(E_{p+k}))\,\right]\Big)\Bigg\}
\end{aligned} \quad (4.96)$$

The noise kernel equals the variance of the stochastic fields:

$$\mathcal{N}_{ab}(x-y) = \langle\xi_a(t,\vec{x})\xi_b(t',\vec{x}')\rangle_\xi \quad (4.97)$$

with the expectation value $\langle . \rangle_\xi$ defined with respect to the Gaussian distribution of the ξ field [NLHB11, Nah11]. We approximate the noise kernel in the same way as we approximated the damping kernel, i.e. we project it onto its longitudinal and transversal components with respect to the mean field,

$$\mathcal{N}_{ab} = \mathcal{N}_L P^L_{ab} + \mathcal{N}_T P^T_{ab} \quad (4.98)$$

and assume for the Fourier transform $\mathcal{N}_{L/T}(\omega, \vec{k})$:

$$\mathcal{N}_{L/T}(\omega, \vec{k}) \approx \mathcal{N}_{L/T}(m_{L/T}, \vec{0}) \tag{4.99}$$

where m_L, m_T are the masses of the longitudinal and transversal meson mean field modes. Then we find ($k^0 = \omega$):

$$\begin{aligned}
\langle \xi_a(t,\vec{x})\xi_b(t',\vec{x'})\rangle_\xi &= \int \frac{d^4k}{(2\pi)^4}\mathcal{N}_{ab}(\omega,\vec{k})\; exp(-i\omega(t-t'))\; exp(i\vec{k}(\vec{x}-\vec{x}')) \\
&\approx \int \frac{d\omega}{2\pi}\left(\mathcal{N}_L(m_L,\vec{0})P^L_{ab} + \mathcal{N}_T(m_T,\vec{0})P^T_{ab}\right)\; exp(-i\omega(t-t'))\;\delta(\vec{x}-\vec{x}') \\
&= \left(\mathcal{N}_L(m_L,\vec{0})P^L_{ab} + \mathcal{N}_T(m_T,\vec{0})P^T_{ab}\right)\delta(t-t')\delta(\vec{x}-\vec{x}')
\end{aligned} \tag{4.100}$$

In this approximation, again only one of the delta functions in equation (4.96) survives. The corresponding factor with the fermion distribution functions can be rewritten as [NLHB11, Nah11]:

$$2n_f(E_p) - 2n_f(E_p) + 1 = \big(1 - 2n_f(E_p)\big)\; coth\left(\frac{E_p}{T}\right) \tag{4.101}$$

which allows to express $\mathcal{N}_{L/T}$ via $\eta_{L/T}$:

$$\mathcal{N}_L(m_L,\vec{0}) = \frac{1}{2}g^2\mathcal{M}_L(m_L,\vec{0})\; coth\left(\frac{m_L}{2T}\right) = m_L\;\eta_L\; coth\left(\frac{m_L}{2T}\right) \tag{4.102}$$

$$\mathcal{N}_T(m_T,\vec{0}) = \frac{1}{2}g^2\mathcal{M}_T(m_T,\vec{0})\; coth\left(\frac{m_T}{2T}\right) = m_T\;\eta_T\; coth\left(\frac{m_T}{2T}\right) \tag{4.103}$$

and thus, we finally obtain for the correlation of the noise fields:

$$\langle \xi_a(t,\vec{x})\xi_b(t',\vec{x}')\rangle_\xi = \left(m_L\;\eta_L\; coth\left(\frac{m_L}{2T}\right)P^L_{ab} + m_T\;\eta_T\; coth\left(\frac{m_T}{2T}\right)P^T_{ab}\right)\delta(t-t')\;\delta(\vec{x}-\vec{x}') \tag{4.104}$$

For vanishing pions we obtain for the correlation of the σ component of the noise fields, i.e. $a = b = 0$, structurally the same result as in [NLHB11, Nah11]. The only difference is the factor of $1/2$ hidden in η which we adressed earlier.

Finally, we have determined all quantities necessary for evolving the chiral mean fields

φ_a with the semi-classical Langevin equation,

$$\partial_\mu \partial^\mu \varphi_a + g\rho_a + \frac{\partial V_{cl}}{\partial \varphi_a} + \eta_{ab}\partial_t \varphi_b = \xi_a \tag{4.105}$$

except for the quark-meson coupling constant g. The particular choice of g determines the order of the phase transition in the model and will be fixed in the next chapters.

4.2. Including the meson propagator

In this section, we will derive the damping and noise kernels originating from a non-vanishing meson propagator. From the influence functional perspective, this corresponds to splitting the meson fields into two parts, containing only the soft and hard modes respectively [Ris98]. We begin again by employing an effective action ansatz and eventually identify the damping and noise kernels as motivated by the influence functional approach.

At one-loop mean field level, for $\Gamma_2 = 0$, the meson propagator equals the free propagator, given by:

$$iG^{-1}_{ab}(x,y) = -([\Box_x + \frac{\lambda}{N}\varphi_c\varphi^c - v^2]\delta_{ab} - 2\frac{\lambda}{N}\varphi_a\varphi_b)\delta(x-y) \tag{4.106}$$

Even in thermal equilibrium its dynamic mass

$$M^2_{ab} = \frac{\lambda}{N}(\vec{\varphi}^2\delta_{ab} + 2\varphi_a\varphi_b - v^2\delta_{ab}) \tag{4.107}$$

becomes tachyonic in the symmetric phase as well as near the phase transition. This is a known problem for the thermal field theory of O(N) symmetric scalar fields. In order to obtain physical masses, we need to go beyond the one loop approximation. One way to do this is to choose the simplest nontrivial truncation of Γ_2:

Γ_2 =  = 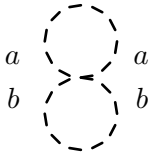 + 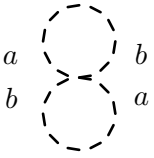

where we have drawn the two distinct diagrams coming from the placement of the meson fields at the vertex. The first diagram has a combinatorical factor of one and the second

carries a factor two. The vertex adds a factor of $\left(-i\frac{\lambda}{4N}\right)$ and the definition of the effective action introduces another overall $(-i)$:

$$\Gamma_2 = -\frac{\lambda}{4N}\int_{\mathcal{C}} d^4x\Big(G_{aa}(x,x)G_{bb}(x,x) + 2G_{ab}(x,x)G_{ba}(x,x)\Big) \tag{4.108}$$

Therefore, the meson self energy is given by:

$$\Sigma_{ab}(x,y) = 2i\frac{\delta\Gamma_2}{\delta G_{ab}(x,y)} = -i\frac{\lambda}{N}(G_{cc}(x,x)\delta_{ab} + 2G_{ab}(x,x))\delta(x-y) \tag{4.109}$$

and so the equation of motion for the meson propagator,

$$iG_0^{-1}G - i\Sigma G = i \tag{4.110}$$

takes the form:

$$\left[-(\Box_x + \frac{\lambda}{N}\vec{\varphi}^{\,2} - v^2)\delta_{ab} - \frac{2\lambda}{N}\varphi_a\varphi_b - \frac{\lambda}{N}(G_{cc}(x,x)\delta_{ab} + 2G_{ab}(x,x))\right] G_{bc}(x,y) = i\delta_{ac}\delta(x-y) \tag{4.111}$$

Before we continue, it is again useful to introduce longitudinal and transversal meson propagators:

$$G_{ab} = P^L_{ab}G_L + P^T_{ab}G_T \tag{4.112}$$

with projection operators onto longitudinal (respectively transversal) parts with respect to the mean-field. Then, equation (4.111) splits into two coupled equations of motion:

$$\begin{aligned}\left\{-(\Box_x + \frac{\lambda}{N}(3\vec{\varphi}^{\,2} - v^2)) - \frac{\lambda}{N}(3G_L(x,x) + (N-1)G_T(x,x))\right\} G_L(x,y) &= i\delta(x-y)\\ \left\{-(\Box_x + \frac{\lambda}{N}(\vec{\varphi}^{\,2} - v^2)) - \frac{\lambda}{N}(G_L(x,x) + (N+1)G_T(x,x))\right\} G_T(x,y) &= i\delta(x-y)\end{aligned} \tag{4.113}$$

The masses of the self-consistent propagators fulfill the gap equations

$$\begin{aligned}M_L^2 &= \frac{\lambda}{N}(3\vec{\varphi}^{\,2} - v^2) + \frac{\lambda}{N}(3G_L(x,x) + (N-1)G_T(x,x))\\ M_T^2 &= \frac{\lambda}{N}(\vec{\varphi}^{\,2} - v^2) + \frac{\lambda}{N}(G_L(x,x) + (N+1)G_T(x,x))\end{aligned} \tag{4.114}$$

which need to be solved simultaneously for given mean fields $\vec{\varphi}$. With equations (4.112), (4.114) the meson equations of motion read (without quark contributions for now):

$$\begin{aligned}\left[\Box_x + \frac{\lambda}{N}(\vec{\varphi}^{\,2} - v^2) + \frac{\lambda}{N}(3G_L(x,x) + (N-1)G_T(x,x))\right]\varphi_a - h\delta_{a,0} = 0 \\ \iff \quad \left[\Box_x + M_L^2 - 2\frac{\lambda}{N}\vec{\varphi}^{\,2}\right]\varphi_a - h\delta_{a,0} = 0\end{aligned} \tag{4.115}$$

As in the derivations from the previous sections, we split the mean field into a slowly varying part $\vec{\varphi}_0$ and a fluctuation part $\delta\vec{\varphi}$ and expand the propagator in fluctuations:

$$\varphi_a = \varphi_{0,a} + \delta\varphi_a \tag{4.116}$$

$$G = (G_{L,th} + \delta G_L + \delta^2 G_L)P^L + (G_{T,th} + \delta G_T + \delta^2 G_T)P^T \tag{4.117}$$

However, we additionally approximate $\Gamma_2 \approx \Gamma_2[\vec{\varphi}_0, G_{th}(\vec{\varphi}_0)]$ and therefore the self energy as

$$\Sigma_{ab}(x,y) \approx -i\frac{\lambda}{N}(G_{th,cc}(x,x)\delta_{ab} + 2G_{th,ab}(x,x))\delta_{\mathcal{C}}(x-y) \tag{4.118}$$

i.e., we consider only the lowest order contribution in fluctuations. The reason is, that without this assumption, we would have to solve coupled gap equations at each order in fluctuations. However, the solutions would then contain contributions from the meson fluctuations implicit to the solutions, i.e. hidden in the numerical values of the propagator masses. Thus, we could no longer find analytic expressions for the damping coefficients and noise correlators. Instead, we would have to think about how to construct observables for comparison and how to extract them from the numerical studies. With our approximation however, we only need to solve gap equations at lowest order and can build up the higher order corrections via the Green's function method which allows to derive damping and noise kernels analogously to the previous sections. At lowest order, we have to solve:

$$\left(\Box_x + M_{L/T}^2(x)\right) G_{L/T,th}(x,y) = -i\delta_{\mathcal{C}}(x-y) \tag{4.119}$$

where M_L, M_T fulfill equations (4.114) with $\vec{\varphi}_0$, $G_{L,th}$, $G_{T,th}$. We require again that the splitting, equation (4.116), ensures a weak x-dependence of $\vec{\varphi}_0$ and thus of $M_{L/T}$ in comparison to the meson propagator. Therefore, the solution to equation (4.119) on the

real time contour is approximately given by:

$$G^{++}_{L/T,th}(p) = \frac{i}{p^2 - M^2_{L/T} + i\epsilon} + 2\pi\, n_B(|p^0|)\, \delta(p^2 - M^2_{L/T}) \tag{4.120}$$

$$G^{--}_{L/T,th}(p) = \frac{-i}{p^2 - M^2_{L/T} - i\epsilon} + 2\pi\, n_B(|p^0|)\, \delta(p^2 - M^2_{L/T}) \tag{4.121}$$

$$G^{+-}_{L/T,th}(p) = 2\pi \left(n_B(|p^0|) + \Theta(-p^0)\right)\, \delta(p^2 - M^2_{L/T}) \tag{4.122}$$

$$G^{-+}_{L/T,th}(p) = 2\pi \left(n_B(|p^0|) + \Theta(p^0)\right)\, \delta(p^2 - M^2_{L/T}) \tag{4.123}$$

with suppressed (weak) spacetime dependence of $M_{L/T}$. Due to (4.118), the corrections to the thermal propagators obey:

$$\mathcal{O}(\delta^1): \quad -\left(\Box_x + M^2_{L/T}(x)\right) \delta G_{L/T}(x,y) = \tfrac{2\lambda\alpha_{L/T}}{N} \varphi_{0,a}(x)\delta\varphi_a(x) G_{L/T,th}(x,y) \tag{4.124}$$

$$\mathcal{O}(\delta^2): \quad -\left(\Box_x + M^2_{L/T}(x)\right) \delta^2 G_{L/T}(x,y) = \tfrac{2\lambda\alpha_{L/T}}{N} \varphi_{0,a}(x)\delta\varphi_a(x)\delta G_{L/T}(x,y) + \tfrac{\lambda\alpha_{L/T}}{N} \delta\varphi_a(x)\delta\varphi_a(x) G_{L/T,th}(x,y) \tag{4.125}$$

with $\alpha_L = 3$ and $\alpha_T = 1$. Suppressing the indices L, T, th and 0, the solutions read:

$$\delta G(x,y) = -i\frac{2\alpha\lambda}{N} \int_{\mathcal{C}} d^4z\, G(x,z)\varphi_a(z)\delta\varphi_a(z) G(z,y) \tag{4.126}$$

$$\delta^2 G(x,y) = -\frac{4\alpha^2\lambda^2}{N^2} \int_{\mathcal{C}} d^4z\, d^4z'\, G(x,z)\varphi_a(z)\delta\varphi_a(z) G(z,z')\varphi_b(z')\delta\varphi_b(z') G(z',y) - \frac{i\alpha\lambda}{N} \int_{\mathcal{C}} d^4z\, G(x,z)\delta\varphi_a(z)\delta\varphi_a(z) G(z,y) \tag{4.127}$$

Now we can turn towards an expansion of the effective action in powers of fluctuations. In the current approximation,

$$\frac{i}{2} Tr(G_0^{-1} G) + \Gamma_2 \tag{4.128}$$

contains terms at various orders in fluctuations. At $\mathcal{O}(\delta^1)$ it provides corrections to the mean field equation of motion which are inconsistent with our current approximations. This is a direct consequence of our approach, sacrificing the self-consistenty of the 2PI effective action ansatz beyond the level of constant mean field in order to extract damping and noise kernels for the off equilibrium dynamics. We will therefore neglect (4.128) for

the mean field equation of motion. To the pressure in thermal equilibrium, however (4.128) provides consistent contributions at $\mathcal{O}(\delta^0)$ which have to be taken into account (see chapter 6.1). For the n-th power of G it can be proved by induction that

$$G^n = P^L G_L^n + P^T G_T^n \tag{4.129}$$

and thus by viewing the logarithm as a power series:

$$\begin{aligned} Tr\, ln\, G &= Tr\, P^L\, ln\, G_L + Tr\, P^T\, ln\, G_T \\ &= Tr\, ln\, G_L + (N-1)\, Tr\, ln\, G_T \end{aligned} \tag{4.130}$$

where in the last step the trace over meson space is performed. Analogously to the quark propagator in the previous section, each of the the log-G terms can separately be expanded in fluctuations. Suppressing again the indices L, T, and the spacetime dependencies, we find:

$$\begin{aligned} \frac{i}{2} Tr\, ln\, G^{-1} = \frac{i}{2} Tr\, ln\, G_{th}^{-1} - \frac{\alpha\lambda}{N} Tr(\varphi_a \delta\varphi_a G_{th}) \\ -\frac{\alpha\lambda}{2N} Tr(\delta\varphi_a \delta\varphi_a G_{th}) + \frac{i\alpha^2\lambda^2}{N^2} Tr(\varphi_a \delta\varphi_a G_{th} \varphi_b \delta\varphi_b G_{th}) \end{aligned} \tag{4.131}$$

The equation of motion is obtained from variation of Γ with respect to the relative fluctuations at vanishing relative variables (with center and relative variables on the time contour as defined above, (4.26)-(4.29)). Thus, the first term on the right hand side of equation (4.131) will drop out in the equation of motion for the meson field and the second term will provide the derivative of the one-loop mean field potential. In the second line we have a term at $\mathcal{O}(\lambda\delta^2)$ which will also drop out as soon as we perform the linear harmonic approximation to the meson field. The last term in equation (4.131) will provide us with the damping and noise kernels originating from the interaction of the meson mean fields with the mesonic part of the heat bath. Dropping the indices "th", "0" as well as the bar for the center variables, we obtain for the trace-log term of

the full meson propagator the expression (see appendix A.1 for details)

$$
\begin{aligned}
-\frac{\lambda}{N}\int d^4x\ \left(3G_L^{++}(x,x)+(N-1)G_T^{++}(x,x)\right)\left(\varphi_a(x)+\frac{1}{2}\Delta\varphi_a(x)\right)\Delta\delta\varphi_a(x)\\
-\frac{i2\lambda^2}{N^2}\int d^4x d^4y\,\Theta(x^0-y^0)\varphi_a(x)\varphi_b(y)\Delta\delta\varphi_a(x)\delta\varphi_b(y)\times\\
\Big(9\Big[G_L^<(x-y)G_L^>(y-x)-G_L^>(x-y)G_L^<(y-x)\Big]\\
+(N-1)\Big[G_T^<(x-y)G_T^>(y-x)-G_T^>(x-y)G_T^<(y-x)\Big]\Big)\\
+\frac{i\lambda^2}{2N^2}\int d^4x d^4y\,\varphi_a(x)\varphi_b(y)\Delta\delta\varphi_a(x)\Delta\delta\varphi_b(y)\times\\
\Big(9\Big[G_L^<(x-y)G_L^>(y-x)+G_L^>(x-y)G_L^<(y-x)\Big]\\
+(N-1)\Big[G_T^<(x-y)G_T^>(y-x)+G_T^>(x-y)G_T^<(y-x)\Big]\Big)
\end{aligned}
\tag{4.132}
$$

where we already ignored terms that drop out of the equation of motion for the meson fields. The first line, in combination with the classical action, leads to the mean field equation of motion (4.115), whereas dissipation and noise enter through the terms $\sim (\lambda/N)^2$. From these latter terms in equation (4.132), we can read off the damping and noise kernels as suggested by the influence functional method.

4.2.1. The damping kernel

The damping kernel is given by:

$$
F_a(x)=-\frac{2i\lambda^2}{N^2}\int d^4y\,\Theta(x^0-y^0)\mathcal{Q}_{ab}(x-y)\delta\varphi_b(y) \tag{4.133}
$$

with

$$
\begin{aligned}
\mathcal{Q}_{ab}(x-y)=\varphi_a\varphi_b\Big(9\Big[G_L^<(x-y)G_L^>(y-x)-G_L^>(x-y)G_L^<(y-x)\Big]\\
+(N-1)\Big[G_T^<(x-y)G_T^>(y-x)-G_T^>(x-y)G_T^<(y-x)\Big]\Big)
\end{aligned}
\tag{4.134}
$$

with suppressed (weak) spacetime dependence of $\vec{\varphi}$. We note that formally the meson flavor space structure of $\mathcal{Q}_{ab}$ is purely longitudinal:

$$\mathcal{Q}_{ab} \sim P^L_{ab} \tag{4.135}$$

but contributions from both, longitudinal and transversal modes enter via the factor in parentheses. In contrast to the previous sections we can thus now introduce $\mathcal{Q}_L$, $\mathcal{Q}_\mathcal{T}$ without confusion as:

$$\mathcal{Q}_{L/T}(x-y) = G^<_{L/T}(x-y)G^>_{L/T}(y-x) - G^>_{L/T}(x-y)G^<_{L/T}(y-x) \tag{4.136}$$

and write $\mathcal{Q}_{ab}$ as:

$$\mathcal{Q}_{ab}(x-y) = P^L_{ab}\,\vec{\varphi}^{\,2}\big(9\mathcal{Q}_L(x-y) + (N-1)\mathcal{Q}_T(x-y)\big) \tag{4.137}$$

In momentum space, $\mathcal{Q}_L$ is given by:

$$\begin{aligned}
\mathcal{Q}_L(\omega,\vec{k}) = \frac{1}{16\pi^2}\int d^3p \frac{1}{E_p E_{p+k}} \times \\
\times\Bigg\{\Big[n_B(E_{p+k})(n_B(E_p)+1) - (n_B(E_{p+k})+1)n_B(E_p)\Big]\delta(\omega + E_p - E_{p+k}) \\
+\Big[n_B((E_{p+k})+1)n_B(E_p) - n_B(E_{p+k})(n_B(E_p)+1)\Big]\delta(\omega - E_p + E_{p+k}) \\
+\Big[(n_B(E_{p+k})+1)(n_B(E_p)+1) - n_B(E_{p+k})n_B(E_p)\Big]\delta(\omega + E_p + E_{p+k}) \\
+\Big[n_B(E_{p+k})n_B(E_p) - (n_B(E_{p+k})+1)(n_B(E_p)+1)\Big]\delta(\omega - E_p - E_{p+k})\Bigg\}
\end{aligned} \tag{4.138}$$

with energies $E_p = \sqrt{M_L^2 + \vec{p}^2}$ (and likewise E_{p+k}) and an analogous expression for $\mathcal{Q}_T$. Just as for the quark induced damping kernel from the previous sections, we have sorted the different terms in $\mathcal{Q}_{L/T}$ according to their energy balance. Again, this sorting reflects the structure of gain minus loss terms for various processes involving interactions of the mean field with the heat bath of meson fluctuations. The gain and loss terms also fulfill the relation (4.64) which is in line with [Wel83]. Since $\mathcal{Q}_{L/T}(\omega,\vec{k})$ is antisymmetric in ω, the derivations from the previous sections, equations (4.66)-(4.87), can easily be applied

to the present case. The result is:

$$F_a(x) \approx \frac{\lambda^2}{N^2}\left[\frac{1}{m_L}\mathcal{Q}_{ab}(m_L,\vec{0})P^L_{bc} + \frac{1}{m_T}\mathcal{Q}_{ab}(m_T,\vec{0})P^T_{bc}\right]\partial_t\varphi_c(x) \tag{4.139}$$

with m_L, m_T the masses of the longitudinal and transversal mean field modes. Inserting equation (4.137) and using

$$\begin{aligned}\mathcal{Q}_{L/T}(m_L,\vec{0}) &= -\frac{1}{4\pi}\int_0^\infty dp\frac{p^2}{E_p^2}\Big(2n_B(E_p)+1\Big)\delta(m_L-2E_p)\\ &= -\frac{1}{4\pi\, m_L}\left(\frac{(m_L)^2}{4}-M^2_{L/T}\right)^{1/2}\left(2n_B\left(\frac{m_L}{2}\right)+1\right)\end{aligned} \tag{4.140}$$

we find that

$$F_a(x) = -\zeta\, P^L_{ab}\partial_t\varphi_b(x) \tag{4.141}$$

with damping coefficient ζ defined as:

$$\begin{aligned}\zeta = \frac{\lambda^2\vec{\varphi}^{\,2}}{4\pi N^2(m_L)^2}&\left[2n_B\left(\frac{m_L}{2}\right)+1\right]\times\\ &\times\left\{9\left(\frac{(m_L)^2}{4}-M_L^2\right)^{1/2}+(N-1)\left(\frac{(m_L)^2}{4}-M_T^2\right)^{1/2}\right\}\end{aligned} \tag{4.142}$$

If $m_L < 2M_L$ or $m_L < 2M_T$, the respective term is set to zero due to the integration over the delta function in equation (4.140).

4.2.2. The noise kernel

From equation (4.132), we see that the mesonic contribution to the noise kernel reads:

$$\begin{aligned}\mathcal{R}_{ab}(x-y) &= \frac{\lambda^2}{N^2}\varphi_a\varphi_b\Big(9\Big[G^<_L(x-y)G^>_L(y-x)+G^>_L(x-y)G^<_L(y-x)\Big]\\ &\quad+(N-1)\Big[G^<_T(x-y)G^>_T(y-x)+G^>_T(x-y)G^<_T(y-x)\Big]\Big)\end{aligned} \tag{4.143}$$

with suppressed weak spacetime dependence of $\vec{\varphi}$. As for the damping kernel, the structure in meson flavor space is purely longitudinal, but contributions from longitudinal and transversal fluctuations enter through the terms in parentheses. We define $\mathcal{R}_L$, $\mathcal{R}_T$

as

$$\mathcal{R}_{L/T}(x-y) = G^{<}_{L/T}(x-y)G^{>}_{L/T}(y-x) + G^{>}_{L/T}(x-y)G^{<}_{L/T}(y-x) \tag{4.144}$$

and consider the corresponding fourier transform ($E_p = \sqrt{M^2_{L/T} + \vec{p}^{\,2}}$):

$$\begin{aligned}
\mathcal{R}_{L/T}(\omega,\vec{k}) = \frac{1}{16\pi^2}\int d^3p \frac{1}{E_p E_{p+k}} \times \\
\times\Bigg\{ \Big[n_B(E_{p+k})(n_B(E_p)+1) + (n_B(E_{p+k})+1)n_B(E_p) \Big]\delta(\omega + E_p - E_{p+k}) \\
+ \Big[n_B((E_{p+k})+1)n_B(E_p) + n_B(E_{p+k})(n_B(E_p)+1) \Big]\delta(\omega - E_p + E_{p+k}) \\
+ \Big[(n_B(E_{p+k})+1)(n_B(E_p)+1) + -n_B(E_{p+k})n_B(E_p) \Big]\delta(\omega + E_p + E_{p+k}) \\
+ \Big[n_B(E_{p+k})n_B(E_p) + (n_B(E_{p+k})+1)(n_B(E_p)+1) \Big]\delta(\omega - E_p - E_{p+k}) \Bigg\}
\end{aligned} \tag{4.145}$$

which features the same gain and loss terms as the damping kernel, but summed instead of mutually subtracted. Applying the zero mode approximation,

$$\begin{aligned}
\mathcal{R}_{ab}(\omega,\vec{k}) &\approx \mathcal{R}_{ac}(m_L,\vec{0})P^L_{cb} + \mathcal{R}_{ac}(m_T,\vec{0})P^T_{cb} \\
&= \frac{\lambda^2\vec{\varphi}^2}{N^2}P^L_{ab}\Big[9\,\mathcal{R}_L(m_L,\vec{0}) + (N-1)\mathcal{R}_T(m_L,\vec{0})\Big]
\end{aligned} \tag{4.146}$$

From equation (4.145) we find

$$\mathcal{R}_{L/T}(m_L,\vec{0}) = \frac{1}{4\pi\, m_L}\left(\frac{(m^L)^2}{4} - M^2_{L/T}\right)^{1/2}\left[2n_B^2\left(\frac{m_L}{2}\right) + 2n_B\left(\frac{m_L}{2}\right) + 1\right] \tag{4.147}$$

and since

$$2n_B^2(\omega) + 2n_B(\omega) + 1 = [2n_B(\omega)+1]\ coth\left(\frac{\omega}{T}\right) \tag{4.148}$$

we find for the contribution of the mesonic heat bath to the noise correlator:

$$\langle\xi_a(x)\xi_b(y)\rangle_\xi = \mathcal{R}_{ab}(x-y) \approx P^L_{ab}\,\delta(x-y)\,m_L\,\zeta\,coth\left(\frac{m_L}{2T}\right) \tag{4.149}$$

with the damping coefficient ζ from equation (4.142). The full equation of motion, including the quark contributions, is:

$$\partial_\mu \partial^\mu \varphi_a + g\rho_a + \left(M_L^2 - 2\frac{\lambda}{N}\vec{\varphi}^2 \right) \varphi_a - h\delta_{a,\sigma} + (\eta + \zeta)_{ab}\, \partial_t \varphi_b = \xi_a \tag{4.150}$$

where the noise correlators from the quarks and mesons add up to the correlator of the effective stochastic field $\vec{\xi}$. The damping coefficients in thermal equilibrium are discussed in sections 5.1 and 6.1. Plots on the full dependence of mean field masses, propagator masses and damping coefficients on the mean field and temperature are collected in appendix B.

Chapter 5.

Results I - Fluctuations and Relaxation for a Pure Quark Heat Bath

In this chapter we will investigate the impact of pionic fluctuations on the dymanics of a system of sigma and pion fields coupled to a heat bath of quarks. For the whole chapter, the equation of motion governing the dynamics of the meson fields is the Langevin equation (4.105), i.e. we neglect contributions from the meson propagator.

5.1. Thermal equilibrium

Before we turn towards the investigations of the nonequilibrium dynamics, we must choose a particular value for the quark-meson coupling constant g. For this purpose, we note that the term

$$g\rho_a + \frac{\partial V_{cl}(\varphi)}{\partial \varphi_a} \tag{5.1}$$

in the equation of motion (4.105) is the field derivative of the effective one-loop potential,

$$V_{eff}(\varphi) = -\frac{i}{\beta V}\Gamma_{(1-loop)} = V_{cl}(\varphi) - \frac{1}{\beta V} Tr\, log\, S^{-1} \tag{5.2}$$

in meson mean field approximation and for a finite spatial volume V. The effective potential evaluates as (see e.g. [KG06] for a computation of the trace-log term and reacall that in our case $\mu_q = 0$):

$$V_{eff}(\varphi) = \frac{\lambda}{4N}(\varphi^2 - v^2)^2 - h\sigma - \frac{n_q}{\beta}\int \frac{d^3k}{(2\pi)^3}\left(\beta E + 2\, log\left(1 + e^{\beta E}\right)\right) \tag{5.3}$$

with energy $E = \sqrt{m_q^2 + \vec{k}^2}$ and quark mass $m_q = g\sqrt{\varphi^2}$. The equilibrium values for the fields fulfill

$$\left.\frac{\partial V_{eff}}{\partial \varphi_a}\right|_{\varphi_{eq}} = 0 \tag{5.4}$$

Due to the explicit symmetry breaking, the pion fields vanish in equilibrium and $\vec{\varphi}_{eq} = (\sigma_{eq}, \vec{0})$ depends on temperature. Thus, also the dynamic quark mass is medium dependent, and the divergent term $\sim \int d^3k\, E$ cannot simply be subtracted but should in principle be carefully renormalized. Many investigations showed that neglecting the divergent term has significant consequences on thermodynamic observables, the type of phase transitions encountered and the phase structure (see e.g. [MME04, PF08, FPP09, PF10, SFN$^+$10]]. However, we will neglect the divergent term completely, since we will anyway tune the coupling constant g so that the model features the various types of phase transition. Furthermore, this ensures for a better comparability to the results in [Nah11, NLB12].

In this spirit, we choose as coupling constants $g = 5.5$, $g = 3.63$ and $g = 3.3$ as in [NLHB11, NLB12]. For the following discussion of the resulting types of phase transitions, see also [Nah11, SMMR01].

With the first choice, $g = 5.5$, the model features a first order phase transition as is shown in figure 5.1 where we plot V_{eff} up to a (temperature dependent) constant for three different temperatures at $\vec{\pi} = 0$. At low temperatures below $T = 108$ MeV, the only minimum of the potential is at values $\sigma \approx f_\pi = 93$ MeV and so the system is in the chirally broken phase. Above the spinodal temperature $T = 108$ MeV, a second minimum appears corresponding to the chirally restored phase. Since this minimum is less deep its associated phase is unstable. With increasing temperatures this minimum gets deeper until at $T = 123.27$ MeV both minima are equally deep. It is at this temperature, that the phase transition occurs and the two phases can coexist. Towards even higher temperatures, the minimum corresponding to the broken phase becomes less deep and thus unstable. Above the upper spinodal temperature there is then only one minimum left. Since the ground state is at the minimum with lowest energy, the σ field jumps at phase transition (see figure 5.4) as is the characteristic behaviour of the order parameter at a first order phase transition.

Lowering g leads to a decreasing barrier at the phase transition until for $g = 3.63$

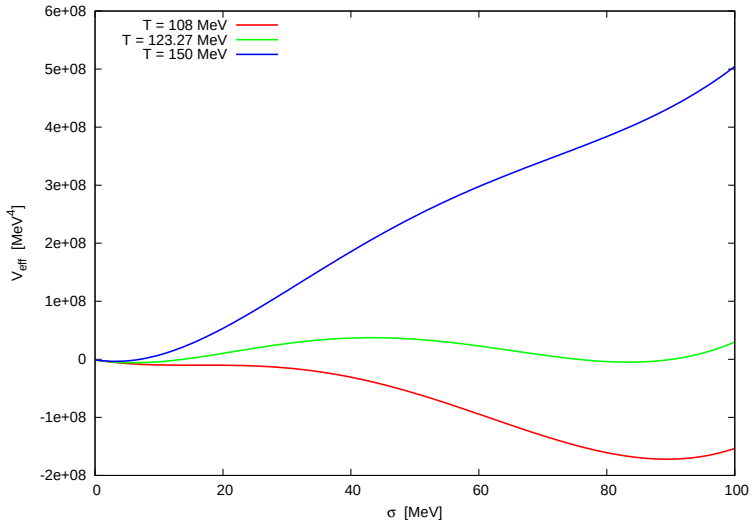

Figure 5.1.: Effective σ field potential (up to a temperature dependent constant) for vanishing pion mean fields and different temperatures. Contributions from the meson propagator are neglected. The quark-meson coupling constant is $g = 5.5$ leading to a first order phase transition at $T = 123.27$ MeV [NLHB11].

we encounter a second order phase transition. The potential for $g = 3.63$ is plotted in figure 5.2 for various temperatures: at the critical temperature $T_c = 139.88$ MeV the potential becomes (nearly) flat between the two phases and so the mass of the σ field drops drastically. This is demonstrated in figure 5.5. Above and below the critical temperature, there are no unstable phases.

For values of $g < 3.63$ the potential shows only one minimum at each temperature as is illustrated in figure 5.3. This minimum moves smoothly from the broken phase to the restored phase for increasing temperature and the model describes a crossover scenario. Since we work with zero quark chemical potential for which lattice QCD predicts a chiral crossover, it is worth noting that for low temperatures the choice of $g = 3.3$ yields a realistic quark constituent mass of about one third of the nucleon mass, $m_q = g f_\pi \approx m_N/3$.

In figure 5.4 we plot the equilibrium values of the σ field and see that it jumps at the first order phase transition while it smoothly changes along crossover transition. The second order scenario is at the boarder between these two cases: The transition is continuous, however, $d\sigma_{eq}/dT \to -\infty$ at the critical temperature. Similarly, the

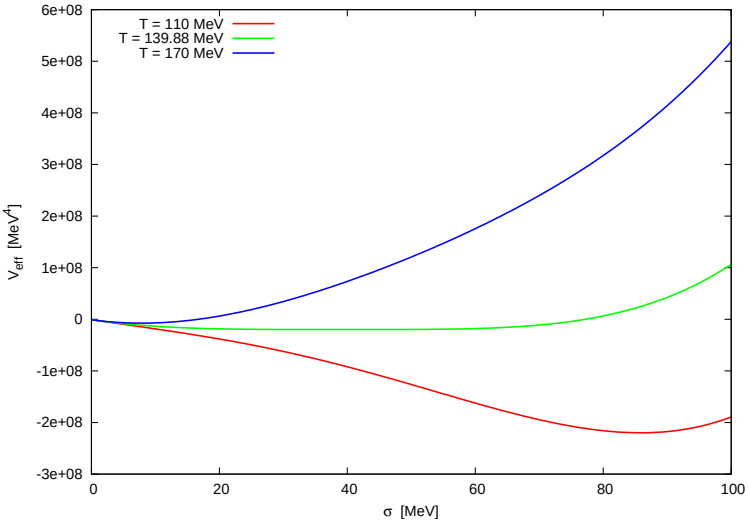

Figure 5.2.: Effective σ field potential (up to a temperature dependent constant) for vanishing pion mean fields and different temperatures. Contributions from the meson propagator are neglected. The quark-meson coupling constant is $g = 3.63$ and the phase transition is of second order. The critical temperature is given by $T_C = 139.88$ MeV [Nah11].

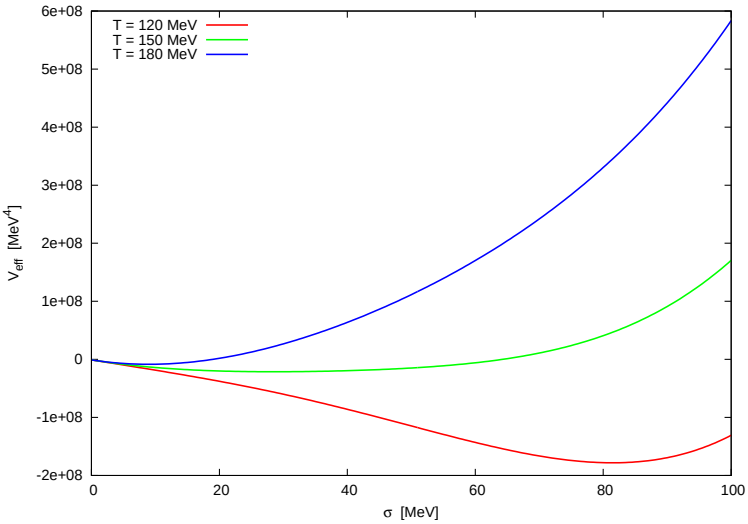

Figure 5.3.: Effective σ field potential (up to a temperature dependent constant) for vanishing pion mean fields and different temperatures. Contributions from the meson propagator are neglected. The quark-meson coupling constant is $g = 3.3$ corresponding to a crossover.

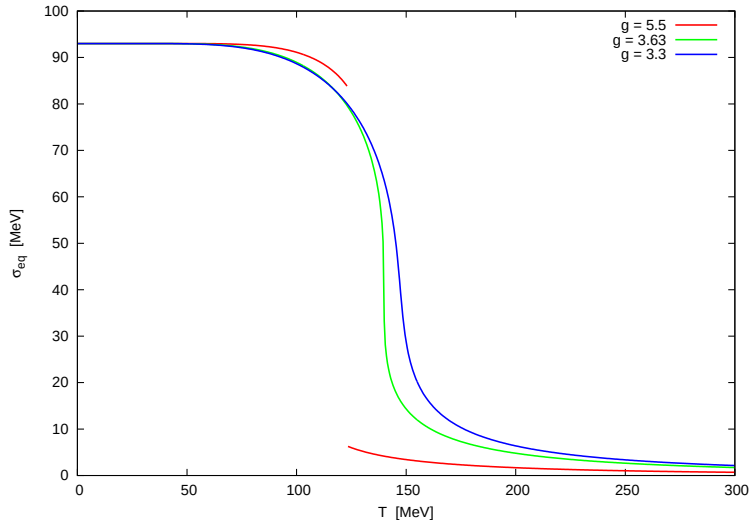

Figure 5.4.: Equilibrium values of the σ field as a function of temperature for different values of the quark-meson coupling constant g. Contributions from the meson propagator are neglected.

equilibrium meson masses, determined by

$$m_\sigma^2 = \frac{\partial^2 V_{eff}}{\partial \sigma^2}\bigg|_{\varphi_{eq}} \qquad m_\pi^2 = \frac{\partial^2 V_{eff}}{\partial \pi_j^2}\bigg|_{\varphi_{eq}} \quad (j = 1, 2, 3) \tag{5.5}$$

which we plot in figure 5.5, show an according behaviour at the first order and crossover transition. At the critical point of the second order phase transition, the σ mass drops very low due to the flat shape of the potential discussed above. However, we see that the mass does not fully drop to zero which means that our choice of $g = 3.63$ is not exactly, but still very close to the case of a second order phase transition. This is appreciated for the numerical implementation of the noise correlator.

Utilizing the equilibrium masses and field values, we can give in figure 5.6 the temperature dependence of the longitudinal and transversal damping coefficients, formulae (4.93),(4.94), in thermal equilibrium. Since in equilibrium the meson four vector points in σ-direction, we can identify the longitudinal damping coefficient η_L with the damping coefficient for the σ and the transversal one with that for the pions. In the broken phase, the decay of zero mode mesons into quark anti-quark pairs and vice versa is kinematically fobidden, since $m_\pi/2 < m_\sigma/2 < m_q \approx g f_\pi$ and so the damping coefficient derived

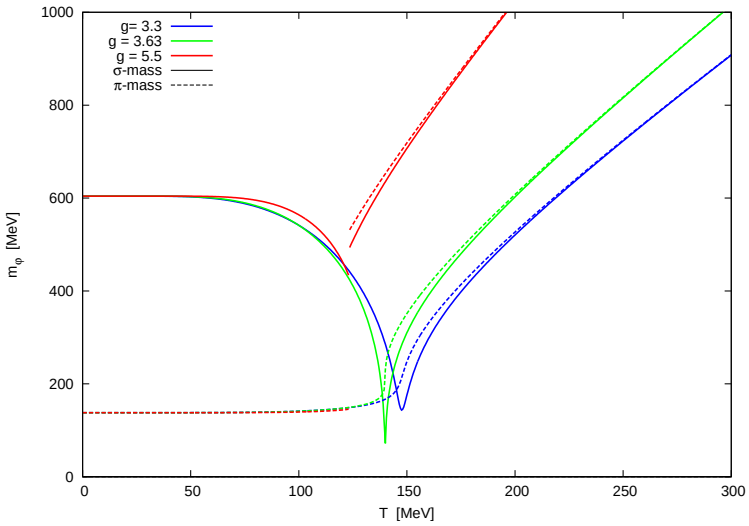

Figure 5.5.: Equilibrium values of the external masses for longitudinal and transversal modes as a function of temperature for different values of the quark-meson coupling constant g. Contributions from the meson propagator are neglected.

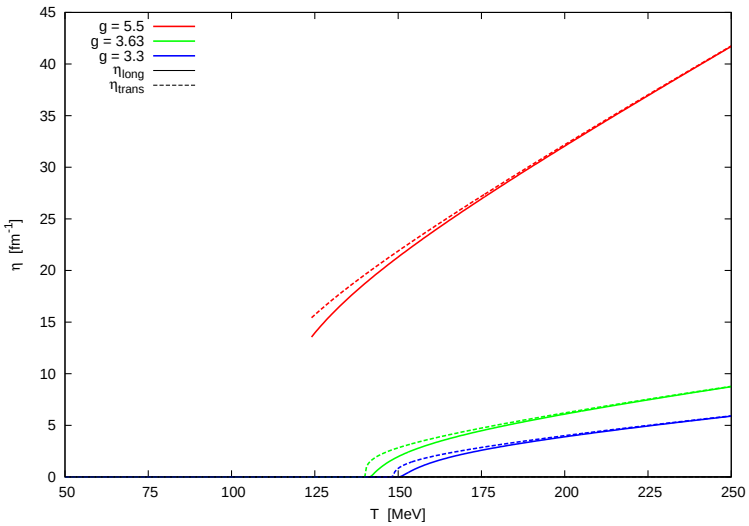

Figure 5.6.: Equilibrium values of the longitudinal and transversal parts of the damping coefficient η as a function of temperature for different values of the quark-meson coupling constant g. Contributions from the meson propagator are neglected.

in the previous chapter vanishes. In the symmetric phase, $m_q \approx 0$ and $m_\pi \approx m_\sigma$ and so we find $\eta_L \approx \eta_T$ from equations (4.93), (4.94) which is also observed in figure 5.6. Thus, the overall deviation between the two damping coefficients is very small. The only noticeable difference occurs in the symmetric phase close to the phase transition where the pion mass exceeds the σ mass. Hence, on the level of the damping coefficient and the noise correlator, we expect the pionic degrees of freedom to have only a small impact on the field dynamics and the effect is best looked for at temperatures just above the phase transition.

5.2. On the Numerical Implementation of the Langevin Equation

We will perform our numerical calculations on a space-time lattice with three spatial dimensions in a cubic volume. We choose $N = 32$ lattice sites in each spatial direction and a lattice spacing of $\Delta x = 0.2$ fm. For the time evolution the Langevin equation is integrated in time steps of $\Delta t = 0.02$ fm using the algorithm presented in [CSFF$^+$12]. At the boundary of the volume, we require the derivatives of the fields normal to the surface to vanish. For the discretized noise field, we follow [NLB12] and choose (with lattice site indices i,j and time step indices n, n')

$$\delta(\vec{x} - \vec{x}')\delta(t - t') \to \frac{1}{V}\delta_{ij}\frac{1}{\Delta t}\delta_{nn'} \tag{5.6}$$

with a factor of $1/V = 1/(N\Delta x)^3$ rather than $1/(\Delta x)^3$. By this, we heavily suppress the amplitude of the noise fields. However, if we did not do so, the small spatial lattice spacing which is required for most simulations of heavy ion collisions and especially such which incorporate hydrodynamic models as used in [Nah11, NHL$^+$13] gives rise to very large noise amplitudes which completely dominate the evolution of the meson fields in an unphysical way. As a remedy one could devise some suitable local spatial averaging which would tame the effect of the noise field to a numerically and physically bearable level. Apart from this, there is also the problem of the field expectation value to depend on the lattice spacing which occurs whenever we treat a field equation with a stochastic force on on a lattice. In order to remove such an unphysical dependence on the lattice spacing one has to identify and subtract the responsible terms [CSFF$^+$12]. By choosing to suppress the noise field in the aforementioned way, we evade both problems.

But we should keep in mind that we will probably underestimate the magnitude of the meson fluctuations. For the damping coefficient and the correlation of the noise fields, equilibrium values (which were given in the previous section) are used for the sake of computational simiplicity. Below the phase transition, η vanishes since the meson masses are too small to allow for the dissipative interactions with the heat bath. However, with $\eta = 0$ we have $\xi = 0$ and thus the equation of motion reduces to that of meson fields oscillating freely in the effective potential. This situation is of course unphysical and we still want nonequilibrium field configurations to relax to an equilibrium state. Therefore, we choose $\eta_{\sigma/\pi} = 3$ fm for $m_{\sigma/\pi} < 2m_q$ based on [Ris98] and used in [NLHB11] which estimates the effects from the interaction of soft and hard meson modes, the latter acting as part of the heat bath.

When presenting the results for the time evolution of the fields we will mostly be interested in the field values averaged over the volume and over different noise configurations. For a given configuration of the noise field ξ_{ijk}, the volume average of the σ field with spatial lattice site indices i,j,k is defined as [CSFF$^+$12, NLB12]:

$$\langle\sigma\rangle_n = \frac{1}{N^3}\sum_{i,j,k=1}^{N}\sigma_{ijk,n} \tag{5.7}$$

The noise average is then obtained by summing over the volume averages for N_ξ different configurations of the noise field:

$$\langle\sigma\rangle_\xi = \frac{1}{N_\xi}\sum_{n=1}^{N_\xi}\langle\sigma\rangle_n \tag{5.8}$$

Further, we define the spatial variance of the sigma field as

$$\langle\sigma^2\rangle_n = \frac{1}{N^3}\sum_{i,j,k=1}^{N}\left(\sigma_{ijk,n} - \langle\sigma\rangle_n\right)^2 \tag{5.9}$$

Accordingly, the corresponding noise average is defined as well as the volume and noise averages for the pion fields.

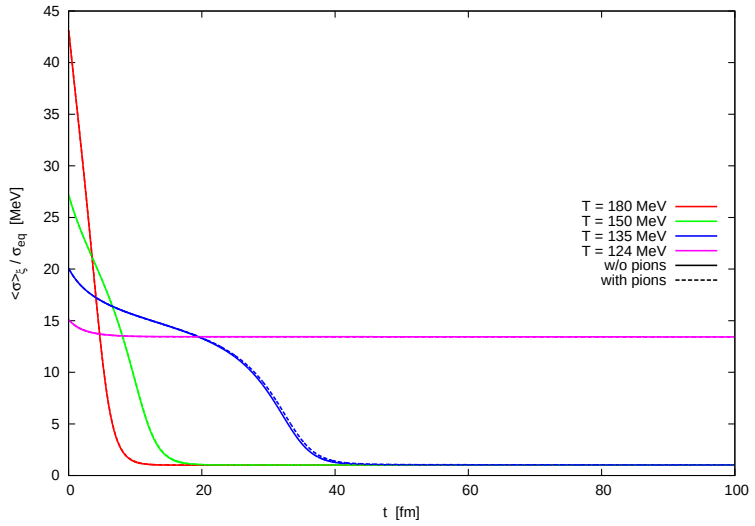

Figure 5.7.: Time evolution of the noise averaged σ field relaxing in a first order phase transition scenario for different temperatures.

5.3. Dynamics With Pionic Degrees of Freedom and a Static Heat Bath

To begin our investiagtions on the impact of pionic degrees of freedom on the relaxation dynamics near the chiral phase transition we assume a static heat bath, i.e. we keep the temperature fixed during the time evolution of the meson fields. Our results for the case of vanishing pion mean field agree with [Nah11, NLB12].

5.3.1. First Order Phase Transition

With the choice $g = 5.5$ the model features a first order phase transition as discussed in the previous sections. We start with temperatures above the phase transition and initialize the field to its zero temperature vacuum expectation value $\vec{\varphi} = (\sigma, \vec{\pi}) = (f_\pi, \vec{0})$.

For high temperatures, the system then relaxes to thermal equilibrium as can be seen from figure 5.7 showing the time evolution of the sigma field averaged over $N_\xi = 20$ noise configurations. At $T = 180$ MeV we see the exponentially damped relaxation to thermal equilibrium and find that adding the explicit propagation of pionic degrees of freedom has no noticeable effect on the dynamics of the order parameter. For $T = 150$ MeV the effective potential in sigma direction is not entirely convex and less steep. It

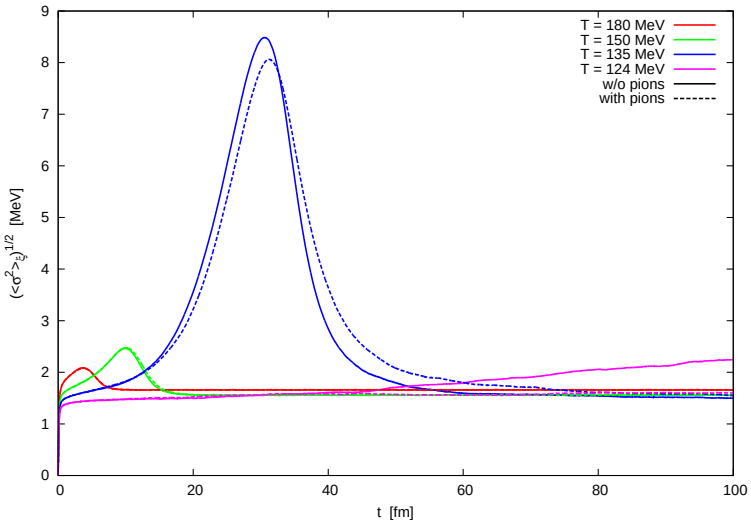

Figure 5.8.: Time evolution of the noise averaged σ fluctuations for relaxation in a first order phase transition scenario for different temperatures.

therefore takes more time for the field to fully relax. The case of $T = 135$ MeV is closer to the upper spinodal temperature but still above it. Thus, there is a larger region $\sigma \approx 60 - 80$ MeV where the potential is less steep compared to smaller ($\sigma \approx 20 - 50$ MeV) or larger ($\sigma \approx 80 - 100$ MeV) field values and so the relaxation process is slowed down while passing through this intermediate region, corresonding to $\sigma/\sigma_{eq} \approx 13 - 17$. For the final part of the relaxation, i.e. at times $t \approx 20 - 40$ fm we see a small effect from the inclusion of pionic degrees of freedom: it seems that including the pion fields leads to a slightly slower relaxation during this time interval. Such an effect is to be exptected since the pions enter the sigma equation of motion only through the absolute value of the chiral field vector, $|\vec{\varphi}| = \sqrt{\sigma^2 + \vec{\pi}^2}$ in the field derivative of the effective potential. So, the sigma field feels the same potential as if the pions were zero and the sigma field correspondingly larger. As a consequence, it takes the sigma field a little longer to drop below $\sigma/\sigma_{eq} \approx 13$ from where the fast relaxation sets in again. The transition from the region of less steep to steeper potential also causes a significant increase in the variance of the sigma field since due to the stochastic force in the equation of motion the tranistion occurs at some lattice sites earlier than at others. The onset of faster relaxation then results in a wider spread of the field values. This is supported by figure 5.8 which for $T = 135$ MeV also shows that the relaxation dynamics including pionic degrees of freedom is slightly slower than without. Very close to the phase transition the field is

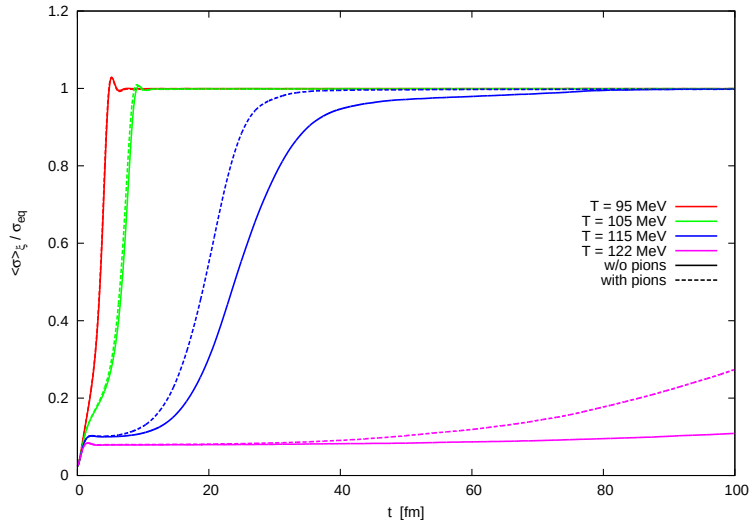

Figure 5.9.: Time evolution of the noise averaged σ field for a quenched system passing a first order phase transition.

trapped in the wrong minimum. Without pionic degrees of freedom the sigma field shows an incresing variance for times $t > 50$ fm indicating that at least at some lattice sites the field approaches the true minimum of the effective potential. Since we are just above the phase transition, this global minimum corresponds to the (approximately) chirally symmetric phase, i.e. low equilibrium values of the sigma field. On inclusion of the pion fields there is no such increase in sigma variance up to $t = 100$ fm which is due the pions causing the sigma field to feel a slightly altered potential as discussed above. This makes it more difficult for the stochastic force to finally push the sigma field over the potential barrier. Applying different initial conditions as for instance a linear distribution for the sigma field as in [Nah11] will cause the system to split into larger regions with different phases. However, the pionic degrees of freedom will eventually drive the system towards the broken phase due to their effect on the sigma potential.

When we quench the system from the symmetric to the broken phase we find a different behaviour for the dynamics of the chiral fields (figure 5.9) and the corresponding fluctuations (figure 5.10): for $T = 95$ MeV and $T = 105$ MeV which are below the lower spinodal temperature the system relaxes rather quickly. Since the damping coefficient is smaller than at temperatures above the phase transition we now see a damped oscillation around the equilibrium configuration (cf also [NLHB11, NLB12]). In these

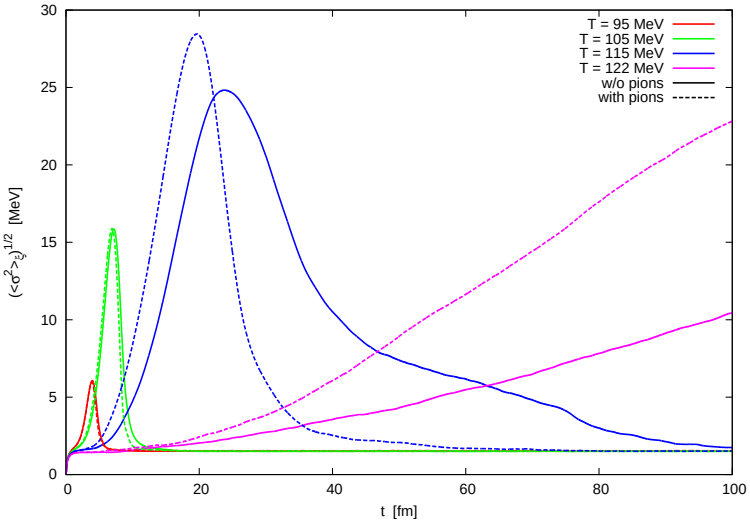

Figure 5.10.: Time evolution of the noise averaged σ fluctuations for a quenched system passing a first order phase transition.

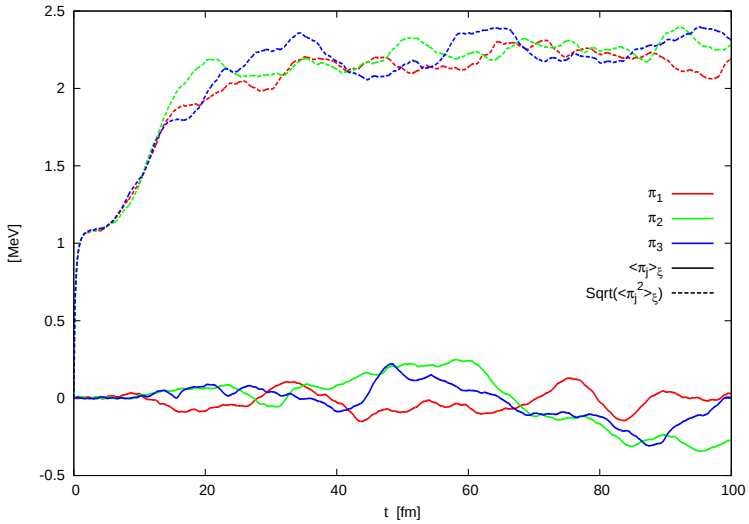

Figure 5.11.: Time evolution of the noise averaged pion mean field and fluctuations for $g = 5.5$. The system is quenched to $T = 115$ MeV and contributions from the meson propagator are neglected.

two cases, explicitly propagating the pion mean fields alongside the sigma field does not significantly alter the dynamics of the latter. However, at $T = 115$ MeV which is above the spinodal temperature we have two minima in the potential which drastically slows down the relaxation. Here, we find that the fluctuating pion fields severely speed up the relaxation process. The time it takes for the sigma average to reach 95% of its equilibrium value is reduced by about $\sim 30\%$ (figure 5.9) and for the full relaxation of the system the effect is even larger ($\gtrsim 35\%$) which we see from figure 5.10. The mechanism behind this is the same as before: the nonzero pion fields cause the sigma field to encounter a slightly shifted potential, as if the value of the sigma field was a little larger. Since relaxation requires the sigma field to be pushed over the potential barrier towards larger field values, the pions now help in achieving this. In order to visualize the pion fluctuations which we refer to so often, we plot in figure 5.11 the noise averages of the single pion field components and the corresponding fluctuations. Since in the vicinity of thermal equilibrium, the potential in pion direction is less steep than in sigma direction, the former are less confined and the magnitude of pion fluctuations $\sqrt{\langle \pi_j^2 \rangle_\xi}$ is larger than the sigma fluctuations by a factor of ~ 1.5. Back to the relaxation of the sigma field we find again that very close to the phase transition at $t = 122$ MeV the system is (almost) trapped in the wrong minimum with a potential barrier too large to overcome quickly. However, since we now want to cross the barrier in the opposite direction as in the high temperature cases of figure 5.7 the pions help: on average the relaxation starts around $t \approx 20 - 40$ MeV. It should be mentioned that also without pions the relaxation sets in at times smaller than 100 fm, as can be seen from the fluctuations in figure 5.10.

5.3.2. Second Order Phase Transition

With the choice $g = 3.63$ the model features a second order phase transition at the critical temperature $T = 139.88$ MeV. We start again with investigating the relaxation dynamics at temperatures above the phase transition. As initial conditions we choose a linear random distribution of the fields in the range $-10\ MeV < \sigma < 110\ MeV$ and $-20\ MeV < \pi_j < 20\ MeV$. Since the potential does not allow for different phases separated by a potential barrier the dynamics are very similar to the case of choosing initially constant field values. The only difference is for times $t \lesssim 0.1$ fm: for initially constant field values the field distribution immediately spreads to gaussian shape. With a random distribution the field fluctuations are so strong that the laplacian operator in the equation of motion dominates and causes the field distribution to relax very fast into

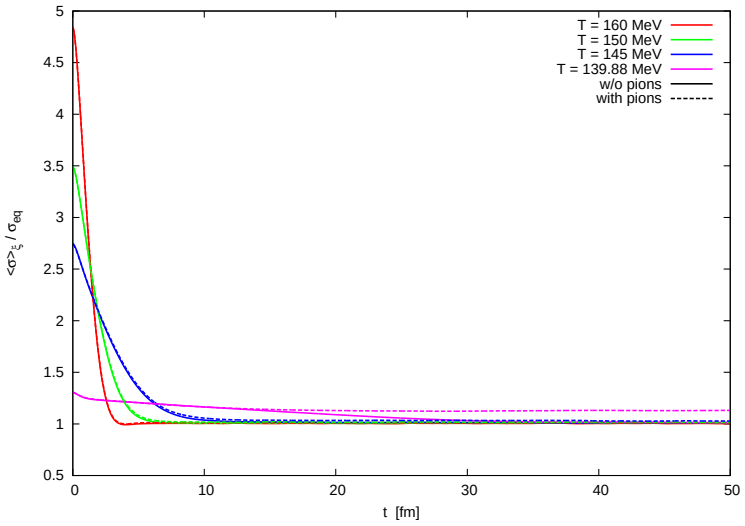

Figure 5.12.: Relaxation of the noise averaged σ mean field for $g = 3.63$, starting with a random field distribution for different temperatures.

same gaussian shape. Thereafter, in both cases the gaussian distribution slides down the potential which is the actual relaxation process we are interested in.

In figures 5.12 and 5.13 we plot the time evolution of the noise averaged sigma field and fluctuations for relaxation at high temperatures. For $T \geq 145$ MeV the sigma relaxes quickly to thermal equilibrium and relaxation occurs faster with increasing temperature. Similar to our previous findings, we see no significant difference in the dynamics of the order parameter when pions are included. However, at the critical point, $T = 139.88$ MeV, there is a noticeable difference: first of all, relaxation is very slow since the potential is (almost) flat in sigma direction. But while without the explicit propagation of pion fields the sigma field relaxes to the correct value, i.e. the minimum of the potential, the system does not seem to fully relax when pions are included. However, in meson space the potential at the critical temperature in the vicinity of thermal equilibrium has an interesting shape: in figure 5.14 we plot the derivative of the potential in sigma direction as a function of the sigma field and the length of the pion mean field vector. In thermal equilibrium, the average squared length of the pion vector may be inferred from the variance of pion fluctuations in figure 5.17 as approximately $\sim 3 \times 1.7\, MeV^2$, so we may look for the equilibrium σ position in figure 5.14 at $|\vec{\pi}| \approx 3$ MeV for which the sigma value is about 9% larger than the equilibrium postition at $\pi = 0$. Since we

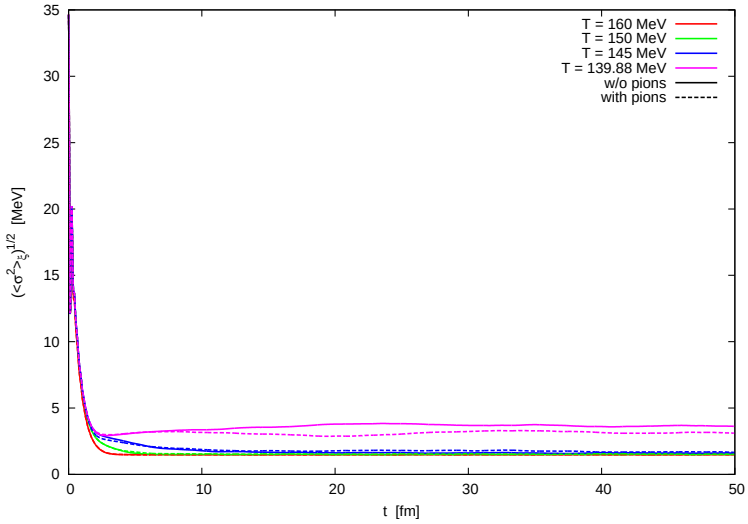

Figure 5.13.: Noise averaged σ fluctuations for $g = 3.63$ during relaxation.

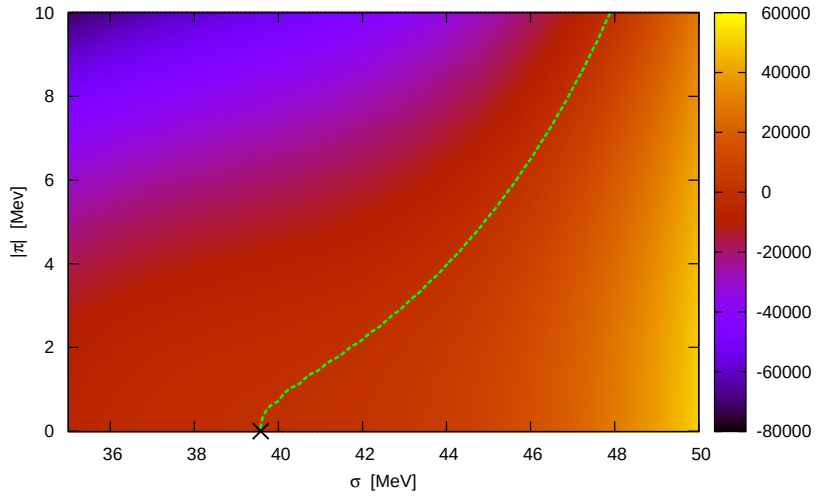

Figure 5.14.: Sigma derivative of the effective potential, $dV_{eff}/d\sigma$ as a function of the sigma mean field and the length of the pion mean field vector. Along the green line this derivative vanishes, corresponding to a stable sigma position for fixed pion vector. The black cross denotes the equilibrium position at zero pion mean field. The scale is given in MeV^3.

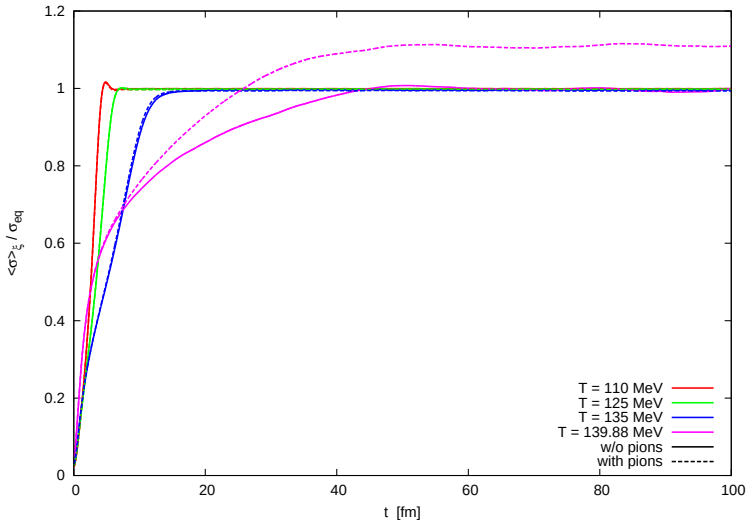

Figure 5.15.: Time evolution of noise averaged σ field for system quenched to different temperatures at $g = 3.63$.

scale the sigma average in figure 5.12 with σ_{eq} at $\pi = 0$ we find our rough estimate to be in good agreement with our observed results.

For a system quenched from the symmetric into the broken phase we find anlaogous results for the time evolution of the noise averaged sigma field and variance which are displayed in figures 5.15 and 5.19 respectively for various temperatures $T \leq T_{crit}$. With a temperature well below the phase transition (e.g. $T = 110$ MeV) we see a damped oscillation around equilibrium and as the critical temperature is approached, the system relaxes more slowly without such oscillations ($T = 125$ MeV and $T = 135$ MeV). While the dynamics of the average sigma field show no significant change on including the pion fields, the fluctuations (figure 5.16) at $T = 135$ MeV reveal that the pions slightly decrease the relaxation time in this case since the peak in the variance typical for relaxation in this model drops a little earlier than without the pions. As reasoned before, at the critical point the pion fluctuations tend to push the sigma field to larger values. At $T = 135$ MeV this effect is too small to be confirmed by figure 5.15, but it helps to minimally speed up the relaxation in our quench scenario where relaxation requires an increase in the sigma value. At the critical point, $T = 139.88$ MeV, we see that relaxation is overall very slow and that the pion fields shorten the relaxation process. However, in line with our previous findings, on inclusion of the pions, the average sigma

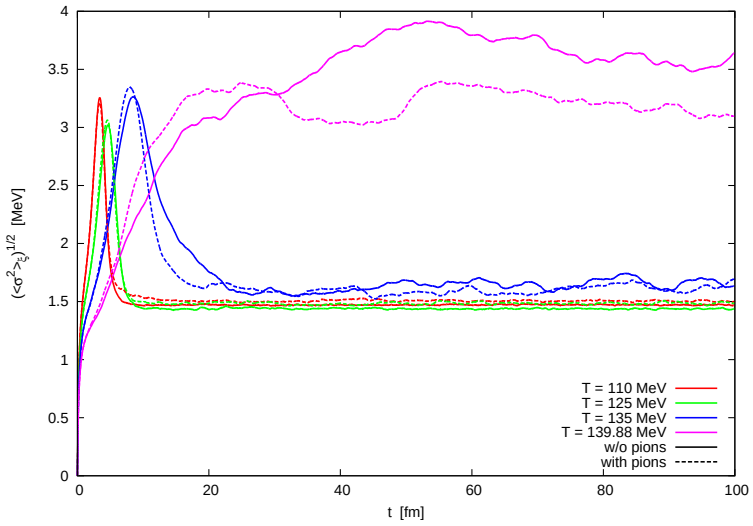

Figure 5.16.: Time evolution of σ fluctuations for system quenched to different temperatures at $g = 3.63$.

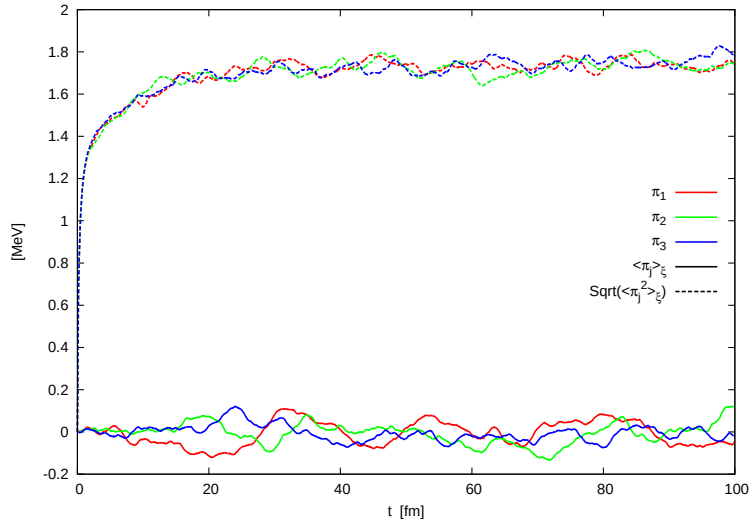

Figure 5.17.: Time evolution of pion mean field and fluctuations at the critical point.

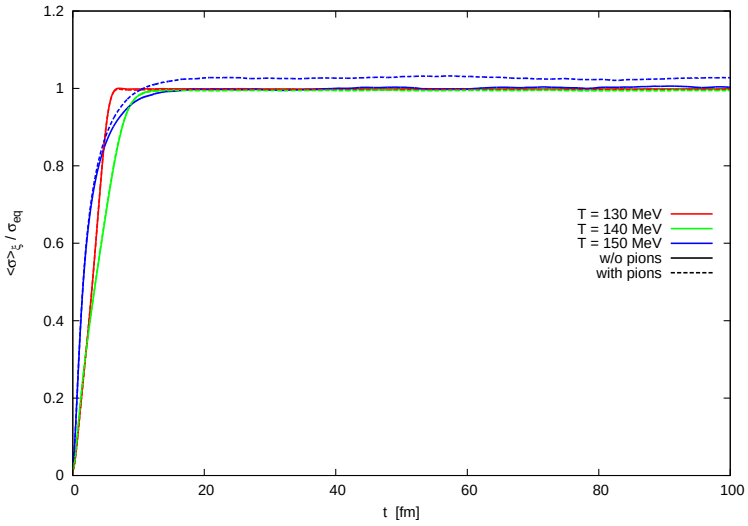

Figure 5.18.: Time evolution of noise averaged σ field for system with crossover ($g = 3.3$) and different temperature quenches.

field exceeds the minimium of the potential an settles down at a value exceeding the ($\pi = 0$)-minimum position of the potential by about 10%, whereas the average sigma fluctuations are reduced. In comparison to the sigma fluctuations at the critical point (figure 5.16) we display the noise averaged pion fields and fluctuations at $T = T_{crit}$ in figure 5.17. Due to the flat potential in sigma direction at $\varphi = (\sigma_{eq}, \vec{0})$ the sigma fluctuations exceed the pion fluctuations in magnitude by a factor of about ~ 1.8.

5.3.3. Crossover

For the sake of completeness we also investigate the crossover scenario, corresponding to a choice of $g = 3.3$. The findings are very similar to the case of the second order phase transition although the effects from the pion fields are less prominent and the relaxation occurs faster. In figure 5.18 we plot the time evolution of the noise averaged sigma field for a system quenched to different temperatures and in figure 5.19 the corresponding sigma fluctuations are displayed. The system relaxes faster for temperatures further away from the phase transition and pions have only a negligible effect on the dynamics of the sigma field. Only at the phase transition ($T \approx 150$ MeV) we see a slight shift of the sigma field to values larger than the actual minimum of the potential for the same reason as in the critical point scenario, only that this time the shift is rather small.

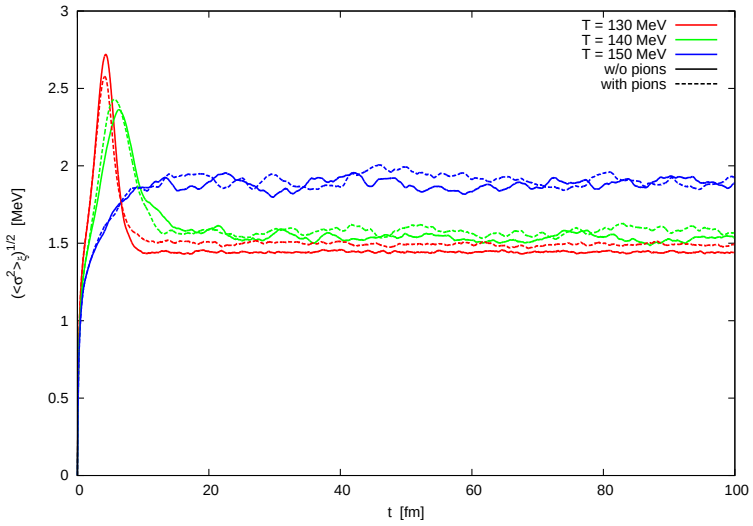

Figure 5.19.: Time evolution of σ fluctuations for system quenched with a crossover, i.e. $g = 3.3$. The system is quenched to different temperatures.

5.4. Dynamics Including Reheating

During relaxation the chiral fields lose energy which is absorbed by the heat bath. In the previous section, this energy transfer has been neglected, but we will now take it into account. For this purpose, we follow [Nah11, NLB12] and identify the energy density of the chiral fields as:

$$\epsilon_\varphi(\vec{\varphi}) = \frac{1}{2}(\partial_t \varphi_a)^2 + \frac{1}{2}\left(\vec{\nabla}\varphi_a\right)^2 + V_{cl}(\varphi) \tag{5.10}$$

with summation over repeated indices. The first term is the kinetic energy density and the second term quantifies the fluctuation energy density of the chiral fields. The last term reflects the potential energy density of course. For the locally equilibrized heat bath of quarks, the energy density fulfills the thermodynamic relation:

$$\epsilon = T\frac{\partial p}{\partial T} - p \tag{5.11}$$

where $p = -\Omega_q$ is given by

$$\Omega_q = V_q = -\frac{1}{\beta V} Tr\ log\ S^{-1} \tag{5.12}$$

and therefore, with $E_q = \sqrt{g^2\varphi^2 + \vec{k}^2}$, and since we neglect the divegent contributions to the potential:

$$\epsilon_q = 2n_q \int \frac{d^3k}{(2\pi)^3} E_q \, n_F(E_q) \tag{5.13}$$

In the following calculations, after each temporal iteration we add the current change in the energy density of the chiral fields to the energy density of the heat bath. The new energy density of the heat bath is then solved for the new temperature. We compute this change in temperature seperately at each spatial lattice site. Consequently, we define the volume and noise averaged temperatures analogously to the corresponding quantities of the chiral fields.

5.4.1. First Order Phase Transition

We begin with a system initialized at $\sigma_{eq}(T = 160\, MeV)$ to different temperatures T_0 below a first order phase transition. While the sigma field relaxes, the energy transferred to the heat bath causes an increase in temperature. In figure 5.20 we plot the time evolution of the noise averaged sigma field, in figure 5.21 the sigma fluctuations and in figure 5.22 the average temperature as a function of time. For quench temperatures $T = 80$ MeV and $T = 100$ MeV we find that the system relaxes faster when the pion mean fields as explicitly propagated degrees of freedom are included. While the effect is minute in the case of $T_0 = 80$ MeV, the time it takes for the system to reach the phase transition temperature $T = 123.27$ MeV for $T_0 = 100$ MeV is decreased by about $\sim 5\%$. In both cases, $T_0 = 80$ MeV and $T_0 = 100$ MeV the system passes from the hot into the cold phase minimum of the potential while the environment heats up and passes the phase transition temperature in the opposite direction. Finally, the sigma field is trapped in the wrong minimum. In the case of $T_0 = 100$ MeV the system has not yet relaxed while passing the phase transition, i.e. a considerable part of the sigma field still needs to overcome the potential barrier. Here, the pion fluctuations help again which is why we see an effect. With $T_0 = 80$ MeV instead the sigma field has already crossed the potential barrier before it even appears at the spinodal temperature of $T = 108$ MeV. For $T_0 = 110$ MeV the system struggles to relax (and the pions are of little help as seen from the sigma fluctuations), but compared to the case of an isothermal heat bath (figure 5.9) one might expect relaxation to set in somewhen between $5\, fm < t < 15\, fm$. Why there is so little happening for the system with reheating is because of the local energy transfer between mean fields and environment. If at a single lattice site the field crosses

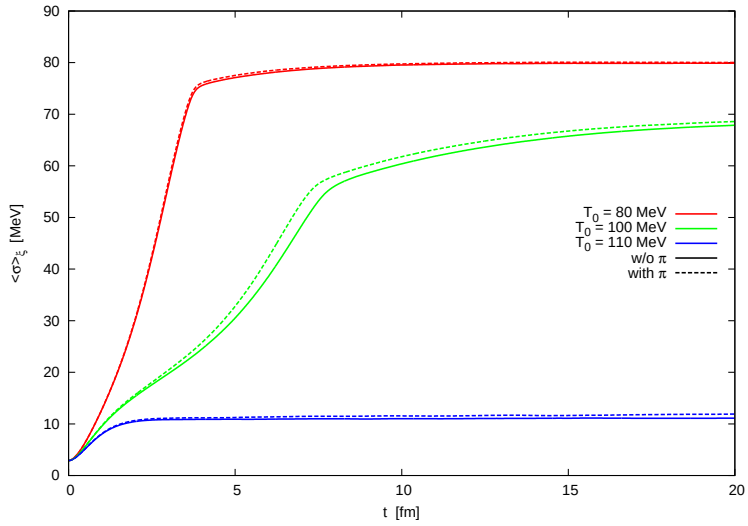

Figure 5.20.: Noise averaged σ field relaxing after a quench in a first order phase transition scenario including reheating.

the potential barrier and reaches values associated with the chirally broken phase, it has caused a local increase in temperature well above the transition temperature and so, locally, the potential pushes the field back to the hot phase minimum (which causes local cooling), and so on. To illustrate this situation, we plot in figure 5.23 the local temperature vs sigma value for each lattice site at $t = 50$ fm.

5.4.2. Second Order Phase Transition

In a critical point scenario the results for relaxation of quenched systems with reheating differ from the case of a first order phase transition mainly because of the missing potential barrier at the phase transition. While the sigma field slides down the potential, the environment heats up and the potential smoothly changes shape until the current temperature and sigma value meet at equilibrium configuration $\sigma(t) = \sigma_{eq}(T(t))$. This is seen in figures 5.24, 5.25 where time evolution of noise averaged sigma field and temperature are displayed for various quench temperatures. (The sigma field was initialized at $\sigma_{eq}(T = 180\,MeV)$.) The closer we get to the critical point, the slower the relaxation occurs, and for low quench temperatures (as e.g.) $T_0 = 90$ MeV we the system overshoots equilibrium and relaxes performing damped oscillations about the final configuration. On inclusion of the pion fluctuations we find no significant difference. We recognize a slightly smaller final temperature ($\Delta T < 0.1$ MeV) which is most likely caused by

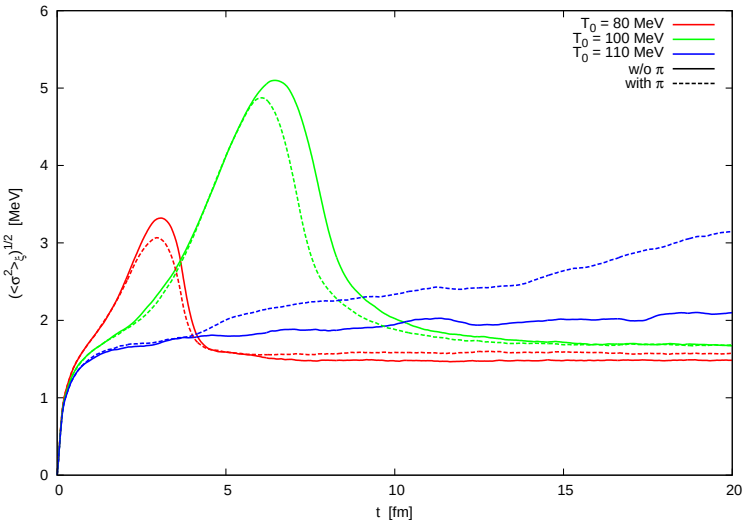

Figure 5.21.: Noise averaged σ fluctuations for a system quenched to different temperatures evolving through a first order phase transition with reheating.

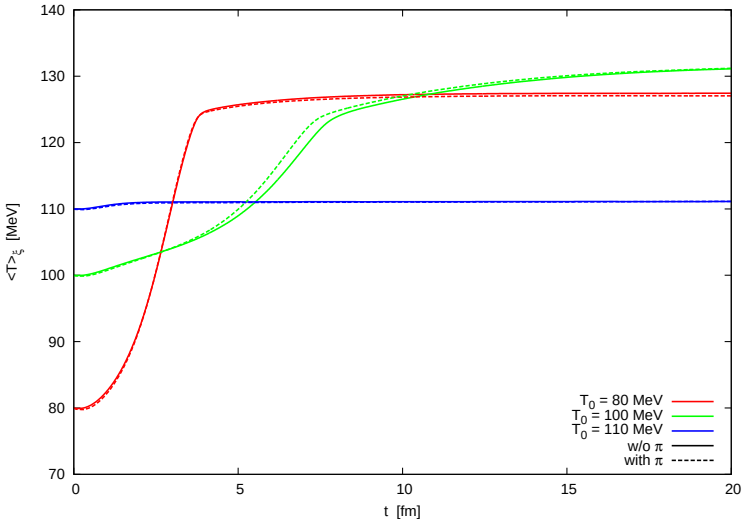

Figure 5.22.: Noise averaged temperature of the heat bath for various quench temperatures in a system with a first order phase transition and reheating.

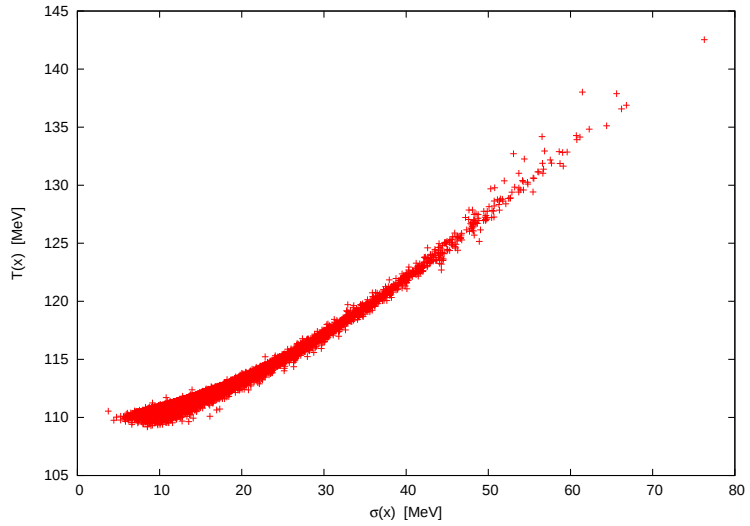

Figure 5.23.: Local temperature vs sigma field value at each lattice site at $t = 50$ fm for a system quenched to $T_0 = 110$ MeV in a first order phase transition scenario including reheating.

the chosen initial conditions (constant field values): immediately after the start of the time evolution, the fields assume the the gaussian distribution from the noise field which means that the mean fields gain energy which is subtracted from the environment and causes a little cooling at $t \lesssim 0.1$ fm. With pions as three additional degrees of freedom the system is thus cooled more (which is also seen in the figure for $t < 0.1$ fm). We could evade this situation by evolving the system in equilibrium in the hot phase for some time and then quench it below the phase transition temperature. However, the overall effect is really small ($< 1\%$), but nevertheless, it helps to explain why we find final sigma values a tiny bit larger when including pions. However, at the critical point, we also found pion fluctuations pushing the sigma field to larger values in case of the isothermal heat bath and in that setup the effect the shift was about 10%. With reheating, the effect is only abuot $2 - 3\%$: if the sigma field is pushed to higher values by means of the pions, the temperature increases and the equilibrium postition is corrected towards lower sigma value which reduces the observed shift in the final sigma average. (Of course, this mechanism also counteracts the small temperature reduction from our choice of initial conditions.)

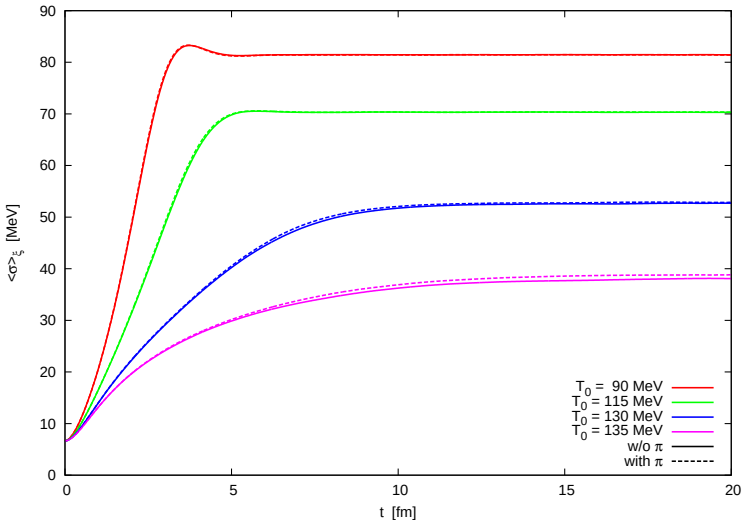

Figure 5.24.: Noise averaged σ field relaxing after a quench including reheating. The case of a second order phase transition is considered (g=3.63).

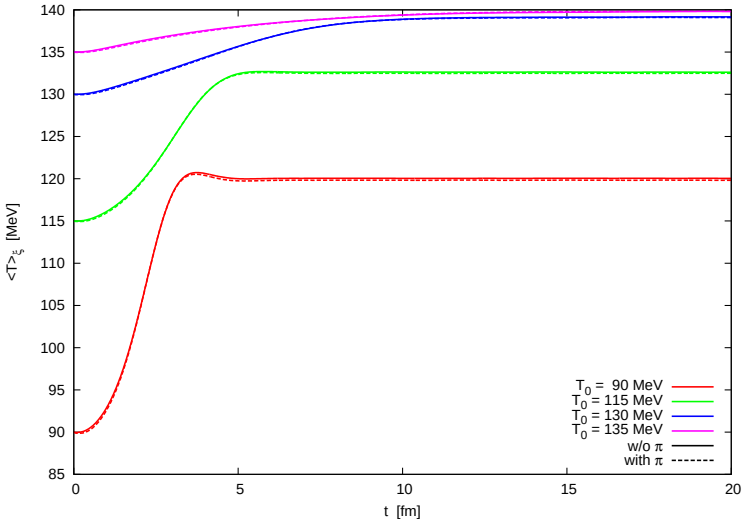

Figure 5.25.: Noise averaged temperature of the heat bath for various quench temperatures in a system with a critical point and including reheating.

Chapter 6.

Results II - Fluctuations and Relaxation for a Heat Bath with Quarks and Hard Meson Modes

In this chapter we investigate the impact of pionic fluctuations on the dynamics of a system of meson mean fields coupled to a static heat bath of quarks and hard meson modes. The interactions in the mesonic sector are accounted for by including the meson propagator in the derivation of the damping coefficient and the correlation of the noise fields in the last section of chapter 4. The equation of motion for the meson fields is

$$\left(\partial_\mu\partial^\mu + M_L^2 - 2\frac{\lambda}{N}\vec{\varphi}^2\right)\varphi_a + g\rho_a - h\delta_{a,\sigma} + (\eta+\zeta)_{ab}\partial_t\varphi_b = \xi_a \tag{6.1}$$

As in the beginning of the previous chapter, we first need to fix the quark-meson coupling constant g. In order to find suitable values we must again take the detour and discuss the thermal equilibrium properties of the model.

6.1. Thermal Equilibrium

In the Langevin equation of motion, (6.1), we recognise the field derivative of the effective potential,

$$\frac{\partial V_{eff}}{\partial\varphi_a} = \left(M_L^2 - 2\frac{\lambda}{N}\vec{\varphi}^2\right)\varphi_a + g\rho_a - h\delta_{a,\sigma} \tag{6.2}$$

which originates from the full effective potential

$$\begin{aligned} V_{eff}(\varphi) &= -\frac{i}{\beta V}\Gamma[\varphi, S, G]\Big|_{\varphi=const} \\ &= V_{cl}(\varphi) - \frac{1}{\beta V}Tr\ log\, S^{-1} + \frac{1}{2\beta V}Tr\ log\, G^{-1} + \frac{1}{2\beta V}Tr\, G_0^{-1}G - \frac{i}{\beta V}\Gamma_2 \end{aligned} \tag{6.3}$$

in thermal equilibrium and with a finite spatial volume V. The first two terms are the classical meson potential and the quark one-loop potential V_q which for $G = 0$ are the only contributions to V_{eff} as was the case in the previous chapter. Now however, we additionally have the trace-log term for the meson propagator which gives the corresponding mesonic one loop potential V_φ, and two remaining terms which we collect into $V_{\varphi\varphi}$ and which result from the nontrivial choice of Γ_2. The one loop meson potential evaluates to (see e.g. [KG06]):

$$\begin{aligned} V_\varphi &= \frac{1}{2\beta V}Tr\ log\, G_L^{-1} + \frac{N-1}{2\beta V}Tr\ log\, G_T^{-1} \\ &= \int \frac{d^3k}{(2\pi)^3}\left(\frac{E_L}{2} + (N-1)\frac{E_T}{2} + \frac{1}{\beta}log\left(1 - e^{-\beta E_L}\right) + \frac{(N-1)}{\beta}log\left(1 - e^{-\beta E_T}\right)\right) \end{aligned} \tag{6.4}$$

In the following, we will omit the divergent terms $\sim \int d^3kE$ as we did for the quark potential. The last two terms in equation (6.3) can be simplified using the explicit expression for the truncated Γ_2 and the meson self-energy, equations (4.108), (4.109). If we neglect again divergent contributions, we find up to an infinite constant:

$$V_{\varphi\varphi} = -\frac{\lambda}{4N}\left(3\overline{G}^2(M_L) + (N^2-1)\overline{G}^2(M_T) + (2N-2)\overline{G}(M_L)\overline{G}(M_T)\right) \tag{6.5}$$

with

$$\overline{G}(M) = \int \frac{d^3k}{(2\pi)^3}\frac{1}{E}\frac{1}{e^{\beta E}-1} \tag{6.6}$$

where $E_{L/T} = \sqrt{M_{L/T}^2 + \vec{k}^2}$.

Within our approximations, at $T = 0$ the effecteve potential is given only by the classical potential. In order to obtain the same vacuum properties as before, we keep $\lambda/N = 20$ fixed and also stick to the values of the symmetry breaking constants v^2, h which we already used in the previous chapter. At finite temperature, we find lower phase transition

temperatures when including the contributions from the meson propagator. However, if we want to investigate systems passing through a phase transition, the transitions should occur at temperatures $T \gtrsim 97$ MeV because otherwise the effective potential would only be defined within the sigma range for which the gap equations can be solved. As we saw in the previous chapter, lower values of the quark-meson coupling constant g shift the phase transition to larger temperatures. A suitable value for which we still find a well developed first order phase transition at a high enough temperature is e.g. $g = 3.7$. We plot the effective potential in figure 6.1 up to a temperature dependent constant for three temperatures: the lower spinodal temperature $T = 97$ MeV, the critical temperature $T_{crit} = 103.43$ MeV for which the system's ground state is degenerate, and $T = 110$ MeV which is above the upper spinodal temperature of $T = 106.5$ MeV. We also note, that the height of the potential barrier is smaller than in the case with a pure heat bath ($g = 5.5$), so we can expect faster relaxation near the phase transition.

Decreasing the quark-meson coupling constant, we eventually find a second order phase transition for $g = 2.4$ with a critical temperature $T_{crit} \approx 117.5$ MeV. In figure 6.2 we plot the potential for three different cases, corresponding to a system in the chirally symmetric phase ($T = 130$ MeV), the broken phase ($T = 110$ MeV) and at the critical point.

Lastly, we choose $g = 2.0$ for studying the model with a crossover which occurs at about $T \approx 120 - 130$ MeV. The effective potential for three different temperatures is given in figure 6.3.

In figures 6.4 and 6.5 we plot the sigma field and the meson masses in thermal equilibrium for the three choices of g: for $g = 3.7$ the sigma field and the pion mass jump at the first order phase transition. In principle, the sigma mass is also discontinuous, but it appears that at the two different minima of the potential the curvature is (almost) the same. With $g = 2.4$ we see a vertical drop of the sigma field and a drastic decrease in the sigma mass at the critical temperature of the second order phase transition while for the model with a crossover, $g = 2.0$, the fields and masses smoothly pass from one phase to the other.

The equilibrium propagator masses are plotted in figure 6.6, i.e. the temperature dependence of the solutions of the gap equations (4.114) for the equilibrium sigma values of figure 6.4. At the phase tranistion both, longitudinal and transversal propagator

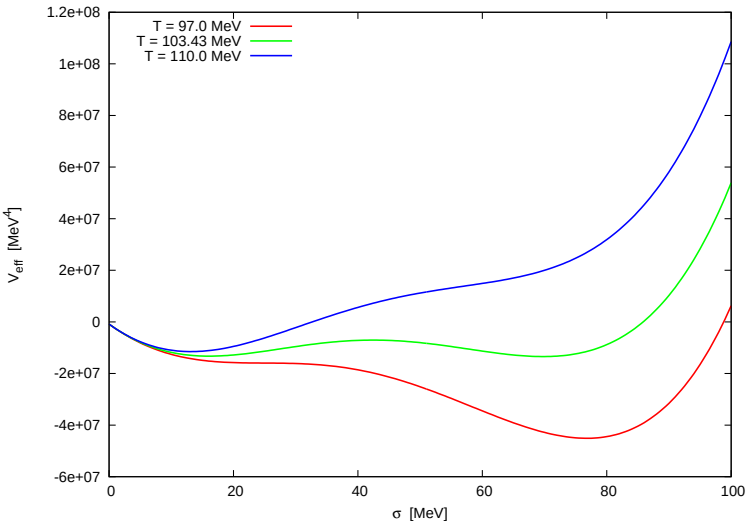

Figure 6.1.: Effective σ field potential (up to a temperature dependent constant) for zero pion mean field and including contributions from the meson propagator. The quark-meson coupling constant is $g = 3.7$ leading to a first order phase transition at $T \approx 103.43$ MeV.

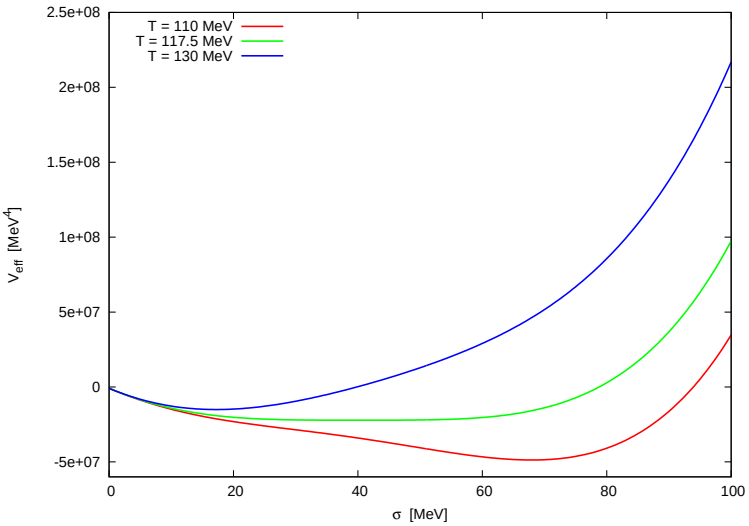

Figure 6.2.: Effective σ field potential (up to a temperature dependent constant) for zero pion mean field and including contributions from the meson propagator The quark-meson coupling constant is $g = 2.4$. The critical temperature for the corresponding second order phase transition is $T_C = 117.5$ MeV.

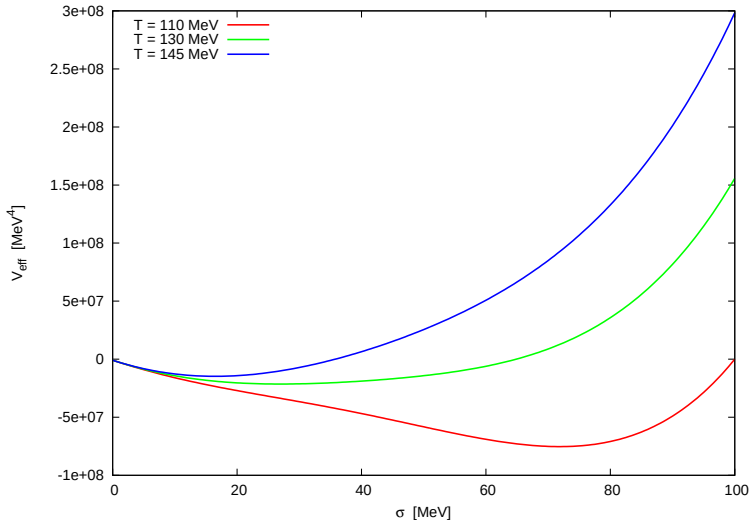

Figure 6.3.: Effective σ field potential (up to a temperature dependent constant) for zero pion mean field and including contributions from the meson propagator. The quark-meson coupling constant is $g = 2.0$ resulting in a crossover.

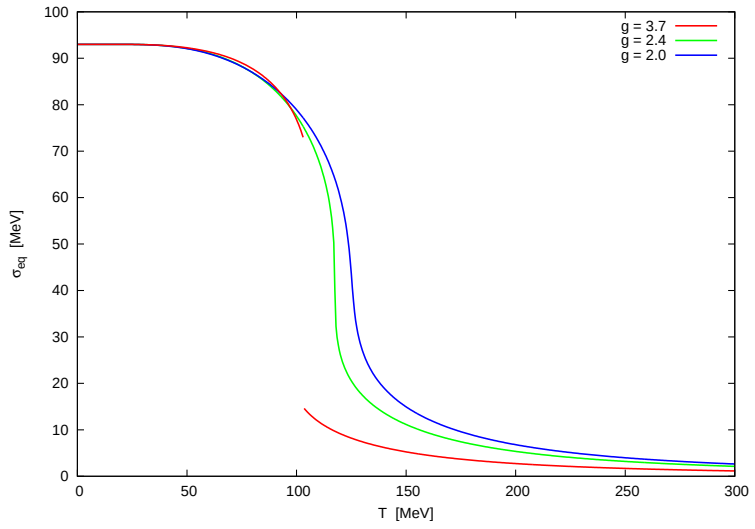

Figure 6.4.: Equilibrium σ values as a function of temperature including contributions from the meson propagator. The quark-meson coupling constant is chosen such that the phase transition is of fisrt order ($g = 3.7$), second order ($g = 2.4$) and a crossover ($g = 2.0$).

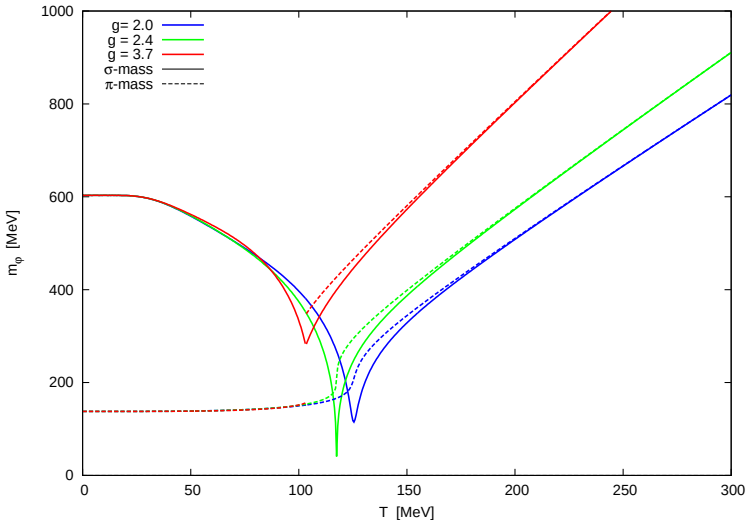

Figure 6.5.: Equilibrium masses of the mean fields as a function of temperature. Contributions from the meson propagator are included in the effective potential.

masses drop, before increasing again towards high temperatures. The way the masses drop, i.e. (dis)continuously respectively smoothly, reflects the type of phase transition. Within the chosen approximations, the gap equations are not explicitly dependent on the quark-meson coupling constant. Only through the particular equilibrium sigma values an implicit g-dependence enters. Since for temperatures sufficiently low or large the equilibrium values of the sigma field are not or at least only weakly dependent on g (cf. figure 6.4) we thus find that the propagator masses in equilibrium are almost independent of g for $T < 50$ MeV and $T > 200$ MeV.

With all equilibrium masses and field values we calculate the damping coefficients: in figure 6.7 we plot the full longitudinal and transversal damping coefficients and in figure 6.8 separately the quark and meson contributions to the longitudinal damping coefficient. In equilibrium , the damping coefficient of the transversal modes gets only the quark contribution. At low temperatures, we find a nonzero damping coefficient which contains contributions from the mesonic sector of the heat bath as well as from the quark sector. To be precise, the latter is only the case for the choices of g with a second order phase transition and crossover, since the small values of g lead to sufficiently small quark masses at low temperatures. At high temperatures the mesonic contribution to the damping coefficients tends to zero and we are left with just the damping from the

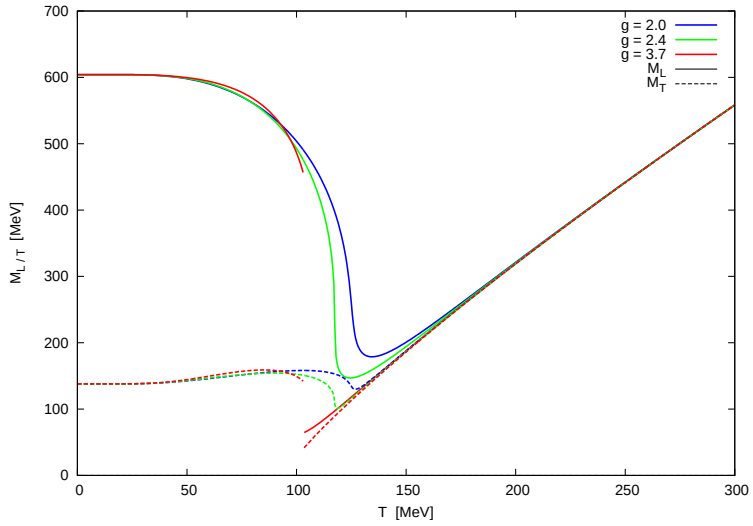

Figure 6.6.: Equilibrium masses of the meson propagator as a function of temperature for different types of phase transitions.

heat bath of quarks. In the vicinity of the phase transition, the damping coefficients vanish in case of the crossover and second order transition. For temperatures just above the critical point, the sigma mass grows fast with increasing T. Together with the drop of the propagator masses and the sigma field at the critical point we thus find for $T > T_{crit}$ two successive bumps in the longitudinal damping coefficient originating from the heat bath of transversal and longitudinal meson modes respectively. In case of a first order phase transition the sudden change in the propagator masses accompanied with the jump in the pion mean field mass leads to a drastic increase in the damping coefficient from the meson heat bath, especially around 103.43 MeV$< T \lesssim$ 110 MeV. At high temperatures however, the damping coefficient is again dominated by the quark sector of the heat bath. Further, it should be remarked that the damping coefficient is still finite at the first order phase transition. Also, we see that for the crossover scenario, there is no meson contribution to the damping coefficient in the hot phase since the mean field masses are too small compared to the propagator masses ($m_L/2 < M_{L/T}$). In contrast to the previous chapter, the longitudinal damping coefficient is nonzero at low temperatures and only vanishes close to the phase transition temperature. Since we require damping for the relaxation but still wish to (at least somehow) respect the temperature dependence of the damping coefficients, we artificially assume a minimum value of $1 fm^{-1}$ for both, longitudinal and transversal damping coefficients. A minimum

of $3fm^{-1}$ as was chosen at low temperatures in the previous chapter would now be too large at high temperatures, since with the smaller choices of g the high temperature damping coefficients are corrspondingly smaller.

However, we confirm that the previous assumption of $\eta = 3\ fm^{-1}$ was a good estimate at low temperatures. This is not surprising since this value is based on [Ris98], where for a chiral O(N) model the damping coefficient was determined from a 1PI ansatz in almost the same fashion as in our case. For the small coupling constants g, we find an additional quark contribution at low temperatures, but for the larger values of g as used in the previous chapter, there is no quark contribution to the damping coefficient in the broken phase and what remains is the meson contribution of about $\sim 3\, fm^{-1}$. In the hot symmetric phase, it was found in [Nah11] that the quark contribution results in much larger damping coefficients than for a pure meson heat bath. The latter was calculated in the linear sigma model without constituent quarks to be $2.2fm^{-1}$ at the critical point [BG97]. In our approximation, we find a smaller meson contribution $\zeta < 1.5\, fm^{-1}$ above the critical point (and $\zeta = 0$ at T_{crit}). In line with [Nah11], the damping in the symmetric phase is thus dominated by the quark contributions (at least for physically reasonable choices of $g \gtrsim 3$).

6.2. Nonequilibrium Langevin Dynamics With Static Heat Bath

In this section, we investigate the impact of pionic fluctuations on the relaxation dynamics of a system passing various types of phase transitions with a static background heat bath of quarks and hard meson modes. Apart from propagting the pion mean field explicitly, the meson contribution to the heat bath can also be regarded as "fluctuations" influencing the mean field dynamics. However, we needed to retune the quark-meson coupling constant in order to find the desired types of phase transition which severely affects the transition temperatures as well as the damping coefficients. Therefore, it is difficult to compare the results of the current chapter with those of the previous one and even more difficult to compare to [Nah11, NLB12, NHL$^+$13].

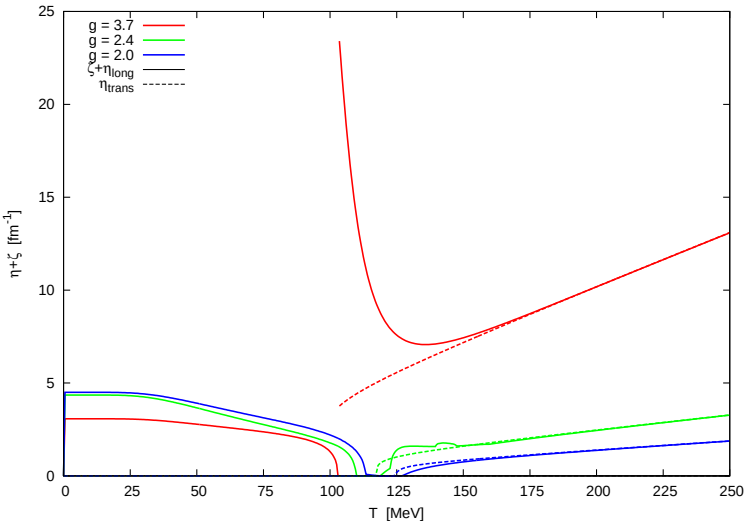

Figure 6.7.: Equilibrium values of the combined damping coefficient from quark and meson heat bath as a function of temperature for different values of the quark-meson coupling constant g. In equilibrium, the meson-meson interactions add only to the damping in longitudinal direction, i.e. in σ direction.

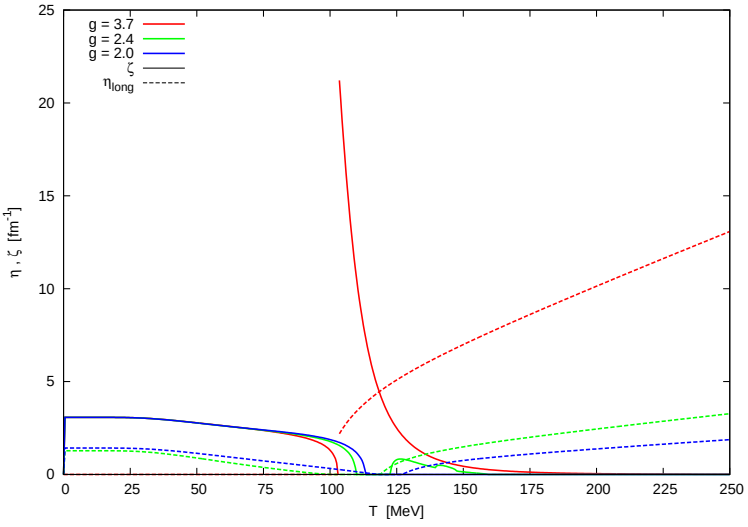

Figure 6.8.: Comparison of different contributions from quarks and mesons to the σ damping coefficient in equilibrium.

6.2.1. First Order Phase Transition

In figure 6.9 we plot the time evolution of the sigma mean field for $g = 3.7$ and a system initialized at the constant value $\vec{\varphi} = (f_\pi, \vec{0})$. For $T = 130$ MeV and $T = 150$ MeV, which is well above the phase transition, the system relaxes very quickly. Since the damping coefficient is smaller (by a factor of roughly 1/2) than for the corresponding first order phase transition setup from the previous chapter the relaxation now occurs faster. Propagting the pion mean field explicitly does not alter the dynamics of the sigma field. This may also be inferred from figure 6.10 where the time evolution of the sigma fluctuations is given. At $T = 110$ MeV which is close but still above the upper spinodal temperature of $T = 106.5$ MeV, we find that the relaxation takes very long. On the one hand, the shape of the potential is of course partially responsible for the slow relaxation. On the other hand, this effect is enhanced by the large damping at temperatures $104MeV \lesssim T \lesssim 110MeV$. Similarly to our previous findings, we see that the explicit propagation of the pion mean fields slightly slows down relaxation for the current setup. For $T = 104$ MeV which is very close to the transition temperature $T = 103.43$ MeV the system is trapped in the wrong minimum due to the large potential barrier. However, the time evolution of the mean field fluctuations indicate that the system might eventually relax on time scales larger than investigated here.

Quenching the system from the symmetric into the broken phase our findings are very similar to the corresponding ones from the previous chapter: As seen in figures 6.11 and 6.12, the sigma mean field relaxes faster if the system is quenched to a lower temperature. Further, since the field now relaxes in the opposite direction, i.e. towards larger field values, the explicit propagation of the pion fields speeds up the relaxation process. This effect becomes more pronounced as we approach the phase transition. Especially at $T = 102$ MeV the pionic degrees of freedom in the equation of motion ensure relaxation while without them the system does not entirely reach thermal equilibrium but remains partially trapped in the wrong minimum. However, as opposed to the case without the meson contributions to the potential and heat bath (see previous chapter), the system (almost) relaxes on a comparably short time scale $t \approx 40 - 60$ fm. In contrast to the previous chapter, we now also see a small oscillation at times $0 < t < 10$ fm when the sigma field is temporarily trapped in the wrong minimum. For $T = 97$ MeV, which is the lower spinodal temperature, there is just a short delay in the relaxation instead of such an oscillation.

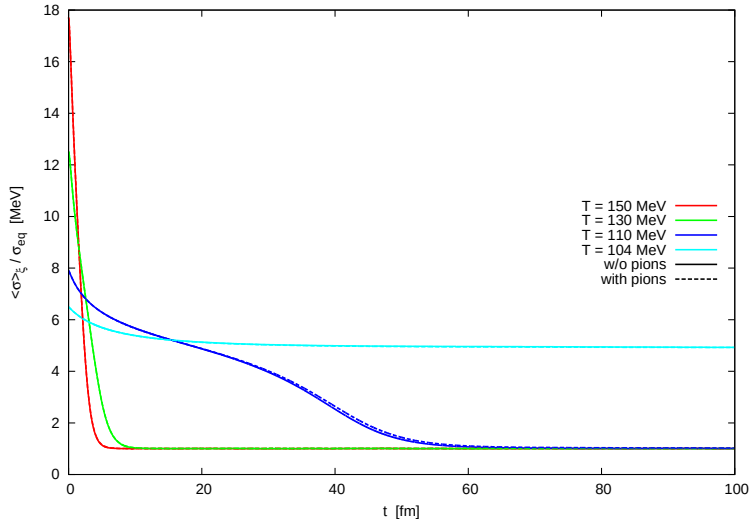

Figure 6.9.: Time evolution of the noise averaged sigma field for different temperatures in a model with first order phase transition, $g = 3.7$. Contribution from the meson propagator to the potential and the heat bath are included.

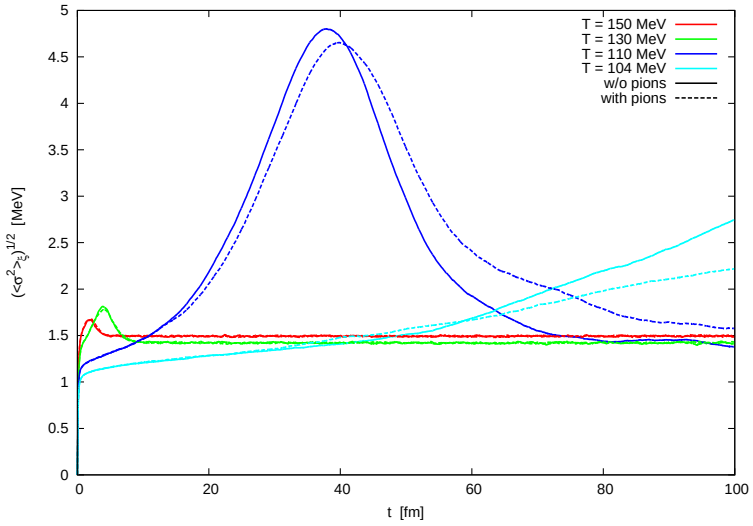

Figure 6.10.: Time evolution of the noise averaged sigma fluctuations for $g = 3.7$ for relaxation at different temperatures.

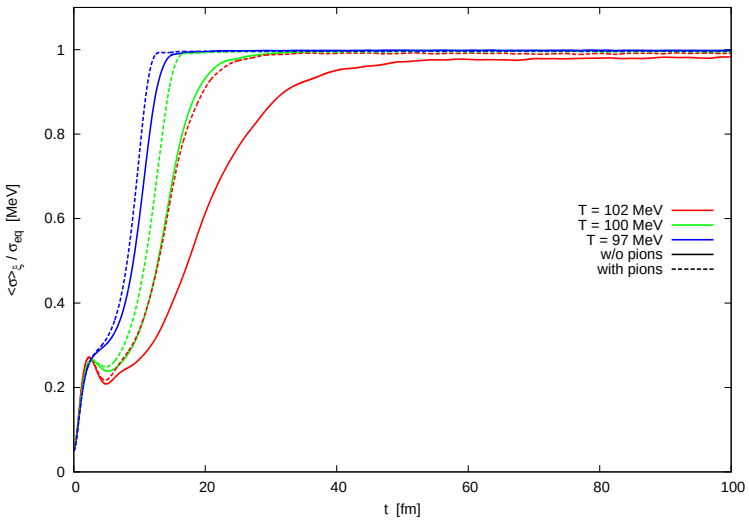

Figure 6.11.: Noise averaged sigma field in a model with first order phase transition, $g = 3.7$ quenched to different temperatures in the chirally broken phase. Contribution from the meson propagator to the potential and the heat bath are included.

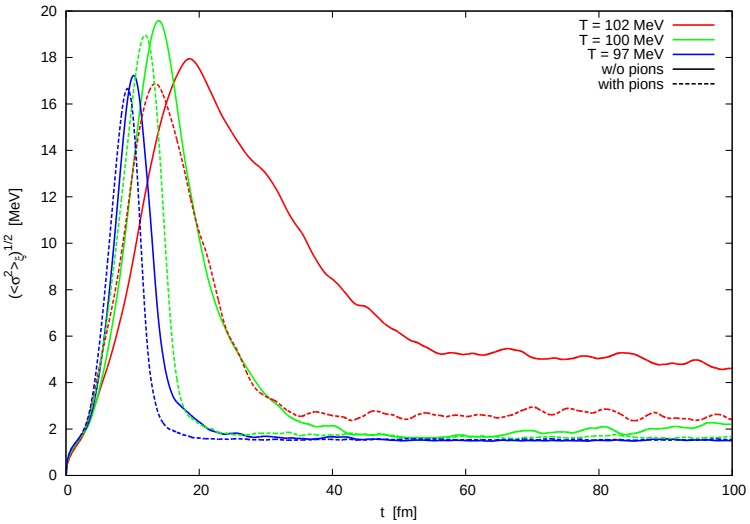

Figure 6.12.: Noise averaged sigma fluctuations for the mean field dynamics of figure 6.11.

6.2.2. Second Order Phase Transition

For the case of a second order phase transition, $g = 2.4$, the time evolution of the sigma field is given in figure 6.13 for a system initialized at the $T = 0$ vacuum expectation value. The corresponding mean field fluctuations are plotted in figure 6.14. For temperatures above as well as at the critical point, the system relaxes quickly ($t < 5 - 10$ fm) and shows damped oscillations around the thermal equilibrium. As the damping coefficients are smaller than those used in the previous chapter, the relaxation times are now much shorter which is especially noticeable at the critical point ($T = 117.5$ MeV). For temperatures above the phase transition, the explicitly propagated pionic degrees of freedom are of no ($T = 130$ MeV) or at least of minor ($T = 120$ MeV) importance for the dynamics of the sigma field. In the latter case, we observe that even without the fluctuating pion mean fields the sigma expectation value is shifted to a value slightly larger than the location of the minimum of the potential: $T = 120$ MeV is just above the critical point where the potential is flat in sigma direction over a wider range. Thus, for temperatures a little above the critical point the flat part of the potential is tilted a bit such that the minimum is in the symmetric phase, i.e. small sigma values. Therefore, in the vicinity of the minimum, the potential grows weaker with increasing than for decreasing sigma. As a consequence, the noise term in the sigma equation of motion then effectively causes the shift of the field expectation value. As we have discussed before, the pion mean fields - if included in the dynamics - tend to push the sigma field in the same direction and so the effect is more pronounced (but still very small) which is accompanied by an increase in the sigma fluctuations. At the critical point, the sigma expectation value is somewhere in the middle of the flat region of the potential and so the sigma fluctuations cancel on average. Thus, for $T = T_{crit} = 117.7$ MeV, in the absence of nonzero pion mean fields, the sigma field relaxes to the correct value while in the precence of the pion mean field dynamics it is again shifted to a higher value. The magnitude of the sigma fluctuations at the critical point is however reduced if pion mean fields are included (see discussion in previous chapter). Overall, the fluctuations become stronger towards the critical point at which we also plot the pion mean fields and fluctuations in figure 6.15. In comparison to the critical point scenario in the previous chapter, the pion mean fields still evolve noisy but they now also show more of an oscillating behaviour. This is basically due to this chapter's damping coefficients being generally smaller than their counterparts from chapter 5.

From what we observed so far, the following findings, for a system quenched from the

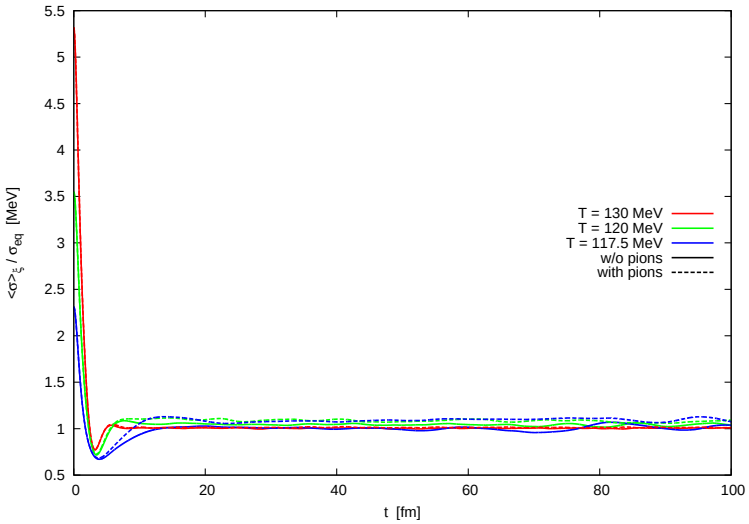

Figure 6.13.: Relaxation of the noise averaged sigma field for $g = 2.4$ for temperatures above and at the critical point of the second order phase transition.

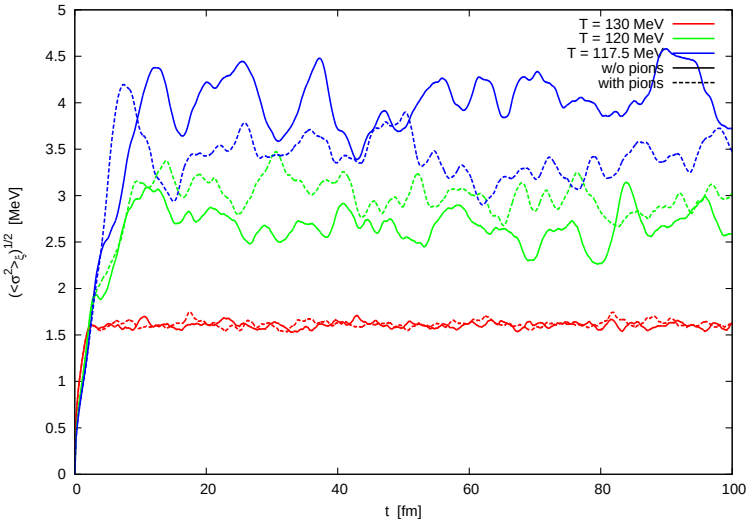

Figure 6.14.: Noise averaged sigma fluctuations for the mean field dynamics of figure 6.13.

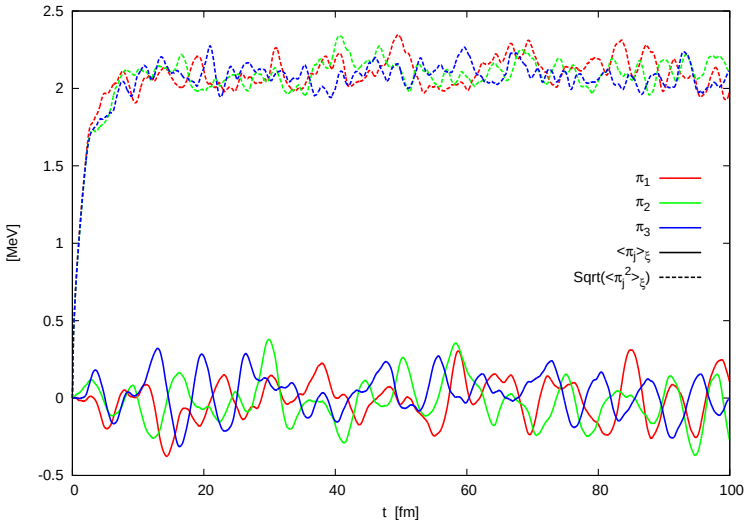

Figure 6.15.: Time evolution of the noise averaged pion mean fields and fluctuations at the critical point, $T = 117.5$ MeV.

hot into the cold phase are straightforward: Relaxation occurs much faster (and with damped oscillation around equilibrium) than for the case where we neglected the meson sector of the heat bath which is due to the smaller damping coefficients. This is seen in figures 6.16, 6.17 where the time evolution of the sigma field and fluctuations are given. For $T = 105$ MeV and $T = 110$ MeV, i.e. well below the critical point the system relaxes to the correct minimum and explicit propagation of the pion mean fields does not alter the dynamics of the chiral order parameter. Just below the critical point, namely at $T = 115$ MeV, we find that the expectation value of the sigma mean field is a little below the minimum of the potential, since now the flat part of the potential is slightly tilted in opposite direction compared to the case of $T = 120$ MeV discussed in figure 6.13 before.

6.3. Dynamics Including Reheating

In this section, we investigate relaxation dynamics of the mean fields coupled to an environment including reheating. The implementation of the energy transfer between mean fields and heat bath follows section 5.4. However, the energy density of the heat bath is now given by

$$\epsilon = \epsilon_q + \epsilon_\varphi + \epsilon_{\varphi\varphi} \tag{6.7}$$

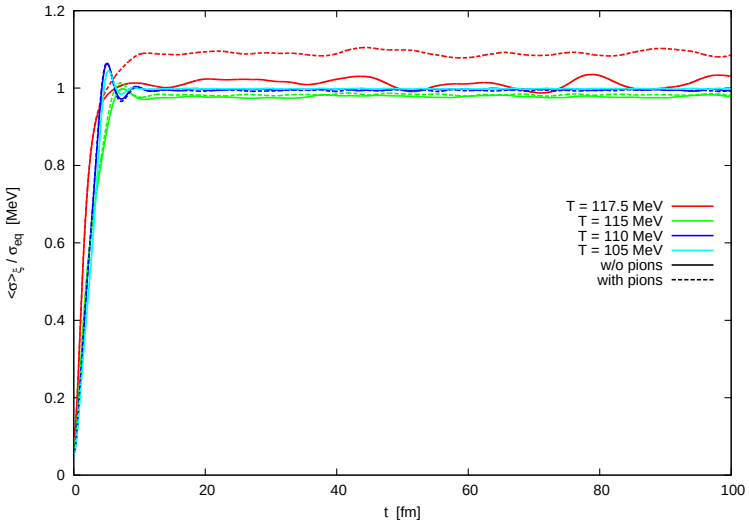

Figure 6.16.: Noise averaged sigma field for $g = 2.4$ after quench to temperatures below and at the critical point.

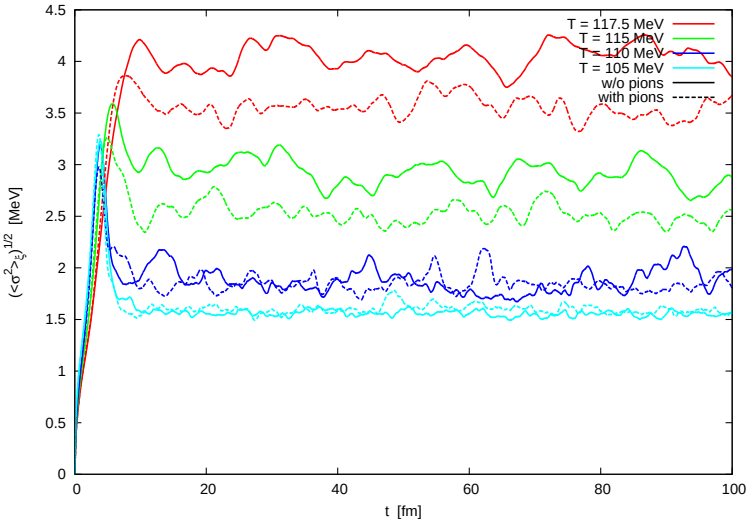

Figure 6.17.: Time evolution of the noise averaged sigma fluctuations for a system with $g = 2.4$ quenched to the chirally broken phase.

with ϵ_q from equation (5.13) and

$$\epsilon_\varphi + \epsilon_{\varphi\varphi} = V_\varphi + V_{\varphi\varphi} - T\partial_T \left(V_\varphi + V_{\varphi\varphi}\right) \tag{6.8}$$

the contributions from the hard meson modes. Since we neglect divergent contributions in the potential, these evaluate to

$$\epsilon_\varphi = \int \frac{d^3k}{(2\pi)^3} \Big(E_L \, n_B(E_L) + (N-1) \, E_T \, n_B(E_T) \Big) \tag{6.9}$$

and

$$\epsilon_{\varphi\varphi} = -\frac{\lambda}{4N} \Big(3\overline{G}^2(M_L) + (N^2-1)\overline{G}^2(M_T) + (2N-2)\overline{G}(M_L)\overline{G}(M_T) \Big) \tag{6.10}$$

with $\overline{G}(M)$ defined in equation (6.6). With reheating implemented locally as in section 5.3, the temperature could drop below $T < 97$ MeV at single lattice sites, where for small sigma values the gap equations for the meson propagator have no solutions. To avoid such a situation, we now average the temperature after each time step and thus work with a global but time-dependent temperature.

6.3.1. First Order Phase Transition

In figure 6.18 we plot the time evolution of the sigma field for a system initialized at $\sigma_{eq}(T = 180\, MeV)$ and quenched to different temperatures below the first order phase transition. The energy dissipated from the meson fields causes changes in the temperature of the heat bath as depicted in figure 6.19. Due to the limited temperature range available in our model below the phase transition (T=103.43 MeV) all considered quenches are above the lower spinodal temperature. In the previous chapter with local temperature fluctuations, we have seen a slow relaxation (if any) in this case. Now, however, things are different since we average the temperature after each time step: in the case of local temperature fluctuations, when the field at a given lattice point takes an increased value, the temperature rises accordingly until above the phase transition temperature the effective potential pushes the sigma field back to lower values. At surrounding lattice sites, the fields do not explicitly notice this particular change of temperature. On the other hand, using a global temperature as in the present case, the field may take large values at few lattice sites without being pushed back by the local potential, since this potential corresponds to the average temperature, which is

lower. At the lower end of the field distribution, the potential reflects a correspondingly higher temperature. Still, while the field relaxes, the environment heats up and the potential barrier grows. However, we now have more collective dynamics and so we see the system running up the potential barrier ($t < 1-2$ fm) and partially oscillating back once ($T_0 = 100$ MeV and $T_0 = 97.5$ MeV), accompanied by a global cooling. Thereafter ($t > 5-6$ fm), a considerable part of the sigma field relaxes to the cold phase (accompanied by renewed heating) and the system shows the extremely slow relaxation close to the first order phase transition which was also observed for the cases of a static heat bath. In the case of $T_0 = 102.5$ MeV this final stage of the relaxation (the slow part) sets in earlier, at $t \approx 0.5 - 1.0$ fm, without initial oscillation, since the transition temperature is reached. The collective character of the dynamics with a global temperature is also evident in the almost identical field values at early times. Only when the system hits the potential barrier for the first time the lines for the average sigma field start to differ (this effect can also be nicely observed for an isothermal heat bath, see e.g. figure 6.11). In the framework with local temperature fluctations the sigma field evolved differently for different quench temperatures from the start (see e.g. figure 5.20).

On inclusion of the pionic degrees of freedom, we see that during the first oscillation ($T_0 \leq 100$ MeV) the temperature is smaller ($\Delta T \approx 0.2$ MeV at the peak), since at the "inner" side of the potential wall, the nonzero pion fields mean a higher meson field energy (due to the classical potential) and so a lower temperature. When the system starts to creep over the potential barrier, we find that the pion fluctuations help in relaxing the sigma field which is in line with our previous findings. In the cases of $T_0 \leq 100$ MeV this leads to a higher global temperature. For $T_0 = 102.5$ MeV however, the majority of the system remains in the hot phase, where the nonzero pion fields raise the meson field energy and lower the temperature which on average leads to lower temperatures despite faster relaxation (as compared to the case without pion fields).

6.3.2. Second Order Phase Transition

Removing the potential barrier by considering a second order phase transition, $g = 2.4$, our findings are analogous to the critical point scenario with a pure quark heat bath. In figures 6.20 and 6.21 we give the time evolution of average sigma field and temperature respectively, for a system quenched to temperatures below the critical point and including reheating. During the relaxation the system heats up until the current

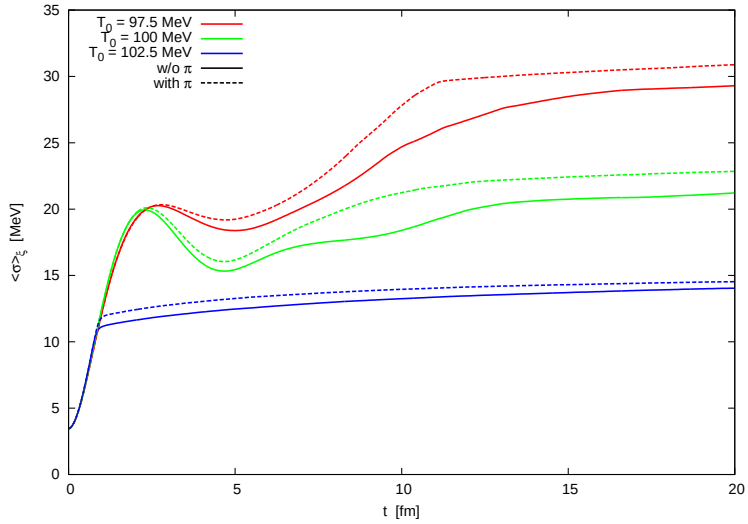

Figure 6.18.: Noise averaged sigma field as a function of time after a quench below the phase transition. The case of a first order phase transition is considered (g=3.7) and reheating of the environment is included.

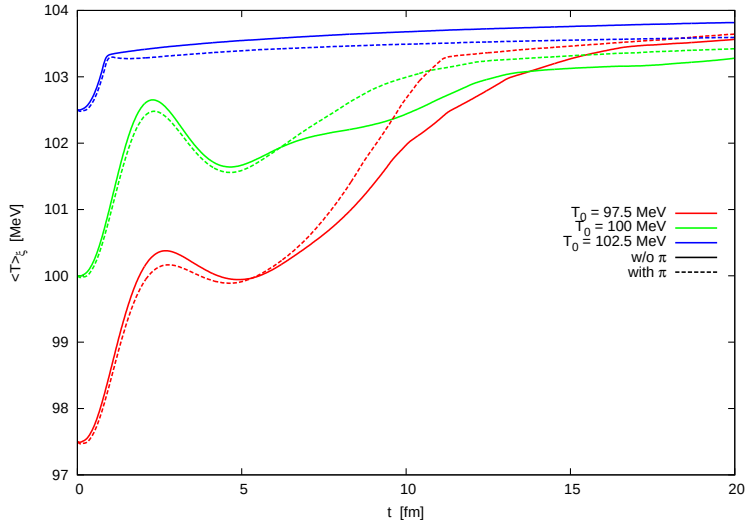

Figure 6.19.: Time evolution of noise averaged temperature in a system quenched below a first order phase transition (g=3.7) including reheating.

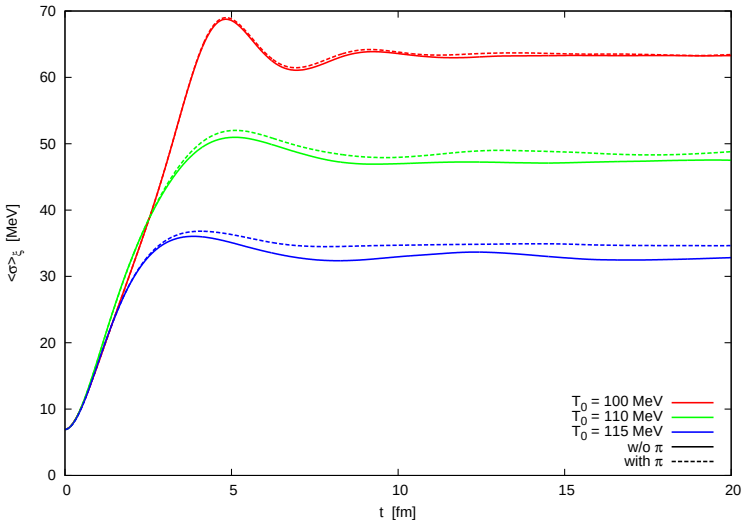

Figure 6.20.: Noise averaged sigma field as a function of time during relaxatin including reheating after a quench below the critical point of a second order phase transition (g=2.4).

field value and the temperature match for equilibrium conditions. Since in the present model the damping coefficient is lower in the corresponding case of the pure quark heat bath, the system exceeds its equilibrium configuration and performs damped oscillations around the thermal configuration. Another difference to the case presented in chapter 5 is that for early times the sigma field evolves almost identically for the various quench temperatures which is again caused by the global temperature treatment. The pionic degress of freedom have nearly no effect on the dynamics of the sigma field, except for small average shifts of sigma above equilibrium value for temperatures close to the critical point (T_{crit} = 117.5 MeV), which is the case for T_0 = 115 MeV and T_0 = 110 MeV.

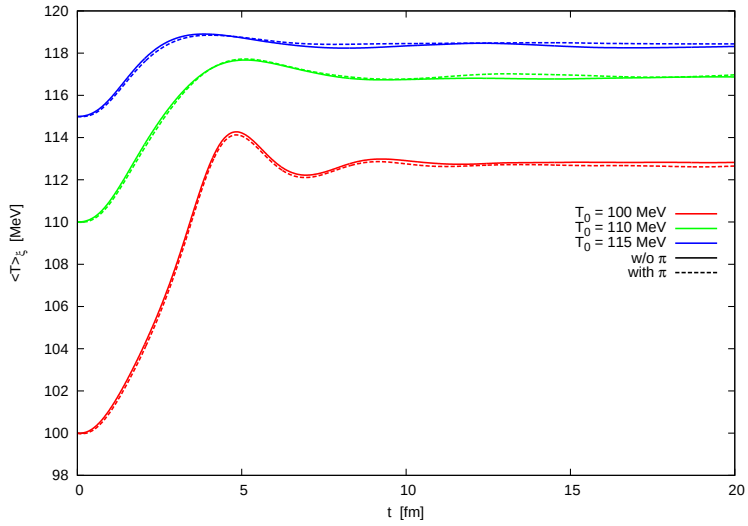

Figure 6.21.: Time evolution of noise averaged temperature for relaxation of a system with a second order phase transition (g=2.4) including reheating.

Chapter 7.

Results III - Meson Fluctuations With Expanding Background Medium

In this chapter, we want to see how the pionic fluctuations influence the dynamics of the sigma field in a more realistic setup as compared to the previous chapters. Such settings are provided in heavy ion collisions where a quark-gluon plasma is formed. The expansion and concurrent cooling of the hot fireball is often described by hydrodynamic models[1].

In [Nah11, NHL+13], the basic model, which we have extended in chaper 4, has been applied to the scenario of heavy ion collisions by evolving the heat bath in the framework of relativistic hydrodynamics. To see how our inclusion of pion fluctuations alters the dynamics of the sigma field during the expansion of a cooling background medium composed of quarks (and hard meson modes), it would thus be nice to perform calculations similar to those in [Nah11, NHL+13]. Unfortunately, we do not have access to a program code for performing such extensive numerical calculations. Instead, we rely on the simulations of heavy ion collisions performed in [Bet09] for central Au-Au collisions at a center of mass energy per nucleon of $\sqrt{s_{NN}} = 200$ GeV as seen at RHIC. In the cited reference, an ideal gas equation of state was assumed for the quark-gluon plasma and the simulation was performed in (2+1)-dimensions. The hydrodynamic evolution was incorporated by means of the so-called SHarp and Smooth Transport Algorithm (SHASTA) [BB73, BBH75, RBM95, RPM95]. We have been provided with two-dimensional tem-

[1] Introductions to relativistic hydrodynamic modelling of heavy ion collisions can be found in many works and textbooks. The idea of applying hydrodynamics to describe the outcome of collider experiments dates back to Landau [Lan53]. Since then, the field has seen great development. For an older review article on the subject, see e.g. [SG86], while a more recent review is given by [DdSKK16].

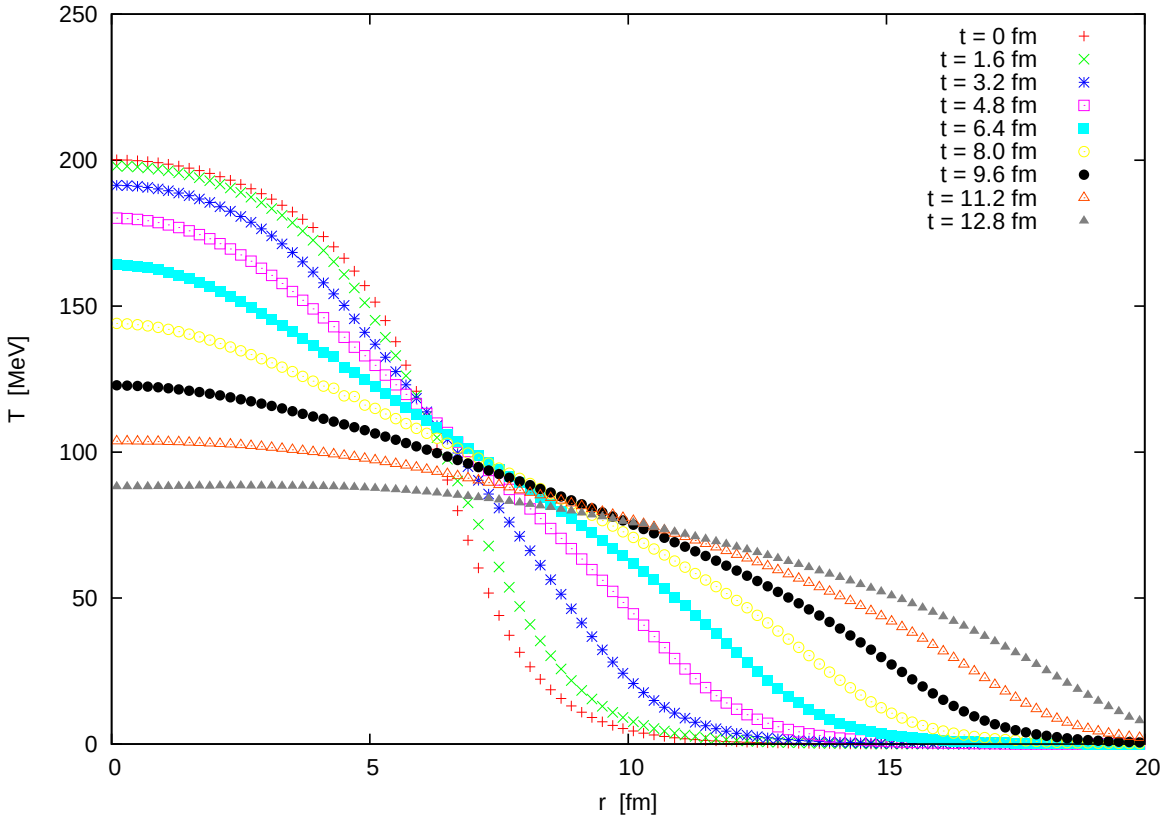

Figure 7.1.: Temperature profiles used as input for expanding background medium. The data is the outcome of numerical simulations peformed in (2+1) dimensions for central Au-Au collisions [Bet09], and has been provided by the cited author.

perature profiles for different times during the expansion of the plasma. They describe the temperature distribution in the plane transversal to the collision axis. We use these temperature profiles as input for the heat bath. They are plotted in figure 7.1 along the radial coordinate in the transversal plane. Since a central collision is assumed, the profiles are radially symmetric.

7.1. Pure quark heat bath

We initialize the meson fields at their local thermal equilibrium values corresponding to the temperature profile at $t = 0$ in figure 7.1. With the time evolution of the temperature, the effective potential as well as the damping coefficient and the noise correlators

also change. For the latter two we use equilibrium values determined by the current temperature at each lattice site respectively. In our first set of runs we neglect meson contributions to the heat bath and the potential, i.e. we use the same model as in chapter 5.

7.1.1. First order phase transition

To begin with, we investigate how the meson fields behave during the expansion and cooling of the heat bath if the system passes a first order phase transition, i.e. we choose $g = 5.5$. In figures 7.2, 7.3 the deviation of the sigma field from its local equilibrium value is given at different times. Whether we include the pion mean fields in the equation of motion or not has no effect on the dynamics of the sigma field in this case. At early times, the laplacian operator in the equation of motion dominates at the phase transition and the field distribution is smoothed out. This is why we find a sudden sharp increase followed by a jump to large negative values which quickly decays for increasing radius. An effect of the expanding medium is however seen in the different magnitude of the peaks: for succeding time steps the radial coordinate where the phase transition occurs decreases and so the smoothed out field configuration follows. However, due to the damping and the potential barrier which the sigma field has to overcome at the first order phase transition the sigma field lags behind the thermal equilibrium value leading to a slightly decreased inner peak and a more pronounced increase in the outer peak. During further time evolution, this effect becomes even stronger until the inner peak vanishes between $7\ fm < t < 8\ fm$ and we have a ring in the x-y plane, where the system sits in the wrong minimum. This ring then becomes broader (up to a thickness of about 1 fm at $t = 9$ fm) until at $t = 10$ fm the whole of the background heat bath has passed to the chirally broken phase. In the central area with radius $r \lesssim 2.5$ fm this transition is like a sudden quench and in this domain the system remains temporarily trapped in the wrong phase. Although this area shrinks from $t = 10$ fm to $t = 12$ fm we cannot continue the time evolution any further for lack of input data.

At this point, we could start to think about possible signatures of the meson fluctuations at the phase transition to be tested by collider experiments. This would lead us straight to the topic of particle production. However, we will first have a closer look at the spatial fourier modes of the chiral fields. For this purpose, we extend the spatial field distribution by placing it in the middle of a larger lattice with $N = 256$ lattice sites

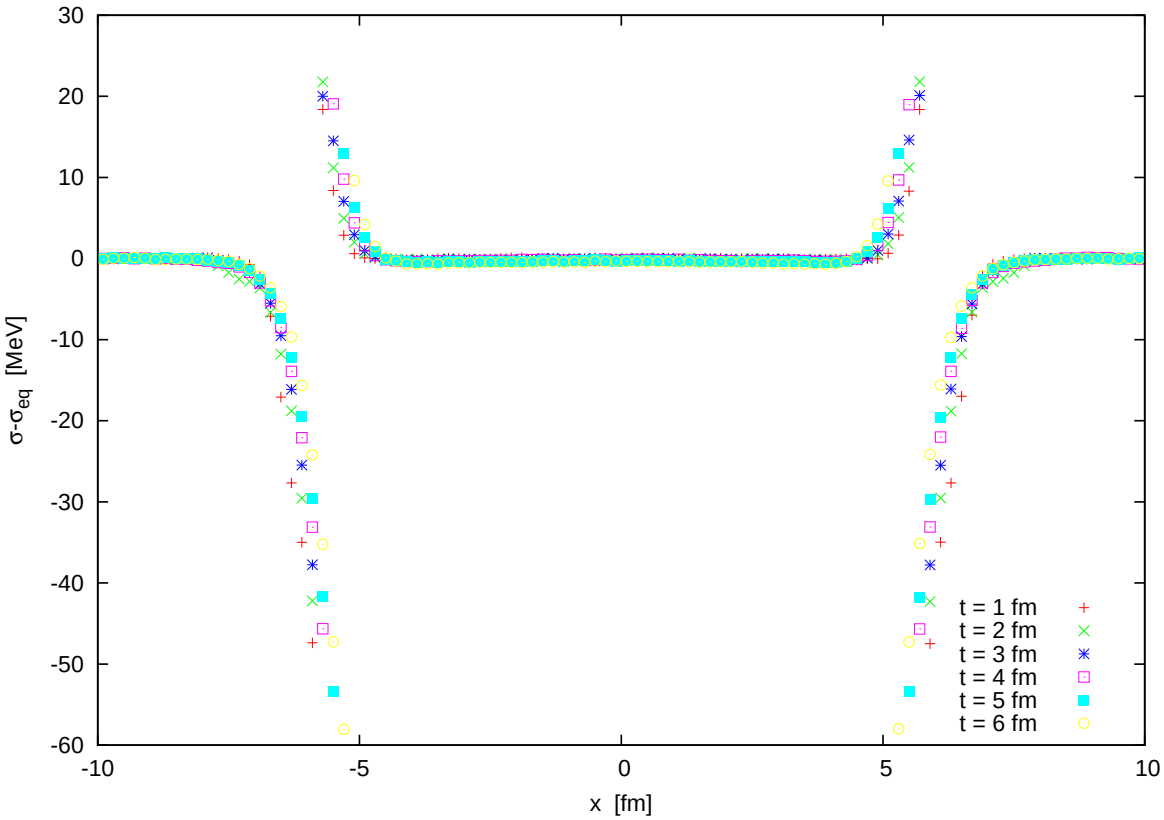

Figure 7.2.: Deviation of the sigma field from its equilibrium value along the spatial x-axis for a system with an expanding background medium at different times. The mesonic sector of the heat bath is neglected and the pion mean fields are kept fixed at zero.

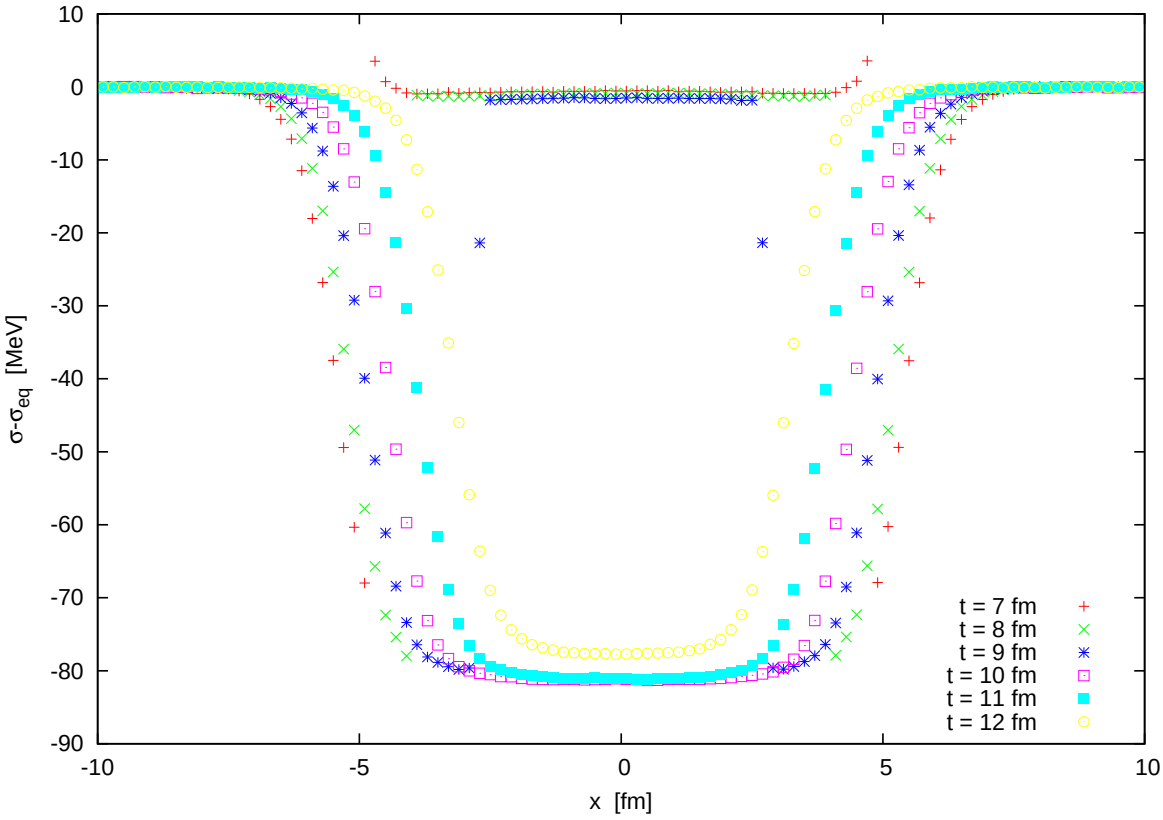

Figure 7.3.: Same as in figure 7.2 but for later times.

in each direction (i.e. $L = 51.2$ fm for a lattice spacing of $\Delta x = 0.2$ fm) and apply a fast fourier transorm [PTVF02]. At the additional lattice points we assume $T = 0$ and $\sigma - \sigma_{eq} = 0$. Due to the radial symmetry of the system we expect the fourier transform of $\sigma - \sigma_{eq}$ to be real valued. Of course, with the noise field in the equation of motion this symmetry is not exact, but we can expect it to have negligible influence on the low momentum modes while it will eventually become important with increasing radial momentum. So let us assume that $\sigma - \sigma_{eq}$ is radially symmetric and let us further assume, that we can approximate the shape of $\sigma - \sigma_{eq}$ e.g. at $t \approx 4 - 5$ fm in figure 7.2 by a superposition of gaussian curves:

$$f(x) = a\left(e^{-\alpha(x-x_0)^2} + e^{-\alpha(x+x_0)^2}\right) - b\left(e^{-\beta(x-x_0')^2} + e^{-\beta(x+x_0')^2}\right) \tag{7.1}$$

with $a, b, \alpha, \beta > 0$. The fourier transform fulfills then

$$f(k) \propto a\, e^{-k^2/4\alpha}\left(e^{ix_0k} + e^{-ix_0k}\right) - b\, e^{-k^2/4\beta}\left(e^{ix_0'k} + e^{-ix_0'k}\right) \tag{7.2}$$

and thus for $\alpha \approx \beta$

$$f(k) \propto e^{-k^2/4\alpha}\left(2a\, cos(x_0k) - 2b\, cos(x_0'k)\right) \tag{7.3}$$

Using

$$cos^2(x) = \frac{1}{2}(1 + cos(2x)) \tag{7.4}$$

$$cos(x)cos(y) = \frac{1}{2}(cos(x+y) + cos(x-y)) \tag{7.5}$$

and assuming $x_0 \approx x_0'$ we find for the squared absolute value of $f(k)$:

$$|f(k)|^2 \propto e^{-k^2/2\alpha}\frac{(a-b)^2}{2}(1 + cos(2x_0k)) \tag{7.6}$$

Thus, we expect the squared amplitude of the fourier transform of $\sigma - \sigma_{eq}$ to be exponentially suppressed and to vanish periodically. For $t \approx 4 - 5$ fm it is $x_0 \approx 5.5$ fm (from figure 7.2) and so this period is approximately

$$\Delta k = 2\pi/2x_0 \approx 113\, MeV \tag{7.7}$$

In figure 7.4 we plot the absolute value of the fourier transform of $\sigma - \sigma_{eq}$ at $t = 4.8$ fm which confirms our expectations: the modes are periodically damped and we find e.g. approximately 13.5 full periods between $0 < |k| < 1.5$ GeV in agreement to our rough estimate, $1.5\,GeV/113\,MeV \approx 13.3$. Further, the modes decrease linearly on the logscale plot for about $100\,MeV \lesssim |k| \lesssim 1500\,MeV$. Below and above these values, our approximations $x_0 \approx x_0'$ and $\alpha \approx \beta$ are not good enough as $exp(-k^2/4\alpha) \neq exp(-k^2/4\beta)$ for small (but finite) k respectively $k(x_0 - x_0') \gtrsim 1$ for large k in the argument of the cosine. Further, for momenta $k > 1.5$ GeV the noise induced sigma fluctuations lead to a correspondingly noisy spectrum. What we also infer from figure 7.4 is that the explicit propagation of the pion mean fields does not change the spectrum of the sigma deviations. For times $1\,fm < t < 6\,fm$, x_0 and x_0' decrease slightly over time (cf figure 7.2) and so the period in the mode spectrum grows accordingly.

At $t = 8$ fm we see from figure 7.3 that we can approximately describe the mode spectrum with equation (7.6) in the limit $a = 0$. Since the width of the peak has increased compared to times $t < 6$ fm, we expect a stronger suppression of modes for increasing momentum. Further, the period in the spectrum is supposed to be larger than at lower times due to the reduced radial coordinate of the phase boundary. This is exactly what we find for the spectrum at $t = 8.0$ fm, plotted in figure 7.5. When the heat bath has passed through the phase transition everywhere and at the center the sigma field is trapped in the wrong minimum, we obatin even stronger exponential suppresion of the modes, because we might think of the coordinate space distribution (see figure 7.3) as consisting of two very broad gaussian curves which overlap. From figure 7.6 we see that at $t = 9.6$ fm the exponential suppression of the modes is so strong that already above $|k| \approx 1.3$ GeV we find only a white noise spectrum from the stochastic force in the langevin equation of motion. At smaller momenta we still find the periodic structure of the spectrum. The corresponding period increases further for later times as the area with the sigma field in the wrong phase becomes smaller.

The total number of sigma particles[2] produced in the x-y-plane is given by [ACBL97,

[2]To be precise, dN/d^dk is the intensity of fluctuations. At later times during relaxation, when the evolution of the system can be approximated by a linearized equation of motion, N can be interpreted as the number of particles emitted. However, we will mostly refer to N as the number of particles straight away.

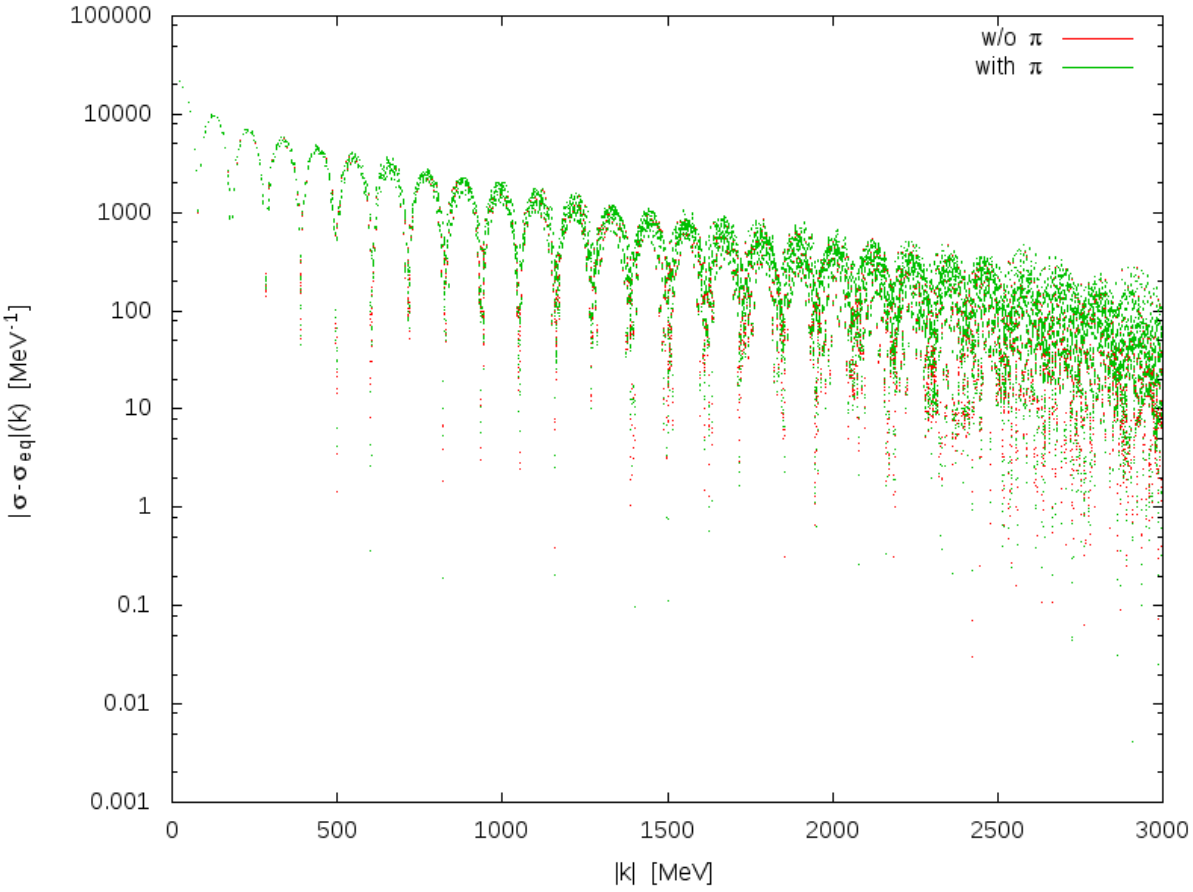

Figure 7.4.: Absolute value of the fourier transformed sigma field deviations $\sigma - \sigma_{eq}$ from thermal equilibrium for a system with an expanding background medium at $t = 4.8$ fm and with $g = 5.5$.

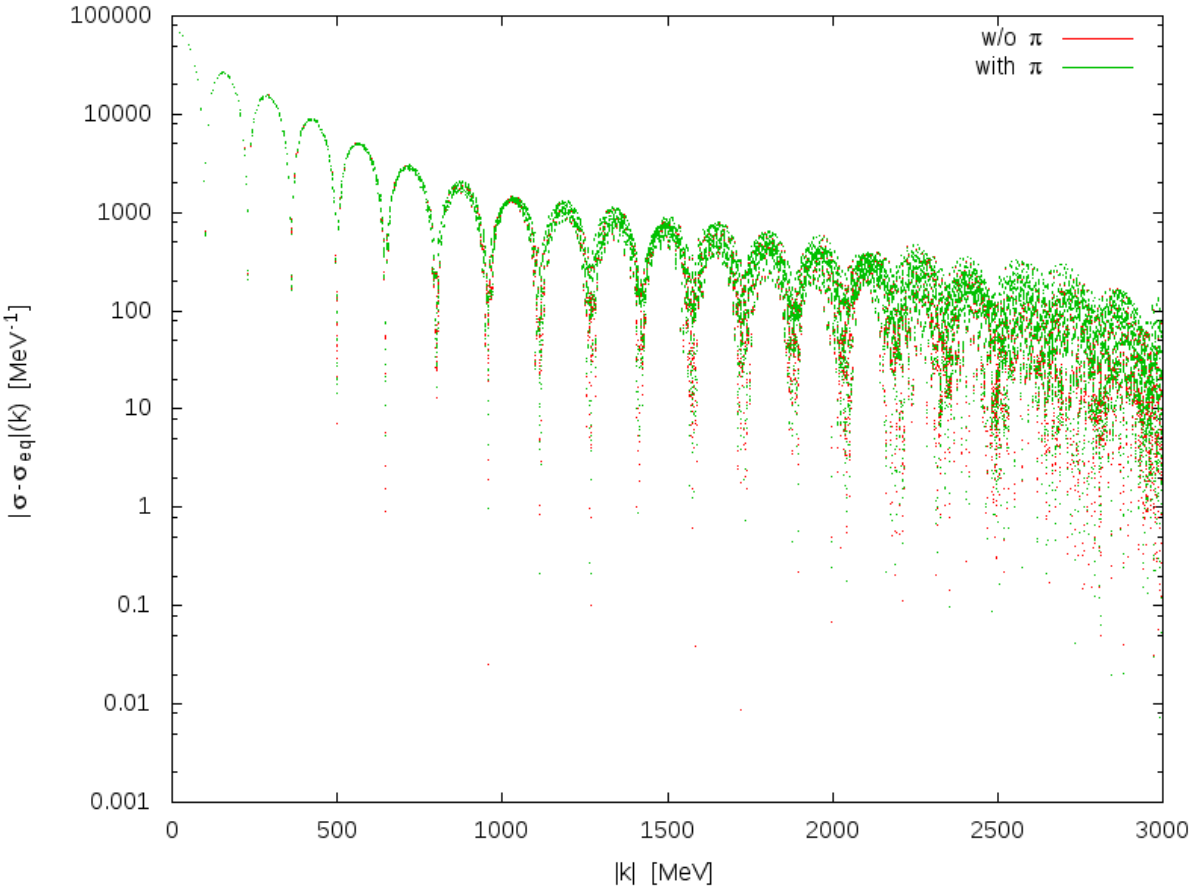

Figure 7.5.: Absolute value of the fourier transformed sigma field deviations $\sigma - \sigma_{eq}$ from thermal equilibrium for a system with an expanding background medium at $t = 8.0$ fm and with $g = 5.5$.

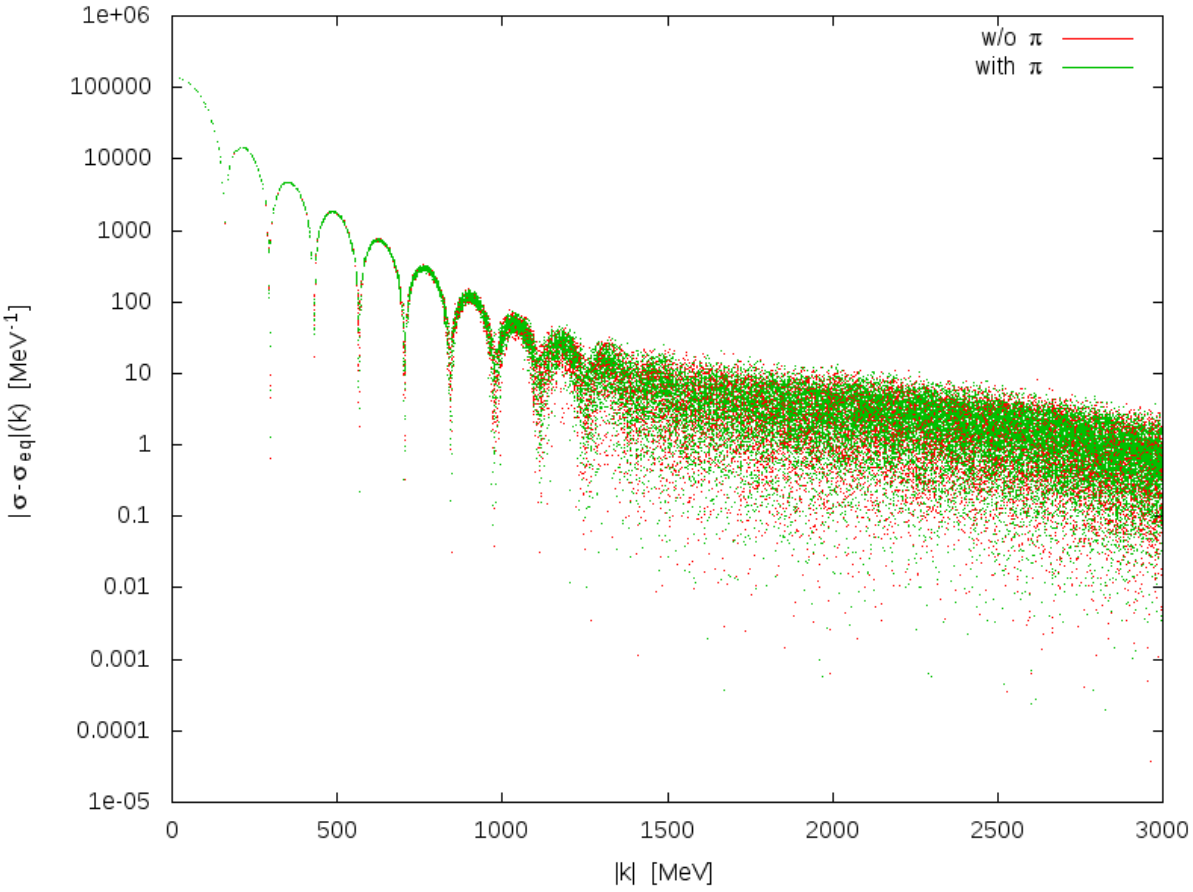

Figure 7.6.: Absolute value of the fourier transformed sigma field deviations $\sigma - \sigma_{eq}$ from thermal equilibrium for a system with an expanding background medium at $t = 9.6$ fm and with $g = 5.5$.

AB97]:

$$\frac{dN_\sigma}{dz}(z=0) = \int \frac{d^2k}{(2\pi)^2\, 2\omega_k} \left(\omega_k^2 |(\sigma - \sigma_{eq})_k|^2 + |\partial_t \sigma_k|^2\right) \tag{7.8}$$

and correspondingly for the pions. $\omega_k = \sqrt{k^2 + m^2}$ is the energy of the modes. In figure 7.7 we plot the number of sigma particles produced for different momenta during the expansion of the heat bath. In figure 7.8 the corresponding number of pions, summed over the three species, is given. We see at first glance that the total number of pions produced directly is negligible compared to the number of sigma particles. At early times, $t \approx 1-3$ fm the the number of sigma particles drops slightly which coincides with the decrease in the negative valued peaks in figure 7.2 where the smoothing out of the sigma field by means of the laplacian operator in the equation of motion is important. Then, during further expansion and cooling the particle numbers grow throughout all low momentum modes until they peak at $9\, fm < t < 10\, fm$ when at the central area the field gets trapped in the wrong phase. Afterwards while the this part of the system melts (or better: cools) away the particle numbers decrease again. In the time evolution of the produced particles we see a signature of the periodic spectrum, most prominently for $8\, fm < t < 1\, fm$ when the line for $150\, MeV < |k| < 200\, MeV$ rises while the line for the neighbouring modes, $100\, MeV < |k| < 150\, MeV$, drops before quickly swapping their order of magnitude. This happens when the periodic suppression of modes passes from one momentum range to the other, as the period increases with time. While on the log-scale plot we can see better what is happening during relaxation, we give the same plot again on a linear scale in figure 7.9, which is a more familiar form and allows for a comparsion to [Nah11, NHL$^+$13]. In agreement to the cited works, we also find a drastic increase in particle numbers produced in the soft mode fluctuations the moment the heat bath cools below the phase transition in the central area while the sigma field is trapped in the wrong minimum. Since our number of particles calculated in two dimensions is actually a line density in three dimensions, we can obtain a dimensionless number, by multiplying with a length. Choosing e.g. $dz \sim 1-2$ fm, we obtain particle numbers of the same order of magnitude as for instance in [Nah11, NHL$^+$13] for the case of temperature dependent damping coefficients. In contrast to the cited works, the major increase in the particle numbers arises at later times, in [Nah11] the phase transition of the heat bath occurs already at $2\, fm < t < 6$ depending on the particular scenario under consideration. This could result from the fact that we impose the time evolution of the heat bath externally. Thus, we do not account for possible backreactions of the sigma field on the heat bath which as we saw in the previous chapter, may cause serious

increase in temperature and would therefore probably drive the expansion of the heat bath instead of lagging behind. Another difference to the findings in the cited works is the relative height of the particle numbers for $|k| > 100$ MeV. Especially a swapping of the lines such as seen at $t = 9$ fm in figure 7.9 is not found in [Nah11, NHL$^+$13]. However, in the cited works an elliptic initial temperature profile in the x-y-plane is chosen corresponding to an off-center collision. In our case of a central collision we obtain the periodic suppression in the mode spectrum.

Finally, we note that figure 7.9 does not change if we include or neglect the pion mean fields as explicitly propagated degrees of freedom. However, this could as well be a consequence of the externally imposed temperature of the heat bath, i.e. the time evolution of the fields is driven by the expansion and cooling of the background. If the meson fields had an impact on the time evolution of the heat bath by means of local reheating, the pionic degrees could be expected to show a noticeable effect on the relaxation of the entire system.

7.1.2. Second order phase transition

If we switch to a model with a second order phase transition, $g = 3.63$, the time evolution of $\sigma - \sigma_{eq}$ is quite different from the findings of the previous section. At earlier times, $0 < t < 6$ fm we find in figure 7.10 a partially familiar profile of $\sigma - \sigma_{eq}$ along the x-axis. The continuous but nevertheless rather sharp change in sigma values at the phase transition is smoothed out by the laplacian operator in the equation of motion. This causes the sigma field to exceed the equilibrium value when approaching the phase transition from the hot phase (i.e. from a lower radial coordinate) and falling below equilibrium value when approaching the transition from the cold phase. However, in contrast to the dynamics with a first order phase transition there is no potential barrier between the two phases. Thus, in the vicinity of the critical point the sigma field is less confined along the flat bottom of the potential and can fluctuate more. Furthermore, the field cannot be trapped in a wrong position and so the peaks of $\sigma - \sigma_{eq}$ at both sides of the phase transition tend to be about equally large for $t \leq 4$ fm (and also coincide roughly with the height of the hot phase peak of the first order scenario). However, when the expansion driven dynamics begin to dominate, i.e. for $t \geq 5$ fm, we find again that the peak in the hot phase shrinks while in the cold phase it grows accordingly. Due to lack of the potential barrier, the cold phase peak remains at about half the magnitude

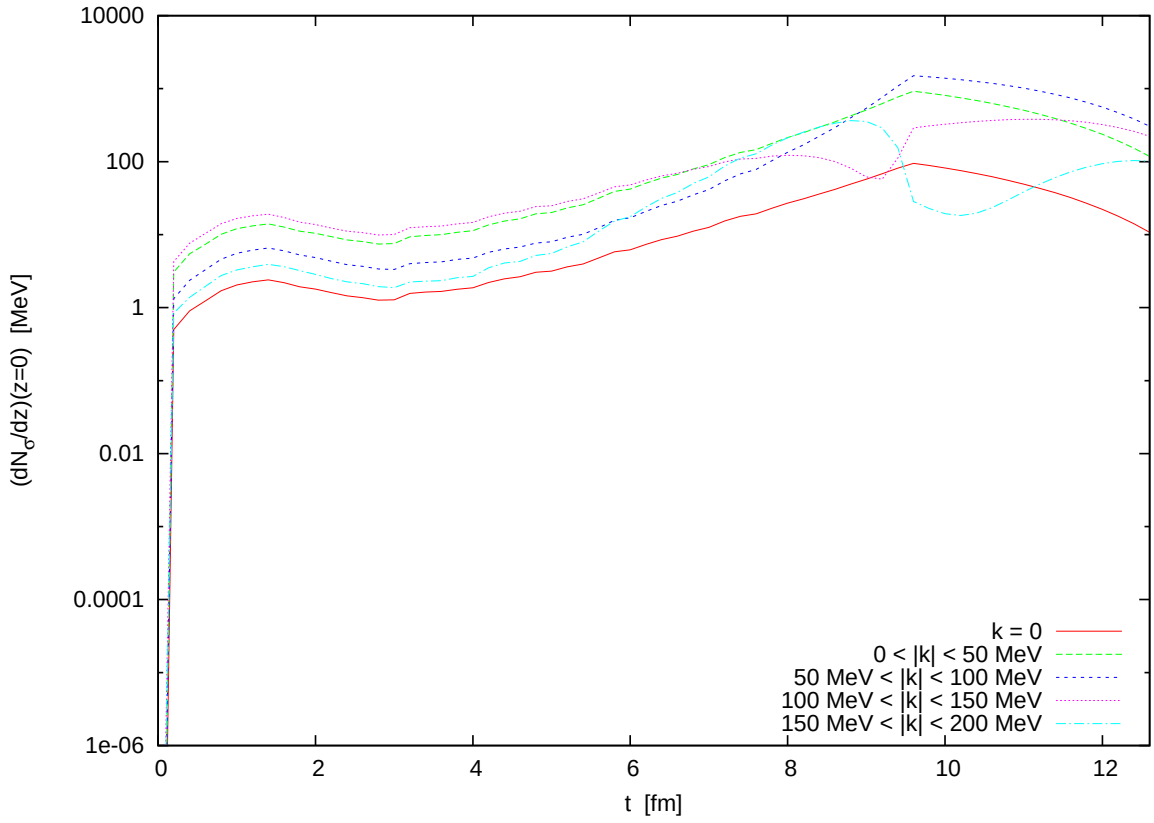

Figure 7.7.: Number of sigma particles produced in the x-y-plane within different momentum ranges for $g = 5.5$ on a logarithmic scale.

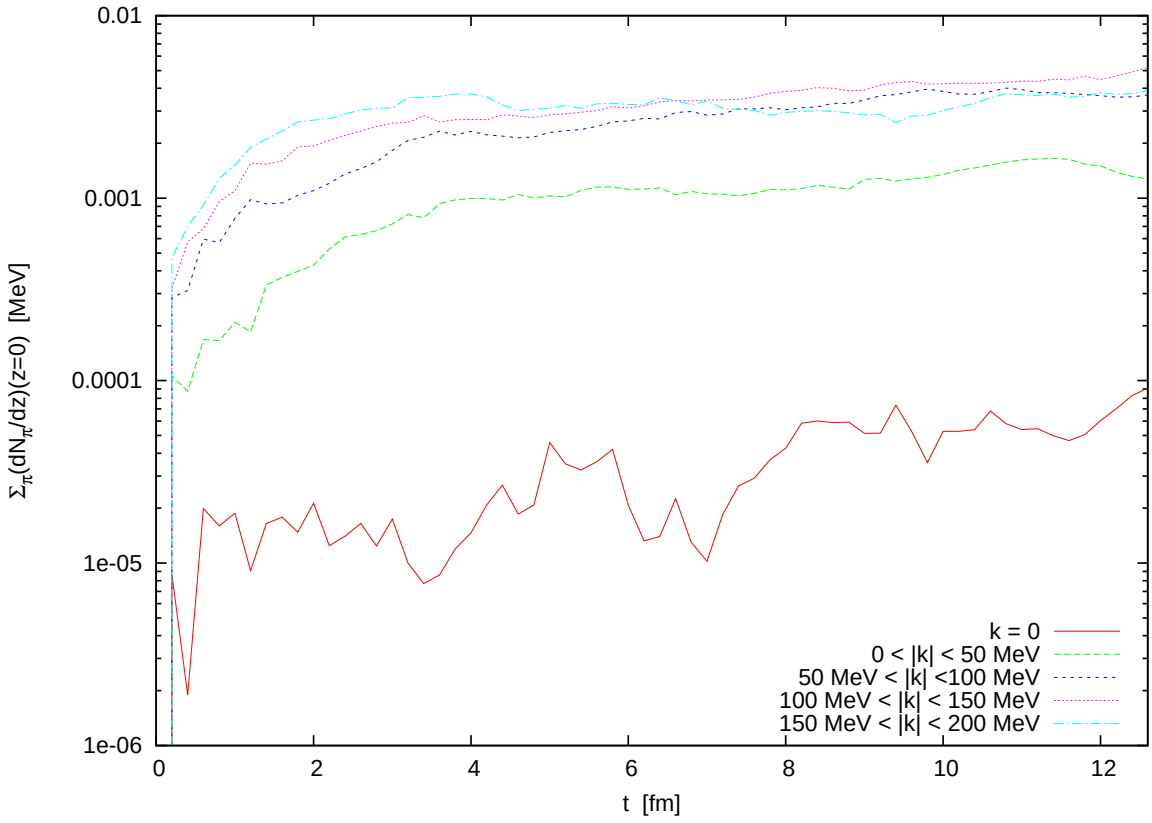

Figure 7.8.: Total number of pions produced in the x-y-plane for different momenta during expansion of the background medium for $g = 5.5$.

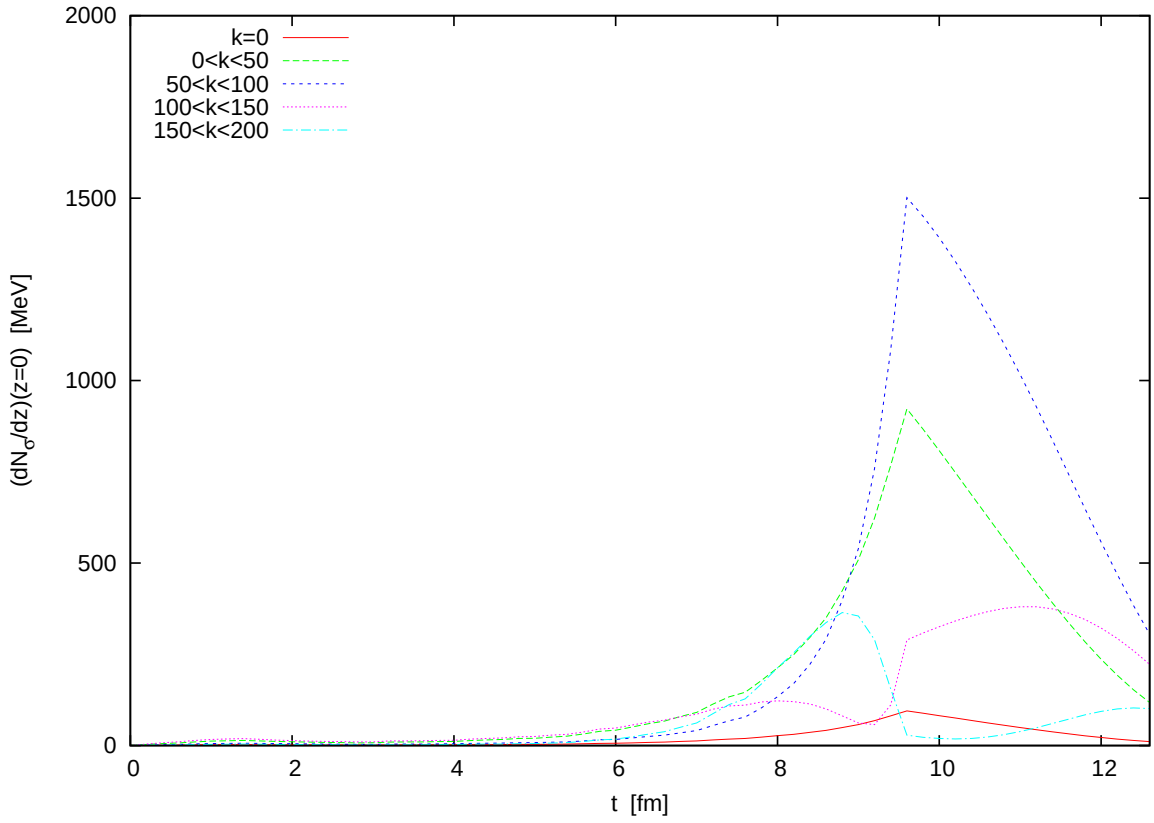

Figure 7.9.: Number of sigma particles produced in the x-y-plane within different momentum ranges for $g = 5.5$ on a linear scale.

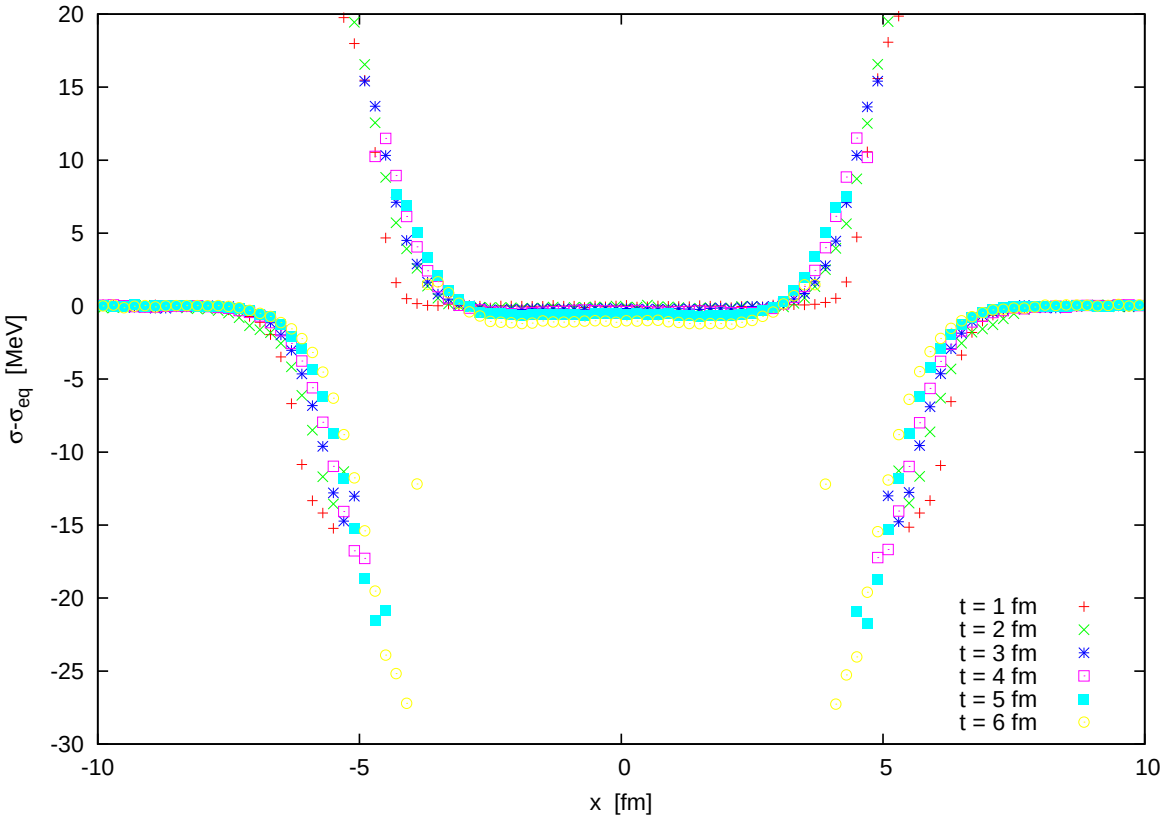

Figure 7.10.: Deviation of the sigma field from thermal equilibrium along the x-axis at different times during the expansion of the pure quark heat bath in a model with a second order phase transition, $g = 3.63$.

of the corresponding first order case for $t < 6$ fm. Since for $g = 3.63$ the phase transition occurs at a higher temperature than for the model with $g = 5.5$, the expanding heat bath drives the chiral fields through the phase transition a little earlier and the phase boundary is at a smaller radial coordinate. In the center of the x-y-plane, the phase transition now occurs between $8\ fm < t < 9\ fm$ as can be seen from figure 7.11 where the profile of $\sigma - \sigma_{eq}$ along the x-axis is plotted for later times. Because of the missing potential barrier the transition between hot and cold phase is not as sharp ($t = 7 - 8$ fm) and the central area where the sigma field is quenched into the cold phase ($t = 9$ fm) shrinks quickly as the field relaxes. At $t = 12$ fm we see that the system overshoots thermal equilibrium. Thereafter, the system would perform damped oscillations around the equilibrium values.

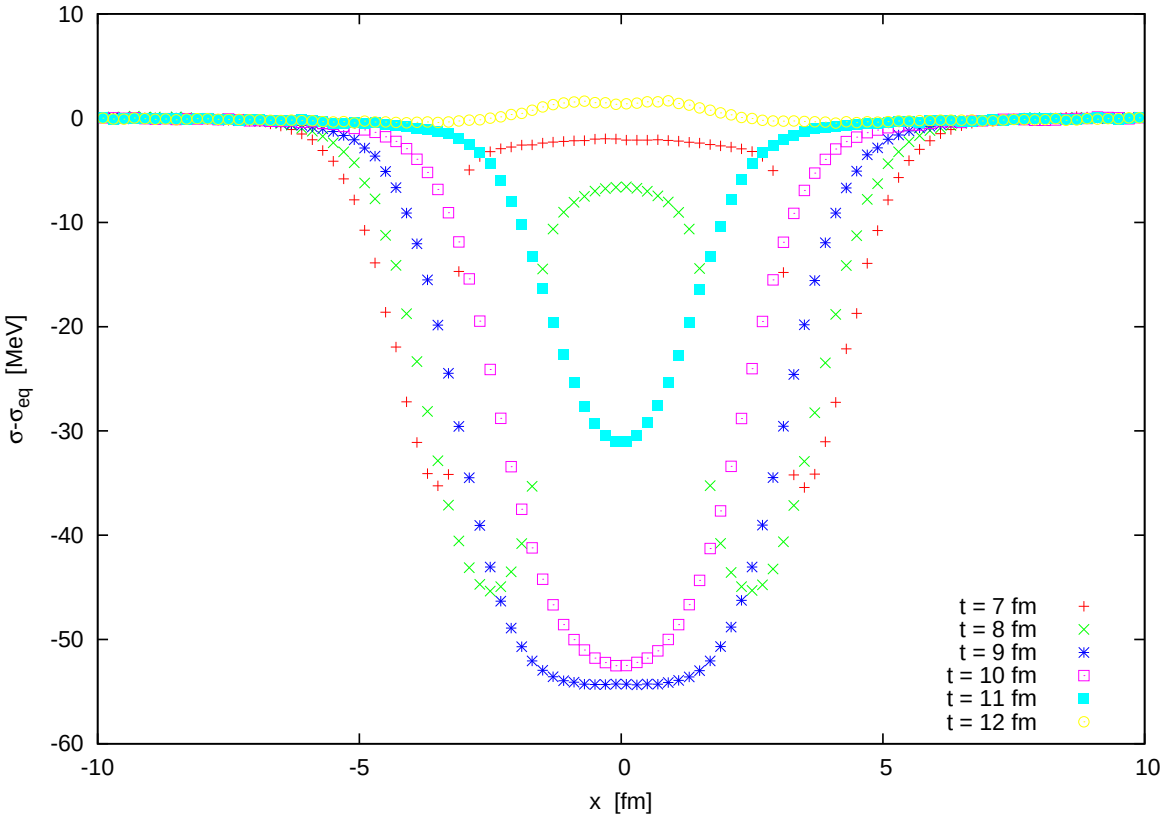

Figure 7.11.: Same as in figure 7.10 but for later times.

In figure 7.12 we plot the absolute value of the spatial Fourier modes of $\sigma - \sigma_{eq}$ for time $t = 1.6$ fm. We see again the periodic structure of the mode spectrum which we can roughly describe by our previously discussed approximation of the fields in coordinate space by gaussian curves. This also explains the (approximately) exponential suppression of the modes. What is new in figure 7.12 is that the low momentum modes are heavily suppressed. This is because the peaks in figure 7.10 on both sides of the phase boundary are of comparable magnitude but of opposite sign. Therefore, the overall offset of the field distribution (or better, its spatial average) is very small and so are the modes for $k \to 0$. When the inner peak in the coordinate space distribution of $\sigma - \sigma_{eq}$ vanishes during the expansion and cooling of the heat bath and the expansion of the heat bath dominates the meson field dynamics, the spatial average of the $\sigma - \sigma_{eq}$ distribution has a significantly larger absolute value than at early times and so, the low momentum modes are no longer suppressed. This can be seen e.g. at $t = 6.4$ fm in figure 7.13. Also, since the radial coordinate corresponding to the phase transition temperature has decreased we find an accordingly larger perdiod in the mode spectrum at $t = 6.4$ fm as compared to the case of $t = 1.6$ fm from figure 7.12. For $t = 9.6$ fm, the heat bath is in the chirally broken phase and in the central area of the x-y-plane the system has only just started to relax and follow the heat bath into the cold phase. In the corresponding spectrum of $\sigma - \sigma_{eq}$, figure 7.14 we see an according enhancement of the low momentum modes. We also infer from the figure, that the distribution in coordinate space may still be approximated by two partially overlapping gaussian curves which leads to the seemingly periodic structure in the spectrum fo $|k| < 700$ MeV. However, these two gaussian curves are wider than in approximations at earlier times leading to a heavy exponential suppression of the modes such that for $k > 700$ MeV the spectrum corresponds to white noise. For later times, i.e. while the field in the central area of the x-y-plane relaxes further, the period in the spectrum increases as well as the exponential suppression. With the system slightly overshooting equilibrium and then oscillating around it only the softest modes $k < 50 - 100$ MeV are enhanced enough to be discernible from the noise.

The number of particles produced by the sigma fluctuations within different ranges of (low) momentum during the expansion are plotted in figure 7.15. Overall, the number of particles produced in each momentum range is smaller than its counterpart from the first order scenario by a factor of ≈ 3 at early times and ≈ 10 later. Similarities to the case with a first order phase transition are the temporary decrease in the particle

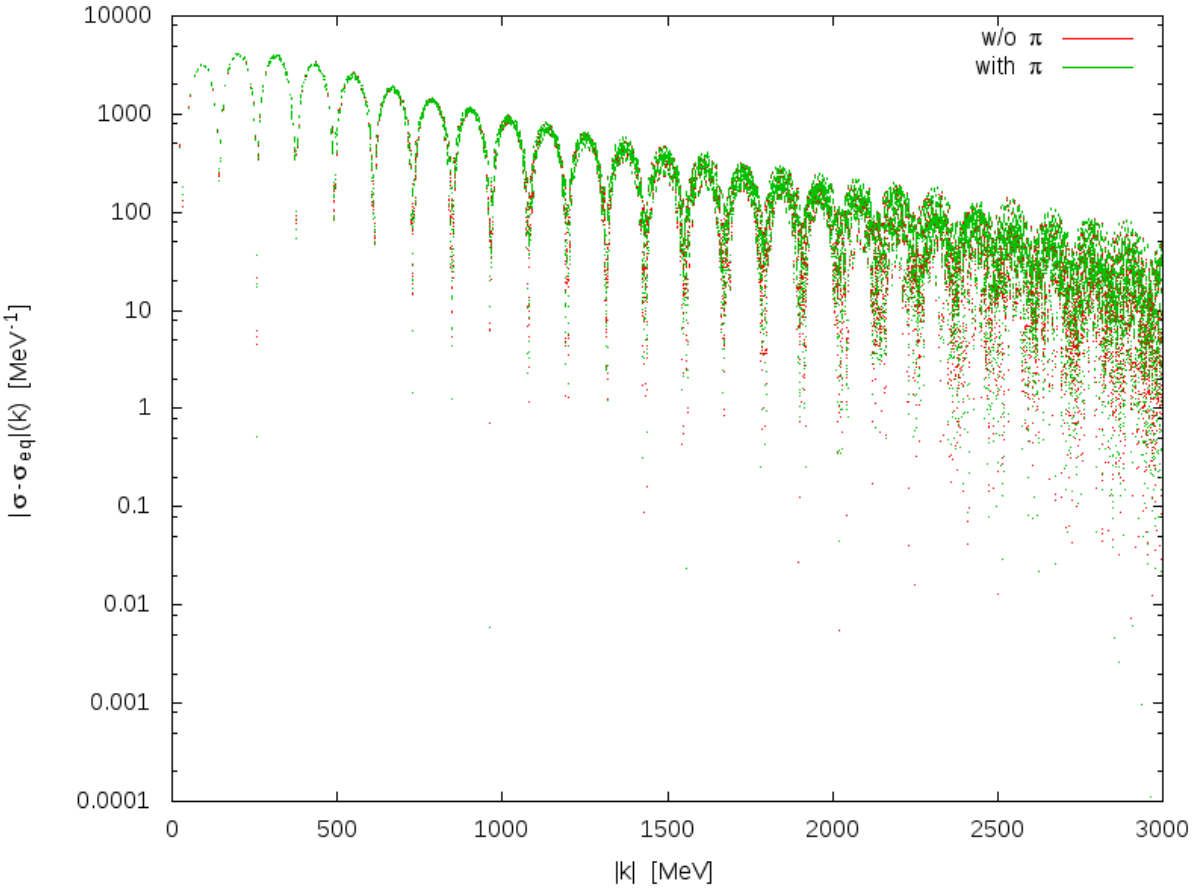

Figure 7.12.: Spatial Fourier modes of $\sigma - \sigma_{eq}$ for a model with an expanding heat bath of quarks at $t = 1.6$ fm and $g = 3.63$.

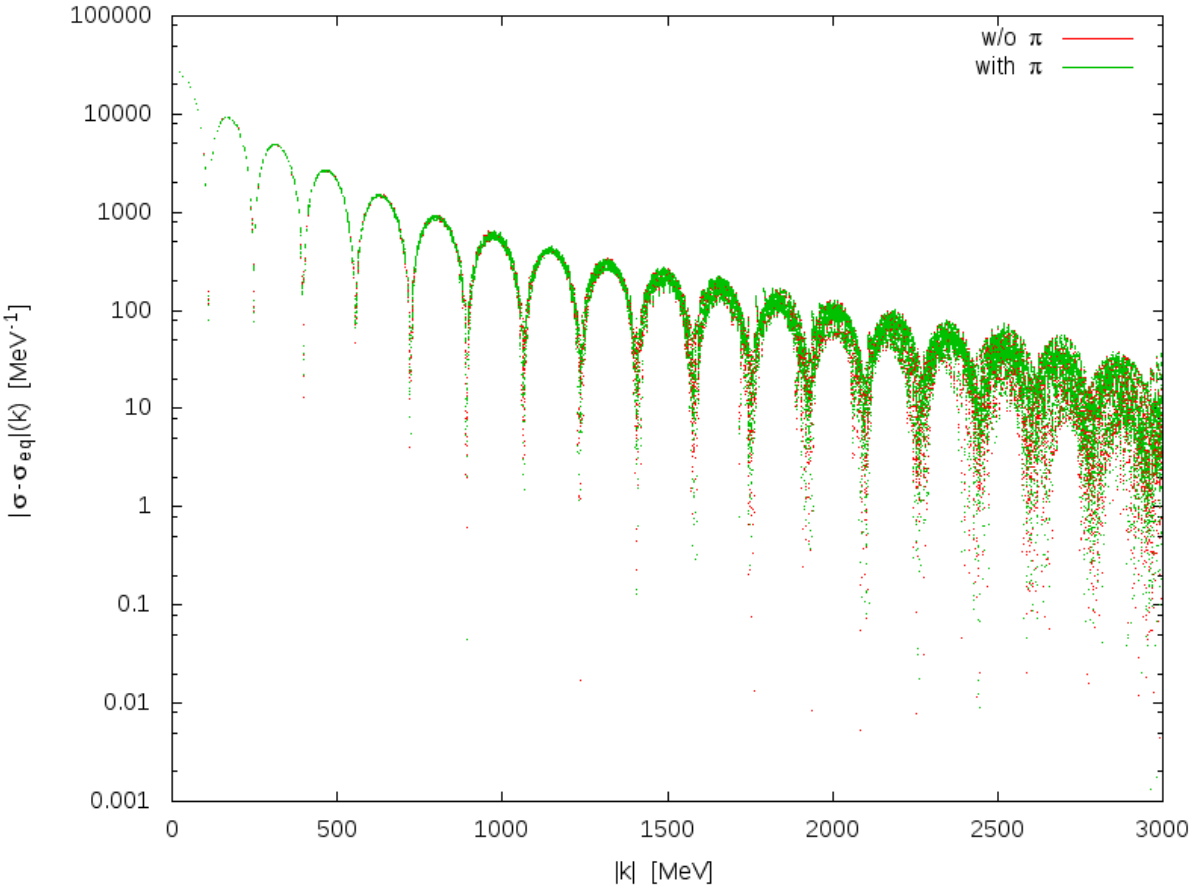

Figure 7.13.: Spatial Fourier modes of $\sigma - \sigma_{eq}$ for a model with an expanding heat bath of quarks at $t = 6.4$ fm and $g = 3.63$.

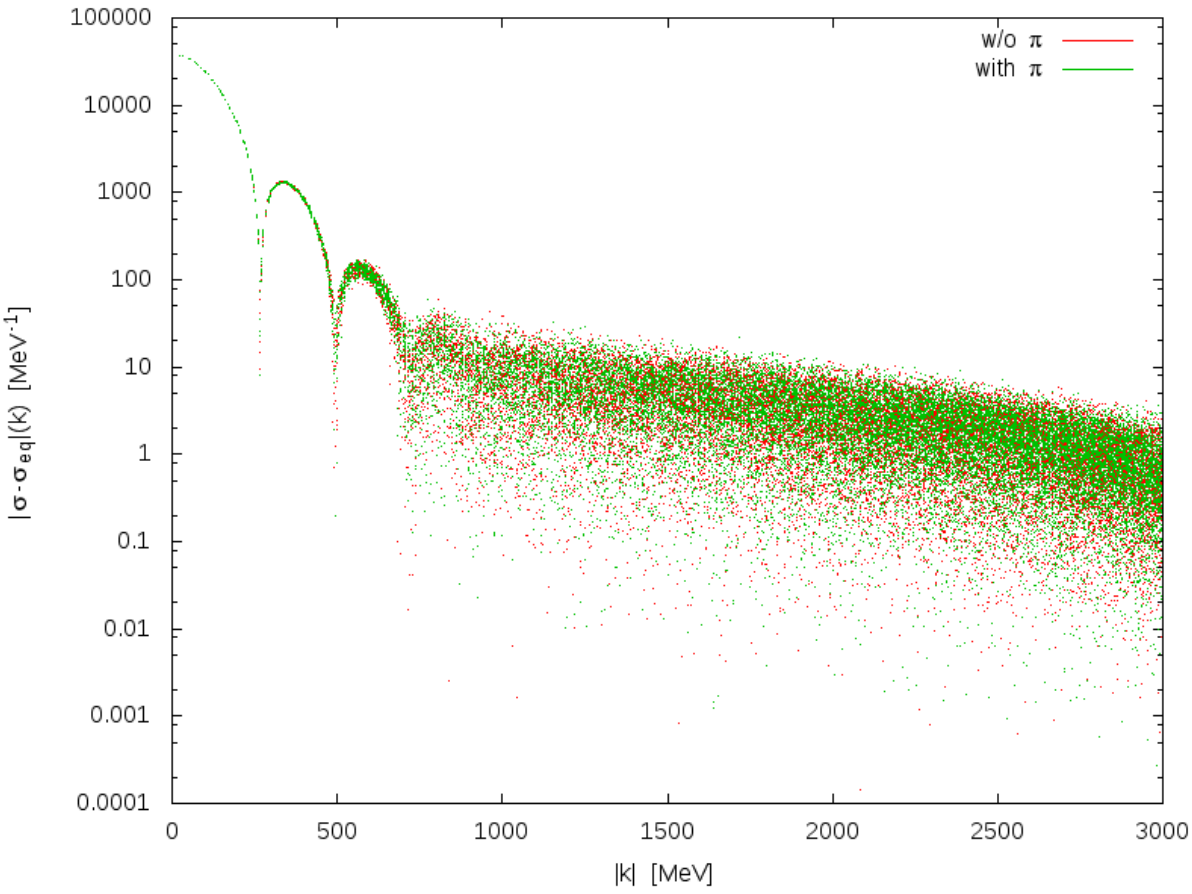

Figure 7.14.: Spatial Fourier modes of $\sigma - \sigma_{eq}$ for a model with an expanding heat bath of quarks at $t = 9.6$ fm and $g = 3.63$.

number at $1\ fm < t < 3\ fm$ while the smoothing of the field distribution dominates the sigma dynamics and then for $t > 3$ fm an increase for all momenta ranges while the sigma field is driven by the expanding medium, until between $t = 8$ fm and $t = 9$ fm the number of produced particles peaks which coincides with the heat bath just having passed through the phase transition also in the central area in coordinate space. Then, during the relaxation, $10\ fm < t < 12\ fm$ the number of particles produced in each momentum range drops quickly. Since the phase transition in the model with the second order phase transition occurs at higher temperature than for the model with a first order transition, the system passes the critical point earlier at each lattice point during the cooling. As a consequence, the periodic suppression in the mode spectrum passes earlier from $|k| < 150$ MeV to $|k| > 150$ MeV and so the sudden swap in the corresponding lines of figure 7.15 occurs already around $t \approx 8$ fm. Since in the setup with a second order phase transition the system relaxes (more or less) fully after cooling below the critical point and exceeds the equilibrium configuration at about $t = 12$ fm and then relaxes further by damped oscillations. This might be the reason for the two kinks in both lines for $|k| > 100$ MeV between $12\ fm < t < 12.8\ fm$. In comparison to [Nah11, NHL$^+$13], our findings are similar to the previous case: the overall reduction in the particle numbers for a second order phase transition as compared to a first order case is also found in [Nah11] although in our case the effect is a little larger. Apart from that, the dominant part of the particle production sets in at later times in our case as compared to the cited work, which might be a consequence of the externally imposed temperature evolution of the heat bath in our case. Moreover, we have the swapping of the lines for two neighbouring mode bins as an imprint of the radial symmetry in the central collision as opposed to the off-center collision regarded in [Nah11, NHL$^+$13].

Let us remark that also for the results presented in the current section the explicit propagation of the pion mean fields is unimportant for the dynamics and spectrum of the sigma field as well as for the particles produced.

7.1.3. Crossover

To complete the investigations of meson fluctuations interacting with an expanding background medium consisting only of quarks we shortly summarize here, without plots, what happens for a model with a chiral crossover, $g = 3.3$. In comparison to the case of the second order phase transition the transition itself occurs a little more smoothly and at

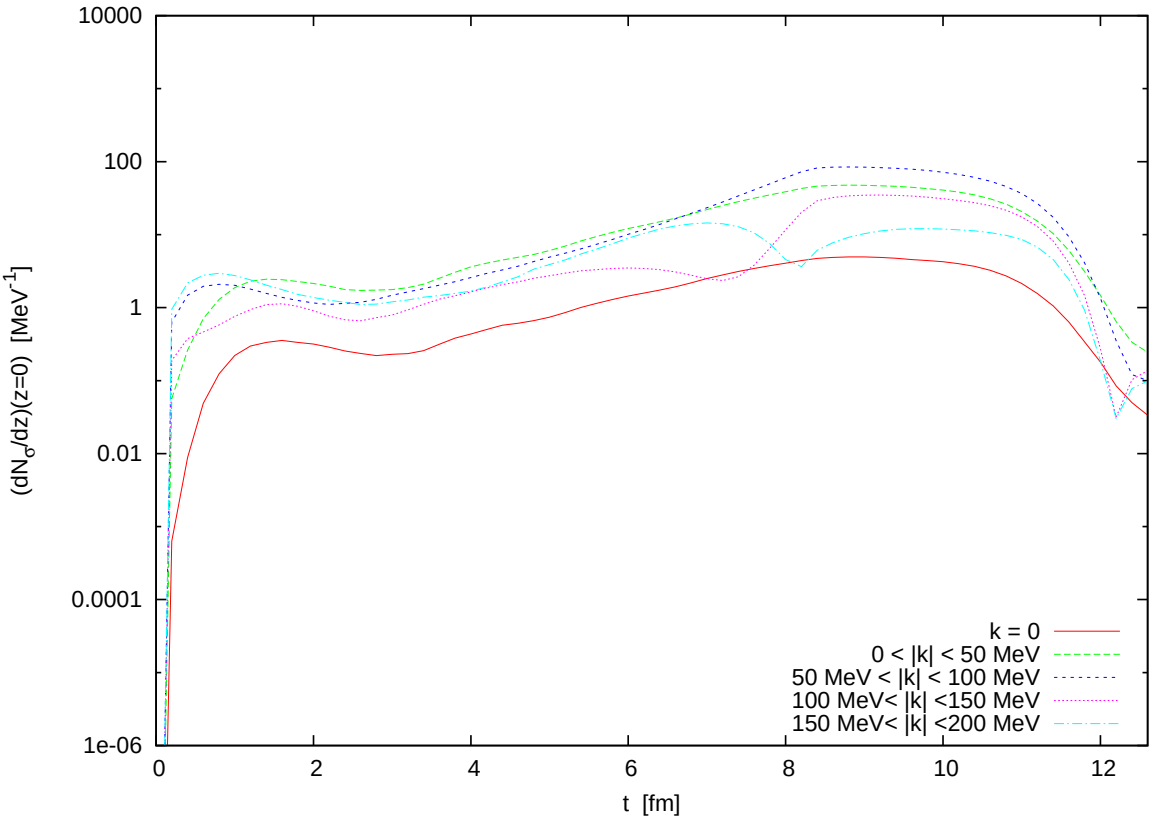

Figure 7.15.: Number of sigma particles produced in the x-y-plane within different momentum ranges for $g = 3.63$.

a higher temperature (cf chapter 5). Thus, the $\sigma - \sigma_{eq}$ profiles in coordinate space are like the ones from the previous section but with the transition occuring at earlier times and the relaxation occuring faster. The mode spectra for the two cases are not too different, the most prominent difference being that the period in the spectrum increases slightly for the crossover due to the transition occuring at smaller radial (spatial) coordinate because of the higher transition temperature. However, for the particles produced by the low momentum fluctuations, this plays no role. Here, again, the main difference to the case with a second order phase transition is that the large peak at the advent of the final relaxation occurs slightly earlier and thereafter the faster relaxation leads to a deeper drop in the particle numbers. Furthermore, on inclusion of the pion mean fields as additional degrees of freedom, the results do not change significantly.

7.2. Heat bath with quarks and mesons

In the previous section we have seen that the explicit propagation of the pion mean fields has no impact on the dynamics of the chiral order parameter interacting with an expanding and cooling external background medium. Now we turn to investigate how meson fluctuations in terms of hard meson modes contributing to dissipation and noise affect the sigma mean field dynamics. Thus, we employ the model derived in chapter 4.2 where the quark and meson propagators are included. The temperature profiles we use as input remain the same.

7.2.1. First Order Phase Transition

For a model with a first order phase transition we choose $g = 3.7$. As discussed in section 6.1, the transition occurs at $T = 103.43$ MeV. From figure 7.1 we see that the comparably low transition temperature leads to an interesting effect: the radial coordinate of the phase transition increases for times $t \leq 8$ fm as the hot medium expands. Only thereafter the cooling leads to a decrease in the radial coordinate of the phase transition. While for early times the peaks in the coordinate space distribution of $\sigma - \sigma_{eq}$ are still at roughly the same radial coordinate as in the previous sections, now the initial expansion of the phase transition radius leads to an increase of the peak in the hot phase (and not in the cold phase as previously), where the system is trapped in the wrong minimum (see figure 7.16). Especially at $t = 6$ fm we see that the magnitude in the peaks is basically interchanged as compared to the case of $g = 5.5$ from section 7.1.1. However,

the absolute value of the large peaks in the two cases differs by about $15 - 20\%$: it is smaller for the present case, since we now have a smaller potential barrier seperating the two phases. At later times (see figure 7.17) the radius corresonding to the phase transition temperature decreases and the peak structure changes to the familiar one from the previous sections. Between $t = 11$ fm and $t = 12$ fm the background medium completely cools down below the phase transition and in the center the sigma field is trapped in the wrong phase. The diameter of this circular region is about the same as in the case of $g = 5.5$, where, however this quench in the center occurs at earlier times ($t \approx 8$ fm). This deviation is of course a direct consequence of the comparably lower transition temperature at $g = 3.7$. The area with sigma in the wrong phase will surely decay eventually, however, we cannot evolve the heat bath much further due to lack of input data beyond $t = 12.8$ fm.

Concerning the fourier components of $\sigma - \sigma_{eq}$ we expect to see a nice periodic structure in the radial direction as predicted by our approximations in section 7.1.1. Further, since the smoothing of the initial spatial field configuration by means of the laplacian operator in the equation of motion (which favors sigma deviations in the cold phase, i.e. at larger radii) is at some point overcompensated by the expansion of the radial coordinate of the phase transition, we expect a drop in the low momentum modes at around $t \approx 2$ fm. Then, around $t \approx 8$ fm we expect another drop in the soft modes because the area of the hot phase shrinks and the sizes of inner and outer peaks in the spatial field distribution interchange (and thus lead to a vanishing volume average $\sigma - \sigma_{eq}$ at some point in time). For $2\ fm < t < 8\ fm$ the mode spectrum should display the familiar exponential and periodic suppression. This behaviour can indeed be seen at $t = 3.2$ fm in figure 7.18 and $t = 8.0$ fm in figure 7.19.

From the above discussion of the fourier mode spectrium it is clear that the number of particles produced in the soft modes from sigma fluctuations shows a sudden drop at $t \approx 2$ fm and at $t = 8$ fm which is observed in figure 7.20 for $|k| < 150$ MeV. Due to the initial increase and subsequent decrease in the spatial radius of the hot phase, leading to the two drops in dN_σ/dz, the particle numbers in the soft modes are are smaller for intermediate times $2\ fm < t < 8\ fm$ as compared to the case of a pure quark heat bath ($g = 5.5$), where the expansion of the heat bath causes steady growth in the intensity of fluctuations from $t \gtrsim 2.5$ fm on. Finally, for $t > 8$ fm when the "standard" cooling of the system (as in the cases discussed in the previous sections) sets in, the particle numbers

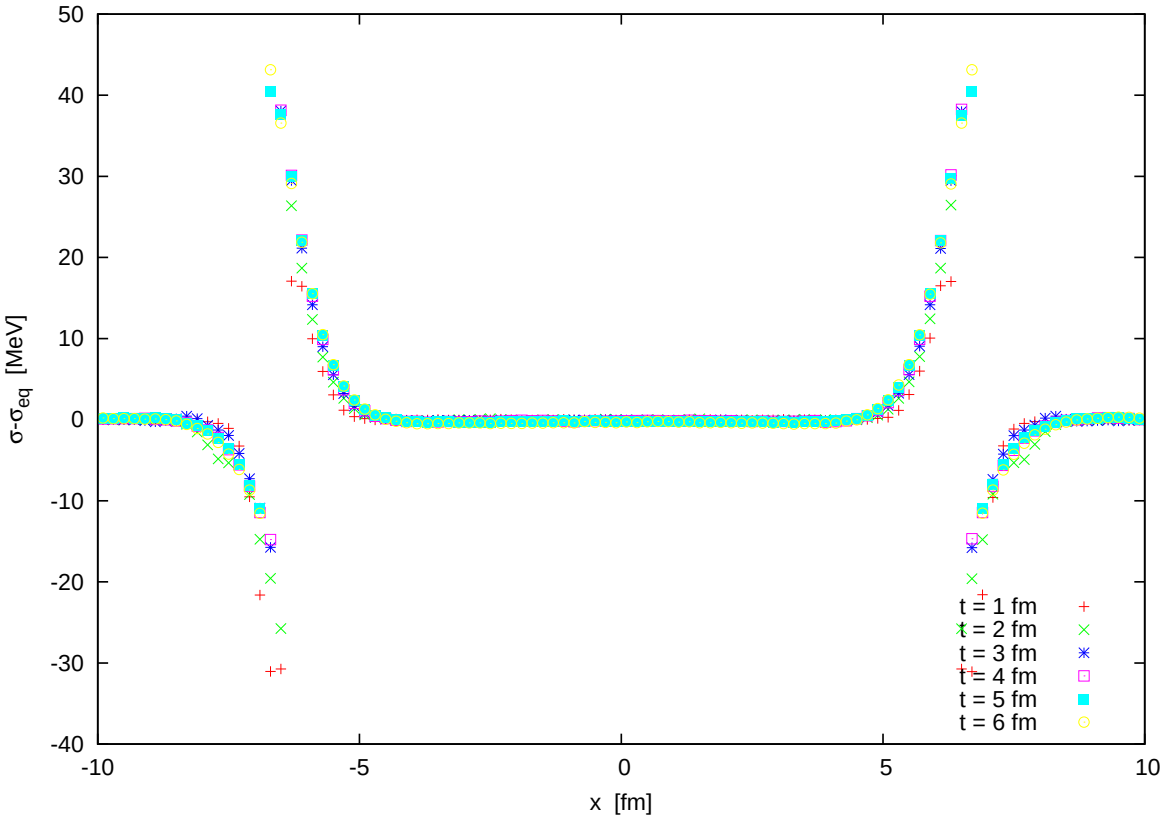

Figure 7.16.: $\sigma - \sigma_{eq}$ along x-axis for different times during expansion of heat bath containing contributions from quarks and hard meson modes. The case of a first order phase transition is considered ($g = 3.7$).

increase until they peak when the central area (in coordinate space) is quenched from the hot into the cold phase. This is again accompanied with a swap in the particle numbers for different momentum ranges, where the periodic mode suppression in the spectrum passes by (see also discussion in section 7.1.1). While for the modes $|k| < 50$ MeV the order of magnitude at peak value is the same as for the case of $g = 5.5$, it is smaller by about $20 - 35\%$ at $50\, MeV < |k| < 100\, MeV$.

Also in the current model, explicit propagation of the pion mean fields does not change the dynamics of the sigma field whose dynamics is completely driven by the expansion and cooling of the heat bath.

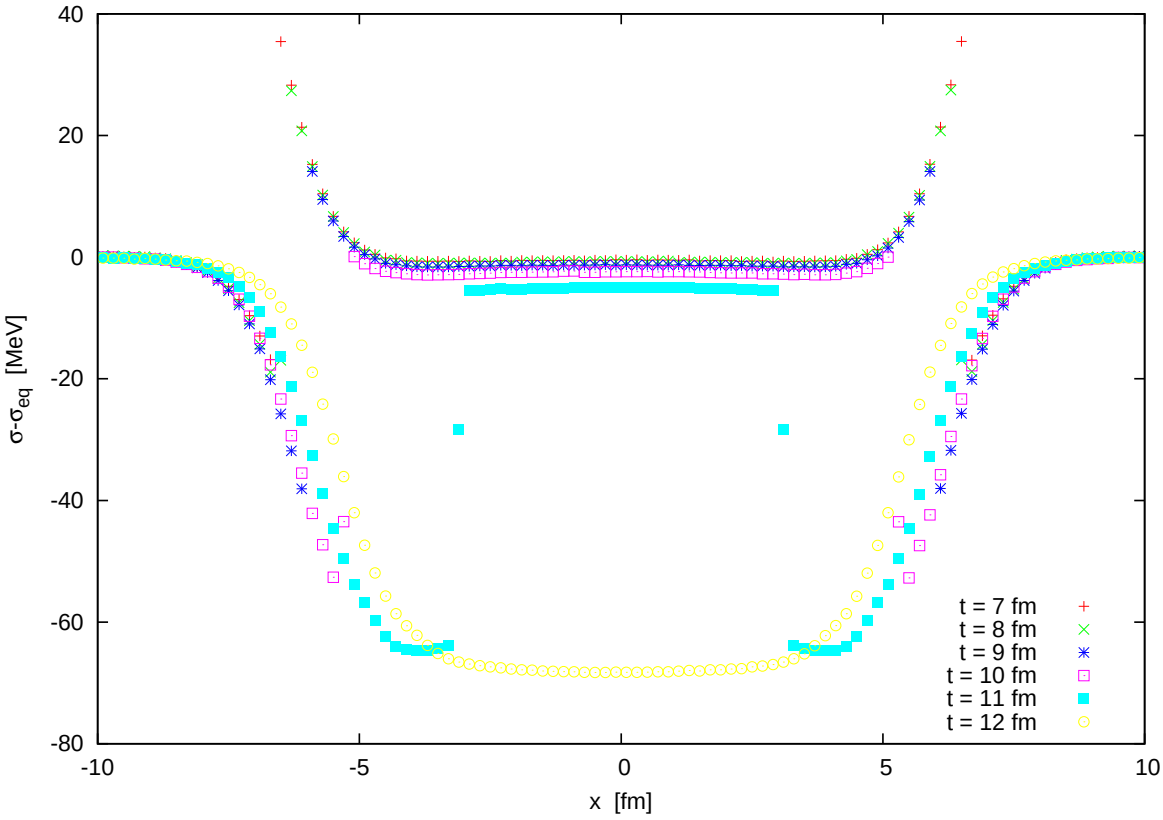

Figure 7.17.: $\sigma - \sigma_{eq}$ along x-axis as in figure 7.16 but for later times.

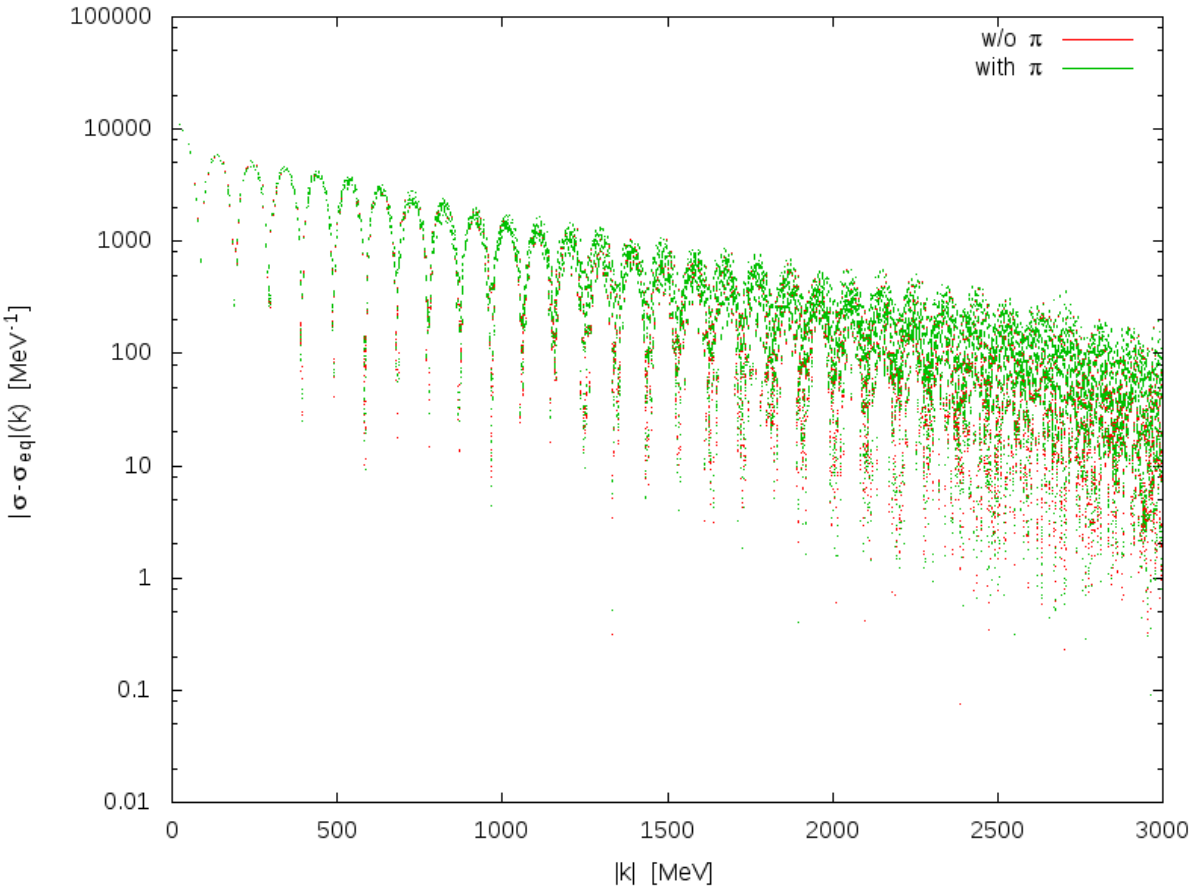

Figure 7.18.: Fourier modes of $\sigma - \sigma_{eq}$ at $t = 3.2$ fm during the expansion of the heat bath which includes contributions from the hard meson modes. The quark-meson coupling constant is chosen as $g = 3.7$ corresponding to a first order phase transition.

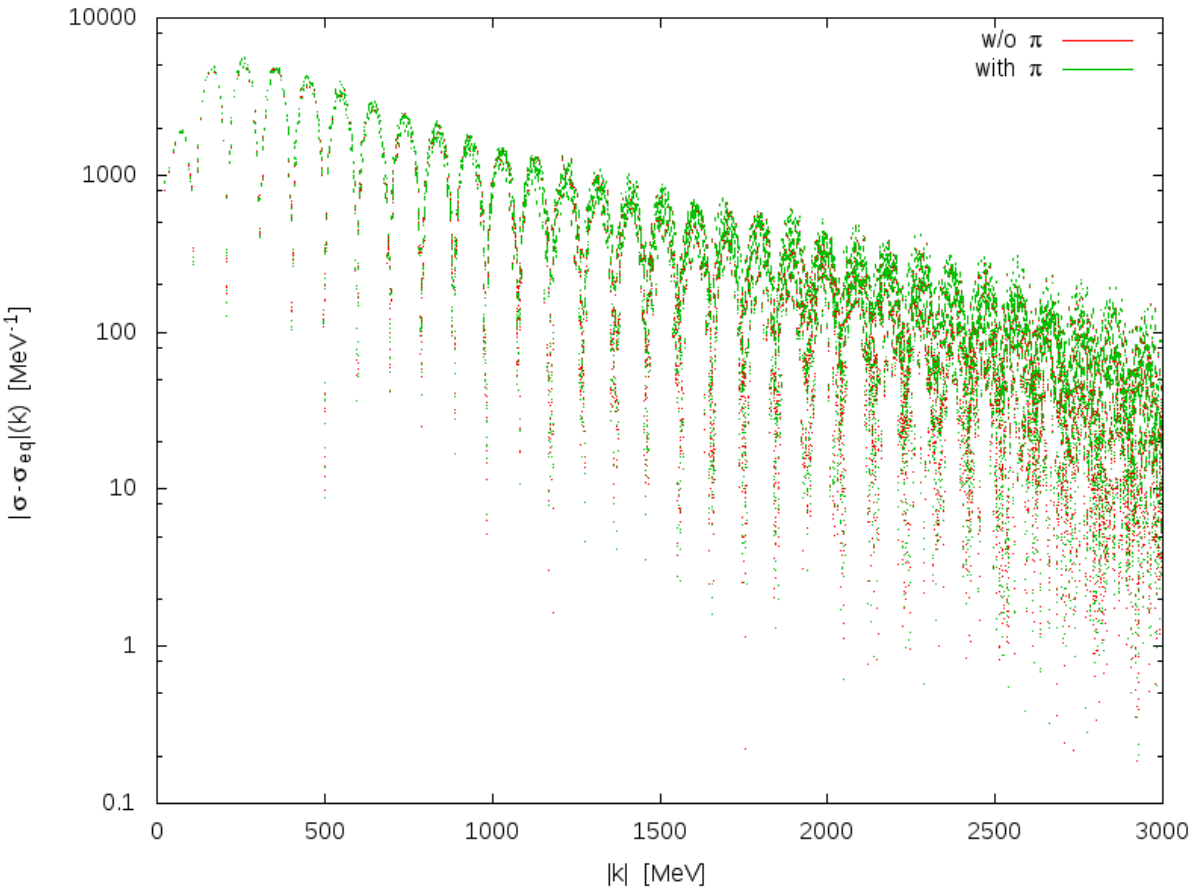

Figure 7.19.: Fourier modes of $\sigma - \sigma_{eq}$ during the expansion of the heat bath as in figure 7.18 but at time $t = 8.0$ fm.

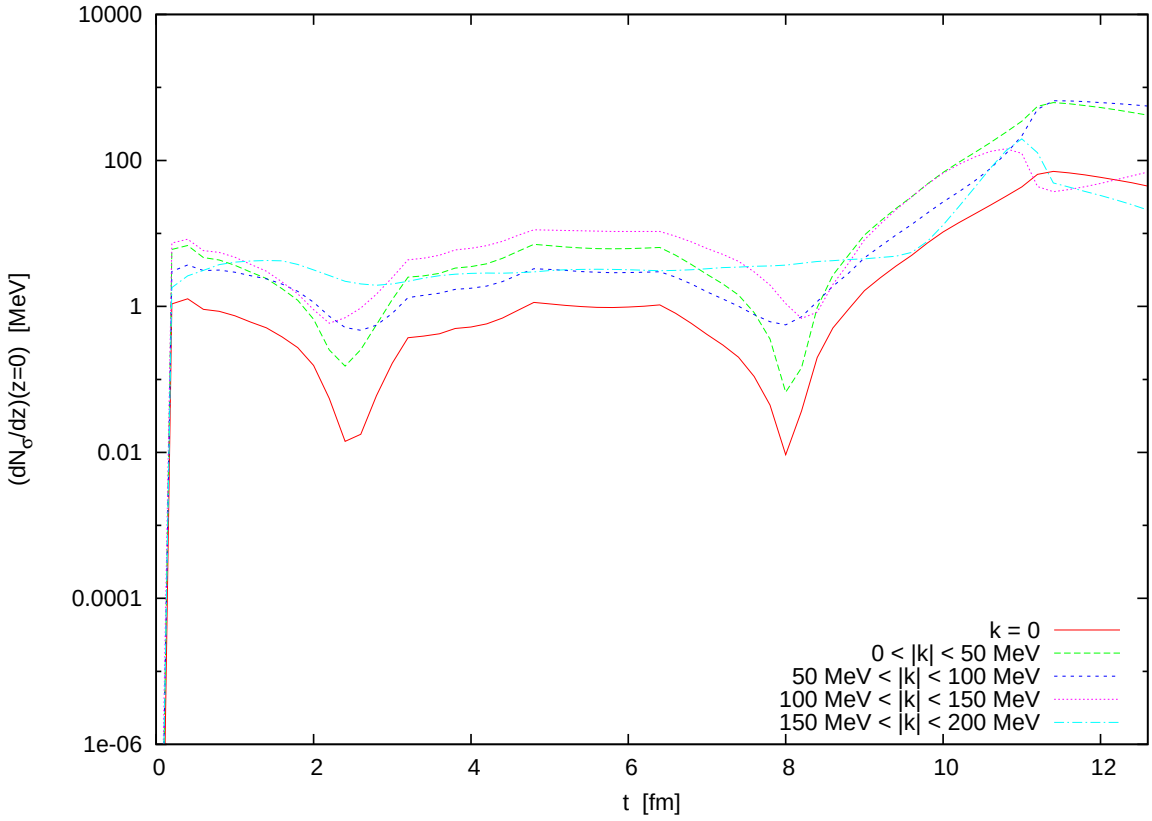

Figure 7.20.: Number of particles produced in low momentum σ modes in $x-y$ plane during expansion of the heat bath consisting of quarks and hard meson modes. It is $g = 3.7$, i.e. a first order phase transition scenario.

7.2.2. Second Order Phase Transition

When including the hard meson modes in the heat bath, the choice of $g = 2.4$ yields a model with a second order phase transition at a critical temperature of $T_{crit} = 117.5$ MeV. At early times, the dynamics of the sigma field during the expansion of the background medium is dominated by the smoothing of the initial field distribution. However, because of the flat potential in sigma direction at the critical point and because of the comparably low damping coefficient, this smoothing process of the initial field configuration overshoots and oscillates around a stable configuration, i.e. the peaks in the distribution of $\sigma - \sigma_{eq}$ in both phases grow and shrink for $t < 2$ fm. In figure 7.21 we only see an intermediate configuration at $t = 1$ fm. Additionally, the damping in the cold phase is larger by a factor of roughly ≈ 2 which means that the stable smooth field configuration in the presence of a heat bath with the given temperature profiles features a larger peak in the hot phase (about 4 to 5 times larger than the cold phase peak at $2\,fm < t < 3\,fm$). For $t \gtrsim 3$ fm, the cooling of the heat bath leads to a decrease in the radius corresponding to the critical temperature and we see a growing peak in the cold phase accompanied by a shrinking peak in the hot phase. This continues for $t > 7$ fm as seen in figure 7.22. Between $t = 9$ fm and $t = 11$ fm the central area is cooled below the critical point. From the intermediate $t = 10$ fm we find that the transition occurs smoothly. At $t = 12$ fm the field in the central area already relaxes towards thermal equilibrium.

During the early stage of expansion, the peaks of $\sigma - \sigma_{eq}$ at both sides of the phase transition are positioned at clearly seperate radii (x_0, x_0' in the notation of section 7.1.1). Therefore, we find the fourier spectrum at e.g. $t = 0.8$ fm in figure 7.23 modulated by a period of about $k_0 \approx 2\pi/(x_0 - x_0') \gtrsim 1.55$ GeV (inferred from a value of $x_0 - x_0' \approx 0.8$ fm at $t = 1$ fm in figure 7.21). During the cooling of the central area below the critical temperature, we can describe $\sigma - \sigma_{eq}$ in coordinate space (figure 7.22) by a superposition of two overlapping and rather broad gaussian curves. For $t = 9.6$ fm, they are centered at radius $r \approx 2.5 - 3.0$ fm. In figure 7.24 we find the periodic suppression of the fourier modes with a period of about $k_0 \approx 222$ MeV corresponding to $r \approx 2.8$ fm from equation (7.6).

In figure 7.25 we plot the number of particles produced from the sigma fluctuations in the low momentum modes. At around $t = 2$ fm we find a drop in the particle numbers in the modes $|k| < 150$ MeV when the process of smoothing out the initial field

distribution abates. Therafter, the cooling of the heat bath leads to a decrease in the radial coordinate at which the system passes the critical point. As in the the previous section, 7.2.1, we find a second drop at $t \approx 5.5$ fm in the zero mode of the sigma fluctuations coinciding with an approximate volume average of $\sigma - \sigma_{eq} = 0$. However, in contrast to the first order scenario where the low transition temperature meant first a growth and then a decrease of the hot phase region, the second drop in the particle number is now due to the smaller damping in the symmetric phase (in combination with a shrinking of that phase). As seen before, during the cooling through the phase transition in the central area the fluctuations intensify to their maximum values. The magnitude of the particle numbers within different momenum ranges is the same as if we neglect the hard meson mode contribution to the heat bath ($g = 3.63$, section 7.1.2), except for $0 < |k| < 50$ MeV where values as for $50\,MeV < |k| < 100$ MeV are reached.

7.2.3. Crossover

In the crossover scenario with $g = 2.0$ the potential is no longer flat at the phase transition as opposed to the case of a second order phase transition ($g = 2.4$) considered before. Therefore, the sigma field is pushed (at least slightly) towards its equilibrium value in the vicinity of the phase transition which reduces the effect of the smoothing of the initial field distribution: the height of the inner peak in the distribution of $\sigma - \sigma_{eq}$ for $t < 2$ fm in figure 7.26 is about $\sim 85\%$ than compared to the second order case. However, the damping in the hot phase at $g = 2.0$ is even lower than in the previous case. The overshooting of the stable configuration (balancing the thermal equilibrium from the temperature profiles versus the smoothing of the fields) leads thus to a distortion with an amplitude of about $2 - 3$ MeV in the hot phase which propagates inwards until it vanishes for $7\,fm < t < 8\,fm$ as seen in figure 7.27. Actually, such a distortion is also observed in the case of $g = 2.4$ in figure 7.21, however, due to the larger damping at $g = 2.4$ the effect is less obvious (amplitude $< 0.5 - 1$ fm) and subsides faster ($t \lesssim 6$ fm). Also, due to the small relative size of the distortion ($\lesssim 15 - 30\%$) the effect on the fourier spectrum is not clearly visible. Apart from this propagating distortion, the time evolution of $\sigma - \sigma_{eq}$ is similar to the second order case, except that now the phase transition occurs at a larger temperature and so the central area is cooled to below the transition temperature at an earlier time $9\,fm < t < 10\,fm$ and the field distribution has relaxed correspondingly further at the end of the time evolution which is enhanced

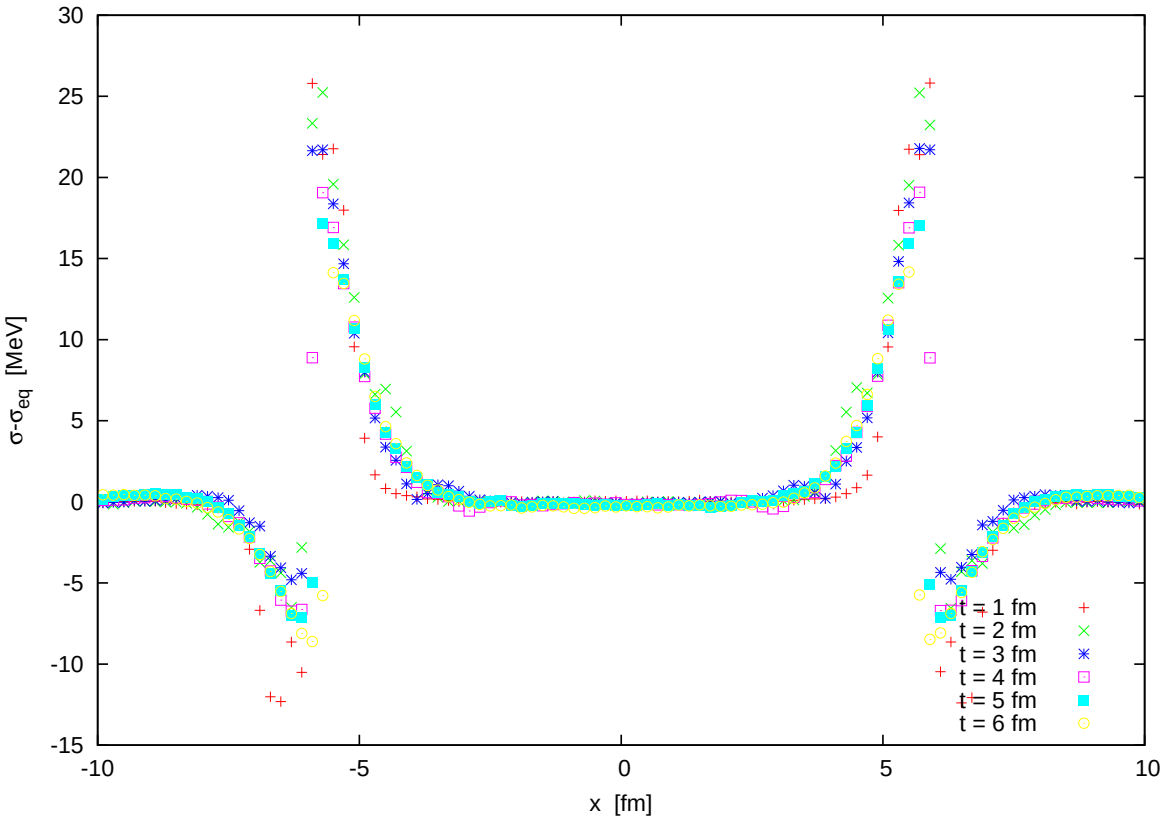

Figure 7.21.: $\sigma - \sigma_{eq}$ along x-axis for different (earlier) times during expansion of heat bath in a critical point scenario. Contributions hard meson modes to the heat bath are taken into account. The quark-meson coupling constant is $g = 2.4$.

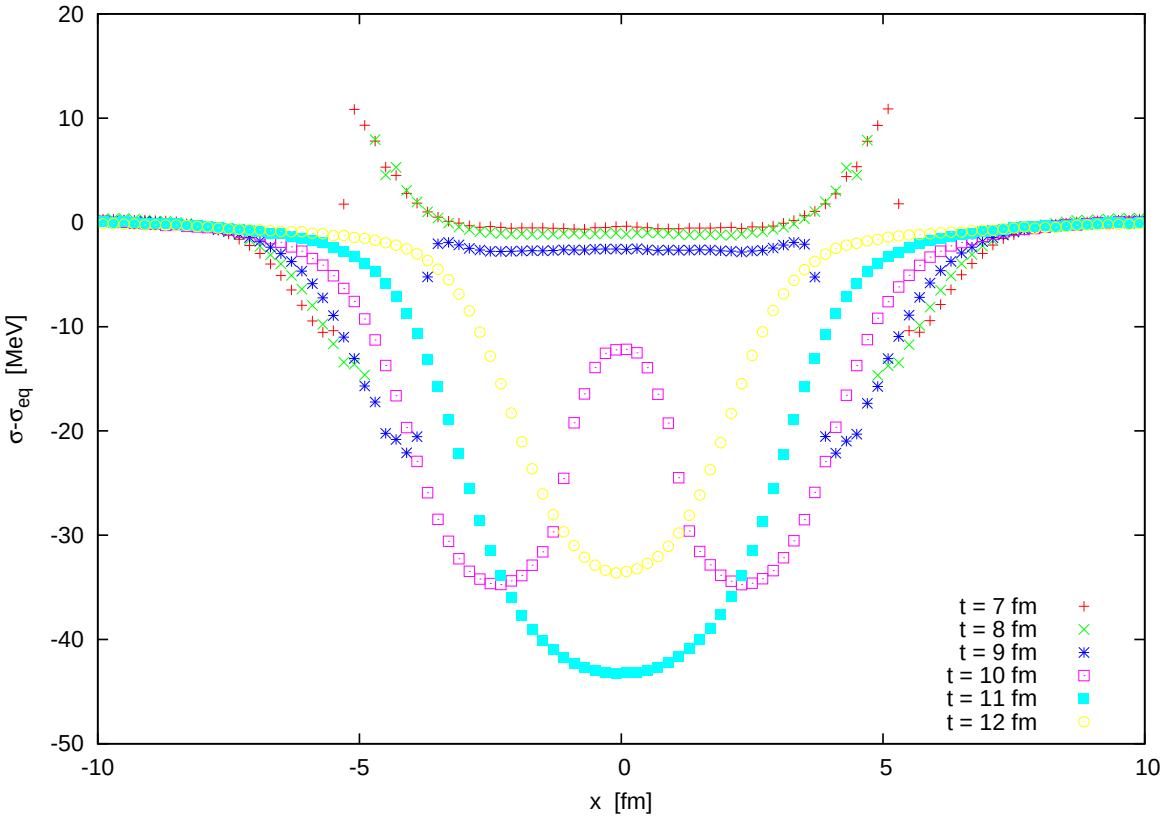

Figure 7.22.: $\sigma - \sigma_{eq}$ along x-axis as in figure 7.21 but for later times.

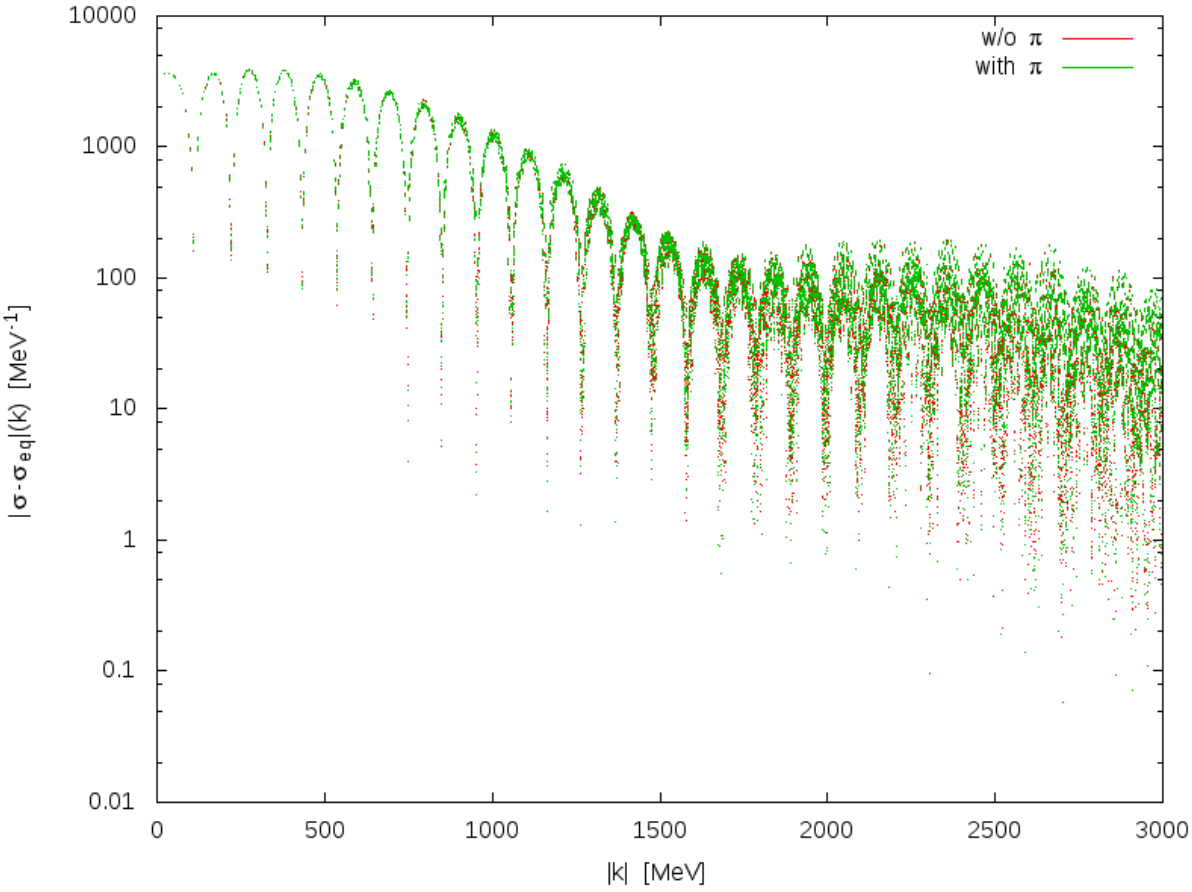

Figure 7.23.: Fourier modes of $\sigma - \sigma_{eq}$ at $t = 0.8$ fm during the expansion of the heat bath including contributions from the meson propagator. The system passes a critical point, $g = 2.4$.

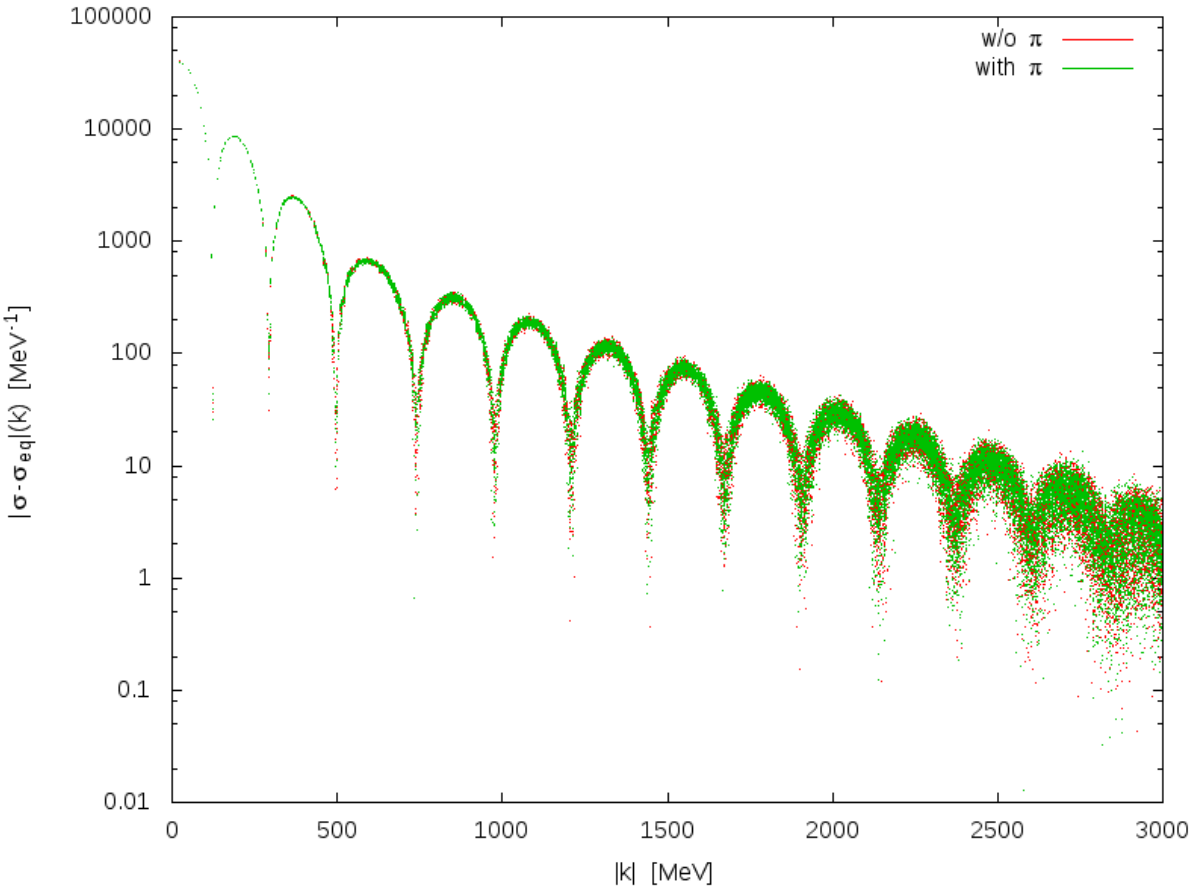

Figure 7.24.: Fourier modes of $\sigma - \sigma_{eq}$ for a system as in figure 7.23 but at $t = 9.6$ fm.

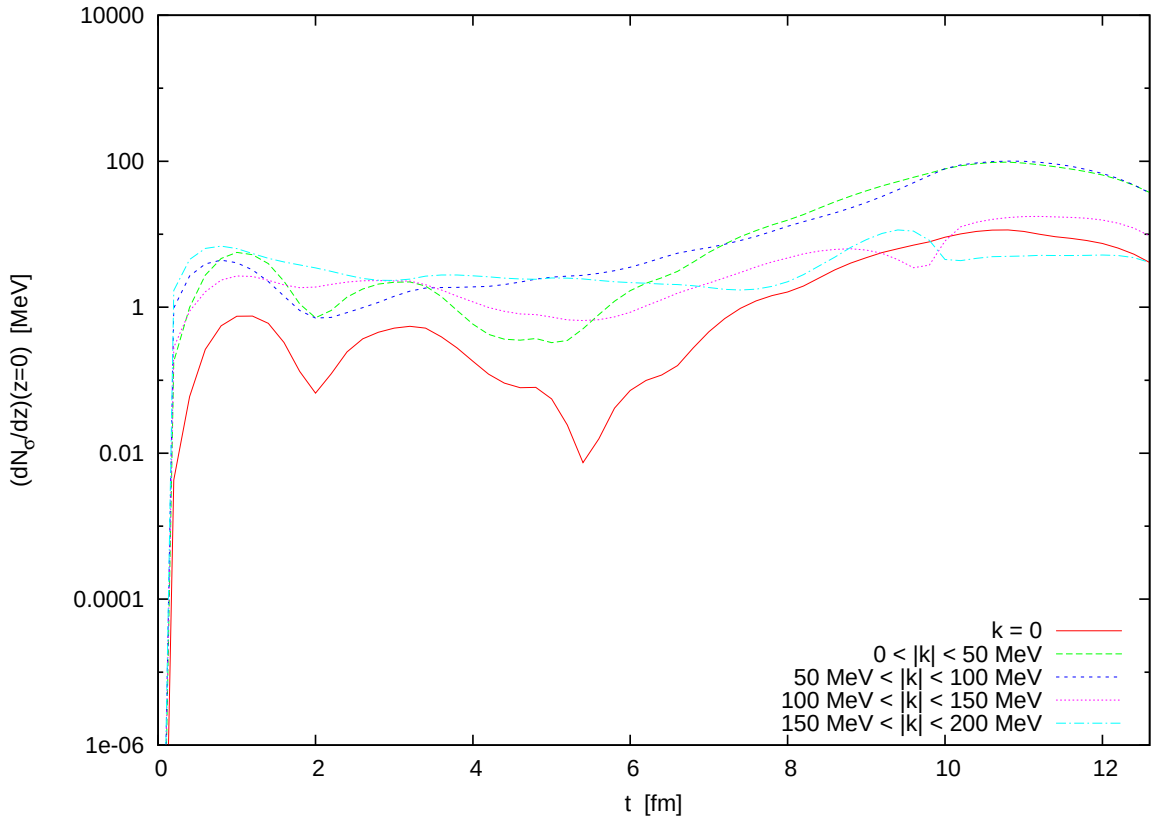

Figure 7.25.: Number of particles produced in low momentum σ modes in $x - y$ plane during expansion of the heat bath. The quark-meson coupling constant is $g = 2.4$ yielding a model with a second order phase transition. Contributions from the hard meson modes are included.

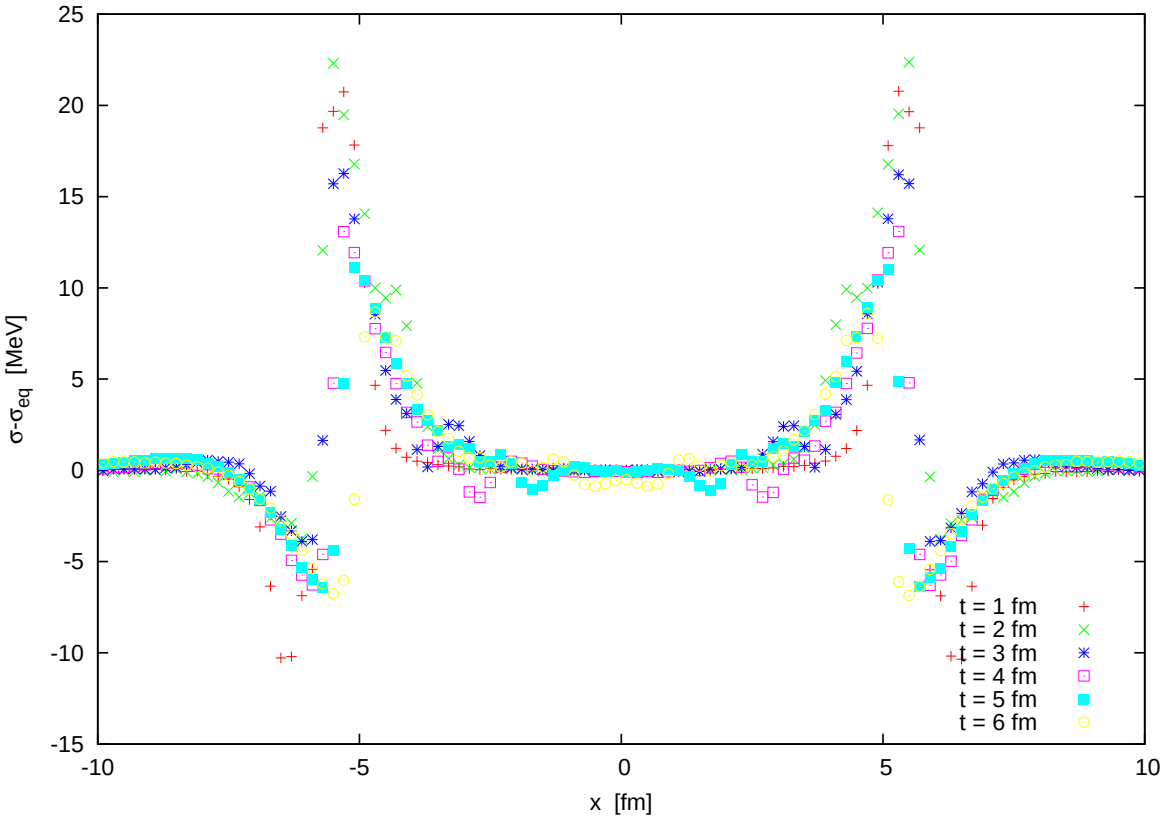

Figure 7.26.: $\sigma - \sigma_{eq}$ along x-axis for an expanding background medium including contributions from the meson propagator. The system passes a crossover transition, $g = 2.0$. The various distributions correspond to early times during expansion.

by the decrease in the damping coefficient. Correspondingly, we find a similar evolution of the particle numbers associated with the soft modes of the sigma fluctuations (figure 7.28) as compared to the critical point scenario in the previous section. The major difference is that the second drop in the particle numbers of the zero mode discussed before, now occurs about $\Delta t \approx 2$ fm earlier at $t \approx 4$ fm. This is an effect of the higher transition temperature meaning an earlier transition at fixed spatial coordinate. Additionally, the drops in the particle numbers are washed out because the transition occurs more smoothly in the crossover scenario.

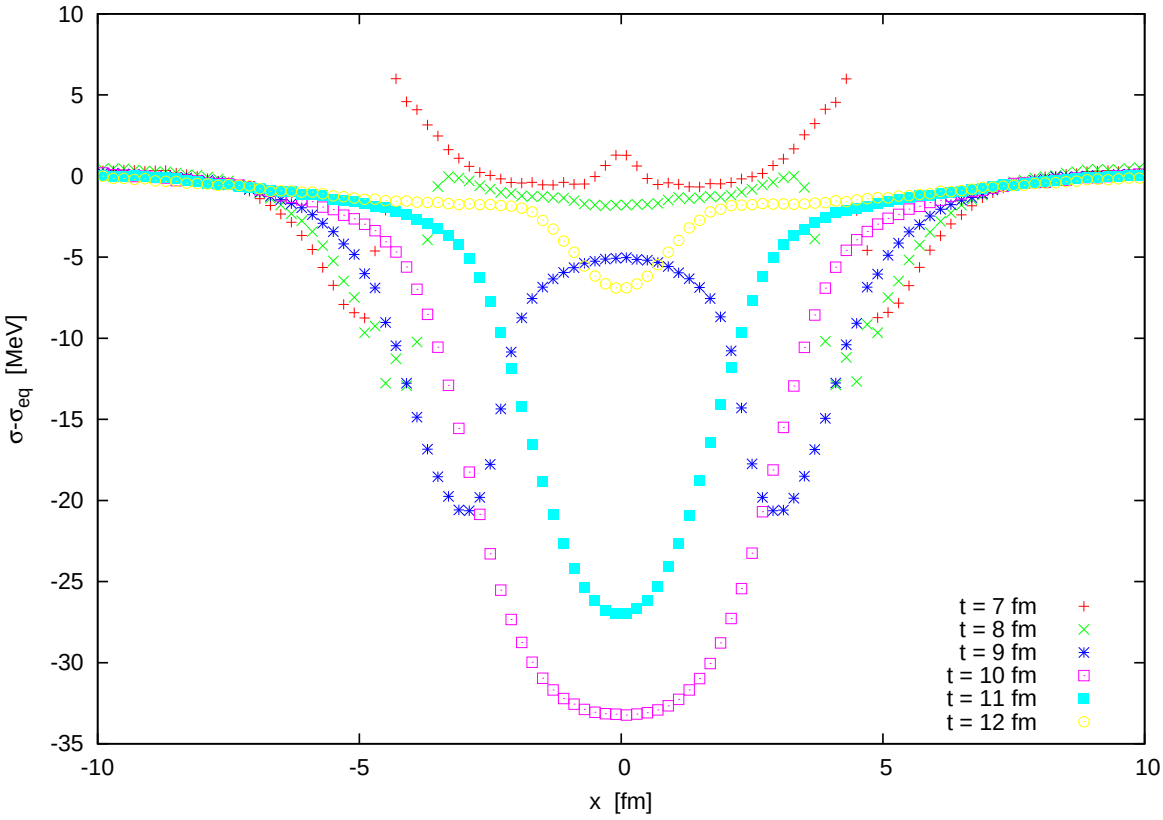

Figure 7.27.: $\sigma - \sigma_{eq}$ along x-axis as in figure 7.26 but for later times.

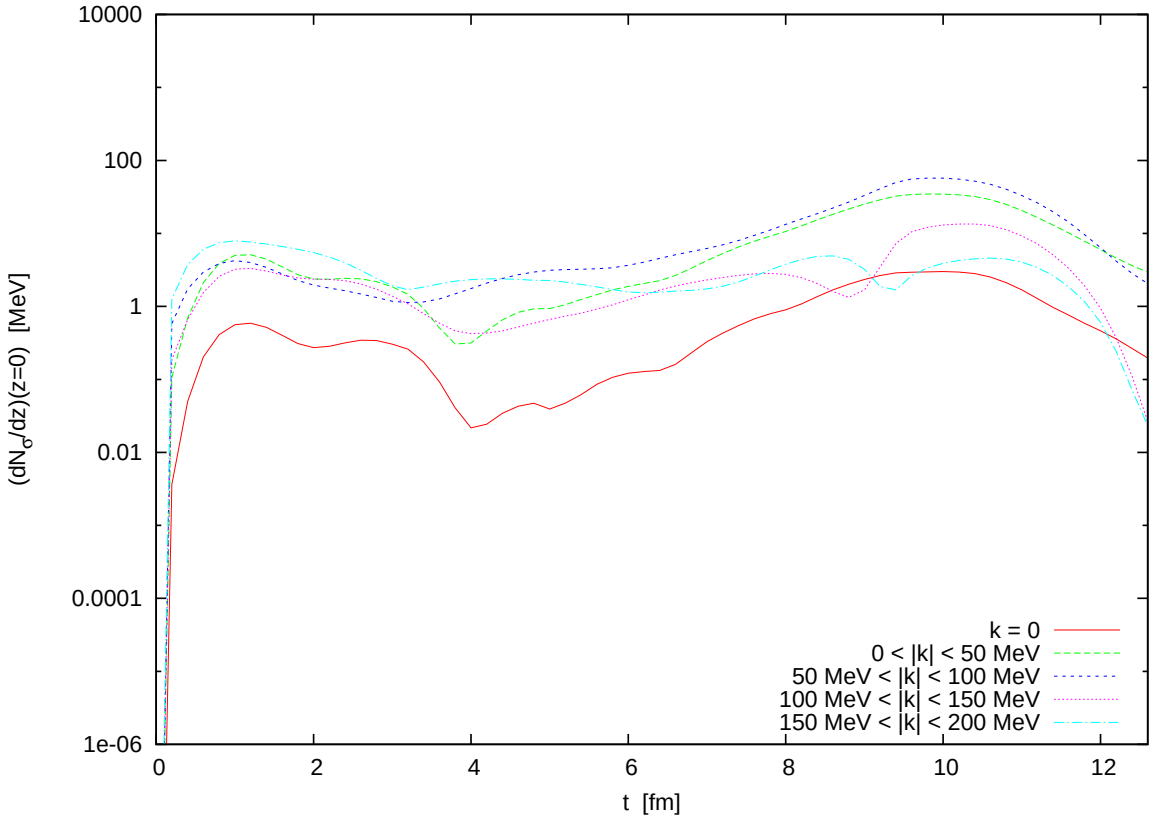

Figure 7.28.: Number of particles produced in soft σ modes during expansion of the heat bath containing contributions from quarks and hard meson modes. The system passes a crossover transition, $g = 2.0$.

Chapter 8.

Summary, Conclusions and Outlook

In this thesis, we have investigated the impact of pionic fluctuations on the dynamics of the chiral order parameter. For this purpose, we have derived a Langevin equation of motion for the chiral fields. Starting point of the derviation was the 1PI effective action for the chiral quark meson model. Motivated by the influence functional formalism, the quarks were considered as a heat bath and an effective description for the interaction of the meson fields with quark environment was obtained. The resulting Langevin equation of motion, in the absence of pion fields, has originally been derived in [Nah11, NLHB11]. In this work we have achieved an extension of this model by including the pion mean fields as explicitly propagated degrees of freedom.

In a second step, we have further extended the model by including pion fluctuations beyond the mean field dynamics. For this purpose, we have included the meson propagator in the effective action. In order to obtain self-consistent propagator masses, we have employed a 2PI effective action ansatz. However, the self-consistency could only be retained at lowest order in mean field fluctuations, a concession we had to make for identifying the dissipation and noise kernels as suggested by the influence functional. In terms of the influence functional, our inclusion of the meson propagator corresponds to accounting for the interaction of the (soft mode) mean meson fields with the hard meson modes as part of the heat bath and resembles the model of [Ris98], where damping and noise kernels have been derived from a 1PI effective action ansatz for an chiral O(N) without quarks.

Our first set of numerical studies concerned the model with a pure quark heat bath. In the case of constant vanishing pion mean field, we could reproduce the results found in [Nah11, NLB12]: For an isothermal heat bath, starting from a non-equilibrium con-

figuration, the system relaxes to the thermal equilbrium. During the relaxation process, the mean field lose energy by dissipation. On the other hand, the thermal fluctuations from the heat bath, encoded in a stochastic force providing the fields with random kicks, ensures a finite spread in the field distribution. In the course of the relaxation process the mean field fluctuations increase temporarily. Close to the phase transition, the relaxation times are generally longer. While at a first order phase transition this is a direct cause of the potential barrier that needs to be overcome for relaxation, at the critical point of a second order phase transition the potential in sigma-direction is flat and so there is no slope for the field to slide down.

Including the pion mean fields as dynamic degrees of freedom we found for the most cases, that they may have a significant effect on the dynamics of the chiral order parameter, but only close to the chiral phase transition: for relaxation in a first order phase transition scenario, we saw that the pion fluctuaions speed up or slow down the relaxation process, depending on the direction in which the phase transition is passed through. On the level of the equation of motion, the pions enter the sigma dynamics by causing the sigma to see the potential slightly shifted, as if the sigma was a bit larger. While the sigma field relaxes along the concave parts of the potential, it is either held back or pushed forward by the pion fluctuations.

There are some cases where the pion degrees of freedom show a considerable effect on the sigma dynamics, such as e.g. quenches from the hot phase to temperatures below the phase transition but above the lower spinodal temperature, where for some cases the relaxation process is drastically shortened by the pionic fluctuations. For quenches to temperatures very closely below the first order phase transition, the effect is most dramatic: where the sigma field without pion fluctuations is trapped in the wrong minimum for extremely long times, the pion fluctuations help overcome the potential barrier comparably quickly. If a system is quenched from the cold to the hot phase, just above the phase transition, the effect is opposite: without pion fluctuations the system shows vague signs of relaxation, but on inclusion of pion fluctuations the sigma field is pushed back while climbing the potential barrier.

For relaxation in a model with a second order phase transition we found the pion fluctuations to have a small effect except at temperatures close to the critical point. Here, the pions push the sigma to value larger than thermal mean field equilibrium

value: while in meson space the potential along the sigma axis is flat, off the axis it has a slope in sigma direction which vanishes at a shifted sigma value for nonzero pion fields.

When we added the energy lost by the chiral fields during relaxation to the thermal energy of the heat bath, we observed that again the pion fluctuations are of little importance for the dynamics of the sigma field away from the phase transition. Only if the reheating increases temperature, such that the relaxation occurs at the first order phase transition, we find again that pion fluctuations speed up relaxation. In case of a second order phase transition, relaxation times are only little shorter on inlcusion of the pions than without.

In a second set of calculations we treated the relaxation dynamics of the chiral fields coupled to a heat bath of quarks and hard meson modes. This model required to readjust the quark-meson coupling constant in order to find the desired type of phase transition. Thus, we first investigated the thermal equilibrium properties. The quark-meosn coupling constants had to be chosen smaller than for the previous model and the phase transitions were found at lower temperatures. Apart from this direct consequence of the inclusion of the hard meson modes into the heat bath, we found similar results from the explicit propagation of the pion mean fields as for the other model: Mostly, the effect is negligible. Only close to the phase transition the pions cause faster or slower relaxation, depending on the direction in which the system passes the phase transition. Especially at a first order phase transition the pion fluctuations might thus either help to push the sigma field over the potential barrier or prevent the relaxation of the sigma field.

In a last set of calculations we tested our model in the more realistic context of a heavy ion collision. We imposed the temperature profiles from hydrodynamic evolution of a plasma computed in [Bet09] for central Au-Au-collisions with an ideal gas equation of state onto the heat bath in our model. As a consequence, we found the dynamics of the meson fields being driven by the evolution of the background medium, which - because of the radial symmetry of the system - resulted in a perdiodic suppression of the fourier modes of the sigma fluctuations. This periodic mode structure translated to the particle numbers produced in the soft momentum modes by the fluctuations. The particle numbers peaked, when the heat bath cools below the phase transition temperature in the (spatial) center of the system. For a first order phase transition the number of produced particles is significantly larger than for a critical point scenario (by a factor > 10). While

the rough shape and order of magnitude of the number of particles produced in the soft modes is comparable to the findings in [Nah11, NLB12], in our case the main relaxation occured at later times ($\Delta t \gtrsim 4$ fm). We assume that this is an effect of not having a backreaction of the meson fields onto the evolution of the heat bath in our setup. For the same reason it might be that we found no impact of an explicit propagation of the pion mean fields on the sigma field dynamics, mode spectrum and particle numbers.

Outlook

Our studies may be carried further in many ways. Apart from a general extension to finite quark chemical potential, especially the model with hard meson modes contributing to the heat bath in addition to the quarks is well suited for various upgrades. In the 2PI effective action ansatz, more diagrams may be included. This could be done e.g. by resumming an infinite number of diagrams up to a given order in a $1/N$ expansion, but it would also be interesting to couple the quark and meson sectors of the heat bath which happens at $\mathcal{O}(g^2)$, respectively at two-loop order. However, if we are to obain a Langevin equation of the likes derived in our work, these upgrades are only at the level of thermal equilibrium.

Another important improvement would be to self-consistently renormalize the divergent terms in the 2PI effective action [vHK01, vHK02b, vHK02a] instead of neglecting them. This would alter the phase structure and we would obtain larger phase transition temperatures as compared to the extremely low values found in chapter 6 (see for instance [PF08, FPP09, PF10]).

In chapter 4, we derived the damping and noise kernels for arbitrary directions of the chiral mean field vector. However, for the numerical simulations in the subsequent chapters, we restricted to equilibrium values of the damping coefficients and noise correlators. In order to further approach full nonequilibrium dynamics, we could use the local field values and temperatures to determine the damping coefficients (see appendix B for plots in the T-φ-plane) and noise correlators[1]

[1] The noise correlators for the mean field components at nonvanishing pion mean field mix longitudinal and transversal noise correlators. In practice, the stochastic fields for the sigma and pion equations of motion can be obtained by drawing random numbers with longitudinal respectively transversal

However, despite all such possible improvements, the Langevin equation is still an approximation to the quantum theory and is obtained by expanding the effective action in mean field fluctuations. It would be great to compare our model to studies performed with a full nonequilibrium 2PI effective action ansatz (see e.g. [BPR09, BGP11] for studies in the quark-meson model) with initial conditions close to equilibrium. Unfortunately, this will not be an easy task since the required framework is very different from the one applied in this work. This includes, that we cannot readily exract damping and noise kernels as in the influence functional setting. Instead, one would have to think about how to construct observables for comparison of the different methods.

Apart from improving the level of approximation on the methodical side, the physical content at the basis can also be upgraded. The starting point for our investigations was the quark-meson model which is designed for describing chiral symmetry breaking. It may be extended to studies of the deconfinement phase transition if gluonic effects, e.g. by means of the Polyakov-loop are taken into account. In [HNB12, HNMB13], this was done for the Langevin framework of [NLHB11]. Combining this Polyakov-loop extended model with our extention by pionic fluctuations would naturally be the next step.

Furthermore, the model we have extended in this work is well suited for the simulation of heavy ion collisions when the heat bath is evolved in a hydrodynamic setting. To perform such calculations self-consistently instead of superimposing temperature profiles from other simulations, would be most desirable, especially since this could lead to noticeable effects on inclusion of the pion fluctuations. Alternatively, instead of a fluid dynamic treatment of the heat bath, one could use a kinetic approach as e.g. on the basis of a Boltzmann-Vlasov equation [vHWMG14, MWvHG14, WvHMG15, GWvHM15].

correlation, $\xi = (\xi_L, \xi_{T,1}, \xi_{T,2}, \xi_{T,3})$ and then applying a O(4) rotation to ξ which rotates the vector $(\varphi, \vec{0})$ into $(\sigma, \vec{\pi})$.

Appendix A.

Details of Calculations

A.1. Evalutation of the term $\sim \lambda^2$ in equation (4.131)

The term

$$Tr(\varphi_a \delta\varphi_a G \varphi_b \delta\varphi_b G) \tag{A.1}$$

reads with G the thermal propagator on the real time contour:

$$\begin{aligned}
&\int d^4x\, d^4y\, \varphi_a^+(x)\delta\varphi_a^+(x)G^{++}(x,y)\varphi_b^+(y)\delta\varphi_b^+(y)G^{++}(y,x) \\
+&\int d^4x\, d^4y\, \varphi_a^-(x)\delta\varphi_a^-(x)G^{--}(x,y)\varphi_b^-(y)\delta\varphi_b^-(y)G^{--}(y,x) \\
-&\int d^4x\, d^4y\, \varphi_a^+(x)\delta\varphi_a^+(x)G^{+-}(x,y)\varphi_b^-(y)\delta\varphi_b^-(y)G^{-+}(y,x) \\
-&\int d^4x\, d^4y\, \varphi_a^-(x)\delta\varphi_a^-(x)G^{-+}(x,y)\varphi_b^+(y)\delta\varphi_b^+(y)G^{+-}(y,x)
\end{aligned} \tag{A.2}$$

In section 4.1 we introduce center and relative variables,

$$\overline{\varphi}_a = \frac{1}{2}(\varphi_a^+ + \varphi_a^-) \tag{A.3}$$

$$\Delta\varphi_a = \varphi_a^+ - \varphi_a^- \tag{A.4}$$

and similarly for $\delta\varphi_a$. In the following we omit the bar in the notation of the center variables, equation (A.3). In section 4.1 we take the derivative of the effective action with respect to $\Delta\delta\varphi$ in order to obtain the equation of motion for the meson fields. Thus, we can drop all terms in expression (A.2) which are not linear or quadratic in

$\Delta\delta\varphi$. Furthermore, said derivative is taken at $\Delta\varphi = 0$, so we may drop these terms as well. This leaves us with:

$$\begin{aligned}
&\frac{1}{2}\int d^4x\, d^4y\, \varphi_a(x)\varphi_b(y)\delta\varphi_a(x)\Delta\delta\varphi_b(y)\times \\
&\quad\times \left(G^{++}(x,y)G^{++}(y,x) - G^{--}(x,y)G^{--}(y,x) + G^{+-}(x,y)G^{-+}(y,x) - G^{-+}(x,y)G^{+-}(y,x)\right) \\
+&\frac{1}{2}\int d^4x\, d^4y\, \varphi_a(x)\varphi_b(y)\delta\varphi_b(y)\Delta\delta\varphi_a(x)\times \\
&\quad\times \left(G^{++}(x,y)G^{++}(y,x) - G^{--}(x,y)G^{--}(y,x) - G^{+-}(x,y)G^{-+}(y,x) + G^{-+}(x,y)G^{+-}(y,x)\right) \\
+&\frac{1}{4}\int d^4x\, d^4y\, \varphi_a(x)\varphi_b(y)\Delta\delta\varphi_a(x)\Delta\delta\varphi_b(y)\times \\
&\quad\times \left(G^{++}(x,y)G^{++}(y,x) + G^{--}(x,y)G^{--}(y,x) + G^{+-}(x,y)G^{-+}(y,x) + G^{-+}(x,y)G^{+-}(y,x)\right)
\end{aligned} \tag{A.5}$$

Interchanging the integration variables and the summation index in the first term, we can collect the first and second term into:

$$\begin{aligned}
&\int d^4x\, d^4y\, \varphi_a(x)\varphi_b(y)\delta\varphi_b(y)\Delta\delta\varphi_a(x)\times \\
&\times \left(G^{++}(x,y)G^{++}(y,x) - G^{--}(x,y)G^{--}(y,x) - G^{+-}(x,y)G^{-+}(y,x) + G^{-+}(x,y)G^{+-}(y,x)\right)
\end{aligned} \tag{A.6}$$

By definition of the thermal propagator on the real time contour, it is with $G^{+-} = G^{<}$, $G^{-+} = G^{>}$:

$$G^{++}(x,y) = G^{>}(x,y)\Theta(x^0 - y^0) + G^{<}(x,y)\Theta(y^0 - x^0) \tag{A.7}$$

$$G^{--}(x,y) = G^{<}(x,y)\Theta(x^0 - y^0) + G^{>}(x,y)\Theta(y^0 - x^0) \tag{A.8}$$

Thus, we have

$$G^{++}(x,y)G^{++}(y,x) - G^{--}(x,y)G^{--}(y,x) - G^{+-}(x,y)G^{-+}(y,x) + G^{-+}(x,y)G^{+-}(y,x)$$

$$
\begin{aligned}
= \quad & \Theta(x^0-y^0)G^>(x,y)G^<(y,x) + \Theta(y^0-x^0)G^<(x,y)G^>(y,x) \\
- \; & \Theta(x^0-y^0)G^<(x,y)G^>(y,x) - \Theta(y^0-x^0)G^>(x,y)G^<(y,x) \\
- \; & G^<(x,y)G^>(y,x) + G^>(x,y)G^<(y,x) \qquad \text{(A.9)} \\
= \; - \; & \big(\Theta(x^0-y^0) - \Theta(y^0-x^0) + 1\big)\,(G^<(x,y)G^>(y,x) - G^>(x,y)G^<(y,x)) \\
= \; - \; & 2\,\Theta(x^0-y^0)\,(G^<(x-y)G^>(y-x) - G^>(x-y)G^<(y-x))
\end{aligned}
$$

In the last line we have additionally used that $G(x,y) = G(x-y)$ for the thermal propagator due to translation invariance of thermodynamic equilibrium [Ber04]. Similarly, we find for the third term in (A.5)

$$
\begin{aligned}
& G^{++}(x,y)G^{++}(y,x) + G^{--}(x,y)G^{--}(y,x) + G^{+-}(x,y)G^{-+}(y,x) + G^{-+}(x,y)G^{+-}(y,x) \\
= \quad & \Theta(x^0-y^0)G^>(x,y)G^<(y,x) + \Theta(y^0-x^0)G^<(x,y)G^>(y,x) \\
+ \; & \Theta(x^0-y^0)G^<(x,y)G^>(y,x) + \Theta(y^0-x^0)G^>(x,y)G^<(y,x) \\
+ \; & G^<(x,y)G^>(y,x) + G^>(x,y)G^<(y,x) \qquad \text{(A.10)} \\
= \; & \big(\Theta(x^0-y^0) + \Theta(y^0-x^0) + 1\big)\,(G^<(x,y)G^>(y,x) + G^>(x,y)G^<(y,x)) \\
= \; & 2\;(G^<(x-y)G^>(y-x) + G^>(x-y)G^<(y-x))
\end{aligned}
$$

Finally, we can write the term (A.1) as

$$
\begin{aligned}
& -2\int d^4x\, d^4y\, \varphi_a(x)\varphi_b(y)\delta\varphi_b(y)\Delta\delta\varphi_a(x)\times \\
& \qquad \times\; \Theta(x^0-y^0)\,(G^<(x-y)G^>(y-x) - G^>(x-y)G^<(y-x)) \\
& +\frac{1}{2}\int d^4x\, d^4y\, \varphi_a(x)\varphi_b(y)\Delta\delta\varphi_a(x)\Delta\delta\varphi_b(y)\times \\
& \qquad \times\,(G^<(x-y)G^>(y-x) + G^>(x-y)G^<(y-x))
\end{aligned}
\qquad \text{(A.11)}
$$

up to terms irrelevant for the final equation of motion.

A.2. Explicit calculation of the term $\sim g^2$ in equation (4.32)

Analogously to the previous section, we now turn to the explicit evaluation of the term

$$-\frac{ig^2}{2}\,Tr(\delta\phi S_{th}\delta\phi S_{th}) \tag{A.12}$$

with the thermal quark propagator S_{th} and the meson fluctuations

$$\delta\phi = \delta\sigma + i\gamma_5\vec{\tau}\delta\vec{\pi} \tag{A.13}$$

On the closed real time contour, the term (A.12) becomes:

$$\begin{aligned}-\frac{ig^2}{2}\int d^4x\, d^4y\, tr\,\Big(&\delta\phi^+(x)S^{++}(x,y)\delta\phi^+(y)S^{++}(y,x)\\ &+\delta\phi^-(x)S^{--}(x,y)\delta\phi^-(y)S^{--}(y,x)\\ &-\delta\phi^+(x)S^{+-}(x,y)\delta\phi^-(y)S^{-+}(y,x)\\ &-\delta\phi^-(x)S^{-+}(x,y)\delta\phi^+(y)S^{+-}(y,x)\quad\Big)\end{aligned} \tag{A.14}$$

where the index "th" has been suppressed. Now we switch again to center and relative variables on the contour,

$$\begin{aligned}\delta\phi^+ &= \delta\overline{\phi} + \frac{1}{2}\Delta\delta\phi\\ \delta\phi^- &= \delta\overline{\phi} - \frac{1}{2}\Delta\delta\phi\end{aligned} \tag{A.15}$$

The equation of motion is obtained by variation of the effective action with respect to the relative flucutations, so we may omit terms independent of $\Delta\delta\phi$. Dropping the "bar" in the notation of the center variables, we find at $\mathcal{O}(\Delta\delta\phi)$ (by swapping integration variables where necessary such that $\Delta\delta\phi(x)$ depends on x and exploiting the cyclicity

of the trace):

$$-\frac{ig^2}{2}\int d^4x\, d^4y\, tr\,\Big\{\Delta\delta\phi(x)\Big(S^{++}(x,y)\delta\phi(y)S^{++}(y,x) - S^{--}(x,y)\delta\phi(y)S^{--}(y,x) + S^{+-}(x,y)\delta\phi(y)S^{-+}(y,x) - S^{-+}(x,y)\delta\phi(y)S^{+-}(y,x)\Big)\Big\} \tag{A.16}$$

Just as in the bosonic case in the previous section, we insert the defining property for the real time contour propagators:

$$S^{++}(x,y) = S^{>}(x,y)\Theta(x^0-y^0) + S^{<}(x,y)\Theta(y^0-x^0) \tag{A.17}$$

$$S^{++}(x,y) = S^{<}(x,y)\Theta(x^0-y^0) + S^{>}(x,y)\Theta(y^0-x^0) \tag{A.18}$$

as well as $S^{+-} = S^{<}$, $S^{-+} = S^{>}$, to obtain:

$$ig^2\int d^4x\, d^4y\, \Theta(x^0-y^0)\, tr\,\Big\{\Delta\delta\phi(x)\Big(S^{<}(x,y)\delta\phi(y)S^{>}(y,x) - S^{>}(x,y)\delta\phi(y)S^{<}(y,x)\Big)\Big\} \tag{A.19}$$

At quadratic order in $\Delta\delta\phi$, we find from (A.14):

$$-\frac{ig^2}{8}\int d^4x\, d^4y\, tr\,\Big\{\Delta\delta\phi(x)\Big(S^{++}(x,y)\Delta\delta\phi(y)S^{++}(y,x) + S^{--}(x,y)\Delta\delta\phi(y)S^{--}(y,x) - S^{+-}(x,y)\Delta\delta\phi(y)S^{-+}(y,x) - S^{-+}(x,y)\Delta\delta\phi(y)S^{+-}(y,x)\Big)\Big\} \tag{A.20}$$

Expressing the propagators again via $S^{>}$, $S^{<}$ and utilizing the cyclicity of the trace in combination with suitable swapping of integration variables, we arrive at:

$$-\frac{ig^2}{4}\int d^4x\, d^4y\, tr\,\Big\{\Delta\delta\phi(x)\Big(S^{<}(x,y)\Delta\delta\phi(y)S^{>}(y,x) + S^{>}(x,y)\delta\phi(y)S^{<}(y,x)\Big)\Big\} \tag{A.21}$$

Appendix B.

Masses and damping coefficients in T-φ plane

Here we list plots of the full temperature and mean field dependence of the various masses (mean field and propagator) as well as of the damping coefficients. We begin with the mean field masses and damping coefficients in the case of a pure quark heat bath and a first order phase transition ($g = 5.5$). This is followed by the mean field masses and damping coefficients for the corresonding model with a critical point ($g = 3.63$) and a crossover ($g = 3.3$). Thereafter, we turn to the models incorporating contributions of the hard meson modes in the heat bath in addtition to the quarks. Here, we begin with the longitudinal and transversal propagator masses which are solutions of the gap equations (4.114). Then we present mean field masses and damping coefficients for the case of a first order phase transition ($g = 3.7$), followed by the second order phase transition ($g = 2.4$) and finally the crossover ($g = 2.0$).

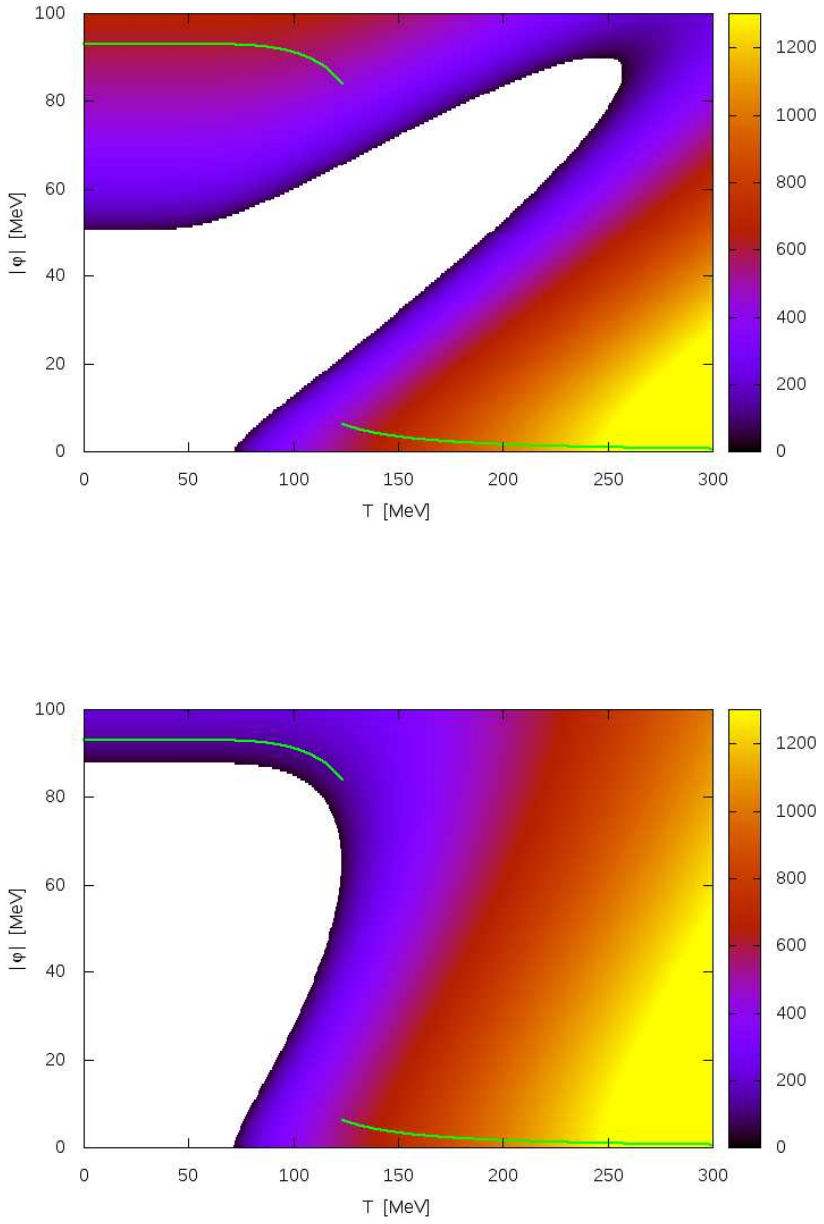

Figure B.1.: Longitudinal (upper figure) and transversal (lower figure) mean field masses $m_{L/T}$ for a model with pure quark heat bath and a first order phase transition (g=5.5). The green line corresponds to thermal equilibrium. In the white area the mass is tachyonic. The scale is given in MeV.

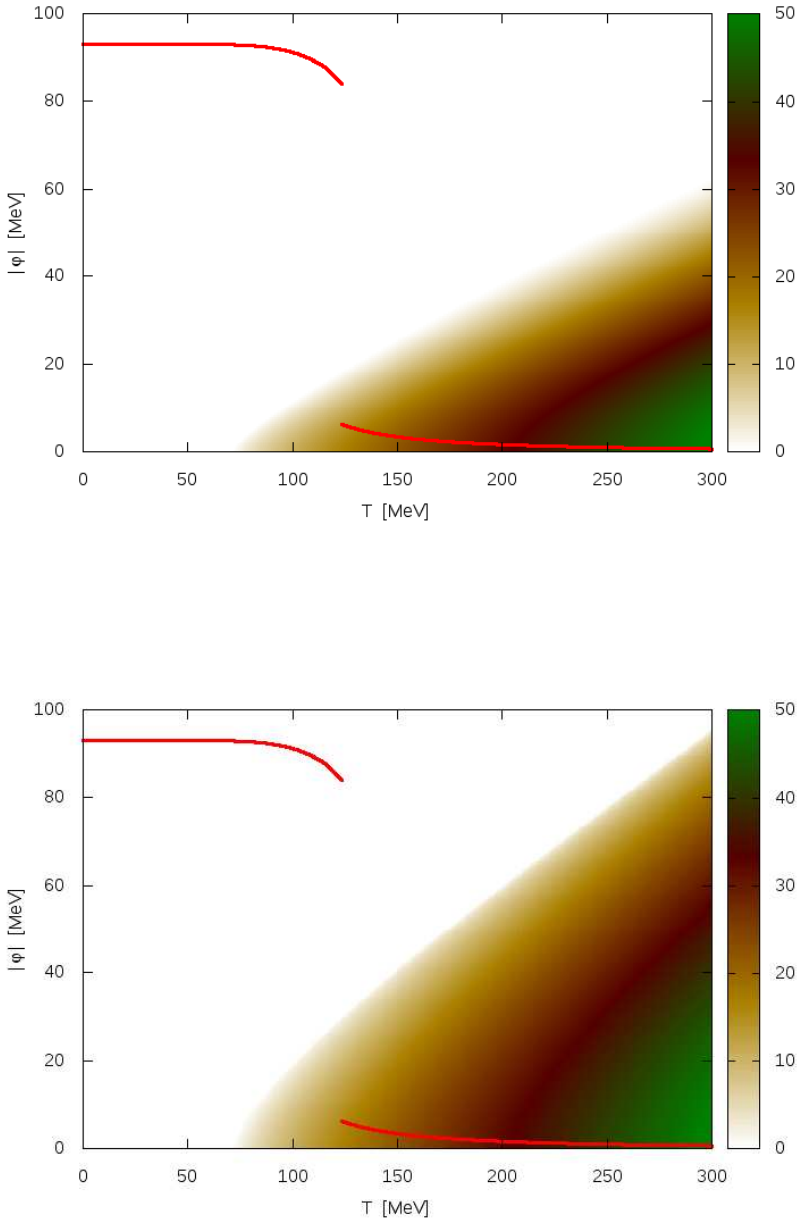

Figure B.2.: Longitudinal (upper figure) and transversal (lower figure) components of the damping coefficient $\eta_{L/T}$ for a model with pure quark heat bath and a first order phase transition (g=5.5). The red line corresponds to thermal equilibrium. In the white area the damping coefficients vanish. All values are given in fm^{-1}.

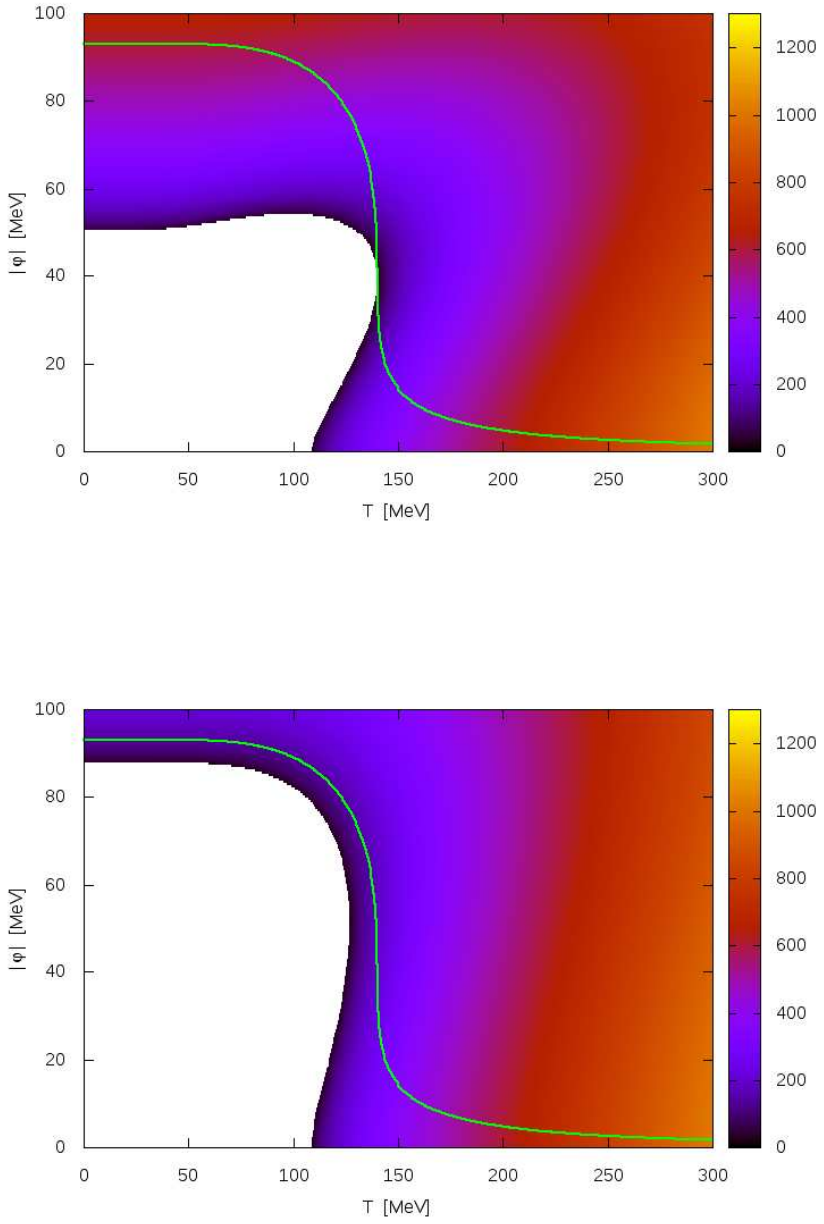

Figure B.3.: Longitudinal (upper figure) and transversal (lower figure) mean field masses $m_{L/T}$ for a model with pure quark heat bath and a second order phase transition (g=3.63). The green line corresponds to thermal equilibrium. In the white area the mass is tachyonic. The scale is given in MeV.

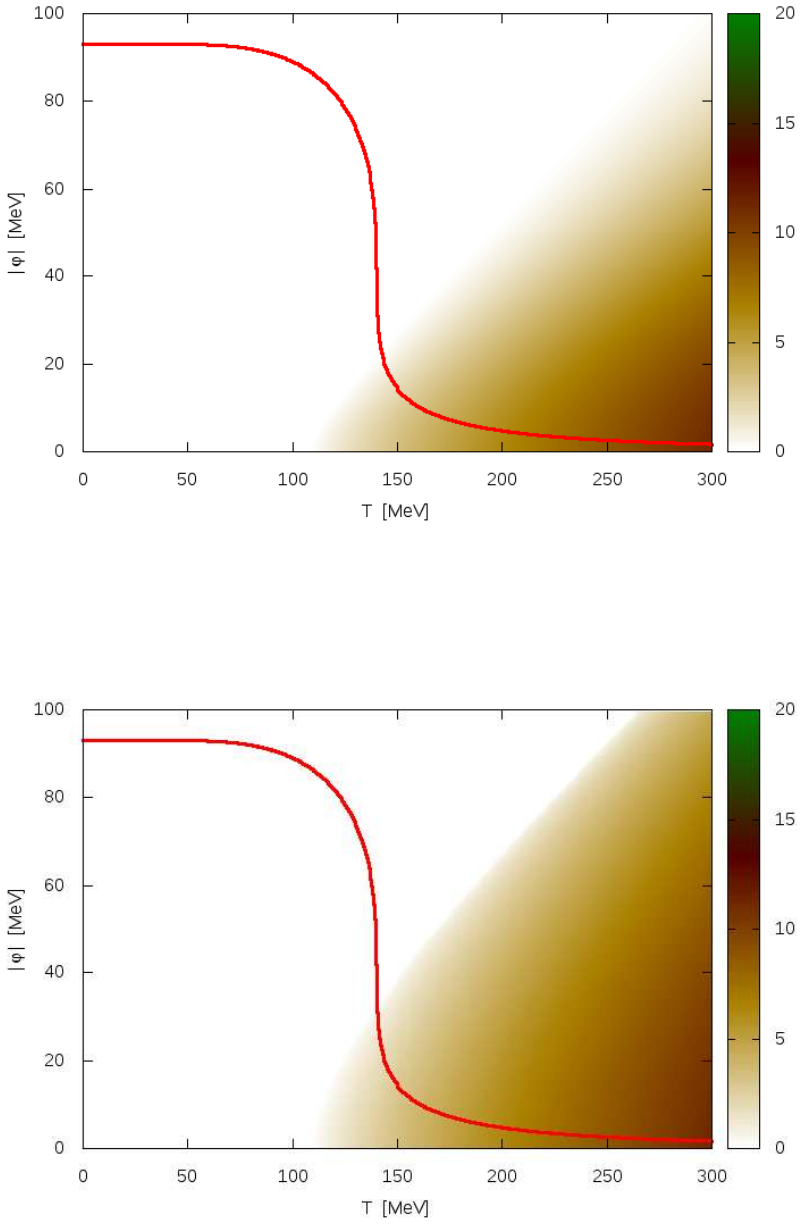

Figure B.4.: Longitudinal (upper figure) and transversal (lower figure) components of the damping coefficient $\eta_{L/T}$ for a model with pure quark heat bath and a second order phase transition (g=3.63). The red line corresponds to thermal equilibrium. In the white area the damping coefficients vanish. All values are given in fm^{-1}.

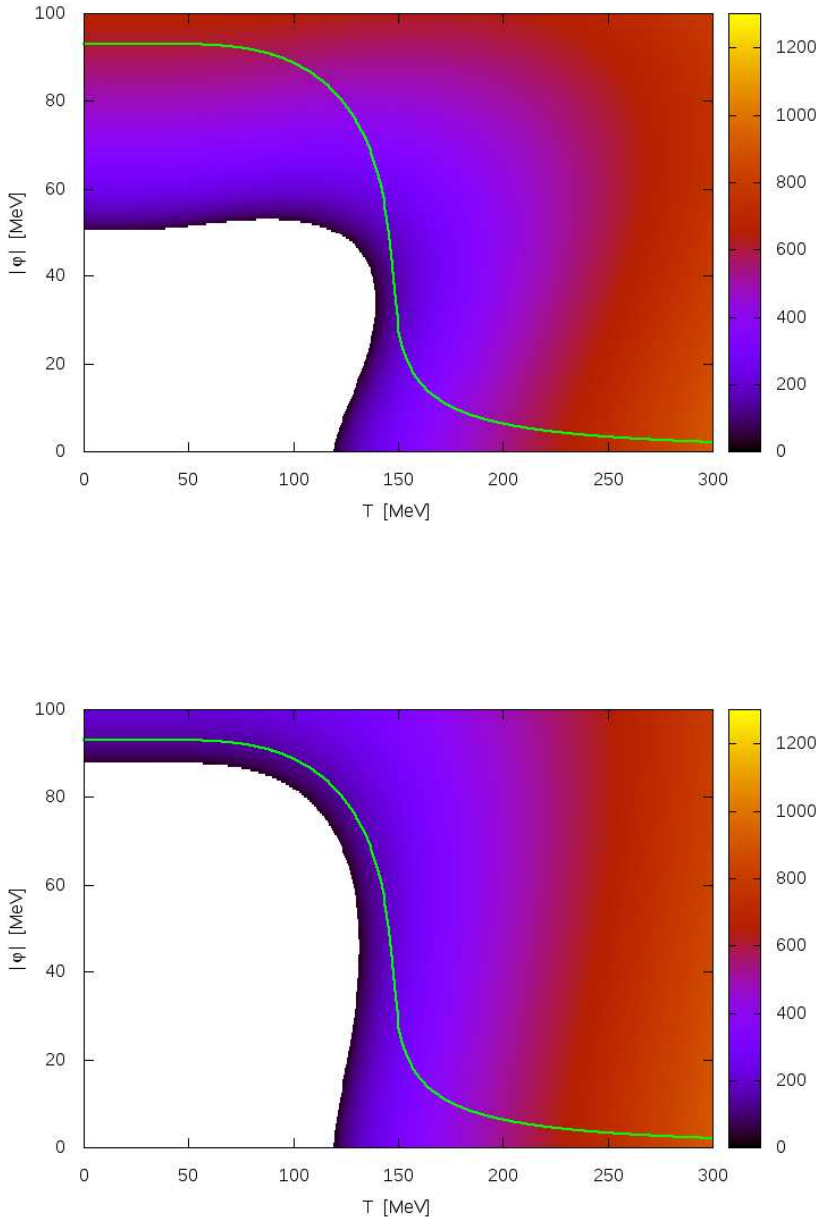

Figure B.5.: Longitudinal (upper figure) and transversal (lower figure) mean field masses $m_{L/T}$ for a model with pure quark heat bath and a crossover phase transition (g=3.3). The green line corresponds to thermal equilibrium. In the white area the mass is tachyonic. The scale is given in MeV.

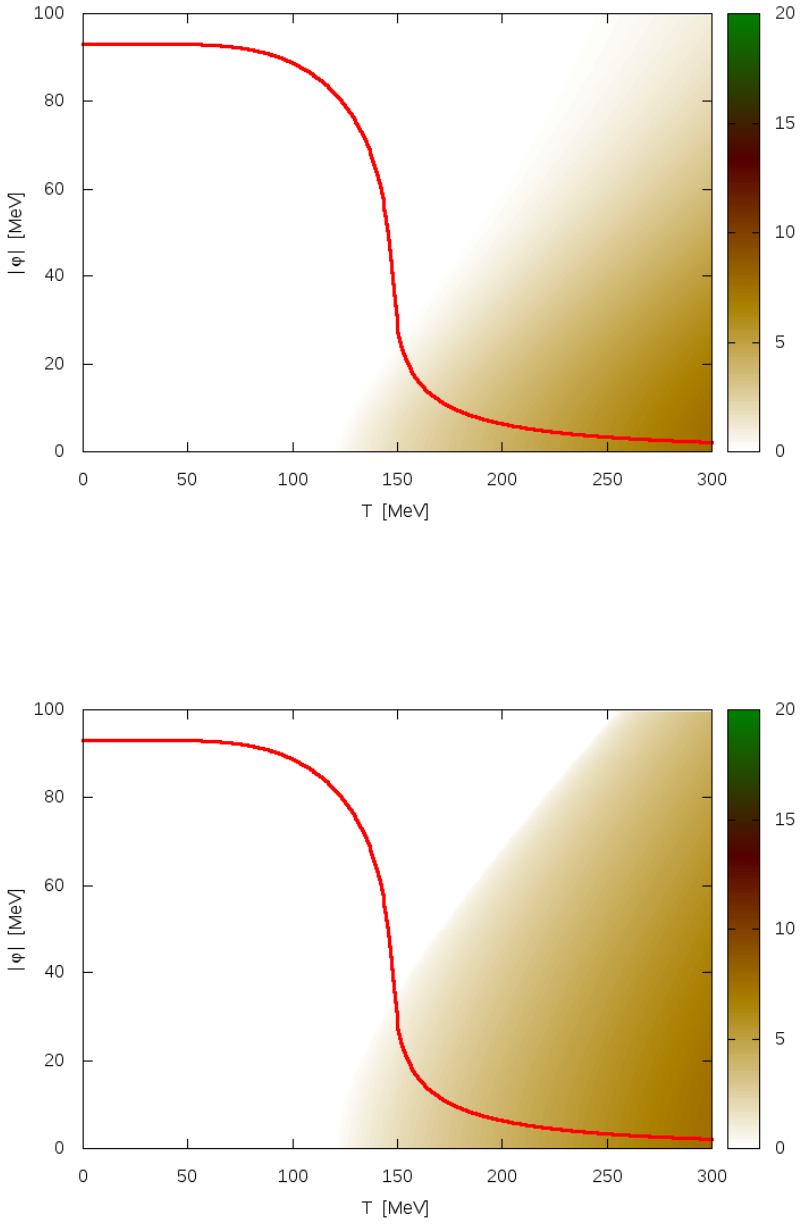

Figure B.6.: Longitudinal (upper figure) and transversal (lower figure) components of the damping coefficient $\eta_{L/T}$ for a model with pure quark heat bath and a crossover phase transition (g=3.3). The red line corresponds to thermal equilibrium. In the white area the damping coefficients vanish. All values are given in fm^{-1}.

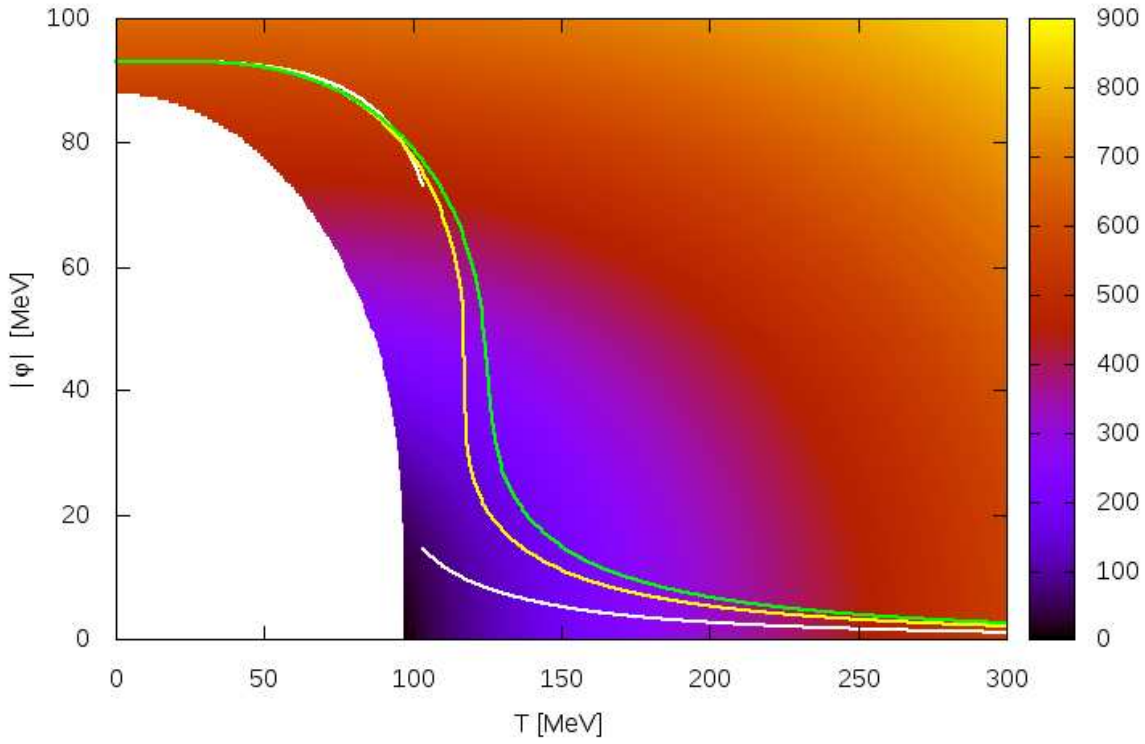

Figure B.7.: Longitudinal propagator mass M_L as solution to the gap equation (4.114). In the white area no solution exists. The scale is given in MeV. The lines correspond to thermal equilibrium in the case of a first order (g=3.7, white line), second order (g=2.4, yellow line) and crossover (g=2.0, green line) phase transition.

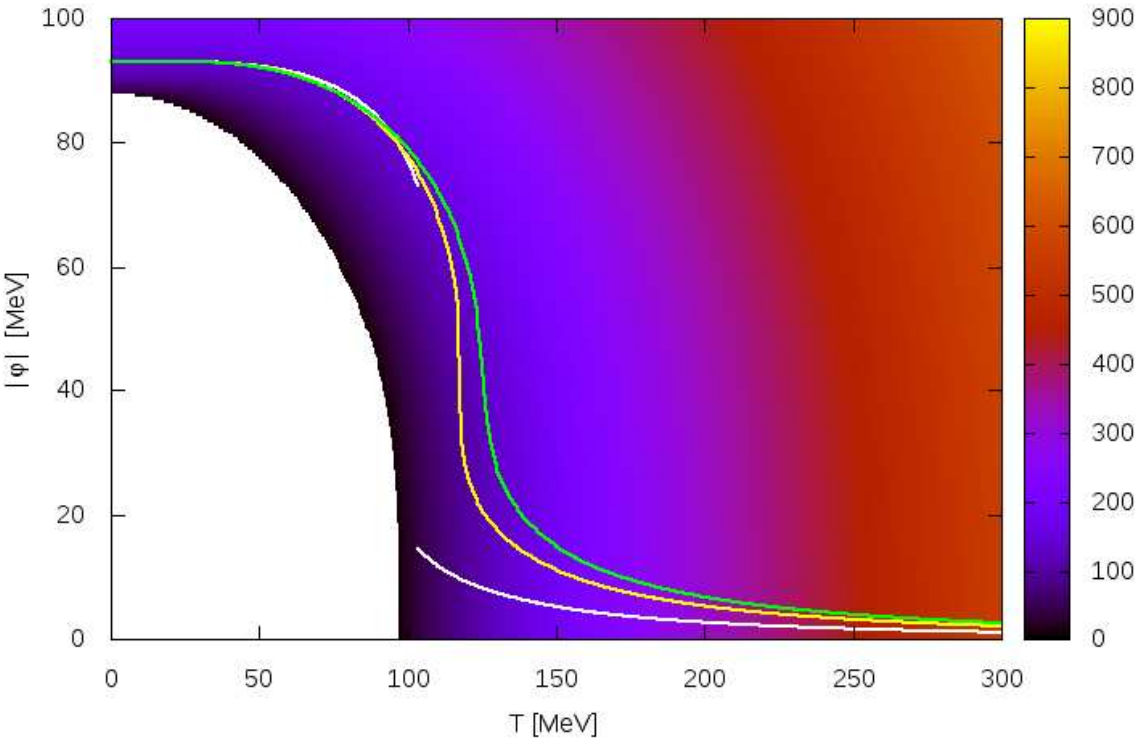

Figure B.8.: Transversal propagator mass M_T as solution to the gap equation (4.114). In the white area no solution exists. The scale is given in MeV. The lines correspond to thermal equilibrium in the case of a first order (g=3.7, white line), second order (g=2.4, yellow line) and crossover (g=2.0, green line) phase transition.

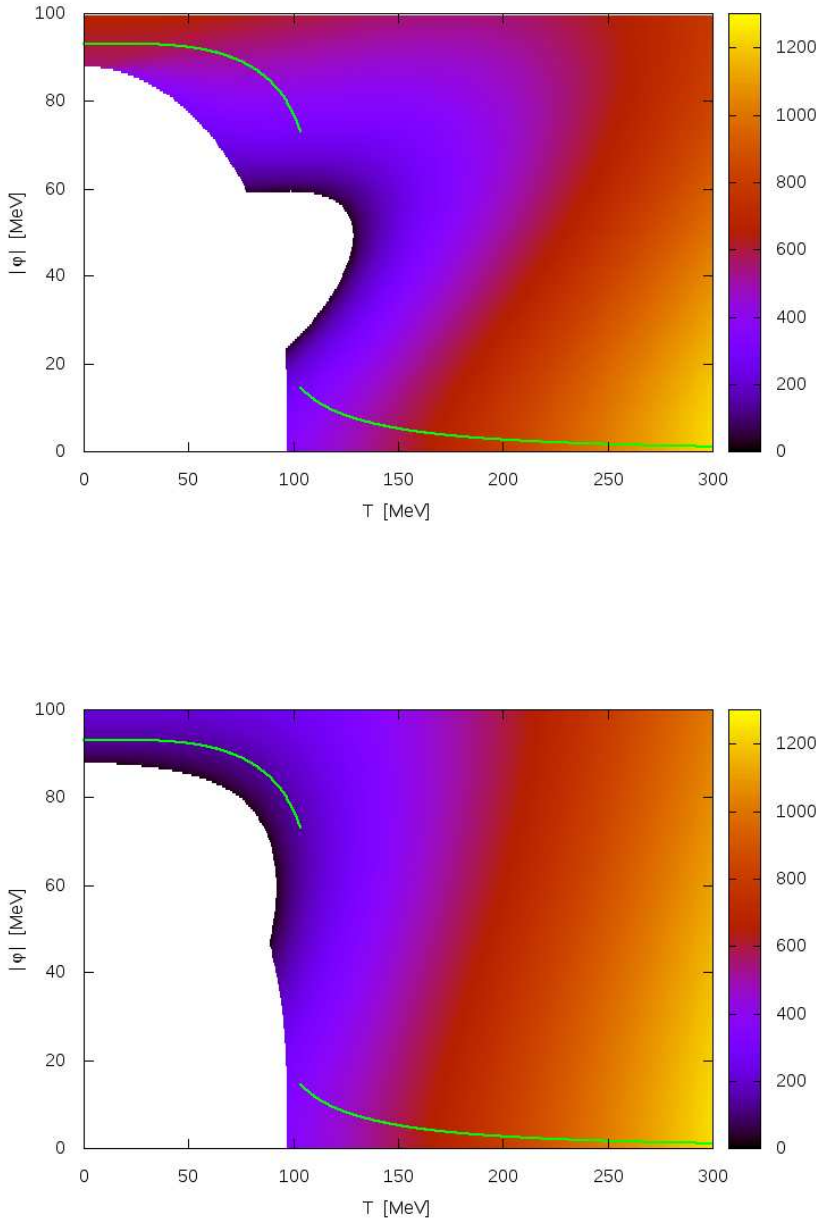

Figure B.9.: Longitudinal (upper figure) and transversal (lower figure) mean field masses $m_{L/T}$ for a model with a heat bath of quarks and hard meson modes and a first order phase transition (g=3.7). The green line corresponds to thermal equilibrium. In the white area the mass is tachyonic. The scale is given in MeV.

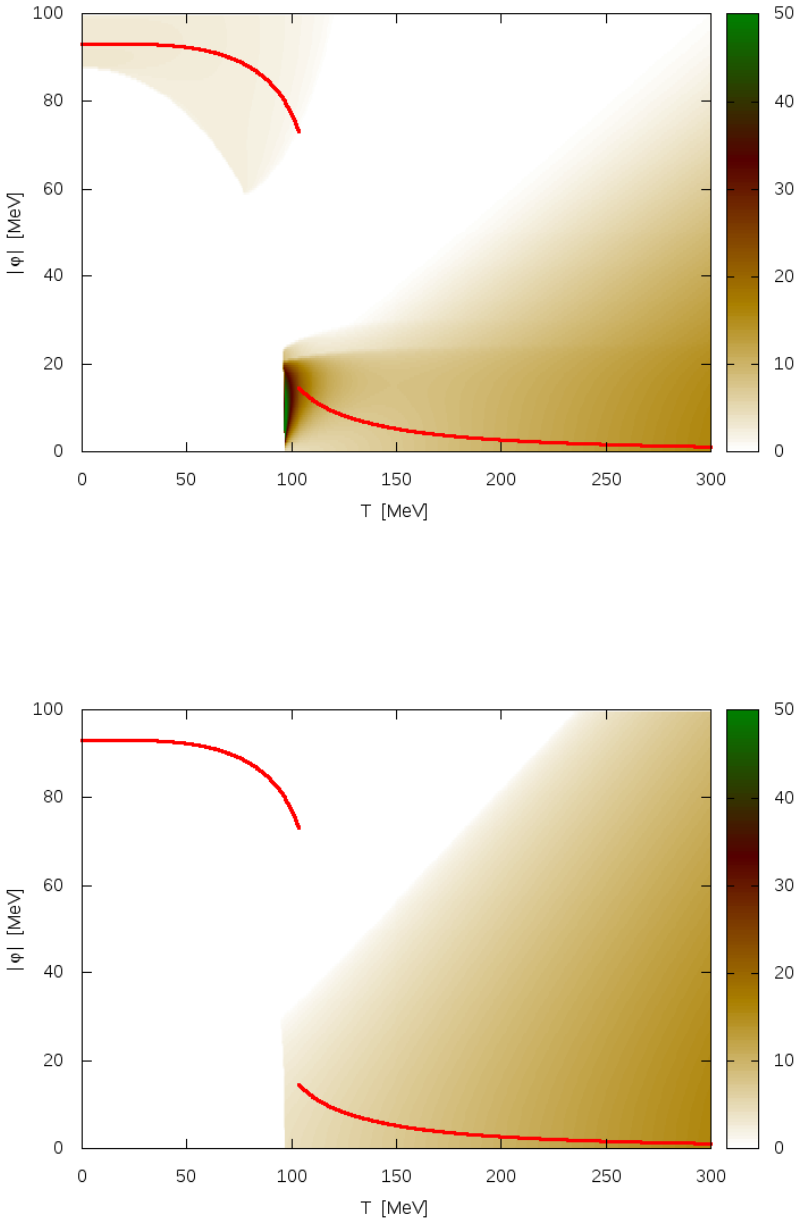

Figure B.10.: Longitudinal (upper figure) and transversal (lower figure) components of the damping coefficient $(\eta + \zeta)_{L/T}$ for a model with a heat bath of quarks and hard meson modes and a first order phase transition (g=3.7). The red line corresponds to thermal equilibrium. In the white area the damping coefficients vanish. All values are given in fm^{-1}.

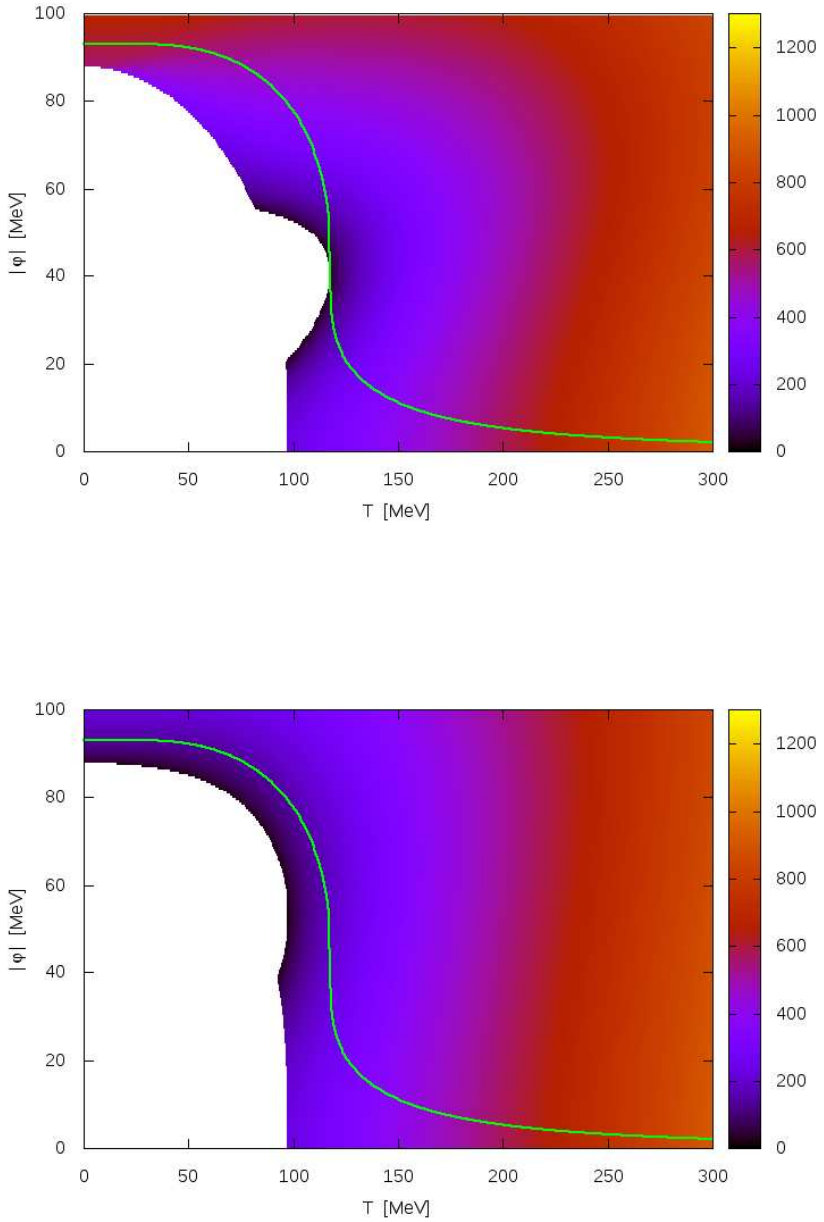

Figure B.11.: Longitudinal (upper figure) and transversal (lower figure) mean field masses $m_{L/T}$ for a model with a heat bath of quarks and hard meson modes and a second order phase transition (g=2.4). The green line corresponds to thermal equilibrium. In the white area the mass is tachyonic. The scale is given in MeV.

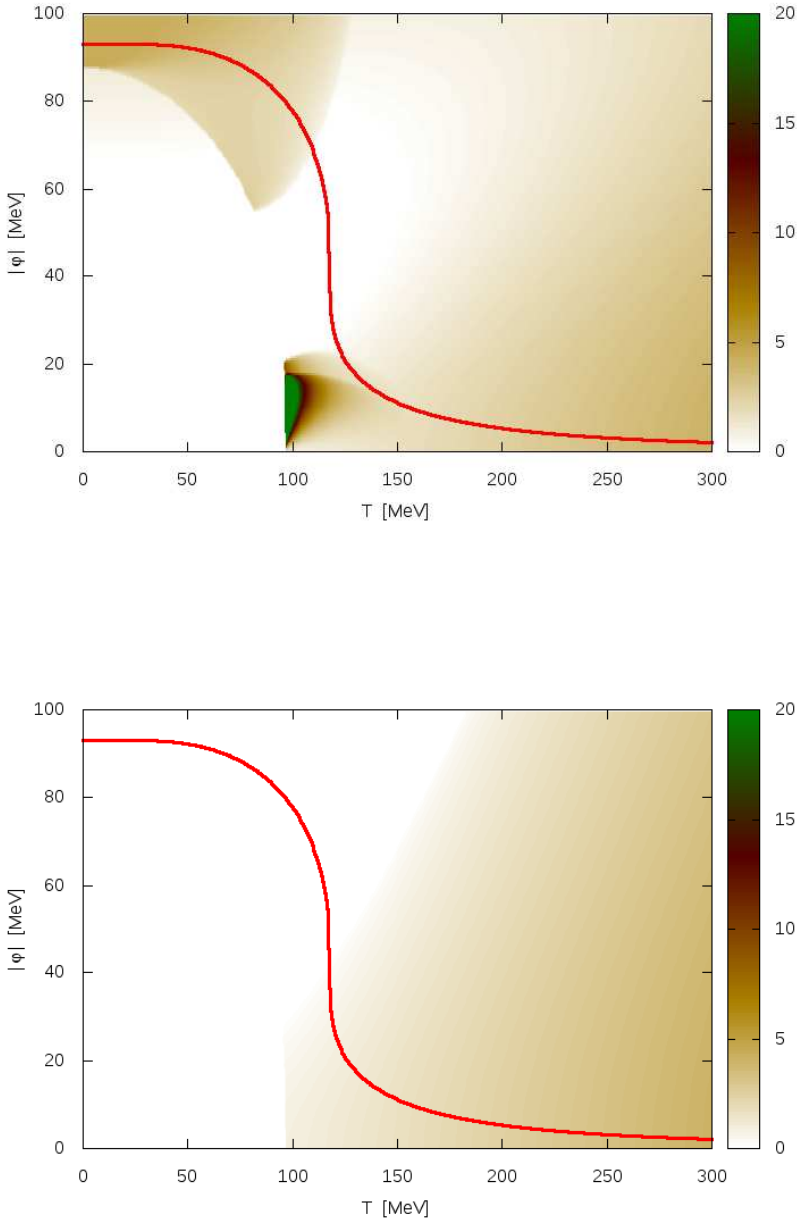

Figure B.12.: Longitudinal (upper figure) and transversal (lower figure) components of the damping coefficient $(\eta + \zeta)_{L/T}$ for a model with a heat bath of quarks and hard meson modes and a second order phase transition (g=2.4). The red line corresponds to thermal equilibrium. In the white area the damping coefficients vanish. All values are given in fm^{-1}.

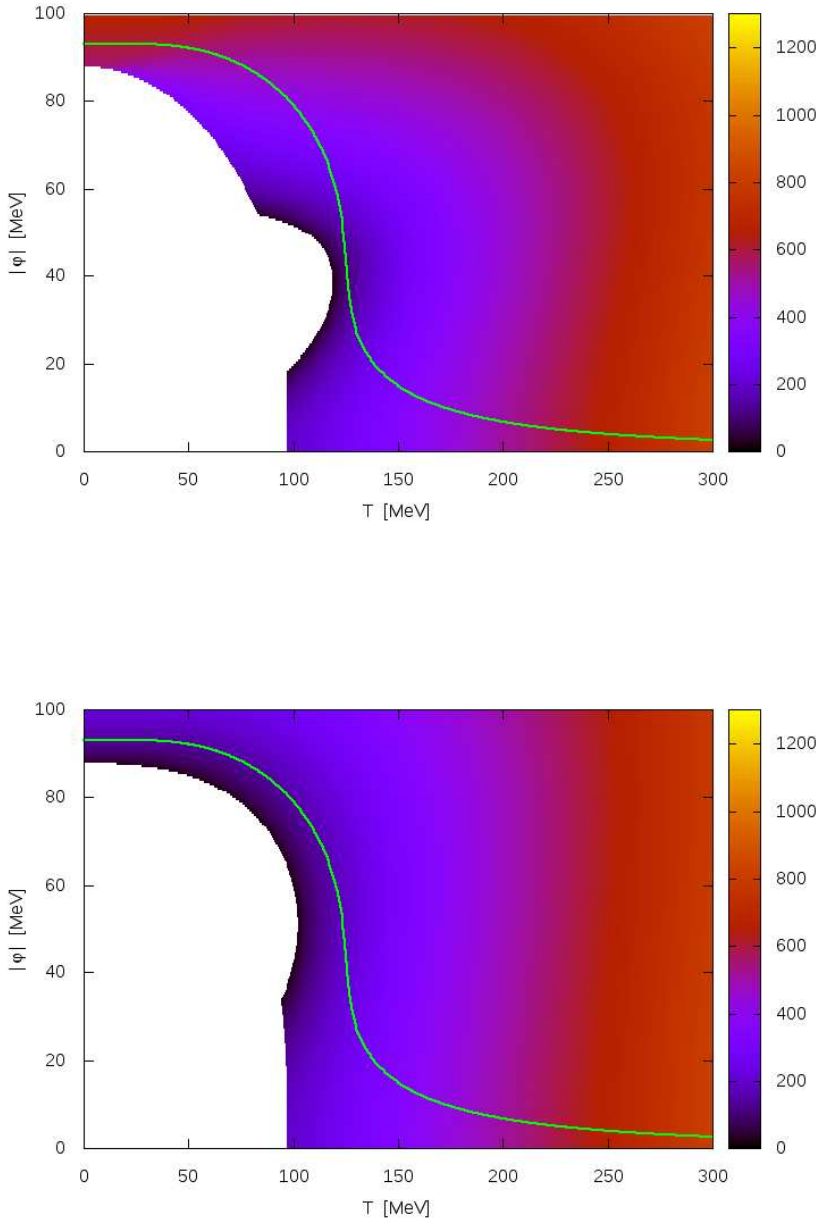

Figure B.13.: Longitudinal (upper figure) and transversal (lower figure) mean field masses $m_{L/T}$ for a model with a heat bath of quarks and hard meson modes and a crossover phase transition (g=2.0). The green line corresponds to thermal equilibrium. In the white area the mass is tachyonic. The scale is given in MeV.

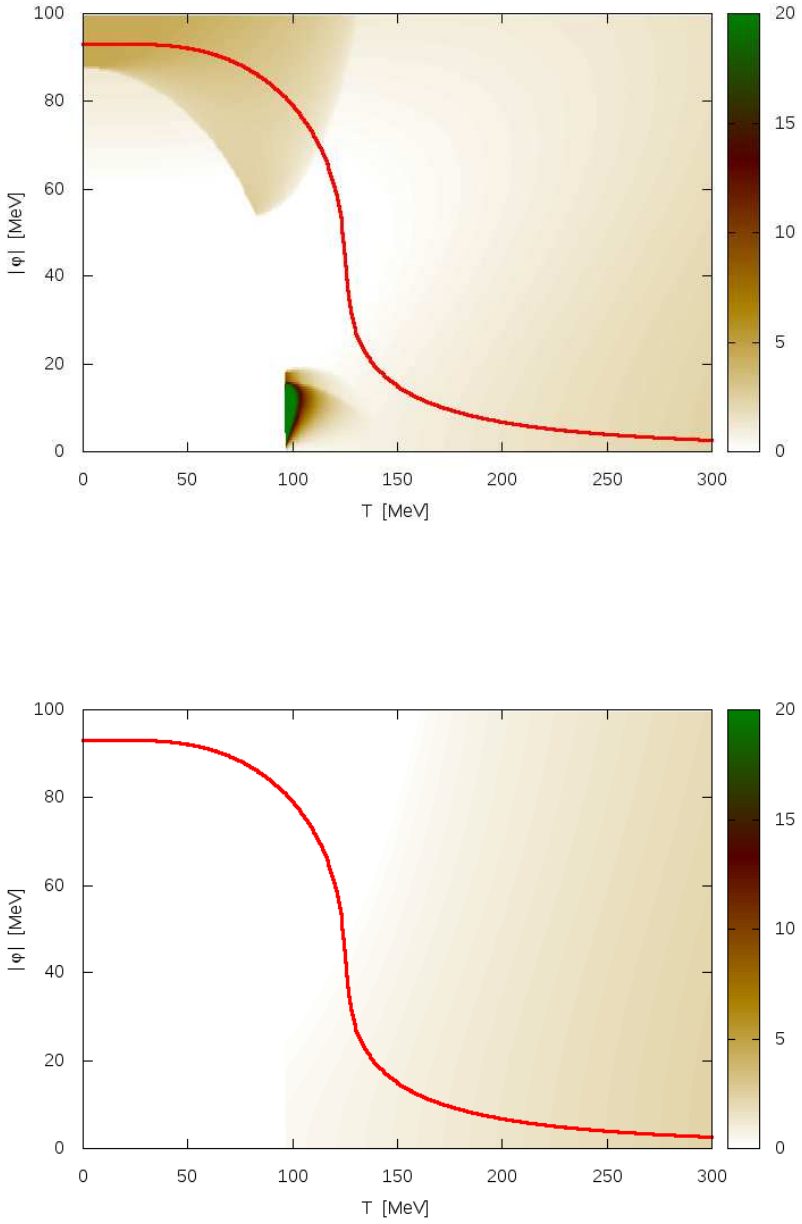

Figure B.14.: Longitudinal (upper figure) and transversal (lower figure) components of the damping coefficient $(\eta + \zeta)_{L/T}$ for a model with a heat bath of quarks and hard meson modes and a crossover phase transition (g=2.0). The red line corresponds to thermal equilibrium. In the white area the damping coefficients vanish. All values are given in fm^{-1}.

List of Figures

Bibliography

[A+05] John Adams et al. Experimental and theoretical challenges in the search for the quark gluon plasma: The STAR Collaboration's critical assessment of the evidence from RHIC collisions. *Nucl. Phys.*, A757:102, 2005.

[AB97] A. Abada and M. C. Birse. Coherent amplification of classical pion fields during the cooling of droplets of quark plasma. *Phys. Rev.*, D55:6887, 1997.

[ACBL97] G. Amelino-Camelia, J. D. Bjorken, and S. E. Larsson. Pion production from baked Alaska disoriented chiral condensate. *Phys. Rev.*, D56:6942, 1997.

[B+69] E. D. Bloom et al. High-Energy Inelastic e p Scattering at 6-Degrees and 10-Degrees. *Phys. Rev. Lett.*, 23:930, 1969.

[B+12] A. Bazavov et al. The chiral and deconfinement aspects of the QCD transition. *Phys. Rev.*, D85:054503, 2012.

[BB73] J. P. Boris and D. L. Book. Flux corrected transport I: SHASTA a fluid algorithm that works. *J. Comp. Phys.*, 11:38, 1973.

[BBH75] D. L. Book, J. P. Boris, and K. Hain. Flux corrected transport II - Generalizations fo the method. *J. Comp. Phys.*, 18:248, 1975.

[BEF+68] C. D. Boley, J. E. Elias, J. I. Friedman, G. C. Hartmann, H. W. Kendall, P. N. Kirk, M. R. Sogard, L. P. Van Speybroeck, and J. K. de Pagter. Experimental Search for a Heavy Electron. *Phys. Rev.*, 167:1275, 1968.

[Bel11] Mi. Le Bellac. *Thermal Field Theory.* Cambridge University Press, Cambridge, UK, 2011.

[Ber02] J. Berges. Controlled nonperturbative dynamics of quantum fields out-of-equilibrium. *Nucl. Phys.*, A699:847, 2002.

[Ber04] J. Berges. Introduction to Nonequilibrium Quantum Field Theory. *arXiv:*, (hep-ph/0409233v1), 2004.

[Bet09] B. Betz. *Jet Propagation and Mach-Cone Formation in (3+1)-dimensional ideal Hydrodynamcis*. PhD thesis, Johann Wolfganb Goethe University, Frankfurt am Main, 2009.

[BFH+10] S. Borsanyi, Z. Fodor, C. Hoelbling, S. D. Katz, S. Krieg, C. Ratti, and K. K. Szabo. Is there still any T_c mystery in lattice QCD? Results with physical masses in the continuum limit III. *JHEP*, 09:073, 2010.

[BG97] T. S. Biro and C. Greiner. Dissipation and fluctuation at the chiral phase transition. *Phys. Rev. Lett.*, 79:3138, 1997.

[BGP11] J. Berges, D. Gelfand, and J. Pruschke. Quantum theory of fermion production after inflation. *Phys. Rev. Lett.*, 107:061301, 2011.

[Bjo92] J. D. Bjorken. A Full Acceptance Detector for SSC Physics at Low and Intermediate Mass Scales: An Expression of Interest to the SSC. *Int. J. Mod. Phys.*, A7:4189, 1992.

[BJW03] J. Berges, D. U. Jungnickel, and C. Wetterich. Quark and nuclear matter in the linear chiral meson model. *Int. J. Mod. Phys.*, A18:3189, 2003.

[BK09] E. S. Bowman and J. I. Kapusta. Critical Points in the Linear Sigma Model with Quarks. *Phys. Rev.*, C79:015202, 2009.

[BM61] G. Baym and N. D. Mermin. Determination of Thermodynamic Green's Functions. *Journal of Mathematical Physics*, 2:232, 1961.

[BP69] J. D. Bjorken and E. A. Paschos. Inelastic Electron Proton and gamma Proton Scattering, and the Structure of the Nucleon. *Phys. Rev.*, 185:1975, 1969.

[BP10] A. Bazavov and P. Petreczky. Deconfinement and chiral transition with the highly improved staggered quark (HISQ) action. *J. Phys. Conf. Ser.*, 230:012014, 2010.

[BPR09] J. Berges, J. Pruschke, and A. Rothkopf. Instability-induced fermion production in quantum field theory. *Phys. Rev.*, D80:023522, 2009.

[Col11] J. Collins. *Foundations of Perturbative QCD*. Cambridge University Press, Cambridge, UK, 2011.

[CP75a] N. Cabibbo and G. Parisi. Exponential Hadronic Spectrum and Quark Liberation. *Phys. Lett.*, B59:67, 1975.

[CP75b] J. C. Collins and M. J. Perry. Superdense Matter: Neutrons Or Asymptotically Free Quarks? *Phys. Rev. Lett.*, 34:1353, 1975.

[Cre83] M. Creutz. *Quarks, gluons and lattices*. Cambridge University Press, Cambridge, UK, 1983.

[CSFF$^+$12] N.C. Cassol-Seewald, R.L.S. Farias, E.S. Fraga, G. Krein, and Rudnei O. Ramos. Langevin simulation of scalar fields: Additive and multiplicative noises and lattice renormalization. *Physica A: Statistical Mechanics and its Applications*, 391(16):4088, 2012.

[Das97] A. K. Das. *Finite Temperature Field Theory*. World Scientific Singapore, New York, 1997.

[DdSKK16] R. Derradi de Souza, T. Koide, and T. Kodama. Hydrodynamic approaches in relativistic heavy ion reactions. *Progress in Particle and Nuclear Physics*, 86:35, 2016.

[DGH14] J. F. Donoghue, E. Golowich, and B. R. Holstein. *Dynamics of the Standard Model*. Cambridge University Press, Cambridge, UK, 2nd edition, 2014.

[DH09] C. DeTar and U. Heller. QCD thermodynamics from the lattice. *Eur. Phys. J.*, A 41:405, 2009.

[DJ74] L. Dolan and R. Jackiw. Symmetry Behavior at Finite Temperature. *Phys. Rev.*, D9:3320, 1974.

[Fey69a] R. P. Feynman. The behavior of hadron collisions at extreme energies. *Conf. Proc.*, C690905:237, 1969.

[Fey69b] R. P. Feynman. Very high-energy collisions of hadrons. *Phys. Rev. Lett.*, 23:1415, 1969.

[FGM72] H. Fritzsch and M. Gell-Mann. Current algebra: Quarks and what else? *eConf*, C720906V2:135, 1972.

[FPP09] E. S. Fraga, L. F. Palhares, and M. B. Pinto. Nonperturbative Yukawa theory at finite density and temperature. *Phys. Rev. D*, 79:065026, 2009.

[FS13] K. Fukushima and C. Sasaki. The phase diagram of nuclear and quark matter at high baryon density. *Prog. Part. Nucl. Phys.*, 72:99, 2013.

[FV63] R. P. Feynman and F. L. Vernon. The Theory of a general quantum system interacting with a linear dissipative system. *Annals Phys.*, 24:118, 1963.

[GL98] C. Greiner and S. Leupold. Stochastic interpretation of Kadanoff-Baym equations and their relation to Langevin processes. *Annals Phys.*, 270:328, 1998.

[GM62] M. Gell-Mann. Symmetries of baryons and mesons. *Phys. Rev.*, 125:1067, 1962.

[GM64] M. Gell-Mann. A Schematic Model of Baryons and Mesons. *Phys. Lett.*, 8:214, 1964.

[GML60] M. Gell-Mann and M. M. Levy. The axial vector current in beta decay. *Nuovo Cimento*, 16:705, 1960.

[Gre64] O. W. Greenberg. Spin and Unitary Spin Independence in a Paraquark Model of Baryons and Mesons. *Phys. Rev. Lett.*, 13:598, 1964.

[Gri08] D. Griffiths. *Introduction to Elementary Particles*. WILEY-VCH Verlag GmBH & Co. KGaA, Weinheim, 2nd edition, 2008.

[GW73a] D. J. Gross and F. Wilczek. Asymptotically Free Gauge Theories. 1. *Phys. Rev.*, D8:3633, 1973.

[GW73b] D. J. Gross and F. Wilczek. Ultraviolet Behavior of Nonabelian Gauge Theories. *Phys. Rev. Lett.*, 30:1343, 1973.

[GW74] D. J. Gross and F. Wilczek. Asymptotically Free Gauge Theories. 2. *Phys. Rev.*, D9:980, 1974.

[GWvHM15] C. Greiner, C. Wesp, H. van Hees, and A. Meistrenko. Monte-Carlo approach to particle-field interactions and the kinetics of the chiral phase transition. *J. Phys. Conf. Ser.*, 636:012007, 2015.

[Hag65] R. Hagedorn. Statistical thermodynamics of strong interactions at high-energies. *Nuovo Cim. Suppl.*, 3:147, 1965.

[HN65] M. Y. Han and Y. Nambu. Three Triplet Model with Double SU(3) Symmetry. *Phys. Rev.*, 139:B1006, 1965.

[HNB12] C. Herold, M. Nahrgang, and M. Bleicher. Fluctuations and correlations in Polyakov loop extended chiral fluid dynamics. *Acta Phys. Polon. Supp.*, 5:529, 2012.

[HNMB13] C. Herold, M. Nahrgang, I. Mishustin, and M. Bleicher. Chiral fluid dynamics with explicit propagation of the Polyakov loop. *Phys. Rev.*, C87:014907, 2013.

[Ito70] N. Itoh. Hydrostatic Equilibrium of Hypothetical Quark Stars. *Prog. Theor. Phys.*, 44:291, 1970.

[JW96] D. U. Jungnickel and C. Wetterich. Effective action for the chiral quark-meson model. *Phys. Rev.*, D53:5142, 1996.

[Kel64] L. V. Keldysh. *Zh. Eksp. Teor. Fiz.*, 47:1515, 1964.

[KG06] J. I. Kapusta and C. Gale. *Finite-temperature field theory: Principles and applications*. Cambridge University Press, Cambridge, UK, 2nd edition, 2006.

[Koc97] V. Koch. Aspects of chiral symmetry. *Int. J. Mod. Phys.*, E6:203, 1997.

[Kub57] R. Kubo. Statistical mechanical theory of irreversible processes. 1. General theory and simple applications in magnetic and conduction problems. *J. Phys. Soc. Jap.*, 12:570, 1957.

[Lan08] P. Langevin. Sur la theorie du movement brownien. *C. R. Acad. Sci.*, 146:530, 1908.

[Lan53] L. D. Landau. On the multiparticle production in high-energy collisions. *Izv. Akad. Nauk Ser. Fiz.*, 17:51, 1953.

[LG97] D. S. Lemons and A. Gythiel. Paul Langevin's 1908 paper "On the Theory of Brownian Motion" ["Sur la theorie du movement brownien," C. R. Acad. Sci. (Paris) 146, 530-533 (1908)]. *American Journal of Physics*, 65:1079, 1997.

[LRSB00] J. T. Lenaghan, D. H. Rischke, and J. Schaffner-Bielich. Chiral symmetry restoration at nonzero temperature in the SU(3)(r) x SU(3)(l) linear sigma model. *Phys. Rev.*, D62:085008, 2000.

[Mal12] M. Maly. Compact Stars in the Quark-Meson Model. Master's thesis, Ruprecht Karls University, Heidelberg, 2012.

[Mat55] T. Matsubara. A New Approach to Quantum-Statistical Mechanics. *Progress of Theoretical Physics*, 14:351, 1955.

[MME04] Á. Mócsy, I. N. Mishustin, and P. J. Ellis. Role of fluctuations in the linear σ model with quarks. *Phys. Rev. C*, 70:015204, 2004.

[Mos89] U. Mosel. *Fields, Symmetries, and Quarks*. McGraw-Hill Book company GmBH, Hamburg, 1989.

[MS59] P. C. Martin and J. S. Schwinger. Theory of many particle systems. 1. *Phys. Rev.*, 115:1342, 1959.

[MS05] B. Mohanty and J. Serreau. Disoriented chiral condensate: theory and experiment. *Phys. Rept.*, 414:263, 2005.

[MWvHG14] A. Meistrenko, C. Wesp, H. van Hees, and C. Greiner. Nonequilibrium dynamics and transport near the chiral phase transition of a quark-meson model. *J. Phys. Conf. Ser.*, 503:012003, 2014.

[Nah11] M. Nahrgang. *Nonequilibrium phase transitions in chiral fluid dynamics including dissipation and fluctuation*. PhD thesis, Johann Wolfgang Goethe University, Frankfurt am Main, 2011.

[Ne'61] Y. Ne'eman. Derivation of strong interactions from a gauge invariance. *Nucl. Phys.*, 26:222, 1961.

[NHL+13] M. Nahrgang, C. Herold, S. Leupold, I. Mishustin, and M. Bleicher. The impact of dissipation and noise on fluctuations in chiral fluid dynamics. *Journal of Physics G: Nuclear and Particle Physics*, 40:055108, 2013.

[NJL61a] Y. Nambu and G. Jona-Lasinio. Dynamical Model of Elementary Particles Based on an Analogy with Superconductivity. I. *Phys. Rev.*, 122:345, 1961.

[NJL61b] Y. Nambu and G. Jona-Lasinio. Dynamical Model of Elementary Particles Based on an Analogy with Superconductivity. II. *Phys. Rev.*, 124:246, 1961.

[NLB12] M. Nahrgang, S. Leupold, and M. Bleicher. Equilibration and relaxation times at the chiral phase transition including reheating. *Physics Letters B*, 711:109, 2012.

[NLHB11] M. Nahrgang, S. Leupold, C. Herold, and M. Bleicher. Nonequilibrium chiral fluid dynamics including dissipation and noise. *Phys. Rev. C*, 84:024912, 2011.

[O+14] K. A. Olive et al. *(Particle Data Group), Chin. Phys. C*, 38:090001, 2014.

[PF08] L. F. Palhares and E. S. Fraga. Perturbative Yukawa theory at finite density: The Role of masses and renormalization group flow at two loops. *Phys. Rev.*, D78:025013, 2008.

[PF10] L. F. Palhares and E. S. Fraga. Droplets in the cold and dense linear sigma model with quarks. *Phys. Rev. D*, 82:125018, 2010.

[Phi10] O. Philipsen. Lattice QCD at non-zero temperature and baryon density. 2010.

[Pol73] H. D. Politzer. Reliable Perturbative Results for Strong Interactions? *Phys. Rev. Lett.*, 30:1346, 1973.

[Pol74] H. D. Politzer. Asymptotic Freedom: An Approach to Strong Interactions. *Phys. Rept.*, 14:129, 1974.

[PS95] M. E. Peskin and D. V. Schroeder. *An Introduction to Quantum Field Theory*. Westview Press, United States of America, 1995.

[PTVF02] W. H. Press, S. A. Teukolsky, W. T. Vetterling, and B. P. Flannery. *Numerical Recipes in C++: The Art of Scientific Computing*. Cambridge University Press, New York, NY, USA, 2 edition, 2002.

[RBM95] D. H. Rischke, S. Bernard, and J. A. Maruhn. Relativistic hydrodynamics for heavy ion collisions. 1. General aspects and expansion into vacuum. *Nucl. Phys.*, A595:346, 1995.

[Ris98] D. H. Rischke. Forming disoriented chiral condensates through fluctuations. *Phys. Rev. C*, 58:2331, 1998.

[RPM95] D. H. Rischke, Y. Pursun, and J. A. Maruhn. Relativistic hydrodynamics for heavy ion collisions. 2. Compression of nuclear matter and the phase transition to the quark - gluon plasma. *Nucl. Phys.*, A595:383, 1995. [Erratum: Nucl. Phys.A596,717(1996)].

[RW93] K. Rajagopal and F. Wilczek. Emergence of coherent long wavelength oscillations after a quench: Application to QCD. *Nucl. Phys.*, B404:577, 1993.

[Sch61] J. Schwinger. Brownian Motion of a Quantum Oscillator. *Journal of Mathematical Physics*, 2:407, 1961.

[Sch82] A. Schmid. On a Quasiclassical Langevin Equation. *Journal of Low Temperature Physics*, 49:609, 1982.

[Sch06] F. Schwabl. *Statistische Mechanik*. Springer-Verlag, Berlin, Heidelberg, 3rd edition, 2006.

[SD99] O. Scavenius and A. Dumitru. A First order chiral phase transition may naturally lead to the 'quench' initial condition and strong soft pion fields. *Phys. Rev. Lett.*, 83:4697, 1999.

[SFN+10] V. Skokov, B. Friman, E. Nakano, K. Redlich, and B.-J. Schaefer. Vacuum fluctuations and the thermodynamics of chiral models. *Phys. Rev. D*, 82:034029, Aug 2010.

[SG86] H. Stoecker and W. Greiner. High-Energy Heavy Ion Collisions: Probing the Equation of State of Highly Excited Hadronic Matter. *Phys. Rept.*, 137:277, 1986.

[SMMR01] O. Scavenius, Á. Mócsy, I. N. Mishustin, and D. H. Rischke. Chiral phase transition within effective models with constituent quarks. *Phys. Rev. C*, 64:045202, 2001.

[SP99] B.-J. Schaefer and H.-J. Pirner. Renormalization group flow and equation of state of quarks and mesons. *Nucl. Phys.*, A660:439, 1999.

[Sre07] M. Srednicki. *Quantum Field Theory*. Cambridge University Press, Cambridge, UK, 2007.

[Sti14] R. Stiele. *On the Thermodynamics and Phase Structure of Strongly Interacting Matter in a Polyakov-Loop-Extended Constituent-Quark Model*. PhD thesis, Johann Wolfgang Goethe University, Frankfurt am Main, 2014.

[Tay] R. E. Taylor. Nucleon Form Factors Above 6-GeV. *Proc. of the Int. Symp. on Electron and Photon Interactions at High Energies, SLAC, 1967. Stanford Univ., SLAC, 1967, p. 78.*

[vHK01] H. van Hees and J. Knoll. Renormalization in Self-Consistent Approximations schemes at Finite Temperature I: Theory. *Phys. Rev. D*, 65:025010, 2001.

[vHK02a] H. van Hees and J. Knoll. Renormalization in self-consistent approximation schemes at finite temperature. III. Global symmetries. *Phys. Rev. D*, 66:025028, 2002.

[vHK02b] H. van Hees and J. Knoll. Renormalization of self-consistent approximation schemes at finite temperature. II. Applications to the sunset diagram. *Phys. Rev. D*, 65:105005, 2002.

[vHWMG14] H. van Hees, C. Wesp, A. Meistrenko, and C. Greiner. Dynamics of the chiral phase transition. *Acta Phys. Polon. Supp.*, 7:59, 2014.

[Wei95] S. Weinberg. *The Quantum Theory of Fields, Vol. II Modern Applications*. Cambridge University Press, Cambridge, UK, 1995.

[Wel83] H. A. Weldon. Simple rules for discontinuities in finite-temperature field theory. *Phys. Rev. D*, 28:2007, 1983.

[WvHMG15] C. Wesp, H. van Hees, A. Meistrenko, and C. Greiner. Monte Carlo framework for noncontinuous interactions between particles and classical fields. *Phys. Rev.*, E91:043302, 2015.

[XG00] Z. Xu and C. Greiner. Stochastic treatment of disoriented chiral condensates within a Langevin description. *Phys. Rev.*, D62:036012, 2000.

[YM54] C.-N. Yang and R. L. Mills. Conservation of Isotopic Spin and Isotopic Gauge Invariance. *Phys. Rev.*, 96:191, 1954.

[Zwe64a] G. Zweig. An SU(3) model for strong interaction symmetry and its breaking. Version 1. *CERN-TH*, 401, 1964.

[Zwe64b] G. Zweig. An SU(3) model for strong interaction symmetry and its breaking. Version 2. *CERN-TH*, 412, 1964.

Acknowledgements

Here I would like to thank all people who contributed to this work or supported me during my PhD studies.

First and foremost, I wish to thank my supervisor, PD. Dr. Jürgen Schaffner-Bielich, who gave me the opportunity to work on an exciting topic. I am very grateful for his suggestions and the fruitful discussions as well as his patience. Also, during his last year at Heidelberg, he made it possible for me to attend several international conferences and workshops.

Secondly, I would like to thank Prof. Dr. Joerg Jaeckel, for agreeing on reviewing this thesis and also for his patience.

Further, I would like to express my gratitude to Dr. Barbara Betz who provided me with the input data from the simulation of heavy ion collisions, and to Dr. Marlene Nahrgang, for kindly answering my many questions.

For the great atmosphere and the discussions during coffee breaks and at conferences, I would like to thank all current and former members of Jürgen's research group. Special thanks go to Dr. Debarati Chatterchee, Dr. Giuseppe Pagliara, Dr. Rainer Stiele, Dr. Simon Schettler, Dr. Torben Graf, Margit Maly and Andreas Zacchi.

Finally, I wish to thank my friends and family (in a wider sense) for their invaluable love and outstanding support, especially Steven Werry, as well as my mother, Jutta Menzer-Weissenborn, and most of all my wife, Karoline.

Eidesstattliche Versicherung gemäß §8 der Promotionsordnung für die Naturwissenschaftlich-Mathematische Gesamtfakultät der Universität Heidelberg:

Bei der eingereichten Dissertation zu dem Thema "On the Impact of Pion Fluctuations on the Dynamics of the Order Parameter at the Chiral Phase Transition" handelt es sich um meine eigenständig erbrachte Leistung.

Ich habe nur die angegebenen Quellen und Hilfsmittel benutzt und mich keiner unzulässigen Hilfe Dritter bedient. Insbesondere habe ich wörtlich oder sinngemäß aus anderen Werken übernommene Inhalte als solche kenntlich gemacht.

Die Arbeit oder Teile davon habe ich bislang nicht an einer Hochschule des In- oder Auslands als Bestandteil einer Prüfungs- oder Qualifikationsleistung vorgelegt.

Die Richtigkeit der vorstehenden Erklärungen bestätige ich.

Die Bedeutung der eidesstattlichen Versicherung und die strafrechtlichen Folgen einer unrichtigen oder unvollständigen eidesstattlichen Versicherung sind mir bekannt.

Ich versichere an Eides statt, dass ich nach bestem Wissen die reine Wahrheit erklärt und nichts verschwiegen habe.

Heidelberg, den 30. Mai 2016